ISBN 978-82-326-2572-7 (printed version)
ISBN 978-82-326-2573-4 (electronic version)
ISSN 1503-8181

Doctoral theses at NTNU, 2017:250

Zhaolong Yu

Hydrodynamic and structural aspects of ship collisions

NTNU
Norwegian University of
Science and Technology
Faculty of Engineering
Science and Technology
Department of MarineTechnology

NTNU
Norwegian University of
Science and Technology

Doctoral theses at NTNU, 2017:250

NTNU

NTNU
Norwegian University of
Science and Technology

Zhaolong Yu

Hydrodynamic and structural aspects of ship collisions

Thesis for the degree of Philosophiae Doctor

Trondheim, September 2017

Norwegian University of Science and Technology
Faculty of Engineering
Science and Technology
Department of MarineTechnology

NTNU
Norwegian University of
Science and Technology

NTNU
Norwegian University of Science and Technology

Thesis for the degree of Philosophiae Doctor

Faculty of Engineering
Science and Technology
Department of MarineTechnology

ISBN 978-82-326-2572-7 (printed version)
ISBN 978-82-326-2573-4 (electronic version)
ISSN 1503-8181

Doctoral theses at NTNU, 2017:250

Printed by Skipnes Kommunikasjon as

Dedicated to my family,
especially my grandpa, who had always expected to witness this moment

Abstract

Ships and offshore installations operating at sea are exposed to the risk of collision accidents, which may cause severe consequences. It is therefore crucial to understand the physics of the collision process and to design structures so that they have sufficient strength to avoid progressive collapses. A traditional way of dealing with ship collisions is to decouple the process into *the external dynamics and the internal mechanics*. *The external dynamics* deals with ship motions and energy absorption while *the internal mechanics* handles the deformation and resistance of structures. The decoupled method is simple to implement and gives fast predictions of the dissipated energy and structural damage. However, the method fails to capture the influence of ship motions and the consideration of hydrodynamic forces is crude, which may lead to poor prediction accuracy in skew collisions with small collision angles and collisions with long durations. To better understand the fluid structure interactions in ship collisions, one main purpose of the thesis is to couple *the external dynamics* and *the internal mechanics* and to discuss the influence of hydrodynamic forces and six degrees of freedom (6DOF) ship motions on the damage prediction of the decoupled method.

By taking advantage of *the user defined load subroutine* and *the user common subroutine*, two coupled approaches for ship collision simulation were developed by implementing two different hydrodynamic models into the nonlinear finite element code LS-DYNA. The first approach uses a traditional ship maneuvering model for the in-plane surge, sway and yaw motions and three single-degree-of-freedom (SDOF) spring-damper vibration systems for the out-of-plane heave, roll and pitch motions. This method provides improved accuracy of hydrodynamic representation, and more importantly, enables a full 6DOF coupled dynamic simulation of ship collisions for the first time without simplifying the collision resistance. The second approach improves the representation of hydrodynamic forces by using linear potential flow theory. Models both with and without considering the forward speed effect were implemented.

Various collision scenarios were simulated with the proposed coupled models, including colliding with oblique plates, grounding on a sloping sea floor, crushing into rigid plates with normal vectors misaligned with coordinate axes, and collision with a submersible platform. Note that the struck objects are assumed to be fixed in the studies, but there should be no limitation for the coupled models to account for the 6DOF motions of the struck objects.

A comparative study was carried out, where the accuracy of the decoupled method to predict the demand for strain energy dissipation and damage extent was checked. A new phenomenon of ‘secondary impacts’ was observed when the periodic motions of heave, roll and pitch were introduced in the coupled method. This is not accounted for in the

de-coupled method. The influence of hydrodynamic forces, 6DOF ship motions and the forward speed effect on the energy dissipation was investigated. The assumptions and simplifications of the external dynamic models were reviewed and the validity was discussed by comparison with the coupled simulation results. Potential limitations of the external dynamic models were pointed out.

In the second part of the thesis, the internal deformation mechanics of two of the most commonly used structural components in offshore industries, i.e. tubular members and stiffened panels, were studied by the use of numerical simulation and simplified analytical methods.

The responses of offshore tubular members subjected to vessel bow and stern impacts were investigated using LS-DYNA. Extensive collision simulations with a total energy of 30-50 MJ were carried out with varying tube diameters, lengths and thicknesses. The effect of ship-platform interaction was considered by modeling both the ship and the tubular braces/legs with nonlinear shell finite elements. An existing analytical denting model was extended to account for distributed loads and was verified against simulation results. The requirements for tubular members to keep compactness were reviewed and discussed. A new concept, 'transition indentation ratio' from local denting to global bending, was proposed for tube deformation. The intention of the concept is to help judge the governing deformation patterns with given tube dimensions and material properties, and to unify existing compactness requirements, providing theoretical support to the R_c (characteristic denting resistance) criterion in the new version DNV-GL RP C204. Design considerations of braces/legs subjected to ship impacts were discussed with emphasis on the ship-platform interactions.

A simplified formulation was proposed for the resistance of large inelastic deformation of stiffened plates subjected to lateral loading. The method is based on rigid plastic material assumptions and the use of yield functions formulated in terms of stress resultants. The method considers the flexibility of the panel ends with respect to inward motion, while the rotational boundary conditions are free or clamped. Concentrated and distributed loads are considered, as well as patch loading. The resistance-deformation curves predicted by the proposed method were compared with results using LS-DYNA. The formulation may be used for quick estimates of the resistance of stiffened panels subjected to abnormal or accidental static and transient transverse loads such as explosions, slamming, hydrostatic pressure, and ice actions.

Acknowledgement

This work has been carried out under the supervision of Professor Jørgen Amdahl at Department of Marine Technology, and Centre for Autonomous Marine Operations and Systems (AMOS), Norwegian University of Science and Technology (NTNU). I would like to express my sincere gratitude to Professor Amdahl for his insightful guidance, continuous support and encouragement during the PhD period. The work would not have been possible without his professional perspective and the enormous talks and discussion with him. Jørgen is a fun and energetic person, an excellent supervisor and also a good friend. I always feel inspired by his deep passion for hiking, biking and skiing, and more importantly for life.

I also wish to thank Dr. Zhiqiang Hu at Newcastle University, Dr. Ge Wang at American Bureau of Shipping (ABS), and Professor Runpei Li at Shanghai Jiao Tong University for the kind support during the PhD application. The committee members, Professor Manolis Samuelides from National Technical University of Athens, Dr. Kristjan Tabri from Tallinn University of Technology, and Professor Sigmund Kyrre Ås from NTNU are gratefully acknowledged. They kindly reviewed the thesis and provided valuable comments.

During the thesis work, I have collaborated with a few devoted and skilled colleagues. I would like to thank my co-supervisor Professor Marilena Greco and her PhD student Yugao Shen for providing the valuable input for the study of the forward speed effect in ship collisions. Thanks also goes to Dr. Martin Storheim for the useful instruction on the use of LS-DYNA and the cluster *vilje*. Dr. Zhenhui Liu generously provided his code of the 6DOF external dynamic model, which makes the comparative study of coupled and decoupled methods and an in-depth discussion possible. This is very much appreciated. Dr. Zhengshun Cheng and Dr. Yanyan Sha have been very helpful for kindly offering guidance on the use of SIMA and USFOS. I wish also to thank the professors from the department of Marine Technology and department of Structural Engineering for giving excellent courses. Knowledge from the lectures has prepared me with solid background and increasing confidence to deal with the PhD work and future challenges.

Studying and living abroad is never easy, but I am so lucky to have you all, the good friends and fellow colleagues from the department and from outside the department. I would like to mention Professor Zhen Gao, Dr. Wei Chai, Dr. Zhengshun Cheng, Dr. Yanyan Sha, Dr. Zhiyu Jiang, Dr. Peng Li, Dr. Ling Wan, Ping Fu, Yuna Zhao, Yugao Shen, Ming Song, Xiaoxian Guo, to name a few who are always helpful. I also wish to thank my office mates, Woongshik Nam, Shaojun Ma and Mohd Atif Siddiqui for the pleasant working atmosphere, fruitful discussion and the wonderful tradition of birthday dinner. I also would like to express my gratitude for the kind help from the administrative staffs, including Sigrid Bakken Wold, Annika Bremvåg, Oddny Kristine

Østhus, Jannike Gripp and Bjørn Tore Bach.

Last but not the least, I would like to give my special thanks to my parents and family in China for their unconditional love, support and encouragement.

Zhaolong Yu

August, 2017
Trondheim, Norway

List of appended papers

This thesis consists of an introductory section and a collection of five journal papers as follows. The five papers are reported in the appendix:

JP 1:
A new approach for coupling external dynamics and internal mechanics in ship collisions
Zhaolong Yu, Jørgen Amdahl and Martin Storheim
Published in *Journal of Marine Structures* (2016), vol. 45, pp. 110-132

JP 2:
Full six degrees of freedom coupled dynamic simulation of ship collision and grounding accidents
Zhaolong Yu and Jørgen Amdahl
Published in *Journal of Marine Structures* (2016), vol. 47, pp. 1-22

JP 3:
Implementation of linear potential-flow theory in the 6DOF coupled simulation of ship collision and grounding accidents
Zhaolong Yu, Yugao Shen, Jørgen Amdahl and Marilena Greco
Published in *Journal of Ship Research* (2016), vol. 60 (3), pp. 119-144

JP 4:
Analysis and design of offshore tubular members against ship impacts
Zhaolong Yu and Jørgen Amdahl
Submitted to journal.

JP 5:
Large inelastic deformation resistance of stiffened panels subjected to lateral loading
Zhaolong Yu, Jørgen Amdahl and Yanyan Sha
Submitted to journal.

Declaration of Authorship

I am the first author of papers 1-5 included in the thesis. I am responsible for initiating ideas, making theoretical derivations, establishing numerical models, performing the analysis and writing the papers. Professor Jørgen Amdahl is the co-author of all the papers. He contributed with constructive ideas, fruitful discussions and critical comments. Dr. Martin Storheim provided useful instructions on the use of LS-DYNA and the cluster *vilje*. He also reviewed paper 1 and provided useful comments. Dr. Yugao Shen is the second author of paper 3, and he was responsible for calculating the hydrodynamic coefficients considering the forward speed effect. Prof. Marilena Greco and Dr. Yanyan Sha are the fourth author of paper 3 and the third author of paper 5, respectively. They reviewed the papers and provided constructive comments.

Additional papers

The following papers were written during the PhD study but are not included as part of the thesis:

AP 1:
Discussion of assumptions behind the external dynamics models in ship collisions and groundings
Zhaolong Yu, Zhenhui Liu and Jørgen Amdahl
Submitted to journal

AP 2:
Influence of 6DOF ship motions in the damage prediction of ship collision and grounding accidents
Zhaolong Yu and Jørgen Amdahl
Proceedings of the 7th International Conference on Collision and Grounding of Ships and Offshore Structures, ICCGS 2016, Ulsan, South Korea.

AP 3:
Design of offshore tubular members against excessive local indentation under lateral impacts
Zhaolong Yu and Jørgen Amdahl
Proceedings of 6th International Conference on Marine Structures, MARSTRUCT 2017, Lisbon, Portugal.

Contents

Abstract i
Acknowledgement iii
List of appended papers v
Declaration of Authorship vi
Additional papers vi
Contents vii
Chapter 1. Introduction 1
1.1 Background 1
1.2 Thesis Objectives and Scope 6
1.3 Thesis Organization 9
Chapter 2. An overview of methodologies for the assessment of ship collisions 11
2.1 Introduction 11
2.2 Hydrodynamic consideration in ship collisions 12
2.3 Structural response assessment in ship collisions 18
2.4 Review of responses of tubular members subjected to lateral impacts 24
2.4.1 Local indentation resistance of tubular braces and legs 24
2.4.2 Residual bending capacity of dented tubes 27
2.4.3 Bending and membrane stretching of tubes 29
Chapter 3. 6DOF coupled dynamic simulation of ship collisions 31
3.1 Introduction 31
3.2 The user defined load and user common subroutine in LS-DYNA 31
3.3 Coupled model 1: implementation of a maneuvering model into LS-DYNA 32
3.3.1 A maneuvering model for planar motions 32
3.3.2 The three out-of-plane degrees of freedom 35
3.3.3 Implementation procedure 36
3.4 Coupled model 2: implementation of linear potential flow theory into LS-DYNA 37

3.4.1 Linear potential flow theory without forward speed effect 37
3.4.2 Linear potential flow theory considering the forward speed effect 39
3.4.3 Implementation procedure 41
3.5 Verification of the proposed methods 42
Chapter 4. Influence of coupling external and internal mechanics on damage prediction 43
4.1 Introduction 43
4.2 Model description and case studies 43
4.2.1 The striking ship 43
4.2.2 The semisubmersible platform 45
4.2.3 Definition of collision scenarios 46
4.3 Discussion of assumptions behind the external dynamic models 47
4.3.1 Constant added masses 49
4.3.2 Proportionality of impact impulses and forces 50
4.3.3 Small collision duration and constant collision angle 54
4.3.4 Determination of the normal vector of the contact plane 56
4.3.5 Restitution factor 58
4.4 The influence of ship motions and fluid-structure interaction 60
4.4.1 Secondary impacts 60
4.4.2 Energy dissipation 62
4.4.3 Penetration path and structural damage 64
4.4.4 The forward speed effect 66
Chapter 5. Analysis and design of offshore tubular members against ship impacts 69
5.1 Introduction 69
5.2 Ship collision with rigid braces and legs 71
5.2.1 FE modelling of supply vessel bow and sterns 71
5.2.2 Resistance to penetration of rigid braces and legs 72
5.3 Denting resistance of braces and legs subjected to lateral impacts 75
5.3.1 Extension of a local denting model 75
5.3.2 Discussion of the models for local denting resistance 76
5.4 Transition from local denting to global bending 78
5.5 Compactness requirements 81

5.5.1 A review of requirements to resist local denting 81
5.5.2 Discussion 82
5.6 Design of offshore tubular members against ship impacts 84
5.6.1 The effect of ship structure interactions 84
5.6.2 Design against ship collisions 86
Chapter 6. Resistance to large inelastic deformations of stiffened panels subjected to lateral loading 87
6.1 Introduction 87
6.2 Yield functions based on generalized forces 88
6.3 Resistance of stiffened panels at finite deformations 90
6.4 Comparison with nonlinear finite element analysis 92
6.4.1 Finite element models 92
6.4.2 Resistance with infinite or finite stiffness against inward motion 94
6.4.3 Resistance to uniformly distributed loads 96
6.4.4 Panels stiffened with L-profiles 97
6.4.5 The influence of transverse shear and inertial forces on the resistance 99
Chapter 7. Conclusions and recommendations for future work 101
7.1 Conclusions 101
7.2 Recommendations for future work 104
References 107
Appendix A: appended papers 117
PAPER 1 117
PAPER 2 143
PAPER 3 167
PAPER 4 195
PAPER 5 235

Chapter 1

Introduction

1.1 Background

Among the most catastrophic accidents that can occur at sea are ship collisions. Ship collisions can be termed as the structural impact between two ships or one ship and a floating or still object such as icebergs, offshore structures, bridges, submerged tunnels and waterfront structures. Ship collision accidents occur frequently although more and more advanced navigational tools and standardized operational regulations have been used. The International Maritime Organization (IMO) reported an average annual occurrence of 23.8 collisions for the last 10 years with very serious casualties (IMO, 2015). The circumstances that lead to these accidents are complex and vary widely. Human error is one of most common causes of maritime collisions, and carelessness or inexperienced crew members can quickly lead to collisions at sea. Next to human error, harsh environmental conditions also contribute significantly, such as extreme waves and currents, fog obstructing vision, high winds and ice flows. Equipment failure is another major cause of ship collisions. For example, ships may lose control due to malfunctioning manoeuvring facilities.

The potential consequences of ship collision accidents vary significantly from minor local structural deformations to major threats to ship integrity, causing progressive collapse of structures, compartment flooding or oil leakage. In the extreme events, the accidental loads may sink the vessel, with associated great economic loss, severe environmental pollutions and loss of human lives. One of the most well-known ship collision accidents may be the *Titanic* accident in 1912. The luxury liner *Titanic*, designed with the latest technology and engineered to be the largest and most luxurious steam ship in the world at that time, was proclaimed to be unsinkable until it collided with the iceberg and sank on its maiden voyage, depriving of more than 1500 people's lives. The sinking of Titanic created worldwide shock and outrage at the huge loss of lives, which still has a wide influence today. More recently in 2012, the Italian cruise ship Costa Concordia collided with a submerged rock and capsized a few hours later, killing 32 people (see Figure 1-1).

The environmental issues at sea are closely related to the transportation safety of oil tankers, which may cause oil spills after ship collisions. The *Exxon Valdez* accident in 1989 is considered one of the most devastating man-made environmental disasters ever to occur at sea. The oil tanker Exxon Valdez slammed into Bligh Reef and spilled more than 11 million gallons of crude oil into the water of Alaska's Prince William Sound region. The coastal ecosystem was severely damaged, with millions of animals died and some species completely perished; see Figure 1-2.

More recently in 2004, the bulk cargo ship *Selendang Ayu* ran aground off the Unalaska Island after the failure of its engine. The ship broke into two with 350,000 gallons of oil spilled into the sea. The *Erika* accident in 1999 off the coast of France and the *Prestige* accident in 2002 off the coast of northwest Spain, were not caused by ship collisions, but led to catastrophic oil spills. Both oil tankers split into two halves due to storms, releasing a large amount of crude oil into the sea water.

Figure 1-1. The grounding accident of the cruise ship *Costa Concordia*

Figure 1-2. (a) Left: the oil spills after the *Exxon Valdez* accident. (b) Right: an oil-soaked bird after the accident.

With the rapid development of offshore oil, gas, and clean energy industry in the past several decades, a large number of offshore structures were constructed and installed worldwide. Offshore structures are exposed to the risk of being collided by visiting vessels, and the consequences can be catastrophic. In July 2005, a multipurpose support vessel struck *the Mumbai High North Platform* and ruptured several marine risers. The resulting gas leak led to catastrophic explosions and fire; see Figure 1-3. After two hours, the entire platform collapsed, leaving only the stump of its jacket above sea level and 22 people dead (Daley, 2013). Fortunately, ship collisions are rare events, and the consequences are generally not as serious as *the Mumbai High North Platform* accident. Kvitrud (2011) summarized the collision events between ships and platforms in Norway in the period 2001-2010. None of the collisions have

caused loss of lives and personnel injuries. The economic consequences have, however, been significant.

As one future trend of the offshore oil and gas exploration and exploitation is to march into the arctic regions, ship collisions with ice flows and icebergs may become more frequent. Collisions between icebergs and ship structures may cause significant structural damage, economic loss and fatalities. The Titanic disaster is one of the most well-known examples. Figure 1-4 shows the damage of the crude oil tanker OVERSEAS OHIO after colliding with an iceberg in 1914. The collision caused extensive damage to the ship bow and had to be repaired in the shipyard.

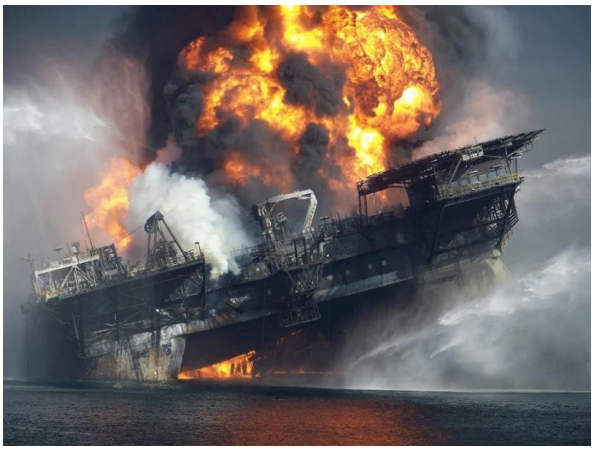

Figure 1-3. The Mumbai High North Platform disaster

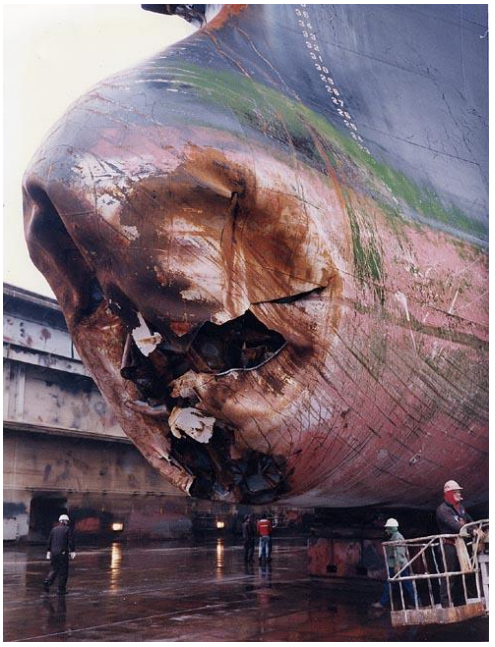

Figure 1-4. The damaged ship bow after *OVERSEAS OHIO* collided with an iceberg

The catastrophic shipping accidents in the history become the key drivers of developing, implementing and enforcing international regulations. For example, the Titanic accident led to the Safety of Life at Sea (SOLAS) Convention. The Oil Pollution Act 1990 (OPA 90) were triggered by the large number of dry bulk carrier losses in the 1980s, and notably the grounding of the Exxon Valdez oil tanker in 1989. The timeline in Figure 1-5 highlights the drivers for changes through the introduction of new or updated legislation attributed to major incidents or a series of incidents focusing on the past 15 years (Pike et al., 2013).

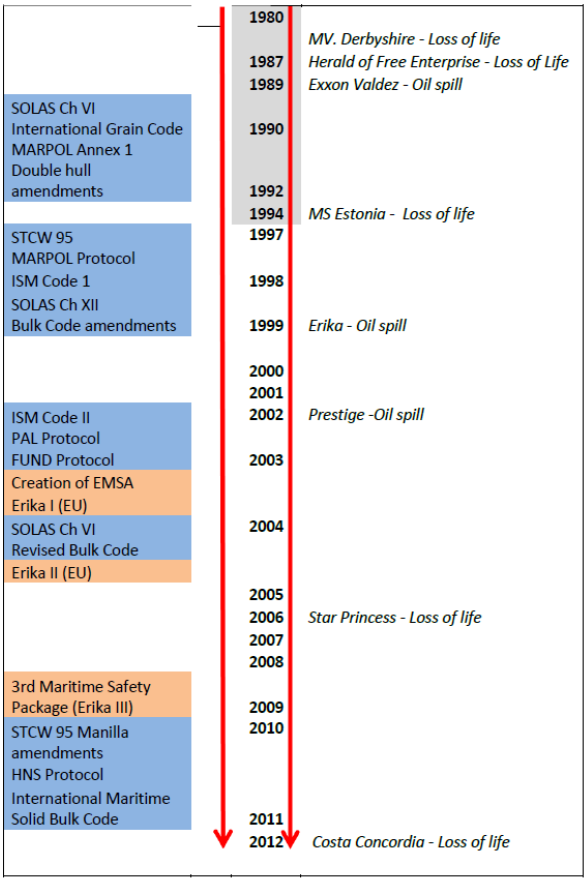

Figure 1-5. The 15 year time line and key shipping accidents and subsequent changes in maritime safety legislation (Pike et al., 2013).

In view of the potential severe consequences of ship collisions, there has been a continuous interest in understanding the underlying collision mechanics and designing crashworthy structures. For exchanging the state-of-the-art developments in the field, the International Conference on Collision and Grounding of Ships and Offshore Structures (ICCGS) was established in 1996. The conference is still very active today with the most recent one held in Ulsan, 2016. Based on the research findings, ship design standards and regulations were enforced by the classification societies and governments for the safe operation and production

at sea. For the offshore industry in Norway, typical design standards are NORSOK-N003 (2007), NORSOK-N004 (2004), DNV-RP-C204 (2010) and DNV-RP-C208 (2013). The current design standard for ship collisions generally follows the content when the standard was first introduced in 1980s (DNV, 1981). According to the NORSOK-N003 (2007) standard, the accidental limit state (ALS) design check should be carried out with a characteristic value of each accidental action which corresponds to an annual exceedance probability of 10^{-4} per installation. This gives the design collision scenario being a standard supply vessel with a displacement of 5000 tons travelling with a speed of 2 m/s. The standard design energy is thus 11 MJ for the bow/stern collisions and 14 MJ for the broadside collisions considering added mass effects. Over the years, significant changes of ship structures and designs have emerged, which pose new challenges for the design of crashworthy structures.

A noticeable change is the increasing tonnage of attendant vessels. Figures 1-6 and 1-7 show supply vessels in 1980 and 2013. The ratio between displacement and dead weight tonnage (DWT) seems to have increased to about 1.65 to 1.75, and the maximum ratio is as high as 2.4 (Moan et al., 2016). The use of DP controlled supply vessels have also increased, which may imply large velocities at impacts. According to risk assessment, Moan et al. (2016) suggested the design energy should be increased to 50 MJ for supply vessel bow collisions with offshore platforms. Parallel with the increase of the design energy, the design standards for ship collisions with offshore structures, notably tubular structures and plated structures, should be modified. In addition, the current standard force-displacement curves in the RP were developed in 1980s (DNV, 1981) and were based on a raked ship bow impact. The design curves are out-of-date for safety considerations today, and will be challenged by modern design of ship structures, like bulbous bows, X-bows, ice-strengthened vessels, etc.

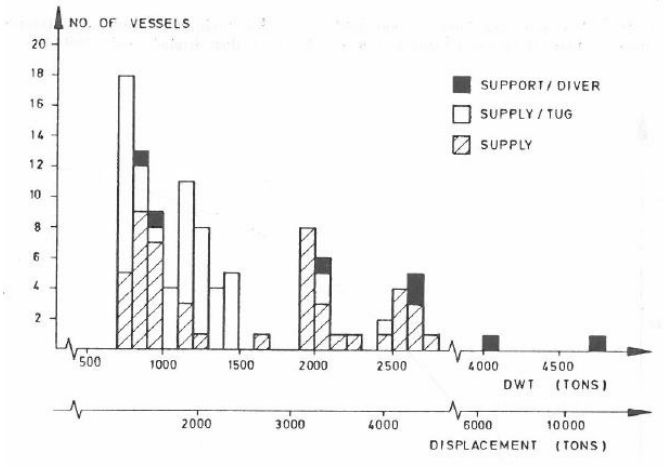

Figure 1-6. Supply vessels with DnV class, 1980 (DNV, 1981)

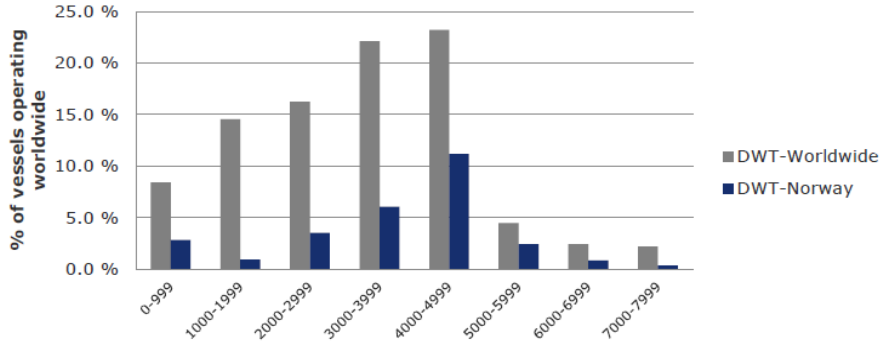

Figure 1-7. Overview of the DWT for 2013 (Moan et al., 2016)

1.2 Thesis Objectives and Scope

This work has been funded by the Research Council of Norway (NFR) through the Centers of Excellence funding scheme (Grant number 223254), at Centre for Autonomous Marine Operations and Systems (AMOS), Norwegian University of Science and Technology (NTNU). The funding is gratefully acknowledged.

The work is carried out under the scope of AMOS project 8 titled 'Consequences of accidental and abnormal events on ships and offshore structures'. The primary aim of AMOS project 8 is to obtain more profound knowledge of the fluid-structure interaction phenomena, improved methods for the simulation of accidental events with NLFEA, verified methods for fast assessment of damage and residual strength, applicable for direct design against accidental events and constituting a fundamental basis for development of decision support systems for emergency situations.

Under the scope of the project, the thesis has two main goals:

- To improve the accuracy of ship collision simulations by developing integrated methods coupling the external dynamics and internal mechanics, and to better understand the influence of hydrodynamic forces and ship motions on the prediction of structural damage in ship collisions.
- To gain deep insights into the deformation mechanics of two widely used structural components in ships and offshore structures, i.e. tubular members and stiffened panels, during ship collisions and by this provide recommendations for their design against accidental actions.

To accomplish it, the following research questions are addressed:

- Is there a way to carry out integrated ship collision analysis, which properly represents the hydrodynamic effects and 6DOF ship motions, but does not lose accuracy of the predicted structural response?
- The decoupled method simplifies the effect of hydrodynamic forces and neglects the interaction between ship motions and structural damage. What is the influence of these assumptions on the prediction accuracy?
- What are the assumptions and simplifications made in the external dynamic models for impact analysis? Under what circumstances will these assumptions become invalid?
- How do tubular members with different dimensions and properties respond in a ship collision event?
- How does ship-platform interaction influence the response of both structures?
- How should tubular members be designed to resist impact actions?
- How do stiffened panels respond under lateral impacts? What is the influence of boundary flexibilities on the structural response?

By addressing these issues, the structural responses in ship collisions can be evaluated with much better accuracy. Prediction accuracy of the decoupled method in different scenarios will be understood, and potential limitations of the method will be conveyed to the engineers. The structural response of tubular members and stiffened panels subjected to collisions should be better understood. The outcome may contribute to development of improved regulations for the design of crashworthy structures.

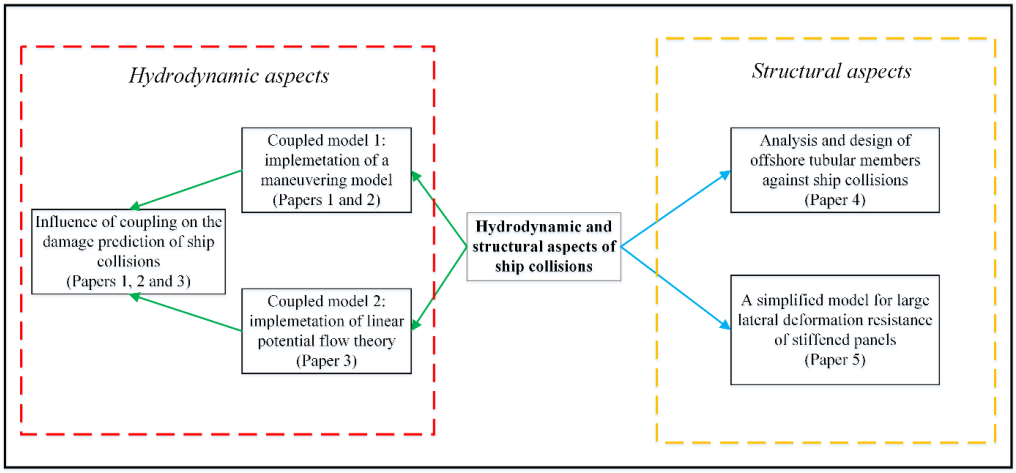

Figure 1-8. Scope of the thesis and the interconnection of appended paper

This thesis is written in the form of a collection of five journal papers provided in the appendices and a summary provided in Chapters 1-7. Figure 1-8 illustrates how the scope of the papers are interconnected. The five papers in the appendices are summarized as follows.

Paper 1: This paper proposes a new model, which efficiently couples the external dynamics

and internal mechanics in ship collision simulation. Collision forces are calculated using the explicit nonlinear finite element code LS-DYNA. Hydrodynamic forces in surge, sway and yaw are calculated using a traditional ship manoeuvring mode. The proposed 3DOF coupled method was applied to calculations of an offshore supply vessel colliding with a rigid plate and a submersible platform. The results were compared with those predicted by a decoupled method.

Paper 2: This paper extends the 3DOF coupled model in Paper 1 to consider full 6DOF ship motions. A traditional ship manoeuvring model is used for the in-plane surge, sway and yaw degrees of freedom, while the out-of-plane roll, pitch and heave motions are simplified as single degree of freedom mass-spring systems. The implementation is verified through free decay tests and SIMO simulation. Several collision and grounding cases are simulated in which a supply vessel crashes into rigid plates with different orientations. Effects of the roll motion, the heave and pitch motions and the full 6DOF motions are studied. Several consecutive impacts were identified in the simulation.

Paper 3: This paper describes the implementation of a model for calculation of hydrodynamic loads based on linear potential-flow theory into the nonlinear finite element code LS-DYNA, facilitating a fully coupled six degrees of freedom (6DOF) dynamic simulation of ship collision and grounding accidents. Potential-flow theory both with and without considering forward speed effect is implemented. With the proposed model, the transient effects of fluid, global ship motions, impact forces and structural damage can all be predicted with high accuracy. The proposed method is applied to calculations of an offshore supply vessel colliding with a rigid plate and with a submersible platform. The results are compared with the decoupled method and discussed with emphasis on the influence of different initial velocities. The influence of forward speed is found to be limited, and can be neglected in ship collisions.

Paper 4: This paper investigates responses of offshore tubular members subjected to vessel bow and stern impacts with the nonlinear finite element code LS-DYNA. The FE models of two 7500 tons displacement supply vessels of modern design have been used. Force-displacement curves for bow and stern indentation by rigid tubes are compared with design curves in the DNV-GL RP C204. Next, both the ship structure and tubular braces/legs are modelled using nonlinear shell finite elements, and the effect of ship-platform interaction on the damage distribution is investigated. A parametric study of denting mechanics with respect to the length, diameter and wall thickness of tubular members is described. An existing analytical denting model is extended to account for distributed loads and is verified against simulation results. Existing requirements to local denting resistance are discussed, and the concept ‘transition indentation ratio’ is introduced. New compactness requirements for the design of tubular members against impacts from ship bow, stern corner and stern end are proposed.

Paper 5: The paper presents a simplified formulation for the assessment of resistance to large inelastic deformation of stiffened panels subjected to lateral loading. The method is based on rigid plastic material assumptions and the use of yield functions formulated in terms of stress resultants. It takes into account the flexibility of panel ends with respect to the inward motion, while rotational boundary conditions are free or clamped. Concentrated and distributed loads

are considered as well as patch loading. Resistance-deformation curves predicted by the proposed method are compared with results using LS-DYNA, and good agreement is obtained for panels that are not dominated by shear failure or tripping and local buckling of stiffeners. The formulation provides a useful tool for quick estimates of panels subjected to abnormal or accidental static and transient transverse loads, such as explosion, slamming, hydrostatic pressure, and ice actions.

1.3 Thesis Organization

The summary section of this thesis consists of the following seven chapters:

Chapter 1 introduces the background, motivation, objectives and organization of this thesis.

Chapter 2 presents an overview of methodologies for the assessment of ship collisions. The coupled ship collision simulation models including hydrodynamic effects are reviewed. Four methods i.e. empirical methods, experimental methods, nonlinear finite element analysis (NLFEA) and simplified analytical methods, for structural response assessments are introduced and discussed. The impact response of an important structural component in offshore industry, i.e. tubular members, is also reviewed and discussed.

Chapter 3 introduces two new models for 6DOF coupled simulation of ship collisions. The theory and implementation procedures are described.

Chapter 4 discusses the influence of hydrodynamic forces and ship motions on the damage prediction of ship collision with respect to energy dissipation, ship trajectories, and structural damage. A secondary impact phenomenon is observed and discussed. A comparative study is carried out between the proposed coupled methods and the traditional decoupled method. The validity of the assumptions behind the external dynamic models are discussed by comparison with coupled simulation results.

Chapter 5 investigates the responses of offshore tubular members subjected to vessel bow and stern impacts with literature review, simplified analysis and the NLFEA simulation. The design resistance curves are checked by comparison with resistance curves from crushing of two modern designed 7500-ton displacement supply vessel bows and sterns. Next, both the ship structure and the tubular braces/legs are modelled using nonlinear shell finite elements, and the effect of ship-platform interaction on the damage distribution is investigated. A parametric study of the denting mechanics with respect to the length, diameter and wall thickness of the tubular members is described. An existing analytical denting model is extended to account for distributed loads and is verified against simulation results. Existing requirements to local denting resistance are discussed, and the concept ‘transition indentation ratio’ is introduced. New compactness requirements for the design of tubular members against impacts from ship bow, stern corner and stern end are proposed.

Chapter 6 proposes a simplified formulation for the assessment of large inelastic deformation

resistance of stiffened panels subjected to lateral loading, taking into account the flexibility of panel ends with respect to the inward motion. Concentrated and distributed loads are considered as well as patch loading. The proposed method is verified of good accuracy against numerical simulation using LS-DYNA. The effects of shear failure or tripping, local buckling of stiffeners, and inertia forces are also studied.

Chapter 7 concludes the thesis work and provides recommendations for future study.

Chapter 2

An overview of methodologies for the assessment of ship collisions

2.1 Introduction

Ship collisions are highly nonlinear and transient, coupled dynamic processes involving large structural deformations and motion in fluid. It is still challenging to capture the coupling between fluid and structures and to accurately assess structural responses in accidental collisions. A few review articles are available from the literature, which focus on the general procedures of risk analysis and structural assessment of ship collisions and groundings, e.g. Pedersen (2010), Ellinas and Valsgard (1985), Wang et al. (2002), etc.

For the past several decades, an important method has been to decouple the problem into two parts: the *external dynamics* and the *internal mechanics*, as suggested by Minorsky (1958); refer Figure 2-1. The *external dynamics* model simplifies the effect of fluid as constant added masses such that the whole collision system is undamped and the conservation of momentum principle applies. This allows for a fast estimation of the dissipated energy with reasonable accuracy. Pedersen and Zhang (1998) proposed a closed form theoretical model for the planar external dynamics problem. Stronge (2004) developed a solution for three dimensional (3D) impacts. Liu and Amdahl (2010) extended Stronge's work for 3D impact cases in a local coordinate system, allowing objects with 3D geometries and eccentricities such as icebergs to be considered. The problem of external dynamics in ship collisions has also been addressed in Brown (2002), Popov et al. (1969), Tabri (2012), etc.

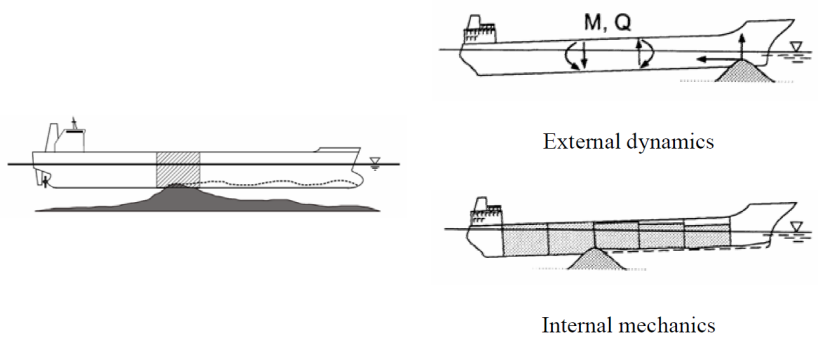

Figure 2-1. External dynamics and internal mechanics in ship grounding (Hong, 2009)

When velocities of the striking and struck ships before and after collision are known from the *external dynamic* calculations, the energy loss during the collision can be obtained. This energy loss is dissipated by structural deformations in the assessment of *internal mechanics*, where the struck ship is normally fixed in space, and the striking ship moves along a prescribed path. The final penetration is obtained when the area under the force-penetration curve equals the energy loss resulting from the *external dynamic* calculations. Both the *external dynamics* and *internal mechanics* are discussed in conjunction with hydrodynamic and structural aspects of ship collisions in this chapter.

2.2 Hydrodynamic consideration in ship collisions

In the assessment of ship collisions, the hydrodynamic effect is often considered secondary. The decoupled method simplifies the hydrodynamic effect as constant added masses, specified as 0.1 and 0.4 times the mass of the ship for bow and side collisions in NORSOK-N004 (2004). Determination of the hydrodynamic coefficients has been studied by Woisin (1988), Valsgard and Jorgensen (1983), Motora et al. (1971), Petersen and Pedersen (1981), Jia and Moan (2010), etc. Generally, the decoupled method is capable of providing fast and reasonable estimations of the dissipated energy and structural damage for most collision cases. However, the method has apparent weakness in several aspects. In certain cases, predicted results show large differences with respect to energy dissipation, motion trajectories, and structural damage.

In the first place, the representation of fluid as constant added masses is overly simplified. The problem of solving for hydrodynamic loads acting on ships during collision is often treated as a radiation problem; i.e. no incident waves and currents are considered. According to the linear potential flow theory, ship collision forces will excite motions of different frequencies. For each frequency, there exists a certain added mass and damping matrix with coupling terms among different DOFs, and it is difficult to select a representative constant added mass that is capable of covering the influence for all frequencies. In addition, as collision occurs when the two bodies are extremely close, fluid multibody interactions may become significant.

Motora et al. (1971) presented a theoretical solution for the equivalent added mass coefficients in ship collisions and conducted model experiments on a nuclear powered ship. Three equivalent added mass concepts were proposed, which gave exact values of acceleration, momentum and absorbed energy at the end of collisions, respectively.

$$M + m' = \frac{f(\mathrm{t})}{a(t)} \tag{2.1}$$

$$M + m'' = \frac{\int_0^t f(\tau) d\tau}{v(t)} \tag{2.2}$$

$$M + m''' = \frac{\int_0^t f(\tau) v(\tau) d\tau}{\frac{1}{2} v^2(t)} \tag{2.3}$$

where M is the ship mass, m', m'' and m''' are the equivalent added masses, and $a(t)$ and $v(t)$ are the acceleration and velocity of the vessel at the end of the collision, respectively. Typically, the equivalent added mass based on energy similarity is used.

Results showed that the equivalent added mass was not always a good approximation and it changed with collision resistances, duration of a collision and the definitions of equivalent added masses; refer Figure 2-2. If the duration is infinitely small, the equivalent added mass is equal to the added mass for infinite frequency. However, if the duration is finite, the equivalent added mass increases as the duration gets larger. Jia and Moan (2010) studied the equivalent added mass using a similar approach, and found that the added mass can also be related to the impact position and the flexibility of the hull girder.

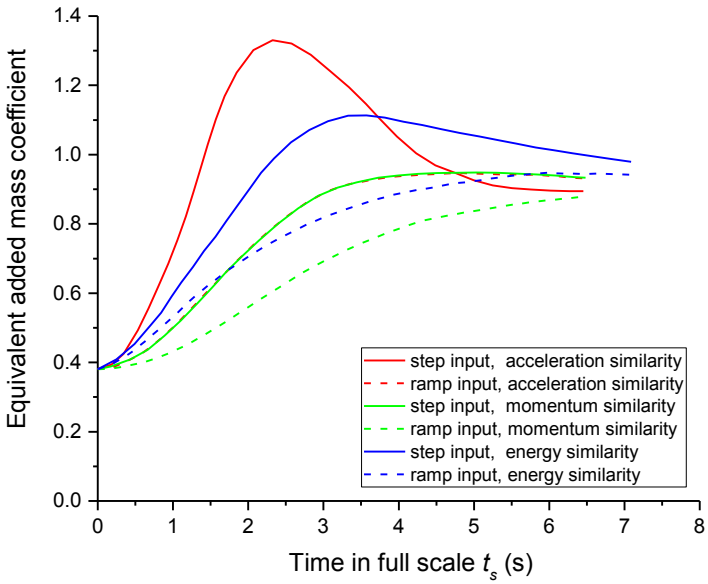

Figure 2-2. Equivalent added masses in sway based on the similarity of acceleration, momentum and absorbed energy, under step and ramp input forces (Motora et al., 1971)

Another consideration of the decoupled method is that ship motion path is prescribed in the assessment of *internal mechanics*, which implicitly assumes that the collision duration is short and the global ship motion are negligible during collisions. Tabri (2012) and Tabri and Broekhuijsen (2011) compared theoretical solutions with experimental data, and found that for

unsymmetrical collisions, especially with small collision angles, the decoupled approach failed to predict the correct penetration paths and the error was large.

For more accurate representation of the effect of fluid and global ship motions, a few researchers have turned to the coupled method, in which the *external dynamics* and the *internal mechanics* are solved simultaneously.

Petersen (1982) presented a coupled simulation procedure considering the planar surge, sway and yaw motions and the transient effects of hydrodynamic loads. The strip theory was used to calculate the hydrodynamic forces. Sectional added masses and damping were calculated using an approximate method utilizing the conformal mapping technique. The ships were treated as essentially stiff bodies with deformation taking place in a zone around the collision point. This deformation zone was simplified by four nonlinear springs; see Figure 2-3. The simulation agreed reasonably with Motora et al. (1971)'s experiments. Figure 2-4 shows transient plots from the ship-ship collision simulation.

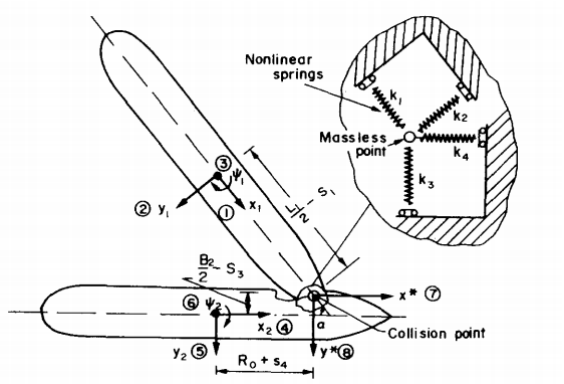

Figure 2-3. The collision model by Petersen (1982)

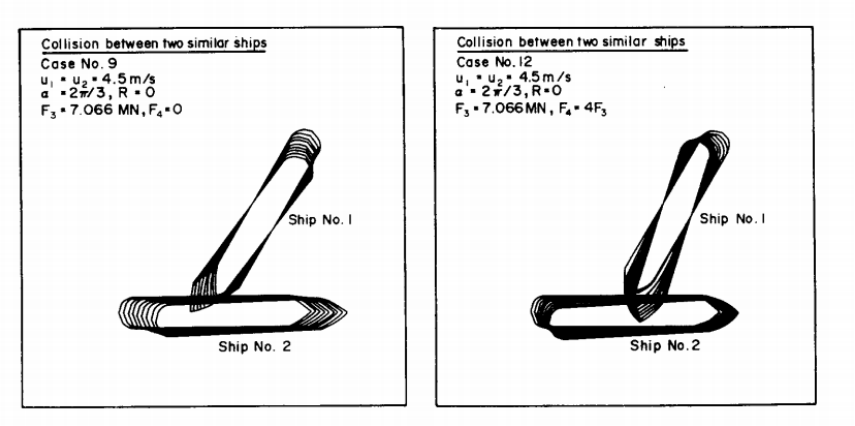

Figure 2-4. Transient plots of ship collisions (Petersen, 1982)

Samuelides and Frieze (1989) presented a procedure for analyzing the consequences of right-

angle ship collisions. It involved coupling of dynamic structural and transient hydrodynamic responses experienced during collision. Both material and geometrical nonlinearities were included in the structural analysis. The accuracy of the procedure was checked against Petersen (1982).

Brown (2002) developed a Simplified Collision (SIMCOL) Model coupling the internal and external mechanics for planar motions. SIMCOL is especially useful in the early design stage. Mitsubishi developed a program entitled MCOL to deal with rigid body dynamics. Le Sourne (2007) and Le Sourne et al. (2012) coupled the MCOL code with the super-element method (Ueda and Rashed, 1984) to tackle the internal and external mechanics simultaneously. The crushing force was determined using the super element method. Crushing resistance and moments were then transmitted to the MCOL program, which solved motion equations and returned new acceleration, velocity, and position of each ship.

Tabri et al. (2008) and Tabri (2010) presented a procedure for simulating nonsymmetrical ship collisions with arbitrary impact locations and collision angles. The model was based on the time integration of twelve equations of motion, six for each ship; see Figure 2-5. The hydrodynamic forces were calculated using linear potential flow theory. The ship stiffness was assumed to be homogeneous, and the contact force was evaluated by integrating the normal and tangential tractions over the contact surface between the colliding bodies. The results compared well with model tests.

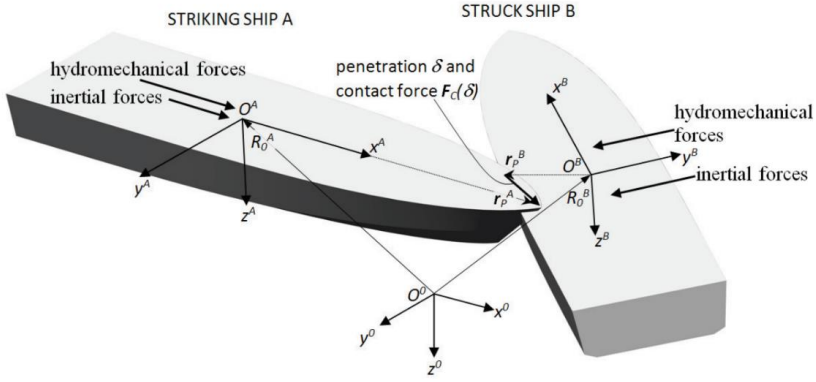

Figure 2-5. The forces acting on the ship in ship-ship impacts; (Tabri, 2010)

Figure 2-6 shows colliding ship trajectories from experiments, the decoupled method and the coupled method. For right angle collisions, the results are quite close. For skew collisions, ship trajectories predicted by the decoupled method deviate from experimental results, while the coupled simulation agrees reasonably well.

The coupled methods described above focus mainly on the hydrodynamic forces acting on the ship and ship motions, while the collision damage and forces are simplified. For example, Petersen (1982) represented the collision forces with four nonlinear springs. Tabri et al. (2010) assumed homogeneous ship stiffness and calculated collision forces by integrating the normal

and tangential tractions over the contact surface. The super-element method in Le Sourne et al. (2012)'s model is based on simplified analytical solutions of the resistance to deformation of the ship structure.

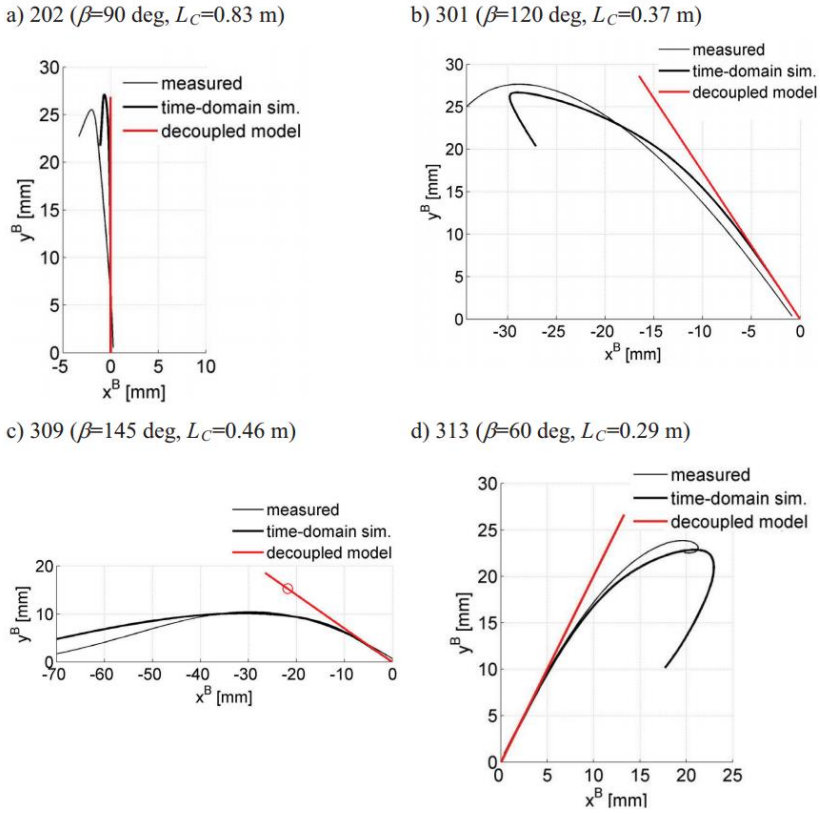

Figure 2-6. Ship trajectories in collisions from the experiments, decoupled model and the coupled model; (Tabri, 2010)

A different way of coupling the *external dynamics* and *internal mechanics* is to ensure that the collision resistances are calculated using the nonlinear finite element method (NLFEM) while the effect of fluid is simplified. Pill and Tabri (2011) used the planar joint technique in LS-DYNA to give constant added masses for motions in the horizontal plane; refer Figure 2-7. The buoyancy, restoring and radiation forces were excluded from the model. Such methods are superior in predicting the collision forces and structural damage as LS-DYNA is directly used to calculate the internal mechanics with a detailed shell finite element model of the structures. Yet, transient effects of hydrodynamic forces are not captured correctly.

Fully coupled dynamic simulation of ship collisions is made possible by the use of the Arbitrary Lagrangian Eulerian (ALE) methods provided in nonlinear finite element codes. Traditional Lagrangian meshes are used to model the structures. In the fluid domain, Eulerian meshes are adopted to avoid possible large mesh distortions. Within each time step, the fluid and structure domains are calculated simultaneously, and the forces and boundary conditions are transferred

between the two domains. Lee et al. (2013), Lee et al. (2012b), Lee and Zhao (2013), Gagnon and Wang (2012) and Song et al. (2016) carried out a series of ship-ship and ship-ice collisions using the ALE the technique. Figure 2-8 shows a comparison between a ship-ice collision experiment and the ALE simulation (Song et al., 2016). The acceleration of the floater wall caused by the ice impact and the relative velocity between the ice and the floater agreed reasonably well. However, the ALE method requires considerable modelling efforts and large computational capacity. Its application is therefore usually limited to small fluid domain problems like slamming impact and in-tank sloshing impact in the fluid cargo tank, see e.g. Wang and Guedes Soares (2012).

Although there are a few coupled ship collision simulation models described in the literature, the decoupled method, which may fail in certain scenarios, is still the most widely used method in academia and industry. It is challenging to couple the internal mechanics and external dynamics efficiently and accurately for general-purpose use. The major obstacle for coupling the *external dynamics* and the *internal mechanics* is that in most numerical codes used for structural analysis, the effect of surrounding water is difficult to be included. Therefore, one main objective of this thesis is to develop a coupled model, which can be used for more accurate ship collision simulations.

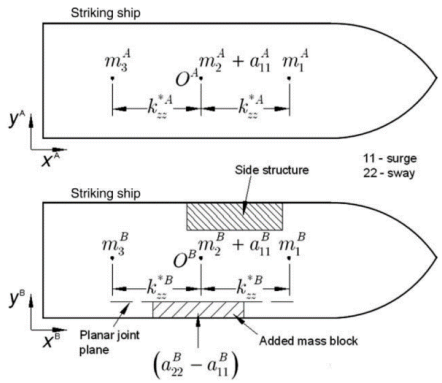

Figure 2-7. Planar joints used in coupled ship collisions (Pill and Tabri, 2011)

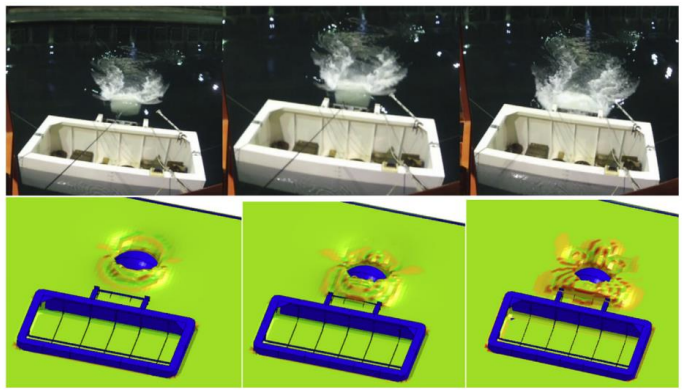

Figure 2-8. Experimental and numerical simulation of ice-stiffened panel collisions (Song et al., 2016).

The behaviors of ships with liquid cargos can be very different with that of 'dry' ships due to in-tank sloshing. Zhang and Suzuki (2007) adopted three different numerical simulation methods, i.e. ALE method, Lagrangian finite element method (FEM) and linear sloshing model to model fluid–structure interaction in liquid-filled cargo tank. The in-tank sloshing was found to have a significant influence on the motion and structural response of the struck cargo tank. Tabri et al. (2009a) and Tabri et al. (2009b) proposed a simplified mechanical model, in which the sloshing water was replaced with a number of oscillating masses; the method predicted reasonable results with the full scale ship collision experiments by TNO (Wevers et al., 1999) and model tests; refer Figure 2-9. For liquid-fill tanks, part of the total kinetic energy was stored by sloshing such that the energy absorption in structures and the damage in the struck vessel were reduced. More research regarding the effect of in-tanking sloshing in ship collisions can be found in Rudan et al. (2010), Tabri et al. (2009b), Lee et al. (2010), Lee et al. (2012a), etc.

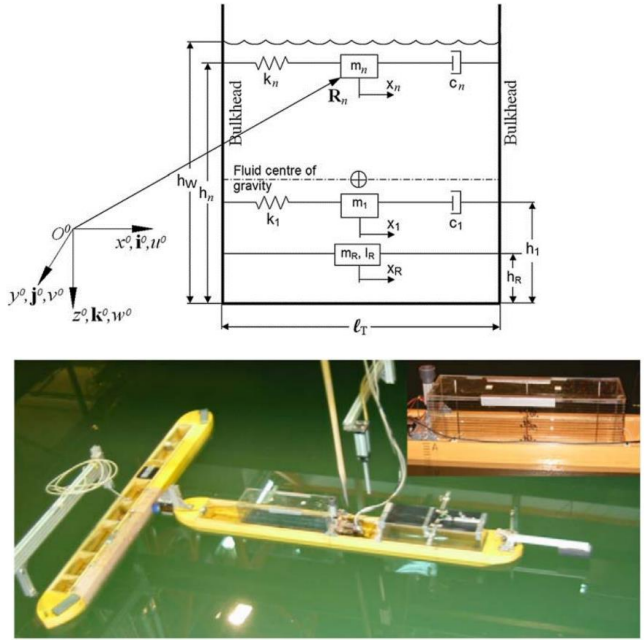

Figure 2-9. Top: a simplified model for sloshing modelling; Bottom: experimental study of in-tank sloshing in ship collisions; from Tabri et al. (2009b)

2.3 Structural response assessment in ship collisions

The assessment of structural damage and deformation resistance is of major concern for researchers and designers. Methods for assessing structural responses in ship collisions can generally be classified into the four categories:

- Statistical or empirical methods
- Experiments
- Nonlinear finite element analysis (NLFEA)
- Simplified analytical methods

Minorsky (1958) conducted pioneering work of the statistical or empirical methods, and he related the absorbed energy of damaged ships to the volume of the damaged material based on investigations of 26 full scale ship collisions reported by U.S. Coastal Guard in Figure 2-10. The simple regression fits the individual data amazingly well in the region of high energy impacts, while there is significant scatter in the low energy region. Considering the simplicity and reasonable accuracy in general, the method is very appealing to ship designers.

However, the method has inherent weaknesses, which limits its application. One thing is the data used for obtaining the curve is from conventional ships. As the design of ship structures changes over time, it is always questionable whether the expression can be transferred to newly designed ships. To overcome the weaknesses and improve the accuracy, Minorsky's method has been modified by a few researchers. Woisin (1979) related the energy absoprtion to the damage of striking and struck ship considering the height of the rupture aperture in the side shell and the side shell thickness. Pedersen and Zhang (2000) derived a new Minorsky expression reflecting differences in structural arrangement, material properties and damage patterns.

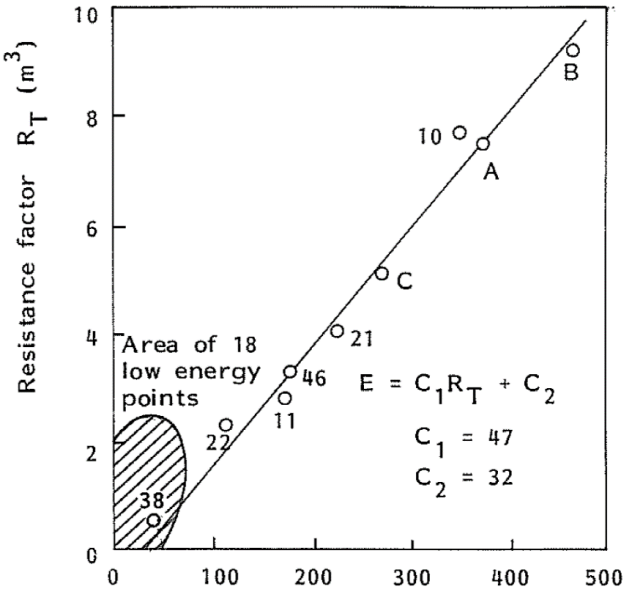

Figure 2-10. Correlation between the absorbed energy and damaged volume of ships; (Minorsky, 1958)

Experimental methods, including full-scale tests and model-scale tests, are considered to be the most straight-forward and accurate methods for structural response assessment. Full scale ship collision experiments provide invaluable data, but are seldom carried out because of the large expenses involved. ASIS (Association for Structural Improvement of Shipbuilding Industry) in Japan launched a seven year project on "Protection of Oil Spills from Crude Oil Tankers" jointly with TNO. In this project, large scale collision (Carlebur, 1995) and grounding (Vredeveldt and Wevers, 1993) experiments were conducted. Wevers et al. (1999) presented results of full-scale collision experiments with two inland vessels to provide further understanding of the deformation mechanisms of ship structures during collision and to validate the methodology of the numerical simulation (see Figure 2-11).

Model scale experiments carried on structural components at reasonable costs, often provide surpreisingly good results. Amdahl (1983) carried out crushing tests of six ship bow models and used the results to verify simplified models for the assesment of the crushing resistance. Ship bow crushing tests have also been carried out by Endo et al. (2002), Yamada and Endo (2008), Calle et al. (2017b) etc. Model scale experiments on the impact resistance, buckling and fracture behavior of ship side/bottom, and stiffened panels were carried out by Alsos and Amdahl (2009), Amdahl and Kavlie (1992), Karlsson et al. (2009), Ohtsubo et al. (1994b), Villavicencio et al. (2014), ect.

Figure 2-11. Full scale ship collision experiments in the Netherlands (Wevers et al., 1999)

Nonlinear finite element methods (NLFEM) are now considered the most powerful tools for simulation of ship collision and grounding. NLFEM simulation resistance and damage are often predicted with high accuracy, and thus often regarded as 'virtual experiments'. A few commercial packages are available, such as LS-DYNA, ABAQUS and MSC/DYTRAN. Special-purpose softwares dedicated for analysis of ship collisions were also developed, e.g. USFOS (Soreide et al., 1999) and SACS. Lehmann and Peschmann (2002) used results of large-scale collision experiment to validate numerical calculations. The simulation was performed of a double–skin structure with austenitic inside wall subject to lateral impacts. Yu and Amdahl (2016a) simulated a ship bulb penetrating a ship side structure using LS-DYNA in a benchmark study based on experiments conducted by Karlsson et al. (2009). The test set-up, numerical models and the crushing resistance are given in Figure 2-12. The resistance agrees quite well with test results, especially in the initial stage, where the outer plate is not ruptured. When fracture occurs, the accuracy degenerates, but it is still acceptable. More numerical simulation on the structural responses in ship collisions and groundings can be found in Kitamura (2002), Yu et al. (2013), Ehlers et al. (2012), Storheim and Amdahl (2014), Valsgard and Jorgensen (1983), Hu et al. (2011), etc.

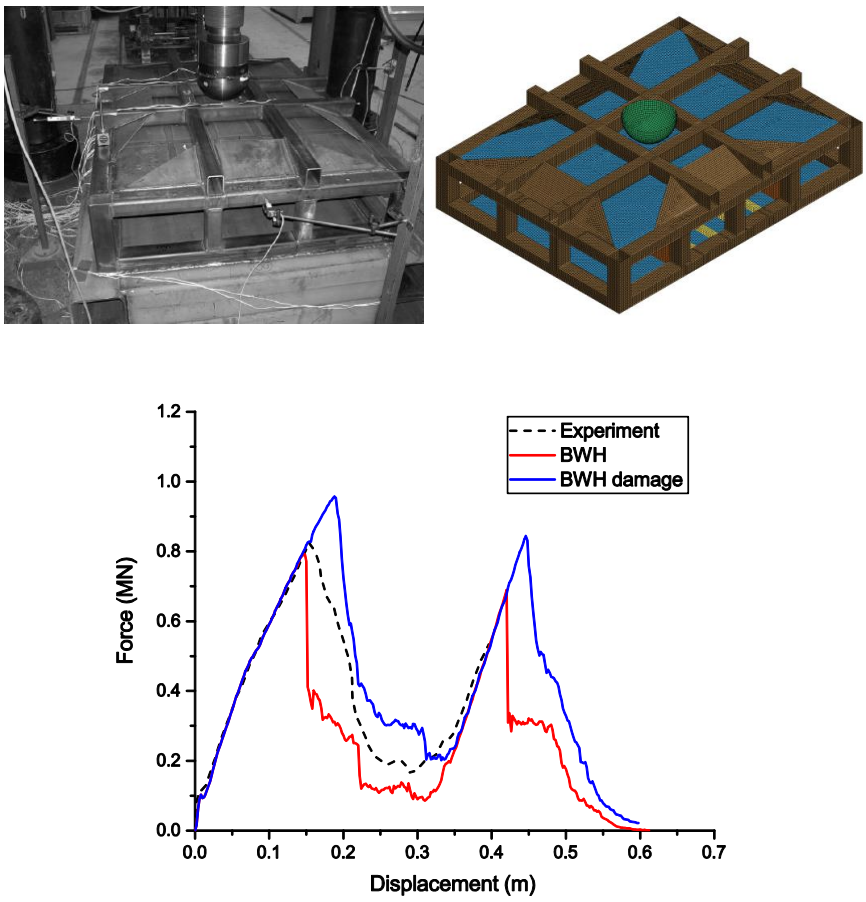

Figure 2-12. Crushing resistance of a ship side structure, from Karlsson et al. (2009) and Yu and Amdahl (2016a)

Although nonlinear finite element methods are powerful and have been used to solve numerous engineering problems, there are still challenges that should be addressed properly in order to obtain sound simulation results. Numerical setup (e.g. mesh generation, hourglass control, element selection, boundary conditions, etc) is a basic operation before carrying out numerical simulation but may influence the results singnificantly. As the NLFEA softwares require users to build finite element models and provide control parameters, one can easily get different results by adjusting parameters. For example, one common mistake is inapproriate control of the hourglass energy (Hallquist, 2006), implying that structural deformation may be dominated by spurious deformation modes. Determination of numerical parameters require good understanding of the studied problems, expertise of softwares, and sound engineering judgement. General recommendations for settings in nonlinear finite element analysis of ship collision and grounding problems, are suggested in Storheim (2016), Maker and Zhu (2000), Bala and Day (2012), Sajdak and Brown (2005), etc.

A big challenge of NLFEA is the calibration of material properties and modelling of fracture

initiation and propogation. When assessing the structural responses using NLFEA, the analyst needs to describe the complete material behavior up to fracture. This includes the stress-strain relationship considering hardening, strain rate effects, and strain and stress state dependent fracture. The representation of material behavior may also be influenced by the statistical uncertainties of material properties. Hogström and Ringsberg (2012) studied the uncertainties of input material parameters on the shape and size of the damage on the struck ship. They showed that the scattering of material properties and choice of fracture criterion would lead to large differences on the outcome of the analysis. Storheim and Amdahl (2017) showed that the material properties of shipbuilding steel and the work hardening model adopted for NLFEA had a large effect on the predicted resistance and energy dissipation during collisions.

What is more challenging is the modelling of fracture initiation and propogation. As ship structures are generally large and thin-walled, shell elements with large sizes rather than solid elements are preferable. However, fracture is a very local phenomenon, and it is very difficult to accurately capture fracture initiation with large shell elements. Walters and Voormeeren (2014) showed that the assumption of plane stress in shell elements is violated as soon as necking begins, causing different stress triaxialities and Lode parameters; the through-thickness behavior becomes important and shoud be accounted for. Fracture propogation is also difficult to capture. The simplest approach is to remove the elements once the critical value of a fracture criteria is reached. However, deleting elements disregards the fact that large stresses can be maintained parallel to the cracks. An improved modelling is to introduce double set of nodes such that the elements are allowed to separate once the critical stress is attained. A drawback with double set of nodes is that the potential location of cracks needs to be defined prior to analysis (Moan et al., 2016). A few models are available for fracture modelling with coarsely meshed shell elements, e.g. the constant critical strain method, Rice-Tracey-Cockroft- Latham (RTCL) fracture criterion by Tørnqvist (2003), Bressam-Willams-Hill (BWH) fracture criterion by Alsos et al. (2008), BWH damage criterion by Storheim et al. (2015a), T-failure criterion by Servis and Samuelides (2006), etc. Different fracture criteria were reviewed and compared with experimental results in review analysis and benchmark studies, such as Storheim et al. (2015b), Calle and Alves (2015), Marinatos and Samuelides (2015), Ehlers et al. (2008), Calle et al. (2017a), etc. Storheim et al. (2015b) and Calle et al. (2017a) showed that the RTCL and BWH fracture models agreed the best with experimental results, but there is still significant room for improvement.

Simplified analytical methods are widely used for quick assessment of the resistance to inelastic deformation, and in the design of crashworthy structrues. Such methods can provide significant insights into the governing deformation processes. They are mathematically tractable, and the predicted results often show surprisingly good agreement with experiments. Various design standards contain simple resistance expressions, e.g. DNV-RP-C204 (2010) and NORSOK N004 (DNV, 2004).

Originating from the upper bound theory, simplified methods require construction of a kinematically admissible displacement field, which is usually based on observation of actual accidents, model tests and numerical simulations. The mechanism should satisfy basic

assumptions in conjunction with the continuity conditions (Wierzbicki and Abramowicz, 1983). An example displacement field for a ship outer plate torn open by a rock is shown in Figure 2-13. The lowest force can be found by equating the internal and external energy dissipation rates.

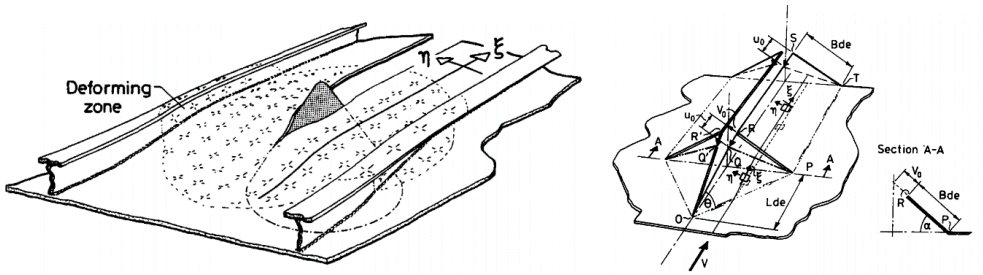

Figure 2-13. Displacement field for a ship outer bottom plate torn open by a rock; from Simonsen (1997)

Alexander (1960) is regarded as a pioneer in the application of plastic methods for analysis of thin-walled structures. Over the years, simplified methods have been used extensively and successfully for structural response analysis of impact and blast actions. Amdahl (1983) derived simplified formulas for the crushing resistance of ship bows by dividing the structure into L, T and X type intersections and summing up. The predicted resistance curves compared reasonably with experimental results. Wierzbicki and Suh (1988) derived simplified equations for the indentation resistance of tubes under combined loading, and the expressions were conveniently used in the design of braces and legs in offshore platforms. Jones (2011) described the upper bound and low bound theorems and presented useful analytical models for the impact responses of beams, plates and shells. Both static and dynamic responses were addressed. The effects of transverse shear and rotatory inertia were discussed. Hong and Amdahl (2013) presented a simplified model for the resistance of a double bottom grounding over a shoal-type rock including crushing of longitudinal girders (Hong and Amdahl, 2008), transverse frames and bottom plates. More simplified methods for the deformation of ship structural components in collisions and groundings can be found in the literature, such as Wierzbicki and Abramowicz (1983) for the crushing of cruciforms, Wang et al. (2000) for the stranding of a double hull, Yu et al. (2015) for the shoal grounding resistance of web girders, Liu et al. (2015b) and Liu et al. (2015a) for crushing resistance of a tanker side, Jones and Shen (1992) for the lateral impact resistance of tubular members, Sun et al. (2015) for the raked bow collision resistance of a ship side, etc.

It should be noted that simplified methods are based on construction of idealized deformation mechanisms. Analysts should be careful to check if these deformations modes are valid for the scenario considered. For example, structural deformation during ship grounding depends significantly on the shape of the rock, and a different rock type may lead to completely different deformation mechanisms. Alsos and Amdahl (2007) defined three types of seabed indenters, namely, ‘rock’, ‘reef’ and ‘shoal’. The accuracy of simplified methods varies; For the purpose of verifying simplified methods, numerical simulation using NLFEA may be preferable, which is efficient and accurate.

2.4 Review of responses of tubular members subjected to lateral impacts

During ship collisions with offshore jacket and jack up platforms, considerable energy will be dissipated through plastic deformation of both the ship and the platform. Often, braces/legs in direct contact with the ship will deform significantly and absorb great energy. The impact response of a single tubular member is complicated, and involves deformation modes in the form of local denting, global bending and membrane deformation, and different deformation modes may overlap. The response behaviors can be influenced by the axial loading, boundary conditions, impact locations, initial inclination angle of tubes, etc.

A series of experiments on the impact responses of tubular members were carried out by Amdahl (1983), Cerik et al. (2016), Cho et al. (2010), Jones et al. (1992), Jones et al. (1992), Sherman (1976), Taby et al. (1981), Zeinoddini et al. (2002) etc. Three deformation models were identified, i.e. local denting of tubular cross sections, global bending of tubes, and membrane stretching. Based on experimental findings, simplified methods were proposed and verified against experimental results.

2.4.1 Local indentation resistance of tubular braces and legs

Many researchers have studied the indentation resistance of tubular members subjected to lateral impacts. They proposed different models for the deformed tubular cross section during indentation, and the commonly used several kinds are shown in Figure 2-14. The model in Figure 2-14(a) is the simplest one and is most widely used by reserchers, such as Furnes and Amdahl (1980), Amdahl (1980), Ellinas and Walker (1983) and Taby and Moan (1988). The model in Figure 2-14(b) was proposed by Wierzbicki and Suh (1988) and used in Buldgen et al. (2014). Figure 2-14 (c) and (d) was proposed by Jones and Shen (1992) for local indentation and combined local denting and global denting. Figure 2-14(d) was used to post process the experimental and numerical data and to separate the local and global deformations, such as, Travanca and Hao (2014), Cerik et al. (2016), etc. Different equations for the denting resistance of tubes have been proposed, ranging from empirical, semi-emprical to completely closed-form solutions.

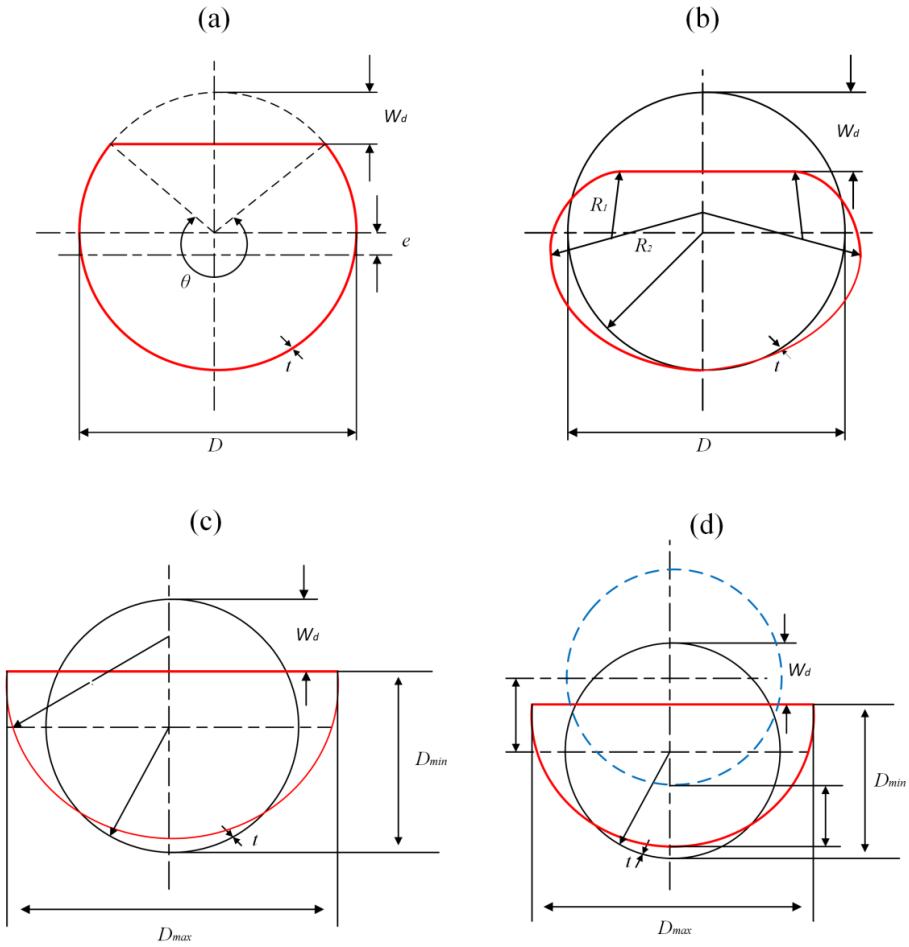

Figure 2-14. Idealized damage to the tube cross sections during local denting

Furnes and Amdahl (1980) defined the following relationship between the indenting force R and the depth of penetration w_d :

$$R = 15 \cdot \frac{1}{4} \sigma_y t^2 \sqrt{\left(\frac{D}{t}\right)\left(\frac{2w_d}{D}\right)} \tag{2.4}$$

Where σ_y is the material yield stress, t is the tube thickness and D is the diameter.

Amdahl (1980) and Skallerud and Amdahl (2002) proposed a local denting model based on plastic yield line analysis, relating the denting resistance to local indentation. The contact width effect was included by fitting with experimental data. This model uses a flat indenter to represent the ship end or side, and the tube is dented with a flattened top section. The model is adopted in NORSOK N-004, and the denting resistance takes the following form:

$$R/R_c = \left(22+1.2\frac{B}{D}\right)\left(\frac{w_d}{D}\right)^{\frac{1.925}{3.5+\frac{B}{D}}} \cdot \sqrt{\frac{4}{3}\left(1-\frac{1}{4}\left[1-\frac{N}{N_p}\right]^3\right)} \tag{2.5}$$

where B is the contact width of the indenter. The last term was borrowed from Wierzbicki and Suh (1988) to account for the effects of axial force in the leg. R_c is a characteristic resistance of the tube defined as:

$$R_c = \sigma_y \frac{t^2}{4}\sqrt{\frac{D}{t}} \tag{2.6}$$

Ellinas and Walker (1983) investigated both local denting and global bending deformation of tubular members. Local deformation was assumed to cease once global bending started. The expression for denting resistance of tubes is empirical and is given by:

$$R = K \cdot \frac{1}{4}\sigma_y t^2 \cdot \left(\frac{w_d}{D}\right)^{\frac{1}{2}} \tag{2.7}$$

K is a constant coefficient representing the shape of the indenter. It is normally assumed as 150 according to experimental observations for concentrated loads.

Wierzbicki and Suh (1988) made the first attempt to derive a closed form solution of the indentation resistance of tubes under combined loading. The problem was decoupled into bending and stretching of a series of unconnected rings and generators. The deformed tube sectional shape in Figure 2-14(b) was used. The indentation resistance is given as:

$$R = 16\sqrt{\frac{2\pi}{3}\frac{D}{t}\frac{w_d}{D}} \cdot \frac{1}{4}\sigma_y t^2 \sqrt{\left(1-\frac{1}{4}\left[1-\frac{N}{N_p}\right]^3\right)} \tag{2.8}$$

A big advantage of this expression is that it is theoretically derived and preserves the appealing form of simplicity for design. According to this formula, the resistance to local denting depends only on the tube thickness and the material yield stress, but not on the tube diameter.

Cho (1990) proposed an empirical equation for the denting resistance considering the contact width:

$$\frac{R}{m_0} = 2.0\left(\frac{D}{t}\right)^{0.2}\left(\frac{E}{\sigma_y}\right)^{0.5}\left(\frac{w_d}{D}\right)^{0.45} \exp\left\{0.1(B/D)\left(\frac{w_d}{D}\right)^{-0.3}\right\} \tag{2.9}$$

where $m_0 = \frac{1}{4}\sigma_y t^2$.

Buldgen et al. (2014) and Jones and Shen (1992) presented analytical solutions for the complete behavior of tubular members including local denting, global bending and membrane stretching. For local denting, Buldgen et al. (2014) extended Wierzbicki and Suh (1988)'s model to consider different orientations and positions of the struck tube, and the shape of the striking ship stem. Jones and Shen (1992)'s denting model requires numerical iterations to obtain resistance

curves. The expressions are complicated and are thus omitted here.

The above equations for the indentation resistance of tubes were all verified to some extent by comparison with experimental results or numerical simulation. The NORSOK model is widely used as it covers the contact width effect. Reasonable accuracy is found in general by Amdahl et al. (2012), Travanca and Hao (2014) and Watan (2011) etc. However, they also found that this model tends to underestimate the indentation resistance in the initial stage and also for cases with large contact widths.

2.4.2 Residual bending capacity of dented tubes

A tube with clamped ends will deform into a three-hinge mechanism when the impact load located at midspan exceeds the plastic bending collapse load $R_0 = 8M_p / L$. However, the maximum cross section bending capacity will often not be reached at beam ends and in the contact region. At the ends, the lower half of the cross section experiences significant compression that may induce local buckling, while the upper half is subjected to large stretching that may cause fracture. This was observed in experiments by Amdahl (1980) as shown in Figure 2-15. In addition, the shear effect may become important for short beams and reduce the maximum bending capacity at beam ends, see e.g. Jones (2011). In the contact region, local indentation of the tube cross section brings about a reduction in the plastic section modulus and produces an eccentricity of the plastic neutral axis. The combined effect will induce a significant loss in load carrying capacity. Considering the deterioration effects at the supports and the contact region, the maximum lateral load for a dented tube with clamped supports can be expressed as:

$$R_0 = \frac{4M_p}{L}\left(\gamma_1 + \gamma_2\right) \tag{2.10}$$

where, γ_1, γ_2 are the effective bending capacity coefficients of tube cross sections at the supports and the dented region, respectively, as suggested in Foss and Edvardsen (1982). $\gamma_2 = M_{res} / M_p$, and M_{res} is the residual bending capacity of a dented cross section.

A few models are available from literature for the bending moment reduction of a dented cross section. The NORSOK standard (DNV, 2004) assumes conservatively that the flat part of a dented cross section is non-effective, and this yields:

$$\begin{aligned} &\frac{M_{res}}{M_p} = \cos\frac{\theta}{2} - \frac{1}{2}\sin\theta \\ &\theta = \arccos\left(1 - 2\frac{w_d}{D}\right) \end{aligned} \tag{2.11}$$

Ellinas and Walker (1983) considered bending equilibrium of the undamaged cross sections and obtained:

$$\frac{M_{res}}{M_p} = \cos\beta - \beta$$
$$\beta = \sqrt{\frac{w_d}{D}} \cdot \left(1 - \frac{D}{t}\left(\sqrt{\frac{16}{9}\left(\frac{w_d}{D}\right)^2 + \left(\frac{t}{D}\right)^2} - \frac{4}{3}\frac{w_d}{D}\right)\right) \tag{2.12}$$

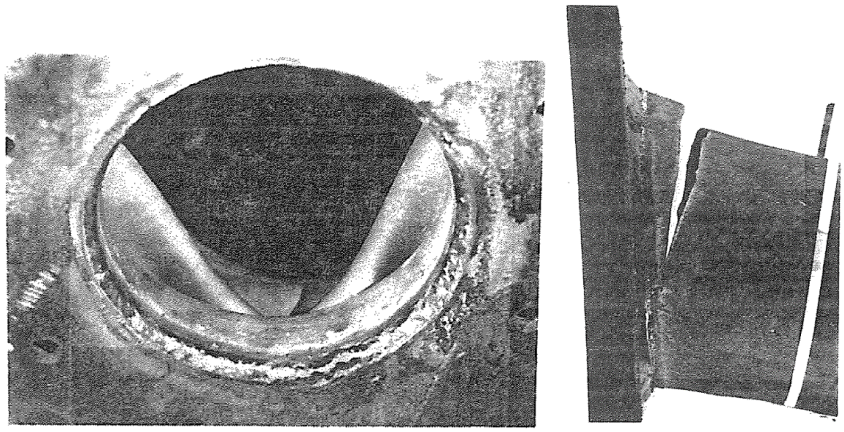

Figure 2-15. Local crippling and fracture of a tube cross section at the supports, from Amdahl (1983)

Cho et al. (2010) proposed an empirical equation by regression analysis of the results from a series of bending tests of dented tubes:

$$\frac{M_{res}}{M_p} = \exp\left[-0.04\left\{\left(\frac{w_d}{D}\right)^{0.7} \cdot D/t\right\} + \left(\frac{B}{D}\right)^{0.1}\right] \tag{2.13}$$

Buldgen et al. (2014) considered the relative positions of the striking ship and the dented tube cross section. For a right angle ship collision on a horizontal tube, the expression becomes:

$$\frac{M_{res}}{M_p} = \frac{1}{2}\left(\left(\frac{w_d}{D}\right)^2 - 1\right)\left(\frac{w_d}{D} - 2\right) \tag{2.14}$$

Jones and Shen (1992) proposed an equation for the development of bending moment with increasing local indentation as:

$$\frac{w_d}{D} = \frac{1}{2} + \frac{\pi\left[\cos\phi - \cos\left\{\left(\phi + \sin\phi\right)/2\right\}\right]}{2(\phi + \sin\phi)}$$
$$\frac{M_{res}}{M_p} = \frac{\pi^2}{2(\phi + \sin\phi)^2} f\left(\phi\right) \tag{2.15}$$
$$f\left(\phi\right) = 2\sin\left(\frac{\phi + \sin\phi}{2}\right) - \sin\phi\left(1 + \cos\phi\right)$$

The above models for the bending moment reduction due to local denting are compared in Figure 2-16. The *D/t* ratio of the tube is set to 30 for the *D/t* dependent models by Ellinas and Walker (1983) and Cho et al. (2010). The various models predict widely different residual

strength. The models by NORSOK standard (DNV, 2004) and Ellinas and Walker (1983) represent a lower bound while the models by Buldgen et al. (2014) and Jones and Shen (1992) give upper bound of the value. The model by Cho et al. (2010) looks promising, which is based on regression analysis of bending test results and predicts an in-between residual bending moment. This model showed reasonable accuracy when it is compared with tests results by Ueda and Rashed (1985) and Paik and Shin (1989).

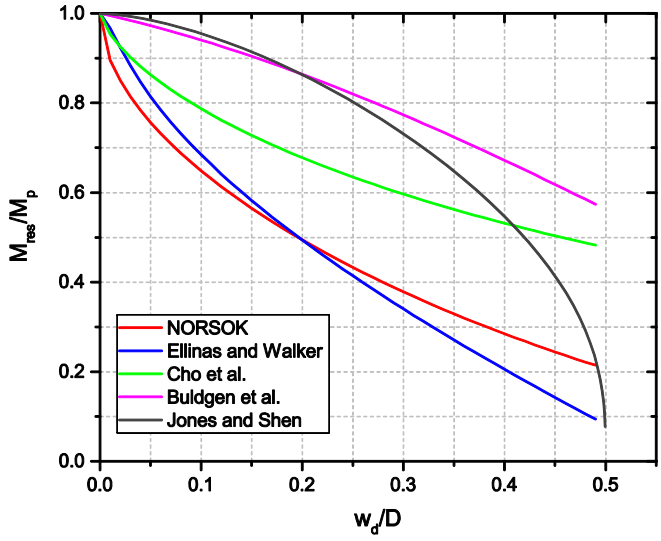

Figure 2-16. Bending moment reduction of a dented tube cross section

2.4.3 Bending and membrane stretching of tubes

Tubes will start global bending and deflect laterally when a certain indentation is reached. In the case of axially restrained boundaries, the membrane force will increase with increasing lateral deflections and later becomes dominant up to the point of fracture. The development of membrane forces depends on the capacity againt the pull-in provided by adjacent members and joints.

Based on rigid-plastic analysis, Soares and Søreide (1983) presented an analytical model for the resistance of laterally loaded tubular members. Local indentation is assumed small and negligible. The interaction between bending moment and axial force is considered. The following expression is obtained:

$$\frac{R}{R_0}=\begin{cases}\sqrt{\left(1-\left(\frac{w_d}{D}\right)^2\right)}+\frac{w_d}{D}\arcsin\left(\frac{w_d}{D}\right); & \frac{w_d}{D}\le 1\\ \frac{\pi}{2}\frac{w_d}{D} & ; \quad \frac{w_d}{D}>1\end{cases} \tag{2.16}$$

This model is good when the denting is small, but deteriorates with increasing local indentations. Based on Sherman (1976)'s experimental results, they suggested that the model applied well for tubular members with D/t of 35 or less and L/D up to 22. Such tubes are compact and can maintain full bending capacity.

De Oliveria (1981) presented a beam deformation model of tubes considering axial and rotational flexibilities at the supports. The interaction between bending moment and membrane forces was accounted for, but the effect of local indentation was neglected. Results showed that the axial stiffness at the supports was very important for the development of membrane forces.

Ellinas and Walker (1983) proposed a tube deformation model considering the denting and bending effects. It was assumed that local denting ceased immediately when the tube started global bending. The ultimate lateral load was reached when the tube started global bending and the force was assumed constant afterwards by neglecting any development of membrane forces.

Jones and Shen (1992) presented a theoretical rigid-plastic formulation for the tube deformation including local denting, global bending and membrane stretching. A big advantage of this model is that it allows local denting deformations to continue in the global deformation phase, which has been considered only semi-empirically in previous work. Good agreement was obtained for the maximum permanent transverse displacements measured in the experiments by Jones et al. (1992). Jones et al. (1992) reported a series of static and dynamic impact results with various tube dimensions and found that regardless of bending or local denting, the dimensionless dissipated strain energy was almost linearly dependent on the maximum permanent transverse displacement. Similar findings were reported by Travanca and Hao (2014) through extensive numerical simulations.

Buldgen et al. (2014) presented an analytical solution for the crushing resistance of an oblique clamped tube impacted by the stem of a striking ship. Different orientations and relative positions of the struck tube, and the shape of the striking ship stem were considered.

Chapter 3

6DOF coupled dynamic simulation of ship collisions

3.1 Introduction

Ship collisions and groundings are highly nonlinear and transient, coupled dynamic processes involving large structural deformation and motion in fluid. It has long been difficult to include all effects in one simulation. *Section 2.2* contained a review of the coupled ship collision simulation models considering the hydrodynamic effects. The literature review showed that it is still difficult today to evaluate simultaneously the *internal mechanics* and the *external dynamics* in one simulation. The major obstacle is that the effect of surrounding water cannot be included efficiently in most of the numerical codes used for structural analysis. By taking advantage of the user defined load (LOADUD) and the user common (USERCOMM) subroutine in LS-DYNA, two new coupled methods, have been developed. They couple the external dynamics and internal mechanics and enable a full 6DOF simulation of ship collisions and groundings. The content of this chapter was presented as part of **Papers 1-3** (Yu et al., 2016a, Yu and Amdahl, 2016b, Yu et al., 2016b).

To determine the hydrodynamic forces acting on a ship during collisions, it is necessary to solve a radiation problem, meaning that no incident waves and currents are considered. The major components of hydrodynamic loads in a ship collision include frequency dependent added masses and damping forces known as radiation forces, and restoring forces. The forward speed effect, which acts like a current in the direction opposite to the ship motion may become important in high speed collisions. The hydrodynamic interaction between the colliding bodies may also become significant as the colliding bodies are extremely close during collisions.

3.2 The user defined load and user common subroutine in LS-DYNA

The user-defined load subroutine (LOADUD) in LS-DYNA has rarely been used by industry and academia. As far as the author knows, there are only few related papers with very limited application. Adoum and Lapoujade (2003) presented a few basic examples demonstrating the application of LOADUD. The user-defined load subroutine in LS-DYNA provides information on nodal displacements, velocities and accelerations for beam, shell and solid elements, and thus allows users to define nodal loads or pressure loads as a function of displacements,

velocities and accelerations and some other user-defined inputs. This should be sufficient to facilitate implementation of the theory of hydrodynamic loads.

However, a problem arises in that nodal accelerations in LOADUD are only available for deformable bodies. If we should use deformable bodies to represent the hull girder, the bodies will generate large vibrations and nodal accelerations that will yield wrong results.

To solve this acceleration problem, the user common subroutine (USERCOMM) is used to track the velocity histories of rigid bodies. The nodal acceleration is then approximated by the velocity history and is expressed as:

$$a(n)=\frac{v_k - v_{k-2}}{t_k - t_{k-2}} \tag{3.1}$$

where nodal velocitity at the k_{th} and the $(k\text{-}2)_{th}$ time step, v_k and v_{k-2}, are used instead of v_k and v_{k-1} because the code will otherwise yield numerical instabilities.

3.3 Coupled model 1: implementation of a maneuvering model into LS-DYNA

The coupled model 1 (presented in **Papers 1 and 2**) represents hydrodynamic forces in the planar surge, sway and yaw motions using a traditional ship maneuvering model with a series of nondimensional coefficients determined from experiments by Van Berlekom and Goddard (1972). For the out-of-plane heave, roll and pitch motions, three SDOF mass-spring systems were used.

3.3.1 A maneuvering model for planar motions

In maneuvering simulations, the roll, pitch and heave motions are generally assumed to be negligible. Only planar motions, i.e., surge, sway and yaw, are considered. The equations of motion constitute the mathematical model of the problem. It is convenient to introduce two coordinate systems, see Figure. 3-1. One is the earth-fixed coordinate system $X_0O_0Y_0$, and the other, XOY, is fixed to the body, with its origin located at the center of gravity (COG) of the ship.

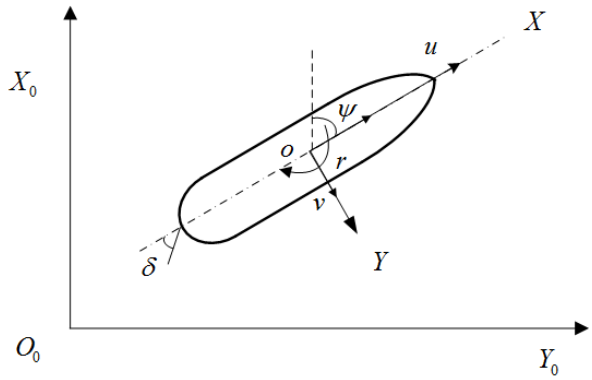

Figure 3-1. Coordinate systems

The governing equations of motion according to Newton's law are given in Eqs. (3.2), (3.3) and (3.4) with reference to the body frame.

$$m(\dot{u} - ru - x_G r^2) = X_{hydro} + X_{dist} \tag{3.2}$$

$$m(\dot{v} + ru + x_G \dot{r}^2) = Y_{hydro} + Y_{dist} \tag{3.3}$$

$$I_{zz}\dot{r} + mx_G(\dot{v} + ru) = N_{hydro} + N_{dist} \tag{3.4}$$

The left hand sides of the equations are the inertial contributions referring to a ship-fixed coordinate system, and the right sides represent the forces or moments acting on the ship. m is the ship mass, and I_{zz} is the moment of inertia in yaw. u,v,r are the velocities in surge, sway and yaw, respectively, in the body-fixed coordinate system. x_G is the position coordinate of the ship COG in the longitudinal x direction. The superscript dot signifies time derivative. The subscript 'hydro' stands for hydrodynamic forces and moments in calm water, and 'dist' stands for disturbance forces and moments due to wind, waves, current, or, in this case, collision forces.

The hydrodynamic forces and moments can, in principle, be regarded as functions of the instantaneous values of velocities, accelerations, the rudder angle, the propeller revolution rate, and engine settings. Thus,

$$X_{hydro} = X(\psi, u, v, r, \dot{u}, \dot{v}, \dot{r}, \delta, n, \rho, \mu) \tag{3.5}$$

$$Y_{hydro} = Y(\psi, u, v, r, \dot{u}, \dot{v}, \dot{r}, \delta, n, \rho, \mu) \tag{3.6}$$

$$N_{hydro} = N(\psi, u, v, r, \dot{u}, \dot{v}, \dot{r}, \delta, n, \rho, \mu) \tag{3.7}$$

where ψ is the yaw angle, δ is the rudder angle, ρ is the water density, n is the nominal propeller revolution rate and μ is the engine output ratio.

The mathematical maneuvering model proposed by Norrbin (1971) is used, where the coefficients are nondimensionalized by means of Froude scaling. The nondimensionalized force expressions are given by:

$$\begin{aligned} X_h &= X_{u|u|}u|u| + X_{uuu|u|}u^3|u| + X_{vr}vr + (X_G + X_{rr})r^2 + X_{u|v|v}u|v|v^2 \\ &+ X_{cc\delta\delta}c^2\delta^2 + X_{vv}v^2 + X_{uvv}uv^2 + X_{c|c|\delta\delta}c|c|\delta^2 + X_{c/c/v}c|c|v + X_{c|c|\beta\delta}c|c|\beta\delta \end{aligned} \tag{3.8}$$

$$\begin{aligned} Y_h &= Y_{ur}ur + Y_{uur}u^2r + Y_{|u|v}|u|v + Y_{u|u|v}u|u|v + Y_{|v|v}|v|v + Y_{|r|r}r|r| \\ &+ Y_{|v|r}r|v| + Y_{v|r|}v|r| + Y_{cc\delta}c^2\delta + Y_{c|c|\delta}c|c|\delta + Y_{c|c|\beta|\beta|\delta}c|c|\beta|\beta|\delta \end{aligned} \tag{3.9}$$

$$\begin{aligned} N_h &= N_{|u|r}|u|r + N_{u|u|r}u|u|r + N_{uv}uv + N_{uuv}u^2v + N_{|v|v}|v|v \\ &+ N_{|r|r}r|r| + N_{|v|r}r|v| + N_{v|r|}v|r| + N_{cc\delta}c^2\delta + N_{c|c|\beta|\beta|\delta}c|c|\beta|\beta|\delta \end{aligned} \tag{3.10}$$

The nondimensional parameters are defined by:

$$u = \frac{u}{\sqrt{gL_{pp}}}, v = \frac{v}{\sqrt{gL_{pp}}}, r = \frac{r}{\sqrt{g/L_{pp}}}, \beta = \frac{v}{u}, n = \frac{n}{\sqrt{g/L_{pp}}}, t = \frac{t}{\sqrt{L_{pp}/g}} \tag{3.11}$$

where β is the drift angle, and L_{pp} is the length between the perpendiculars of the ships.

The origin of the body-fixed coordinate system is set at the ship COG to eliminate nonzero terms in Eqs. (3.2), (3.3) and (3.4). The nondimensional motion equations are given by:

$$(1 - X_{\dot{u}})\dot{u} = X_h + X_{dist} \tag{3.12}$$

$$(1 - Y_{\dot{v}})\dot{v} - Y_{\dot{r}}\dot{r} = Y_h + Y_{dist} \tag{3.13}$$

$$-N_{\dot{v}}\dot{v} + \left(\frac{I_{zz}}{mL_{pp}^2} - N_{\dot{r}}\right)\dot{r} = N_h + N_{dist} \tag{3.14}$$

The coefficients $-X_{\dot{u}}, -Y_{\dot{v}}, -Y_{\dot{r}}, -N_{\dot{v}}, -N_{\dot{r}}$ are added mass in surge, added mass in sway induced by sway acceleration, added mass in sway induced by yaw acceleration, added mass in yaw induced by sway acceleration, and added mass in yaw induced by yaw acceleration. $-Y_{\dot{r}}$ and $-N_{\dot{v}}$ in Eqs. (3.13) and (3.14) are zero, according to the maneuvering data in Van Berlekom and Goddard (1972). This implies that the added mass coefficients for yaw and sway are not coupled; coupling terms only exist among velocities.

To properly simulate ship maneuvering motions, the effects of propeller, rudder and engines should be included. Three auxiliary equations were given by Van Berlekom and Goddard (1972), where propeller thrust *T*, torque *Q* and flow velocity *c* at the rudder are defined as follow:

$$T = T_{uu}u^2 + T_{un}un + T_{|n|n}|n|n + T_{nn}n^2 \tag{3.15}$$

$$Q = Q_{uu}u^2 + Q_{un}un + Q_{|n|n}|n|n + Q_{nn}n^2 + Q_{\mu}^{E}\mu + Q_{n}^{E}n + Q_{f}^{E}n|n| \tag{3.16}$$

$$\begin{aligned} c^2 &= c_{uu}u^2 + c_{un}un + c_{|n|n}|n|n + c_{nn}n^2, \ for\ c \geq 0 \\ c^2 &= 0, \ for\ c < 0 \end{aligned} \tag{3.17}$$

The rate of propeller revolution per minute is given by:

$$dn = Q / (\mathrm{K}_p^2 - \mathrm{Q}_{\dot{n}}) \cdot dt \tag{3.18}$$

3.3.2 The three out-of-plane degrees of freedom

It is assumed that the out-of-plane ship motions are not coupled with the in-plane ship motions and there is no coupling among roll, pitch and heave motions. Then, the roll, pitch and heave can be simplified as three single degree of freedom spring-damper vibration subsystems. The governing equations are then:

$$(M_{33} + A_{33})\ddot{z} + B_{33}\dot{z} + C_{33}z = 0 \tag{3.19}$$

$$(I_{44} + A_{44})\ddot{\alpha} + B_{44}\dot{\alpha} + C_{44}\alpha = 0 \tag{3.20}$$

$$(I_{55} + A_{55})\ddot{\gamma} + B_{55}\dot{\gamma} + C_{55}\gamma = 0 \tag{3.21}$$

where A_{33}, A_{44}, A_{55} are added masses for heave, roll and pitch, respectively. α and γ are the roll and pitch angles, and z is the heave displacement. The restoring forces are

$$C_{33} = \rho g A_w \tag{3.22}$$

$$C_{44} = \rho g \nabla \cdot GM_T \tag{3.23}$$

$$C_{55} = \rho g \nabla \cdot GM_L \tag{3.24}$$

where A_w is the water plane area, ∇ is the ship displacement, and GM_T and GM_L are the transverse and longitudinal metacentric heights, respectively.

By moving the hydrodynamic terms of the motion equations to the left side, the hydrodynamic forces for heave, roll and pitch are expressed as:

$$F_{33} = -A_{33}\ddot{z} - B_{33}\dot{z} - C_{33}z \tag{3.25}$$

$$M_{44} = -A_{44}\ddot{\alpha} - B_{44}\dot{\alpha} - C_{44}\alpha \tag{3.26}$$

$$M_{55} = -A_{55}\ddot{\gamma} - B_{55}\dot{\gamma} - C_{55}\gamma \tag{3.27}$$

The natural period of oscillation for a single degree of freedom vibration system is given by

$$T = 2\pi\sqrt{\frac{I+A}{C}} \quad or \quad T = 2\pi\sqrt{\frac{M_{33}+A_{33}}{C_{33}}} \tag{3.28}$$

By simplifying the roll, pitch and heave as independent single degree of freedom systems, it is assumed that the coupling effect between different motions is secondary in ship collisions, and the natural periods are only determined by Eq. (3.28). The added masses for heave, pitch and roll are determined by using empirical equations proposed by Popov et al. (1969). The equations are shown in the appendix in **Paper 2** (Yu and Amdahl, 2016b). Given the natural periods calculated with potential theory using the code HydroD, the values of the restoring terms for the proposed method are readily obtained according to Eq. (3.28).

The damping effect is usually considered secondary in ship collision and grounding problems. Here, the damping terms for roll, pitch and heave are expressed empirically as *n* fraction of the value for critical damping:

$$B = nB_{crit} = n\left\{2[(I+A)C]^{0.5}\right\} \tag{3.29}$$

3.3.3 Implementation procedure

The coupling algorithm between structural and hydrodynamic solvers is shown in Figure 3-2. During simulation, LS-DYNA first passes nodal displacements, velocities of ship COG in the current timestep to the user subroutine. The velocity histories of COG are then stored with the user common subroutine. The time increment is typically in the order of 10^{-6} s in ship collision simulations. To maintain efficiency without losing accuracy, the velocity histories are stored every 400 steps, i.e. around every 10^{-3}s. The mass scaling technique is adopted to maintain a constant timestep during simulation. With the above information, hydrodynamic loads can be calculated in the user load subroutine. The obtained hydrodynamic loads are applied on the ship COG, and the program returns to the structural solver. LS-DYNA solves structural deformations and global motions, and gives motion information for the next timestep.

HydroD and SIMO softwares are used for verifying the proposed method as shown in Figure 3-2. With the ship panel model, HydroD calculates the hydrodynamic coefficients and natural periods of roll, pitch and heave of the vessel. The obtained natural periods are used as input to the user subroutine to ensure that exactly the same natural periods are used for both methods. This can be achieved by adjusting the restoring terms. The obtained 6DOF collision forces and moments from LS-DYNA and the hydrodynamic coefficients are imported into SIMO. SIMO then calculates the global motion response of the vessel under the action of collision forces. The results can then be compared to those obtained with the proposed method.

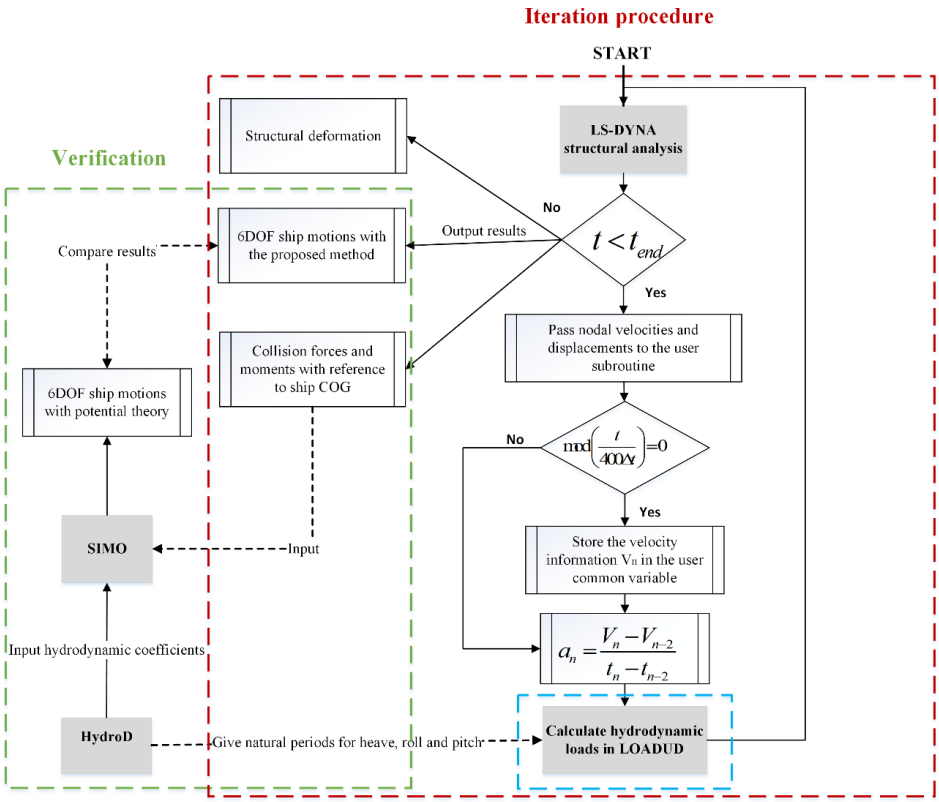

Figure. 3-2. Illustration of the coupling algorithm

3.4 Coupled model 2: implementation of linear potential flow theory into LS-DYNA

In coupled model 2, hydrodynamic loads are calculated on the basis of linear potential-flow theory by the use of the user subroutine in LS-DYNA. This approach facilitates a 6DOF coupled dynamic simulation of ship collision and grounding accidents. Potential-flow theory both with and without considering the forward speed effect was implemented to study the speed influence. With the proposed model, the transient effects of the fluid, global ship motions, impact forces and structural damage can all be predicted with high accuracy. The content is covered in **Paper 3** (Yu et al., 2016b).

3.4.1 Linear potential flow theory without forward speed effect

A right-handed orthogonal seakeeping coordinate system $O_s xyz$ is used as shown in Figure 3-3.

The origin is located in the plane of the undisturbed free surface $z = 0$ with the-axis z pointing upwards through the center of gravity of the ship in its mean position and x pointing towards the bow. The coordinate system $O_s xyz$ is inertial and fixed to the mean position of the vessel,

and it moves with the speed of the vessel, but it does not oscillate.

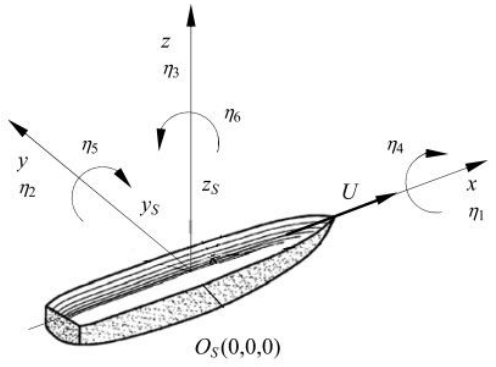

Figure 3-3. The seakeeping coordinate system

To simplify the problem, the forward speed effect is first disregarded. The forces acting on a ship during collision and grounding accidents are the results of the propeller and rudder forces, hydrodynamic forces and collision forces. Before collision, propeller and rudder forces are in equilibrium with the hydrodynamic forces acting on the hull. Departure from this state due to a sudden change in the external forces causes a change in the hydrodynamic forces acting on the hull (Petersen, 1982). The governing motion equations are:

$$\sum_{k=1}^{6}\left[\left(M_{jk}+A_{jk}(\infty)\right)\ddot{\eta}_k+\int_0^t K_{jk}(t-\tau)\cdot\left[\dot{\eta}_k(\tau)-\dot{\eta}_k(t=0)\right]d\tau+C_{jk}\eta_k\right]=F_j(t)\left(j=1,2,...,6\right) \tag{3.30}$$

where M_{jk}, $A_{jk}(\infty)$, and C_{jk} are components of the generalized ship mass matrix, the added mass of infinite frequency and the restoring matrix of the ship. The index $j=1,...,6$ represents surge, sway, heave, roll, pitch and yaw, respectively. $\dot{\eta}_k(t=0)$ is the velocity component of the striking ship in the k_{th} degree of freedom just before impact and $F_j(t)$ is the generalized collision force in the j_{th} degree of freedom. $\int_0^t K(t-\tau)\cdot\dot{\eta}(\tau)d\tau$ is the convolution integral connected with free-surface memory effects and $K_{jk}(t)$ is the so called impulse-response - or the retardation function connected with direction *j* and *k*. It provides a radiation load in *j* direction acting on the vessel at the actual time *t* as a consequence of an impulse speed in *k* direction experienced by the ship at a previous time instant *t*-τ. $K_{jk}(t)$ is given by:

$$K_{jk}(t)=\frac{2}{\pi}\int_0^\infty B_{jk}(\omega)\cos\omega t d\omega=\frac{2}{\pi}\int_0^\infty\left(A_{jk}(\infty)-A_{jk}(\omega)\right)\omega\sin\omega t d\omega \tag{3.31}$$

$A_{jk}(\omega)$ and $B_{jk}(\omega)$ are frequency-dependent added masses and linear wave radiation damping for zero forward speed, respectively.

In order to estimate the impulse response functions, the hydrodynamic coefficients must be estimated for all frequencies. This is done numerically in the frequency domain by means of boundary element methods (BEM). The challenge is connected with estimating the added-mass and damping coefficients at large frequencies because they imply short waves, which require suitably small elements to be handled. In other words, there is an upper limit of the frequency ω up to which the added mass and damping coefficients can be calculated accurately for the chosen discretization. Here, the integral is performed from 0 to Ω_e, where Ω_e is the highest frequency possible for computation of damping coefficients. A correction term δK_{jk} can be introduced to compensate for the truncation error,

$$K_{jk}(t) = \frac{2}{\pi}\int_0^{\Omega_e}\left[B_{jk}(\omega_e)\cos(\omega_e t)\right]d\omega_e + \delta K_{jk} \tag{3.32}$$

$$\delta K_{jk} = \frac{2}{\pi}\int_{\Omega_e}^{\infty}\left[\tilde{B}_{jk}(\omega_e)\cos(\omega_e t)\right]d\omega_e \tag{3.33}$$

where $\tilde{B}_{jk}$ is an analytical approximation for damping coefficients. Here, $\tilde{B}_{jk}(\omega_e > \Omega_e) = \frac{c_1}{\omega_e^2}$ is used, as the formula is simple and applicable for all coefficients. c_1 is a constant determined by the cut-off frequency.

3.4.2 Linear potential flow theory considering the forward speed effect

Forward speed will influence ship hydrodynamic forces in several aspects. First, it will modify the time derivative through bringing in a convective term in the Bernoulli equation. This gives an explicit change in the pressure. An implicit variation is caused by the changes in the boundary value problem for the velocity potential. In particular, the free surface and body boundary conditions change when the forward speed effect is accounted for. The forward speed will also modify the frequency felt by the ship when interacting with incident waves. This encounter frequency effect is not included as incident waves are normally disregarded in ship collision and grounding problems.

Here the added mass and damping coefficients considering the forward speed are computed by the use of the 3D hybrid method proposed by Thys (2013), which is a combination of the Salvesen–Tuck–Faltinsen (STF) strip-theory method (Salvesen et al., 1970) and a 3D zero forward speed Green function method implemented in the seakeeping commercial code WAMIT. Hybrid method can provide better results for relatively blunt body than that by STF, where the hydrodynamic coefficients are evaluated from ship cross sections. The detailed

theory for added mass and damping coefficients with the forward speed is shown in the appendix of **Paper 3**.

The governing equations of ship motion considering the forward speed effect are given by:

$$\sum_{k=1}^{6}\begin{bmatrix}\left(M_{jk}+A_{jk}\left(u,\infty\right)\right)\ddot{\eta}_k+B_{jk}\left(u,\infty\right)\left[\dot{\eta}_k\left(\tau\right)-\dot{\eta}_k\left(t=0\right)\right]\\ +C_{jk}\eta_k+\int_0^t K_{jk}\left(t-\tau,u\right)\cdot\left[\dot{\eta}_k\left(\tau\right)-\dot{\eta}_k\left(t=0\right)\right]d\tau\end{bmatrix}=F_j\left(t\right)\left(j=1,2,...,6\right) \tag{3.34}$$

where the impulse response function terms are calculated by means of the speed and frequency dependent damping coefficients

$$K_{jk}\left(t,u\right)=\frac{2}{\pi}\int_0^{\infty}\left[B_{jk}\left(u,\omega_e\right)-B_{jk}\left(u,\infty\right)\right]\cos\left(\omega_e t\right)d\omega_e \tag{3.35}$$

It is convenient to express the impulse-response function in terms of speed-independent and speed-dependent contributions. The retardation function can thus be expressed as:

$$K_{jk}\left(t,u\right)=K_{jk}^0\left(t\right)+uK_{jk}^u\left(t\right)+u^2K_{jk}^{u^2}\left(t\right)+\delta K_{jk} \tag{3.36}$$

where for $k=1,2,3,4$,

$$\begin{aligned}K_{jk}^0&=\frac{2}{\pi}\int_0^{\Omega_e}B_{jk}^0\left(\omega_e\right)\cos\left(\omega_e t\right)d\omega_e\\ K_{jk}^u&=\frac{2}{\pi}\int_0^{\Omega_e}-\left[dA_{jk}^0\left(\omega_e\right)-dA_{jk}^0\left(\infty\right)\right]\cos\left(\omega_e t\right)d\omega_e\\ K_{jk}^{u^2}&=0\end{aligned} \tag{3.37}$$

for $k=5$

$$\begin{aligned}K_{j5}^0&=\frac{2}{\pi}\int_0^{\Omega_e}B_{j5}^0\left(\omega_e\right)\cos\left(\omega_e t\right)d\omega_e\\ K_{j5}^u&=\frac{2}{\pi}\int_0^{\Omega_e}\left[B_{j3}^0\left(\omega_e\right)\frac{\sin\left(\omega_e t\right)}{\omega_e}-\left(dA_{j5}^0\left(\omega_e\right)-dA_{j5}^0\left(\infty\right)\right)\cos\left(\omega_e t\right)\right]d\omega_e\\ K_{j5}^{u^2}&=\frac{2}{\pi}\int_0^{\Omega_e}dB_{j3}^0\left(\omega_e\right)\frac{\cos\left(\omega_e t\right)}{\omega_e^2}d\omega_e\end{aligned} \tag{3.38}$$

and for $k=6$

$$\begin{aligned}K_{j6}^0&=\frac{2}{\pi}\int_0^{\Omega_e}B_{j6}^0\left(\omega_e\right)\cos\left(\omega_e t\right)d\omega_e\\ K_{j6}^u&=\frac{2}{\pi}\int_0^{\Omega_e}\left[-B_{j2}^0\left(\omega_e\right)\frac{\sin\left(\omega_e t\right)}{\omega_e}-\left(dA_{j6}^0\left(\omega_e\right)-dA_{j6}^0\left(\infty\right)\right)\cos\left(\omega_e t\right)\right]d\omega_e\\ K_{j6}^{u^2}&=\frac{2}{\pi}\int_0^{\Omega_e}-\left[dB_{j2}^0\left(\omega_e\right)\frac{\cos\left(\omega_e t\right)}{\omega_e^2}\right]d\omega_e\end{aligned} \tag{3.39}$$

The definitions of dA_{jk}^{0} and dB_{jk}^{0} are given in the appendix of **Paper 3**. The correction term can also be divided into speed-independent and speed dependent contributions. The detailed expressions are omitted here, but can be found in the appended **Paper 3**.

3.4.3 Implementation procedure

The coupling algorithm between structural and hydrodynamic solvers is shown in Figure 3-4. Before starting a simulation (i.e. step 0), a text file with impulse response functions should be prepared by users. Information inside the file will be read and stored permanently in the first simulation timestep. The hydrodynamic coefficients and subsequent impulse response function coefficients are computed by use of the 3D hybrid method proposed by Thys (2013).

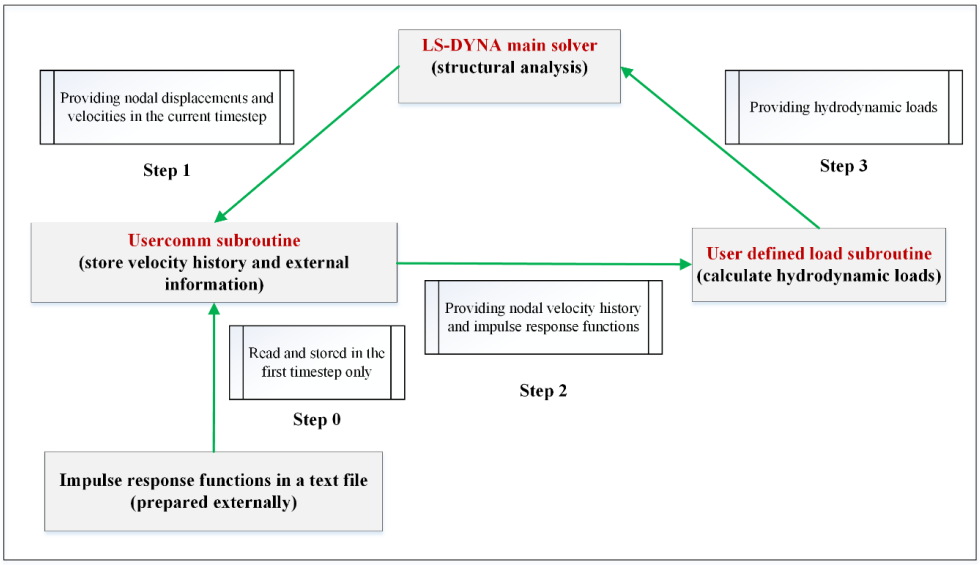

Figure 3-4. The implementation procedure of coupled model 2

During the simulation, LS-DYNA first passes information of nodal displacements, velocities and accelerations at the ship COG in the current timestep to the user subroutine. The velocity history is stored with the user common subroutine for calculating the convolution integral and approximating the acceleration. The time increment is typically in the order of 10^{-6} s in ship collision simulations. To maintain efficiency without loss of accuracy, velocity histories are stored every 10^{-3}s. The mass scaling technique is adopted to maintain a constant timestep during simulation. With the above information, hydrodynamic loads can be calculated in the user load subroutine. The simple trapezoidal integration method is used for the convolution integration. The accuracy is good as the timestep is quite small. The obtained hydrodynamic loads are applied on the ship COG, and then the structural LS-DYNA solver calculates structural deformation and global motions, and gives motion information for the next timestep.

3.5 Verification of the proposed methods

The implementation of the coupled models 1 and 2 in LSDYNA was verified by comparison with SIMO and a user generated code. The collision forces were extracted from the coupled simulation, and were applied as external forces on the ship in SIMO and the user code. The obtained ship motions were compared with those from the coupled simulation. Results showed that ship motions of the coupled models agreed with SIMO and the user code. Excellent agreement with linear potential flow theory was found, especially for coupled model 2. The accuracy of coupled model 1 is less, but still acceptable for ship collision simulations. Detailed information of the verification can be found in **Papers 1-3**.

Figure 3-5 shows snapshots of a coupled collision simulation using model 2. All the 6DOF ship motions can be clearly observed and the trajectories are complicated, demonstrating the soundness of the implementation.

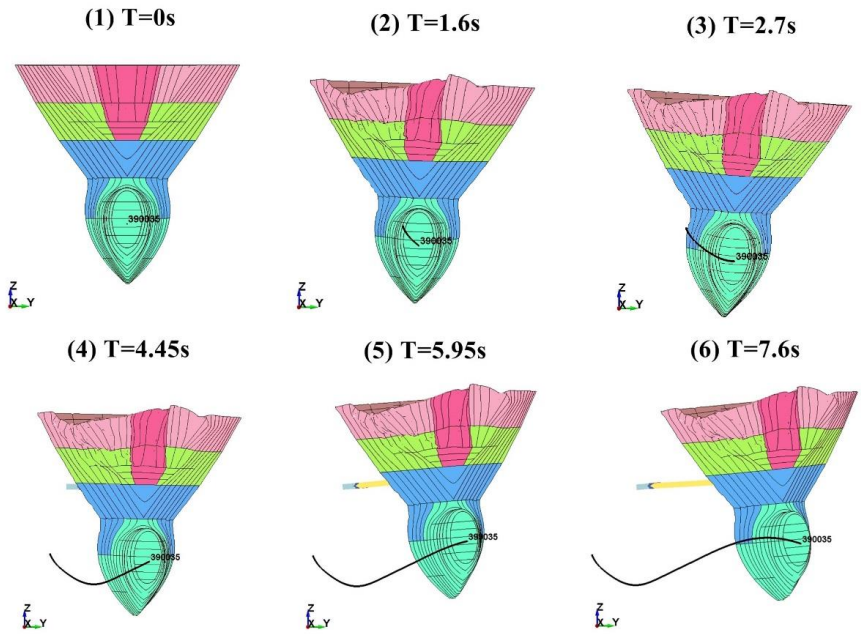

Figure 3-5. Snapshots of a coupled collision simulation using model 2

Chapter 4

Influence of coupling external and internal mechanics on damage prediction

4.1 Introduction

In this chapter, the proposed models in *chapter 3* are used to carry out planar 3DOF and full 6DOF coupled dynamic simulation of ship collision and grounding accidents. A comparative study with the traditional decoupled method is conducted, and the validity of the basic assumptions behind the decoupled method is discussed. The influence of fluid structure interactions on the damage prediction of ship collisions is also studied. The content in this chapter is included as part of **Papers 1-3** and a conference paper in Yu and Amdahl (2016c).

4.2 Model description and case studies

An offshore supply vessel colliding with rigid walls of different orientations and a semi-submersible platform were simulated. The wall was modelled as a plate with much larger extension than the vessel.

4.2.1 The striking ship

The striking ship is a modern supply vessel with a bulbous bow. The principal dimensions of the vessel are given in Table 4-1.

Table 4-1. Principal dimensions of the striking vessel

Displacement	7500	ton
Length overall	90	m
Length between perpendiculars	78.8	m
Breadth	18.8	m
Depth	7.6	m
Draft	6.2	m

Finite element model of the ship bow

The bow FE model is shown in Figure 4-1. The element size is generally 120 mm. The plate thickness varies from 7 mm for the decks to 12.5 mm in the bulb. The stiffener spacing is approximately 600 mm, with ring stiffeners and breast hooks of approximately 250 × 15 mm in the bulb. The bulbous part is almost cylindrical and is relatively strong. The forecastle protrudes

1.2 m ahead of the bulb.

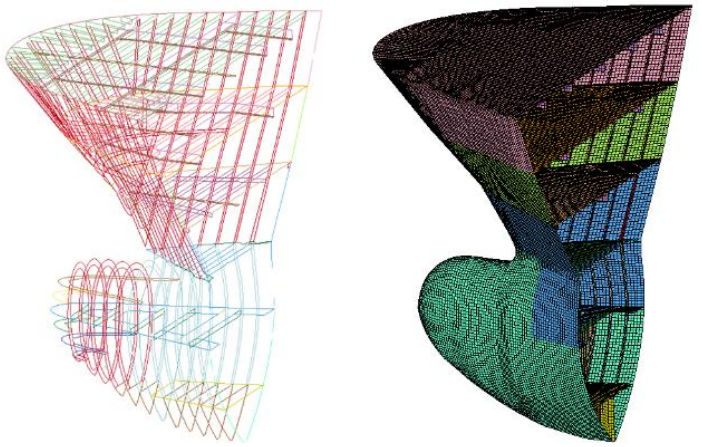

Fig. 4-1. The FE model of the bulbous bow

The ship's hull girder is represented by a long rigid beam from the bow back towards the COG of the vessel, see Figure. 4-2. The beam properties are calibrated so as to represent correctly the total mass and inertia of the ship with respect to the center of gravity taking into account the contribution of the bow model. The 6DOF hydrodynamic forces and moments are applied as user-defined loads at the COG of the ship. Because the user defined load subroutine does not allow applying bending moments, the bending moments have to be transformed into force pairs. Therefore, several small beams are created for applying bending moments in roll, pitch and yaw. The assumption of rigid hull girder is reasonable according to Pedersen and Li (2009), and they showed that elastic energy absorbed by the struck ship through global hull girder vibrations was normally small and varied from 1% to 6% of the energy released for crushing.

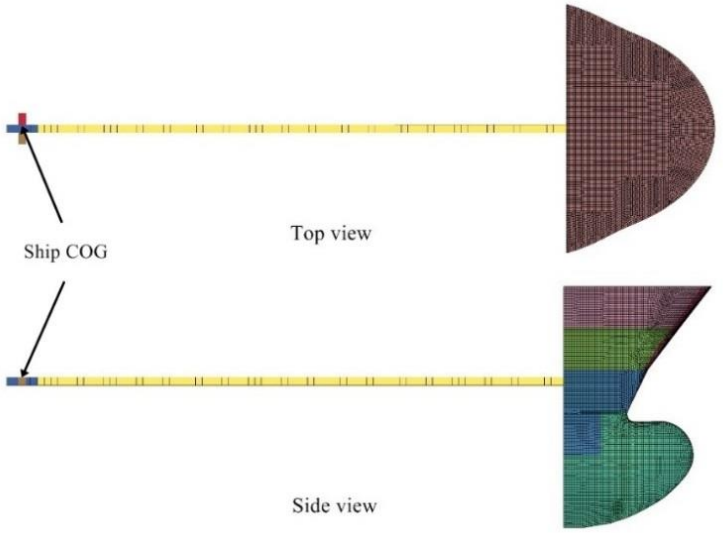

Figure 4-2. The FE model of the striking ship

The ship panel model

The panel model of the striking supply vessel analyzed by the seakeeping solver is shown in Figure 4-3 with a total number of 3506 elements. For simplicity, the bulbous bow part is not modelled in the panel model. Its influence is considered minor. Representative components of the resulting hydrodynamic coefficients and the impulse response functions are given in Appendix B of **Paper 3**. The hydrodynamic coefficients are correctly calculated back from the impulse response function, demonstrating the soundness of the results.

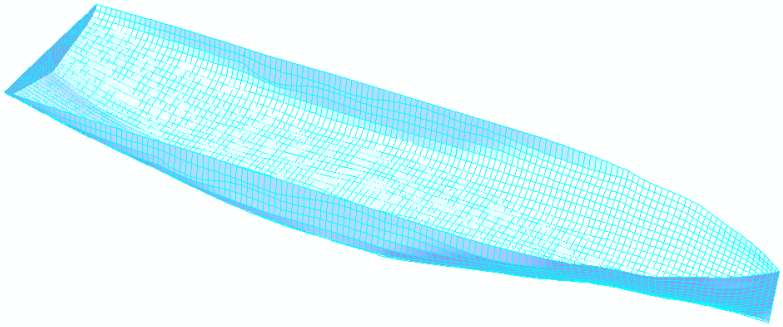

Figure 4-3. The panel model of the striking supply vessel

4.2.2 The semisubmersible platform

The platform is a four-legged semisubmersible with ring-pontoons. The global motion is small and has little interaction with local deformations. Only the front part of the column including the sponson at the impact point is modelled; see Figure 4-4.

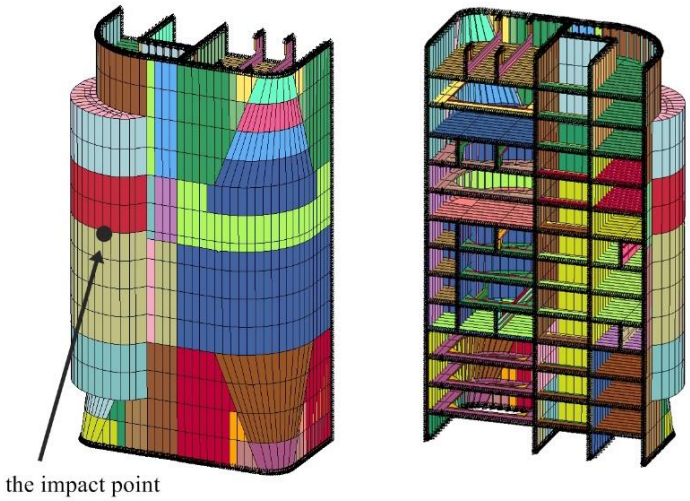

Figure 4-4. FE models of the semi-sub platform column

The mass of the platform is considerably larger than that of the striking ship. Hence, the platform

motions are small and are neglected for simplicity. The nodes on the platform boundary edges, marked in black in Figure 4-4, are constrained against all translations and rotations.

4.2.3 Definition of collision scenarios

A supply vessel is assumed to run into rigid bodies with different orientations and a deformable semisubmersible platform. Five scenarios are defined as shown in Figure 4-5. The scenarios are (1) colliding with oblique plates, (2) grounding on a sloping sea floor (3) crushing into a rigid plate with the normal vector of $\vec{n}_1 = [-0.74, 0.24, 0.63]$, (4) crushing into a rigid plate with the normal vector of $\vec{n}_2 = [-0.86, 0.42, -0.30]$, (5) collision with a submersible platform. For each scenario, several cases are simulated with different attack angles and impact velocities.

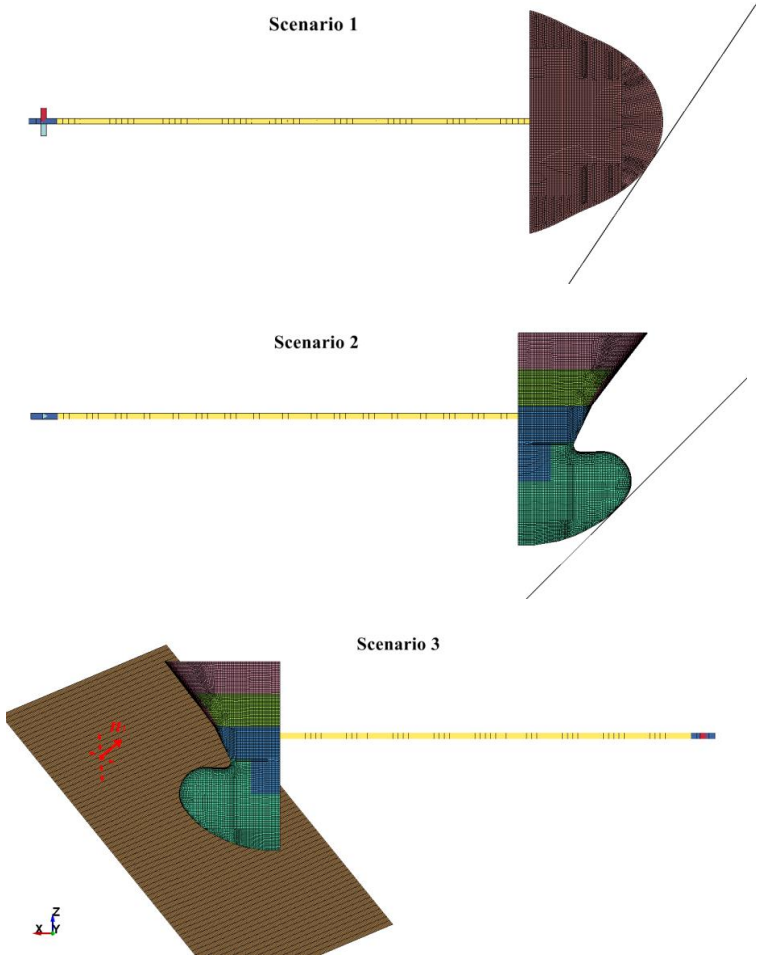

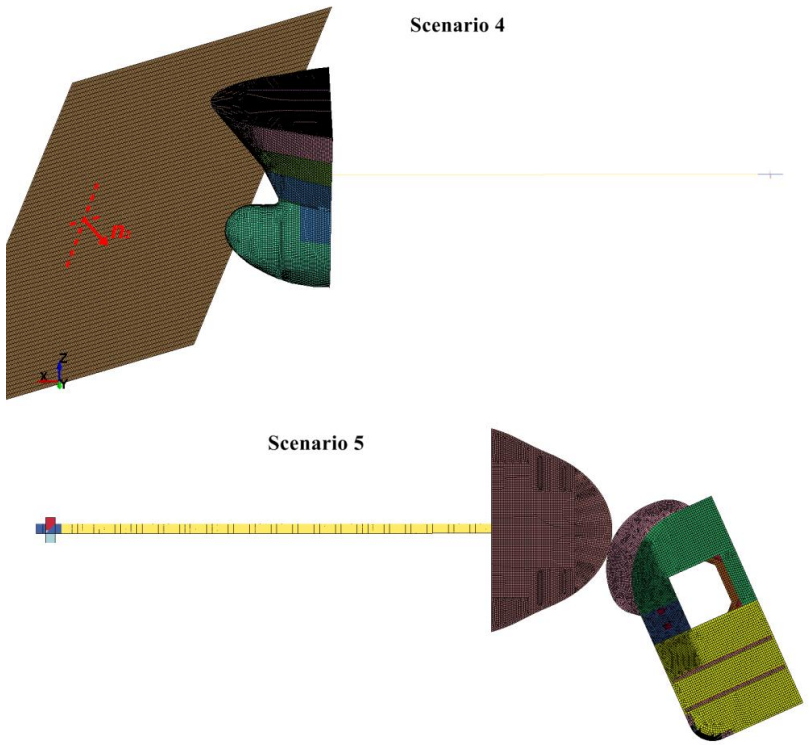

Figure 4-5. Collision scenarios

4.3 Discussion of assumptions behind the external dynamic models

Pedersen and Zhang (1998) proposed an external dynamic model considering planar surge, sway and yaw motions; refer Figure 4-6(a). A local coordinate $\xi\eta$ system is established with the ξ direction normal to the contact point. The ships are allowed to rebound from each other in the ξ direction by introducing a coefficient of restitution e. The relative velocity in the ξ direction at the end of the impact can be directly obtained as $-e\cdot\dot{\xi}(\mathrm{t}=0)$. The parameter e is 0 for an entirely plastic collision and is 1 for a perfect elastic collision. The ratio of impact impulses in the η and ξ direction $\mu = I_{\eta 0} / I_{\xi 0}$ is introduced to judge whether the striking and struck ships will stick or slide against each other.

If $|\mu| \le |\mu_0|$ (μ_0 is the friction coefficient), the two ships will stick together, and the relative velocity after collision is zero in the η direction. The collision forces are assumed to satisfy the relation $F_\eta = \mu \cdot F_\xi$, where μ is the ratio of impact impulses.

If $|\mu| > |\mu_0|$, the two ships will glance off each other. Then, $F_\eta = \mu_0 \cdot F_\xi$ according to Coulomb's friction law.

With these assumptions, the relative velocities in the ξ and η directions and the subsequent dissipated energy after the collision are readily obtained. Liu and Amdahl (2010) extended the external dynamic model to consider the full 6DOF motions. The collision forces are given in the right-handed global XYZ coordinate as defined in Figure 4-6 (b). It is assumed that the normal and tangential friction factors μ_n and μ_t are constant and are given as

$$\mu_n = sign(dp_1)\frac{\sqrt{dp_1^2 + dp_2^2}}{dp_3} \tag{4.1}$$

$$\mu_t = \frac{dp_2}{dp_1} \tag{4.2}$$

where dp_1, dp_2 and dp_3 are the impulses in each direction in the local coordinate in Figure 4-6 (b). For sliding cases, μ_n is assumed to be equal to the friction coefficient μ_0. For both models, it is implicitly assumed that the collision angles do not change during the collision process. The validity of the assumptions of the external dynamic models is discussed using the coupled simulation results.

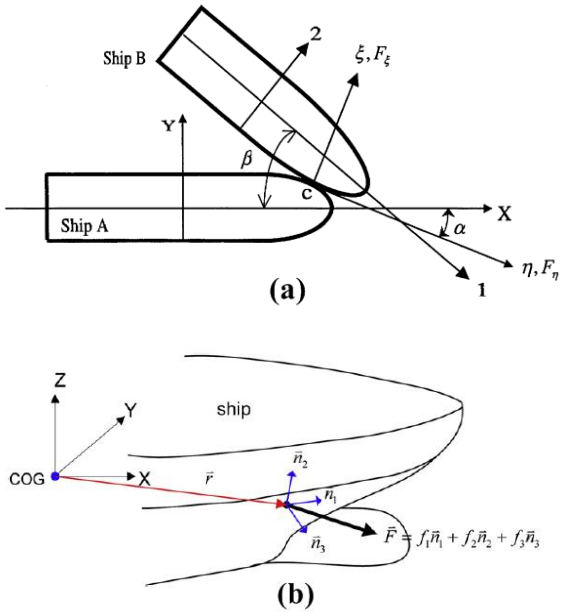

Figure 4-6. External dynamic models (a). 3DOF model by Pedersen and Zhang (1998); (b). 6DOF model by Liu and Amdahl (2010)

4.3.1 Constant added masses

The external dynamic models are based on conservation of energy and momentum, while ship collision including the surrounding water is actually not an undamped system considering the damping terms such as wave making damping, viscous damping, structural damping, etc. The damping terms are generally negligible in view of the large collision forces.

As discussed in *Section 2.2*, the constant added mass representation of fluid cannot fully reflect the complicated behavior of the fluid during a collision. From linear potential flow theory point of view, ship collision forces will excite ship motions in different frequencies. For each frequency, there exist certain added mass and damping matrices with coupling terms among different DOFs. Fourier transformation of the collision forces is useful to check the frequency content. The single-sided amplitude spectrums of the collision forces in scenario 3 and scenario 4 with an impact velocity of 2.78 m/s are plotted in Figure 4-7. The frequency distribution is quite dispersive, and the amplitudes are considerable from low frequencies to high frequencies with respect to ship motions. It is difficult to find a representative frequency to determine the constant added masses as inputs of the external dynamic models; In addition, as collision occurs when the two bodies are extremely close, fluid multi-body interactions may become significant.

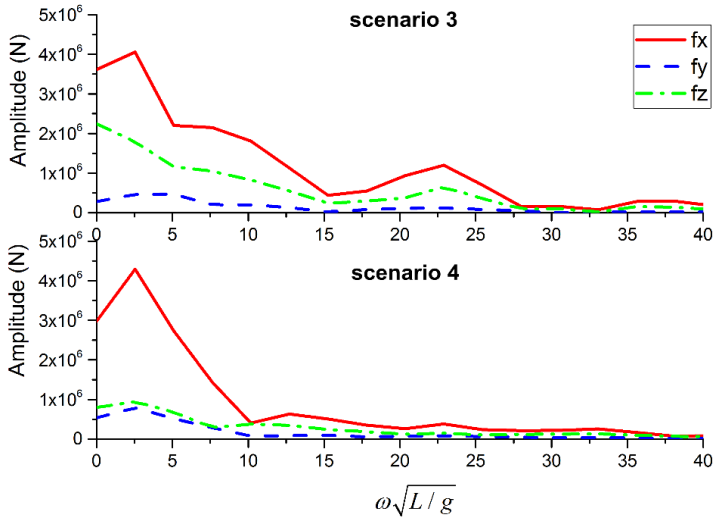

Figure 4-7. Single-sided amplitude spectrum of collision forces

The determination of constant added masses to be used in the external dynamic models will also introduce some errors. Liu and Amdahl (2010) adopted the empirical equations by Popov et al. (1969), which were derived for the purpose of investigating the ice loads exerted on ship structures. Determination of hydrodynamic coefficients were also studied by Valsgard and Jorgensen (1983), Motora et al. (1971), Petersen and Pedersen (1981), Jia and Moan (2010), etc.

The sensitivity of dissipated total energy to added mass coefficients is checked using collision scenario 1 with a collision angle of 35° and 56°. An initial impact velocity of 2.25m/s is assumed, which gives a kinetic energy of about 20 MJ considering the added mass effect. Figure 4-8 plots the dissipated total energy predicted by the 6DOF external dynamic model with varying sway and yaw added mass coefficients ranging from 0.3 to 1.0. The maximum and minimum values of dissipated energy are marked with green triangles, where added mass coefficients in sway and yaw have the same value of 1.0 and 0.3, respectively.

The dissipated total energy increases with added mass coefficients. The differences between the maximum and minimum values of dissipated energy are about 1.4 MJ and 1.1 MJ, corresponding with an error of 22% and 7% for the two cases. The differences are similar in absolute value, but the relative error increases with decreasing collision angles. The varying added mass coefficients in sway and yaw have little influence on the total energy absorption for large collision angle cases, but the influence tends to become important with decreasing collision angles.

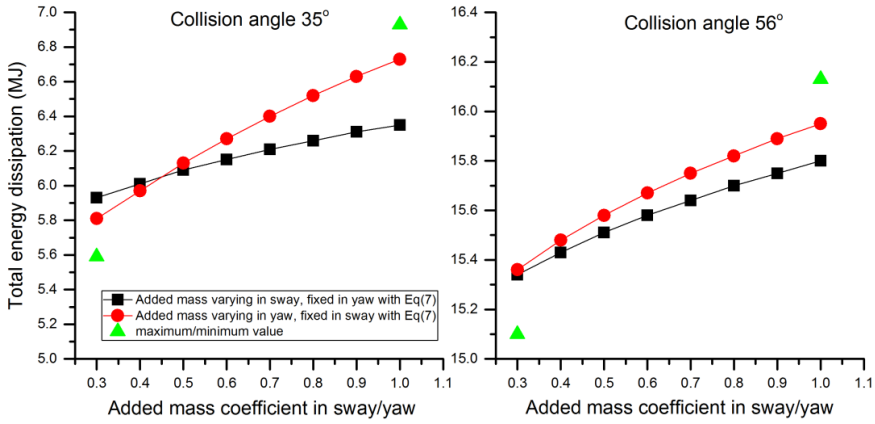

Figure 4-8. Variation of dissipated total energy with sway and yaw added mass coefficients

4.3.2 Proportionality of impact impulses and forces

The assumption of proportionality of impulses is checked using results from coupled simulation. *Scenario 1* is selected, where the supply vessel collides with oblique rigid plates with collision angles of 35°, 44°, 56° and 80°. The first three collision angles represent sliding cases while the 80° case is an example of sticking. The collision angle is defined in Figure 4-9. Three coordinate systems are used, i.e. global earth fixed coordinate, ship fixed coordinate and local coordinate at the impact point.

- *3DOF external dynamic model*

In the first place, *the 3DOF coupled and decoupled models* are used and the roll motion is neglected. Collision forces of the 35° and 56° cases are plotted in the earth-fixed $X_0O_0Y_0$ coordinate in Figure 4-10. The collision force changes drastically at about 1.3 s for the collision

angle 56° because the bulbous bow starts to be crushed. During sliding, the Coulomb's friction law gives $F_\eta = \mu_0 \cdot F_\xi$. Transformed into the global coordinate system, the ratio of the vertical and horizontal forces becomes:

$$\lambda = \frac{F_{Y_0}}{F_{X_0}} = \frac{F_\xi \cdot \cos\alpha - F_\eta \cdot \sin\alpha}{F_\xi \cdot \sin\alpha + F_\eta \cdot \cos\alpha} \tag{4.3}$$

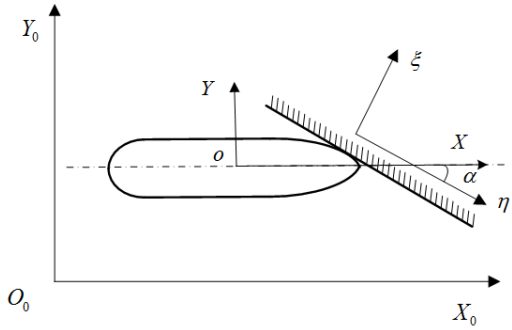

Figure 4-9. The coordinate systems

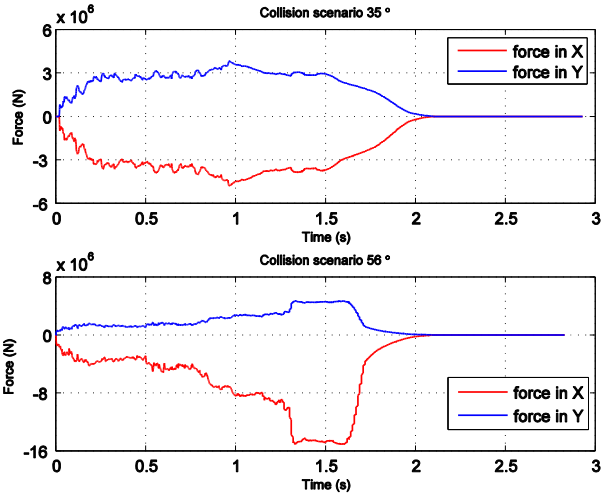

Figure 4-10. The time sequence of collision forces in the global coordinate system

$\mu_0 = 0.3$ is used in the simulation. The force ratio versus collision angle in the global coordinate system is shown in Figure 4-11, and can be used to check the change in the collision angle during collisions. Note that this ratio is only valid for sliding cases. The force ratios for collision angles of 35° and 56° are plotted in Figure 4-12. Despite some small oscillations, the force ratio remains generally constant. According to Figure 4-11, the decoupled method should have a force ratio of 0.31 and 0.79 for collision angles of 56° and 35°, respectively. These values agree well with simulation results shown in Figure 4-10. The same also applies for the collision angle

44°, which confirms the validity of the assumption of a constant force ratio for the sliding cases in the 3DOF external dynamic model.

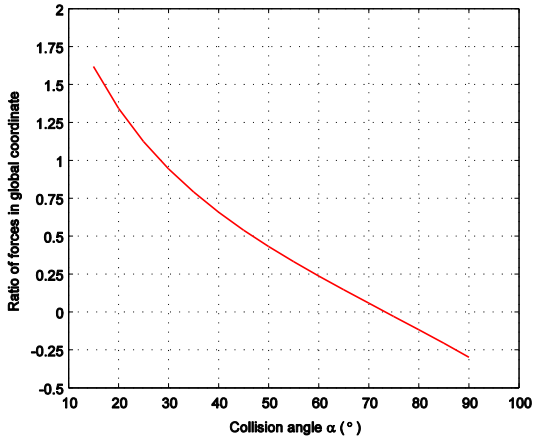

Figure 4-11. Collision force ratio versus collision angles in the global coordinate system for μ=0.3

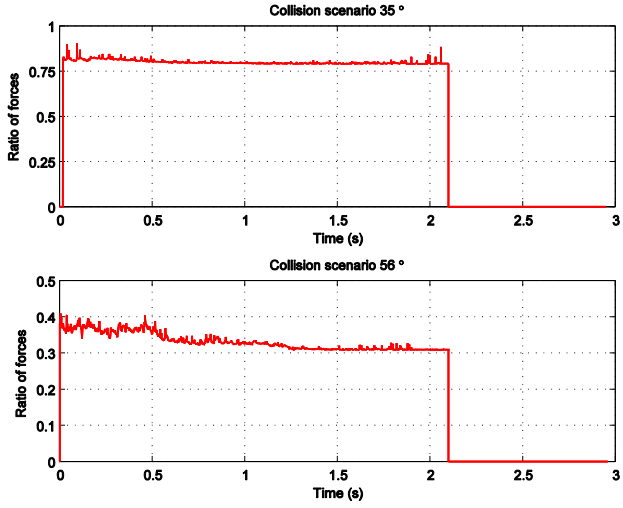

Figure 4-12. The ratio of vertical and horizontal forces in the global coordinate system

For the sticking 80° case, the force ratio equals to the ratio of impact impulses in the η and ξ direction, which is approximately $\mu = I_{\eta 0} / I_{\xi 0} = 0.18$ in the local $\xi\eta$ coordinate system and 0 in the global coordinate system. Collision forces in the longitudinal and transverse directions and the force ratios with the coupled method are plotted in Figure 4-13. It is observed that the force ratio varies significantly but remains within ±0.1. The proportionality of impulses is not strictly satisfied in the sticking case, but the mean value of the force ratio is reasonable.

- *6DOF external dynamic model*

In the 6DOF coupled methods and 6DOF external dynamic models, the roll motion is taken into account. Figure 4-14 shows time histories of the roll and the yaw angles in the 44º and 56º cases. The yaw and roll motions are more intense in the 44º case, because in the 56º case, the bulbous bow gets involved in the collision process, which gives a large rolling moment that tends to counteract that produced by deformation of the forecastle, yielding a small resultant bending moment in roll.

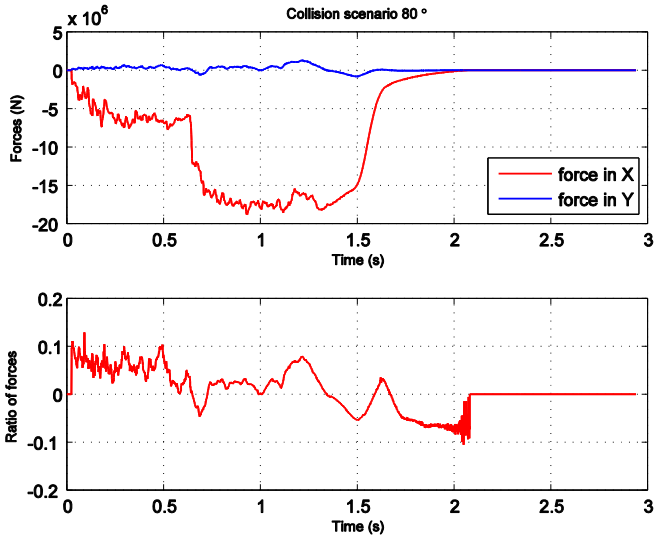

Figure 4-13. The collision forces and force ratio

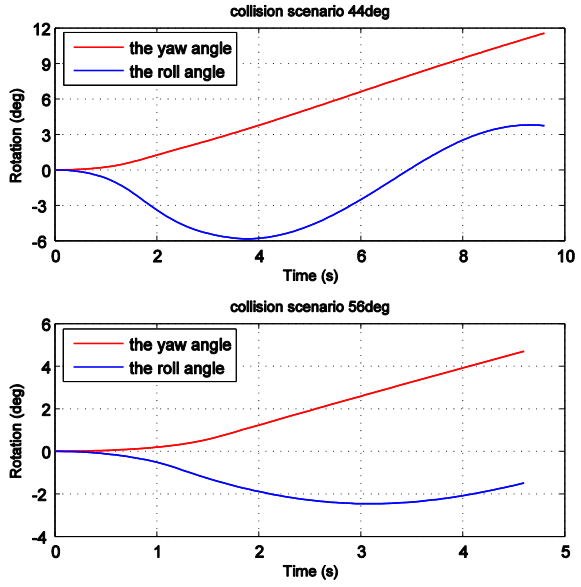

Figure 4-14. The time history of roll and yaw angles during collision

The collision forces and ratios of impulses for the 44º cases are presented in Figure 4-15. The peak forces using the 3DOF and 6DOF coupled methods are quite similar, but the peak values last shorter when the roll motion is considered. This is because the roll gives a velocity at the collision point that tends to separate the ships at the contact point. It is interesting to see that when the 6DOF coupled model is used, the collision force drops to zero at 2.1s and rises up again at 2.8s when secondary impact occurs. The secondary impact extends significantly the total collision duration, but shortens the first impact duration.

From Figure 4-15, the normal force ratio μ_n is virtually constant except some small oscillations and is equal to the sliding friction coefficient 0.3. This is consistent with the conclusions for the 3DOF model. However, the tangential force ratio μ_t is not quite constant. This may lead to inaccurate energy contributions in the n_1 and n_2 directions. However, the total sum of energy dissipation on the n_1 and n_2 directions can still be acceptable. The calculation of μ_t for the sliding case is not straightforward. The solution proposed by Liu and Amdahl (2010) regarding μ_t does not have theoretical background, but it is a pragmatic way to assume proportionality of the forces. More investigations should be performed.

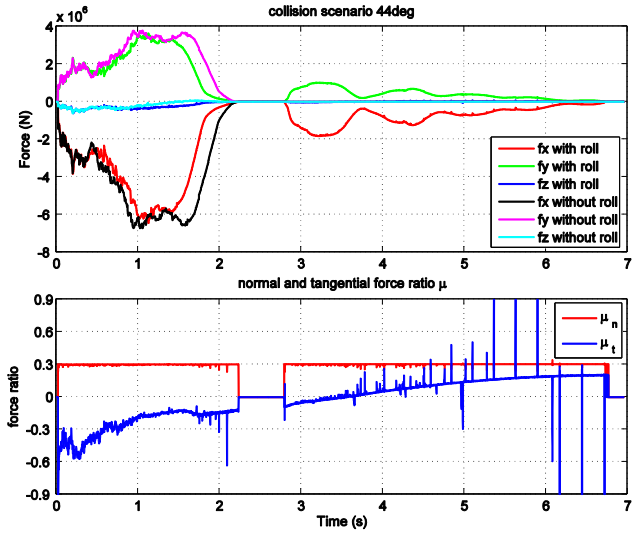

Figure 4-15. The collision forces and impulse ratios for the 44º case

4.3.3 Small collision duration and constant collision angle

Although external dynamic models consider momentum changes of different motions, the initial collision configuration is always used by assuming that collision duration is short and changes

of the collision angle during collision are negligible; otherwise numerical iterations will be needed.

Figure 4-16 shows ship motions for scenario 1 using the 3DOF coupled model. The yaw motion is generally within 3°. However, if the 6DOF coupled model is used, the roll motion is significant and secondary impacts occur. The yaw motion can be as large as 10° at the end of secondary impacts. The assumption of constant collision angle may cause large errors with respect to the total energy dissipation and ship motion trajectories in scenarios with secondary impacts and long durations.

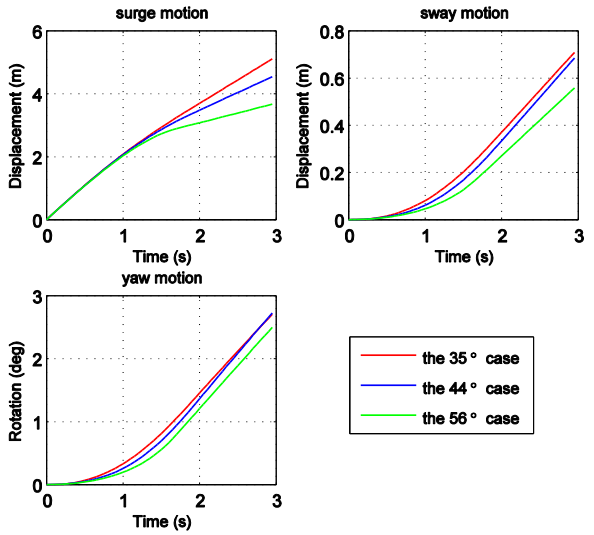

Figure 4-16. Ship motions in scenario 1

The external mechanics models are actually derived based on collisions between rigid bodies, i.e. the normal vectors of the contact plane will not change. However, large structural deformations may change the normal direction of the contact surface and also the collision angle. Figure 4-17 shows a sliding collision case between a supply vessel and a semisubmersible platform with a collision angle of 56°. The collision resistances and the force ratios are compared in Figure 4-18.

The duration of the collision process is much longer than that for collisions against a rigid plate. Unlike the ship-rigid plate collision, the force ratio oscillates more intensively. In the first 2 seconds, it oscillates about a mean value of 0.28. This value is close to 0.31 predicted by the decoupled method. However, the force ratio decreases after 2s and oscillates intensively about zero until the end of the collision. The curved geometry of the struck object and the deformation changes the collision angle significantly.

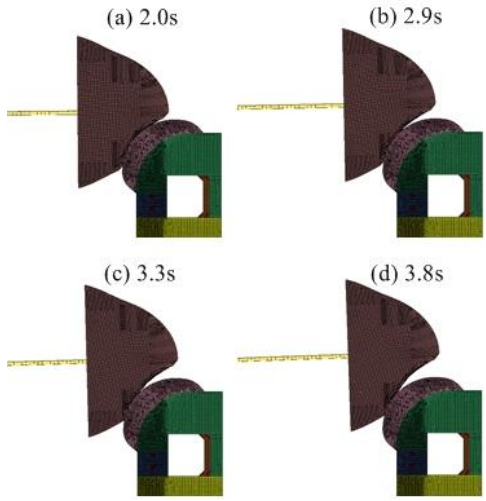

Figure 4-17. Snapshots during ship collision with the semisubmersible platform

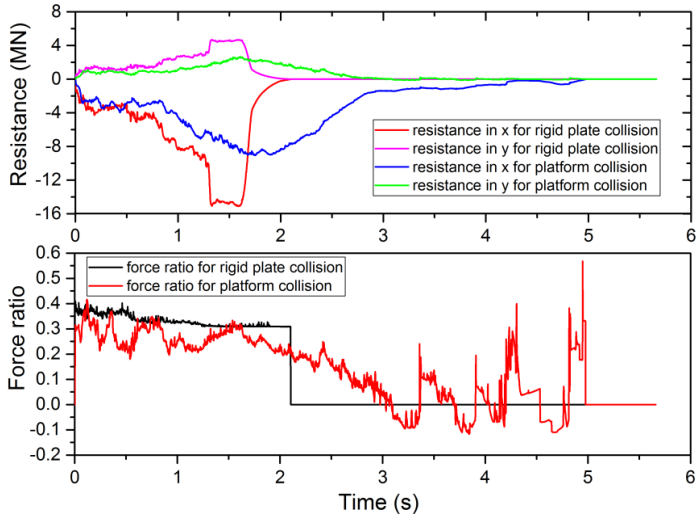

Figure 4-18. A comparison of the collision resistances and the force ratio

4.3.4 Determination of the normal vector of the contact plane

In the impact mechanics models, it is assumed that collisions occur between rigid bodies, and the striking and struck objects have a common contact plane at the contact point, thus a unique normal vector can be found. However, the colliding bodies are deformable in reality and the initial surfaces of both bodies do not necessarily share a common tangent plane before impact; in other words, the surfaces are initially nonconforming. It is therefore not straightforward to determine the input normal vector for the 6DOF external dynamic model. The normal vector may be based on either the undamaged surface of the striking or the struck object at the contact point.

It may be considered to use the stronger object to determine the normal vector. For example, for ship collisions with rigid plates in scenarios 1 - 4, the normal vector should be determined by the orientation of the rigid plates. For supply vessel-platform collisions in scenario 5, the normal vector is given by the stronger platform. Good accuracy is obtained in these cases. However, it is not always correct to use the normal vector of the stronger object as input. For example, if a rigid ship bow is assumed in scenario 5, the ship penetrates into the platform shell, and the platform deformation follows the shape of the bow front (see Figure 4-19). The out-of-plane ship motions are locked by the deformation of the platform, and little 3D effects are observed. This is somewhat analogous to bow collision with a ship side, where the ship side is weaker and deforms significantly. Figure 4-20 compares the energy dissipation from the coupled simulation with predictions from the external dynamic model with normal vectors from both the ship bow and the platform. It is found that the normal vector from the weaker platform gives the best results. The internal and friction energy are underestimated to some extent mainly due to the effect of the curved geometries; refer *Section 4.3.3*. Failure to identify the correct normal vector will yield inaccurate estimation of energy dissipation.

It requires good engineering judgements to determine the appropriate normal vector. From the limited simulation results, it may be recommended to use the normal vector of the initial surface of the stronger structure as input for structures, where 6DOF motions are not restricted by structural deformations. If the struck object is able to cover the ship, ship motions may be locked by structural deformations, and the 3DOF external dynamic model neglecting the roll motion is recommended for conservative consideration.

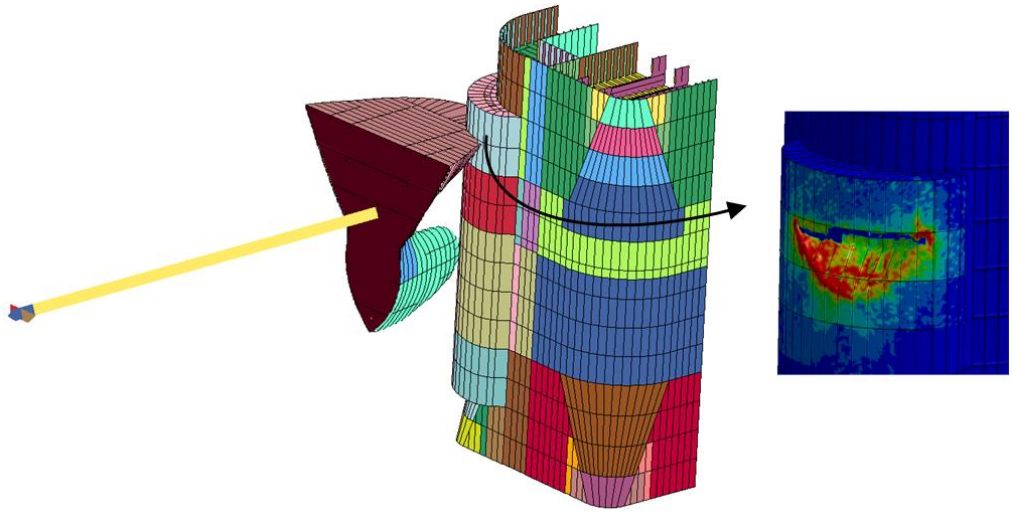

Figure 4-19. Damage created in a rigid ship-deformable platform collision

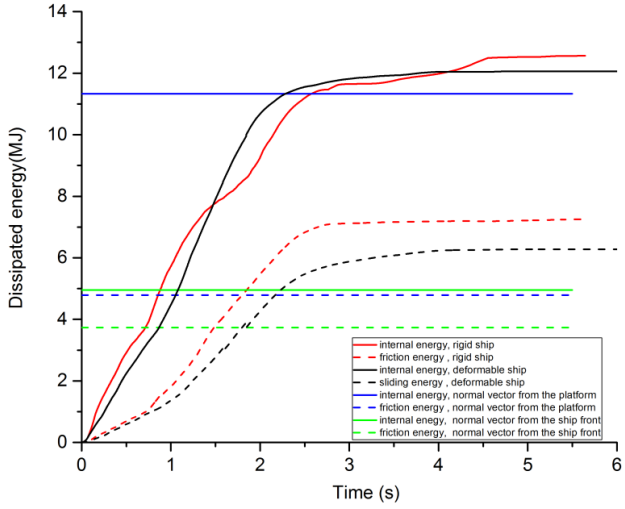

Figure 4-20. Energy dissipation with coupled and decoupled methods

4.3.5 Restitution factor

The restitution factor e in the external dynamic models is defined as the ratio between the normal relative velocity before and after impact (refer Eq. (4.4)), which is termed as the kinematic coefficient or Newton coefficient (Newton, 1686). If it is set as 0, it means that there is no relative velocity in normal direction (v_3^t=0). It is traditionally believed to be "conservative" with respect to energy dissipation. This enforced condition is one of the key boundary conditions for solving the motion of equations. However, zero restitution factor cannot guarantee a conservative prediction of energy dissipation since the velocity changes on the tangential plane are not included. The variation of dissipated energy with different restitution factors using the decoupled method is shown in Figure 4-21 for the 35° collision case in scenario 1. It is observed that the internal energy reaches its maximum when e equals 0 and decreases with an increase of the restitution factor. However, the friction energy increases continuously with e. The increase is virtually linear. The total energy is maximized when a certain non-zero restitution factor is used. The value is about 0.5 in this case.

$$e = -\frac{v_3^t}{v_3^0} \tag{4.4}$$

In general, the restitution ratio to maximize total energy dissipation varies with cases. This ratio can be found by iterating the external dynamic program with the restitution factor ranging from 0 to 1. However, in some cases, the maximum dissipated energy is reached for a restitution factor of 1.0 according to Liu and Hu (2017), which is not realistic. To be conservative without being unrealistic, it is recommended to use a restitution factor of 0.1 for engineering practice

based on observations from numerical simulations; see Table 4-2.

A different way to solve the problem has been proposed by Stronge (2000). He found that the use of the kinematic restitution factor in eq. (4.4) may lead to nonconservation of energy before and after collisions. To solve the energy inconsistence, he proposed a new definition of the coefficient termed as the energetic coefficient of restitution, see eq. (4.5). It is calculated from the ratio of elastic strain energy released during restitution over the internal energy during compression.

$$e_*^2 = -\frac{W_n(p_f) - W_n(p_c)}{W_n(p_c)} \tag{4.5}$$

where $W_n(p_c)$ is the work of normal force during compression, and $W_n(p_f)$ is the final work of normal force.

The energetic coefficient should be 0 for pure plastic impact. This definition has rarely been used in the external mechanic studies for ship or offshore structure collision problems. Further study on this aspect is recommended.

Table 4-2. Measured restitution factors for scenario 1 with varied collision angles

Collision angle (scenario 1)	35°	44°	56°	66°	88°
Measured restitution factor	0.19	0.18	0.12	0.08	0.08

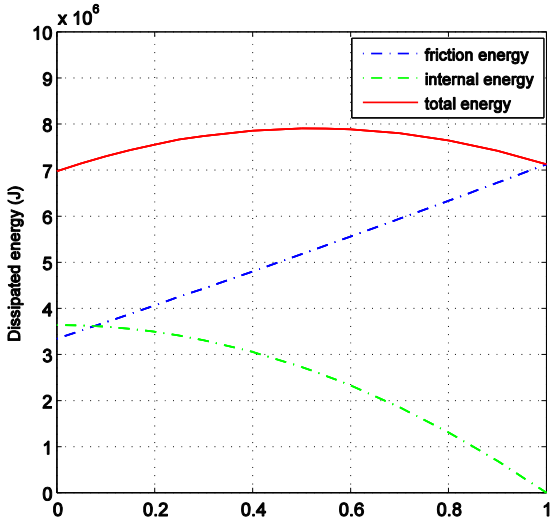

Figure 4-21. Variation of dissipated energy with the restitution factor for the 35° collision case

4.4 The influence of ship motions and fluid-structure interaction

4.4.1 Secondary impacts

Secondary impacts are observed in Figure 4-15 for collision against a rigid plate. They are mainly due to the periodic motions in heave, roll and pitch. Take the simple case in Figure 4-22 as an example, where the ship collides with a 35° oblique rigid plate with an initial velocity of 2.25 m/s. Roll motion is excited. The collision force histories, plotted in Figure 4-23, witness of secondary impacts. The ship normal velocity at the contact point decreases with excitation of sway, yaw and roll motions. The collision finishes when the relative velocity at the collision point in the normal ξ direction decreases to zero and rebound starts, i.e. $V_\xi - V_{sway,\xi} - V_{yaw,\xi} - V_{roll,\xi} \le 0$ (see Figure 4-24). Unlike sway and yaw motions, the roll motion is periodic. After $V_{roll,\xi}$ reaches its maximum, it decreases and may change sign. This increases V_ξ again and causes a second collision to occur. The same considerations apply also to heave and pitch motions. The velocity history for the roll motion is plotted in Figure 4-25. According to Figure 4-23, the first impact event ends at t=1.65s, which is close to the time when the roll velocity reaches its maximum (i.e. t=1.50s). It is the roll angular velocity rather than the roll angle itself that governs the secondary impact phenomenon. According to Figure 4-23, $V_{roll,\xi}$ is given as

$$V_{roll,\xi} = V_{roll} \cdot \frac{h_1}{\sqrt{h_1^2 + h_2^2}} \cdot \cos\alpha = \dot{\theta} h_1 \cos\alpha \tag{4-5}$$

$h_1 = 6.2m$, and the roll angular velocity is about $\dot{\theta} = 0.05\ rad/s$ at 1.65 s. Then $V_{roll,\xi}$ is calculated as 0.25 m/s. The energy carried by the roll motion is estimated to be only 0.33 MJ, which is quite small. However, during the period of contact loss, the yaw motion changes the collision angle significantly, yielding quite different energy dissipation (refer section 4.4.2).

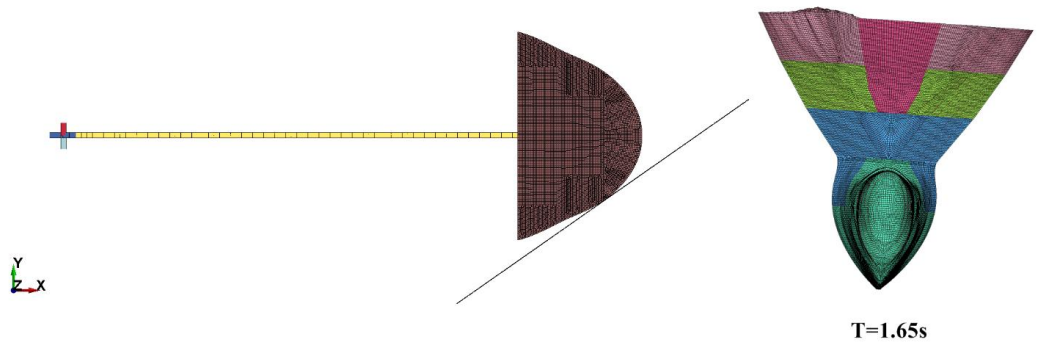

Figure 4-22. Ship collision with a 35° oblique rigid plate

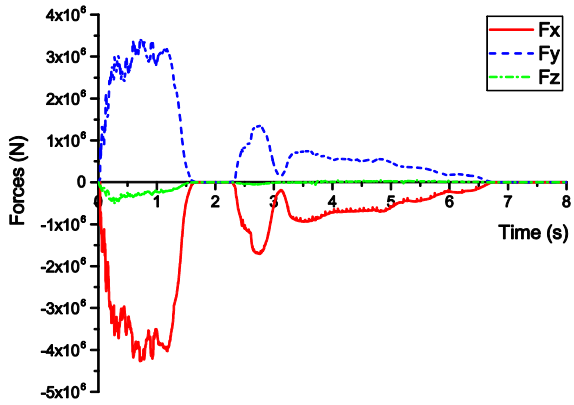

Figure 4-23. The collision forces for the oblique collision case, α=35°

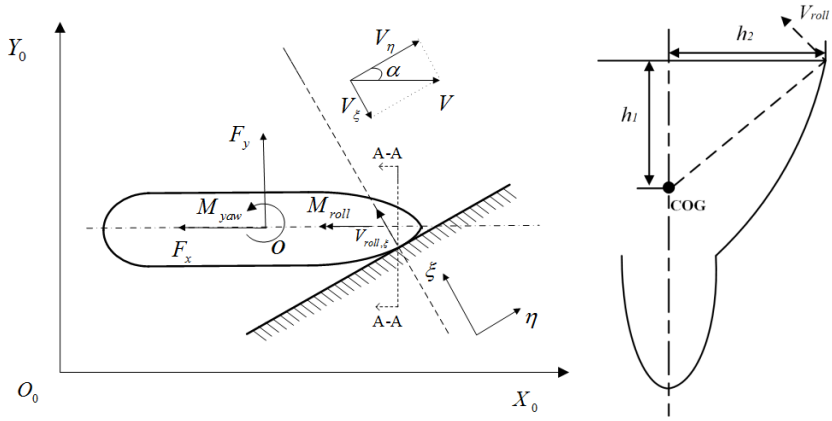

Figure 4-24. Loads and velocities during collision

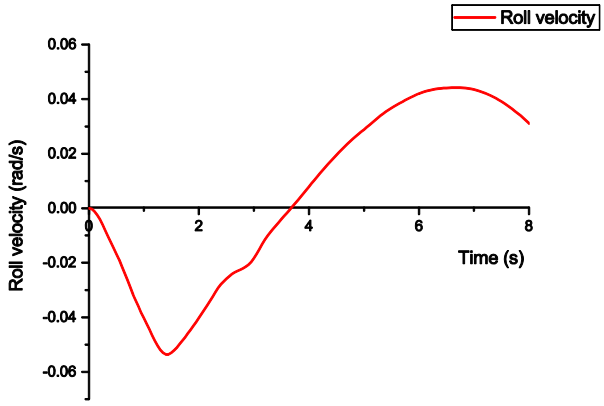

Figure 4-25. The roll velocity versus time for the oblique collision case

4.4.2 Energy dissipation

Figure 4-26 shows the dissipated internal and friction energy curves for scenario 1 with the collision angle of 35° and 56°, scenario 2 with the collision angle of 45°, and scenario 3. It is observed that for cases where the periodic motions are intense, secondary impacts will occur and dissipate considerable energy. The increased energy in secondary impacts mainly comes from friction energy contribution while the increase from the internal energy contribution is minor. For scenario1-35° where the roll motion is significant, it is found that the energy curves using the 3DOF and 6DOF coupled methods can be very different if secondary impacts occur. In cases where the roll velocity is small, the 3DOF and 6DOF coupled methods predict quite similar curves; refer scenario1-56°. The roll motion is small because of the counteracting effect of the bulbous bow.

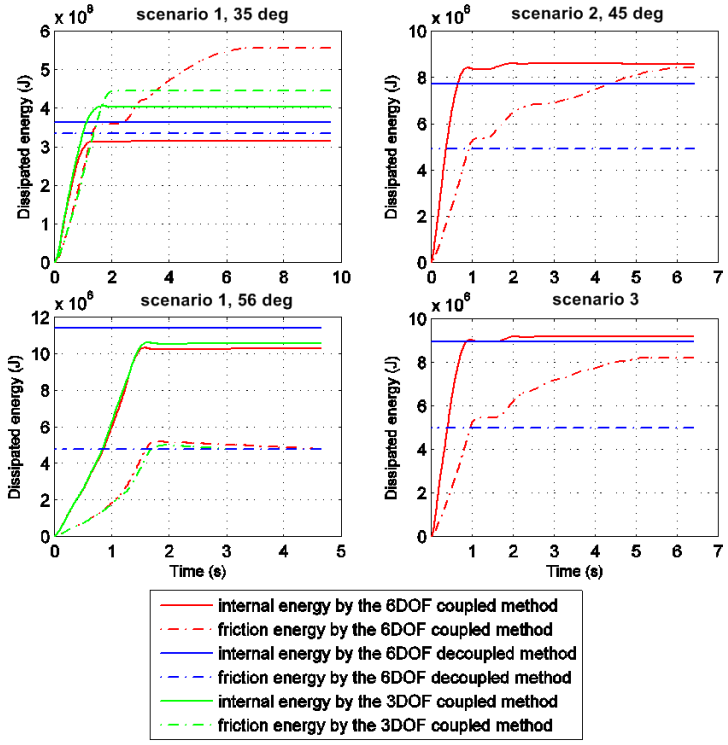

Figure 4-26. Dissipated energy of several typical cases

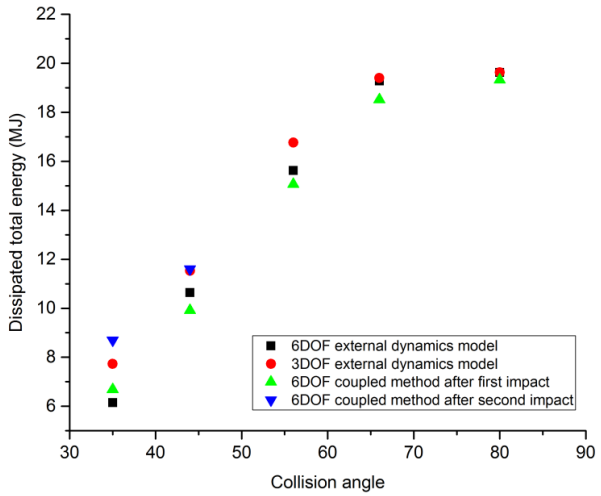

Figure 4-27. The predicted total energy absorption for scenario 1 with different methods

The dissipated energy for all cases are summarized in Table 4-3. The dissipated total energy of scenario 1 with different collision angles are plotted in Figure 27. It is found that, the energy dissipation predicted by the 6DOF decoupled method agrees well with results at the end of the first impact period for the 6DOF coupled model. In cases with secondary impacts, the decoupled method can be very unconservative since it captures only the first collision period, and underestimates significantly the entire friction energy.

At the end of the entire collision, the total energy is quite close for the 3DOF coupled method and the 6DOF coupled method, but the contributions from the internal and friction energy are different. This is because the roll motion is periodical. If the plate is long enough, the kinetic energy absorbed by the roll motion at the end of the first collision period will be dissipated in secondary impacts, anyhow. The internal energy and friction energy contributions are different because the collision angle changes significantly due to the yaw motion. The yaw angle is much larger for cases with secondary impacts. Therefore, to be conservative, it is recommended to use the planar 3DOF decoupled method, because the 6DOF decoupled method will significantly underestimate the total energy when a second collision occurs. The conclusions agree with experimental observations in Zhang et al. (2017).

Table 4-3. A comparison of dissipated energy with different methods (MJ)

Case No.	6DOF coupled method after the first impact			6DOF decoupled method		
	internal energy	friction energy	total	internal energy	friction energy	Total
Scenario1-35°	3.1	3.6	6.7	3.6	3.3	6.9
Scenario1-44°	5.4	4.6	10.0	5.5	4.3	9.8
Scenario1-56°	10.3	4.8	15.1	11.3	4.8	16.1
Scenario1-66°	14.4	4.1	18.5	16.0	3.3	19.3
Scenario1-80°	17.3	2.0	19.3	19.3	0.4	19.7
Scenario2-45°	8.3	5.4	13.7	7.7	4.9	12.6
Scenario2-60°	14.9	4.1	19.0	14.7	4.2	18.9
Scenario2-75°	18.4	1.7	20.1	19.0	0.7	19.7
Scenario3	8.9	5.5	14.4	8.9	5.0	13.9
Case No.	3DOF coupled method			6DOF coupled method after secondary impact		
	internal energy	friction energy	total	internal energy	friction energy	total
Scenario1-35°	4.0	4.4	8.4	3.2	5.6	8.8
Scenario1-44°	6.6	5.1	11.7	5.4	6.2	11.6
Scenario1-56°	10.6	4.8	15.4	--	--	--
Scenario1-66°	14.6	4.1	18.7	--	--	--
Scenario1-80°	17.4	2.1	19.5	--	--	--
Scenario2-45°	--	--	--	8.6	8.4	17.0
Scenario2-60°	--	--	--	--	--	--
Scenario2-75°	--	--	--	--	--	--
Scenario3	--	--	--	9.2	8.2	17.4

-- Not applicable

4.4.3 Penetration path and structural damage

Figure 4-28 presents the penetration paths of collision cases in scenario 1 evaluated by the decoupled method, the 3DOF coupled method and the 6DOF coupled method. The markers on the curves represent time points when the collision ends. For the decoupled method, 'collision end' means the point where the dissipated energy evaluated in the assessment of internal mechanics equals the energy calculated from the external dynamic models. For the coupled method, 'collision end' represents the moment when collision forces decrease to zero. Curves with two markers represent cases with secondary impacts.

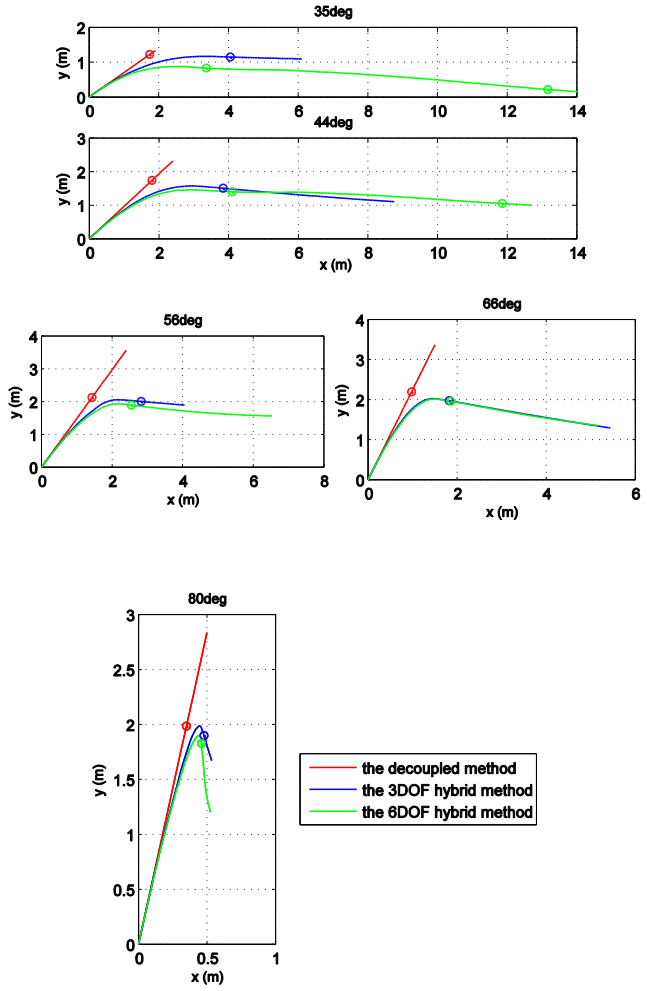

Figure 4-28. Global motions of the striking ship

It is observed that the decoupled approach predicts deeper penetrations normal to the contact plane but shorter transverse extent. The deviation is especially obvious for cases with small collision angles. The transverse damage is underestimated by about 50% for the 35°, 44°, 56° and 66° impact cases, where the striking ship and the rigid plate slide over each other. The deviation is small for cases with large collision angles, see for example case scenario1-80°. In cases with secondary impacts, the decoupled method is not able to capture a second collision. As ship structures are not homogeneous in general, the structural consequences can be very different for different collision paths. Tabri and Broekhuijsen (2011) compared the deformation energy required to breach an inner hull using the decoupled method and a coupled method. They found that the difference in required energy with the two methods could be up to 90% due to the path deviation.

The path deviation is mainly induced by the yaw motion. However, the roll motion also has

some influence as shown in the comparison of the blue and green curves in Figure 4-28. It is found that the penetrations are generally smaller when the roll motion is considered. In general, when more degrees of freedom are released, more kinetic energy will remain after collision because the structures are more compliant. The colliding bodies separate more easily, and less strain energy is dissipated. Similarly, in the grounding cases in scenario 2, the pitch and heave motions will induce path deviations.

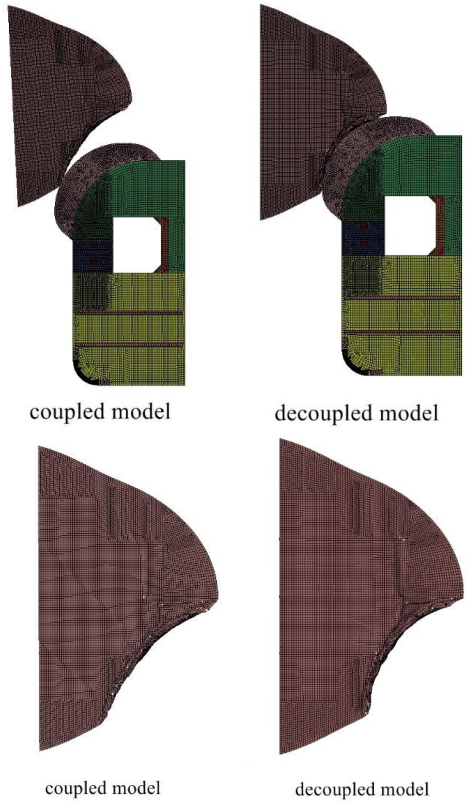

Figure 4-29. Structural damage with the coupled and decoupled method at the end of the collision

The damage extent calculated by the coupled and decoupled methods for the supply vessel collision with a cylindrical column of a semi-submersible platform is different as shown in Figure 4-29. The penetration normal to the collision plane is shallower with the decoupled method, and the tangential damage extension is larger. The deformation is elliptical rather than circular with the decoupled method. The coupled approach gives more realistic predictions of penetration paths and structural damage. In view of possible large prediction deviations of energy dissipation and structural damage when using the decoupled method, it is suggested to verify the critical cases with the coupled method.

4.4.4 The forward speed effect

The influence of forward speed is studied with the coupled model 2 by simulating up to a high collision velocity. Figure 4-30 compares ship motions with and without the forward speed effect

included for collision scenario 4. The speed is 5.56 m/s corresponding to a Froude number of 0.2. The kinetic energy is 116 MJ. Here t=0 represents the instant when the colliding bodies start to crush each other. The forward speed is found to have a limited effect up to a Froude number of 0.2, which is a significant speed for most collision scenarios. Consequently, it is concluded that zero speed potential-flow theory for seakeeping problems is sufficiently accurate for most collision and grounding scenarios if no incident waves are assumed.

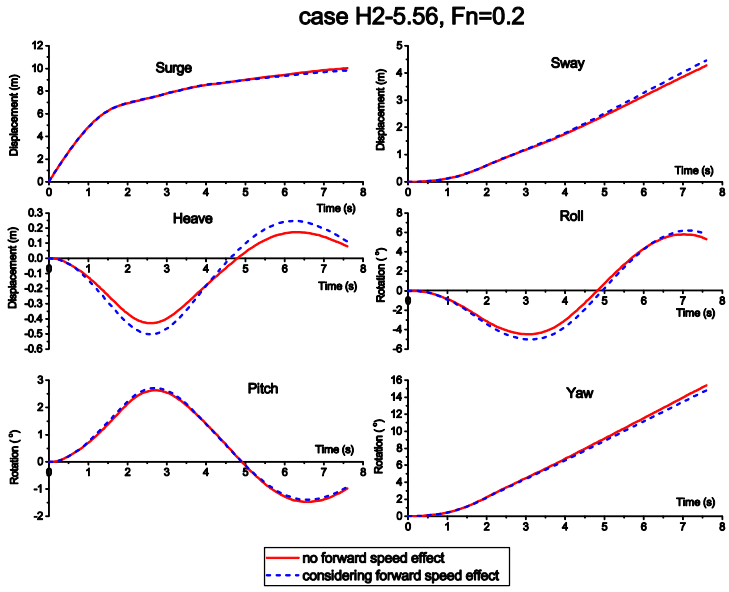

Figure 4-30. Ship motions with a collision velocity of 5.56 m/s

Chapter 5

Analysis and design of offshore tubular members against ship impacts

5.1 Introduction

Since the1980s, significant changes have taken place for collisions between service vessels and offshore platforms, notably the increase of supply vessel displacements, collision velocities, and new structure designs. A noticeable demonstration of the damage potential is the well workover vessel Big Orange XVIII collision with the Ekofisk 2/4 jacket platform. The kinetic energy was about 60 MJ, which is far beyond the current design energy 11 MJ. The accident caused severe damage to the three legged jackets and also the bow, see Figure 5-1. Several braces of the jackets were ruptured and the jacket had to be dismantled. This has triggered the need for revision of recommended practices for ship collisions design, and a new version DNV-GL RP C204 is under preparation.

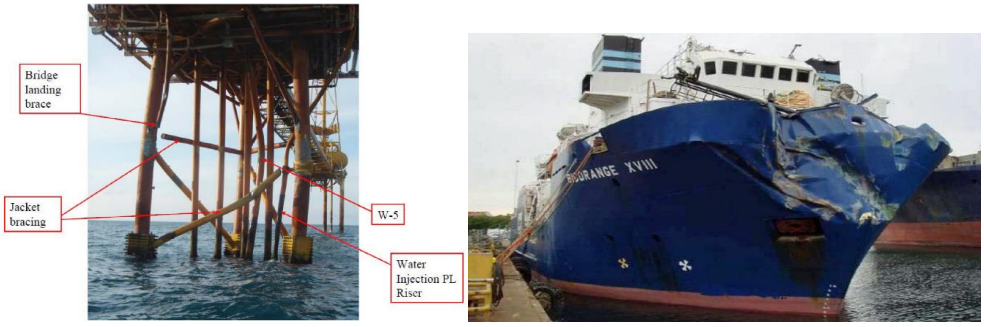

Figure 5-1. Big orange-Ekofisk 2-4/W collision

As concerns the impact responses of tubular members in offshore structures, an idealized model may be described as follows: the tubular brace/leg deforms first with local denting. At the same time, the plastic bending capacity of the dented brace is reduced. When a certain indentation is reached, the brace starts to collapse as a beam via a three-hinge mechanism. Upon further crushing of the brace, axial membrane forces develop and get dominant up to fracture if the adjacent structures are capable of providing sufficient strength against pull-in of the brace ends. Local denting may either cease or continue in the beam deformation stage. The responses of a single tubular member subjected to impacts were reviewed in *section 2.4*. The governing parameters for the impact responses of a brace/leg are quite a few such as tube length, diameter,

thickness, material properties, contact width, restraint conditions at tube ends, axial loading, striker geometry, impact locations, etc. The high number of parameters make the deformation mechanics of tubular members complicated.

Regarding the distribution of strain energy between two ships or a ship and a platform, three categories are often assumed: strength design, ductile design and shared-energy design; refer Figure 5-2.

- **Strength design** implies that the installation is strong enough to resist the collision force with minor deformation, so that the ship is forced to deform and dissipate the major part of the energy.
- **Ductility design** implies that the installation undergoes large, plastic deformations and dissipates the major part of the collision energy.
- **Shared energy design** implies that both the installation and ship contribute significantly to the energy dissipation.

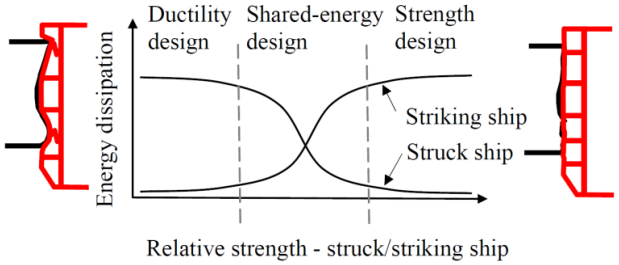

Figure 5-2. Energy dissipation for strength, ductile and shared-energy design (DNV, 2004)

Normal seized jacket braces are not strong enough to resist ship impact forces, and hence ductile design is often applied for tubular braces where the installations are assumed to dissipate most of the collision energy. However, as the design collision energy in NORSOK N-003 increases significantly, a single member cannot absorb the total collision energy in general. Based on a risk assessment, Moan et al. (2016) suggested the standard design energy for supply vessel bow collisions with offshore platforms should be increased from 11 MJ to 50 MJ. This will apply unless vessel size, operational restrictions etc are not put in place. Ductile design of braces and legs may not be appropriate because they will be subjected to very large deformations. This was shown by e.g. Amdahl and Johansen (2001), who simulated high energy ship bow-jacket collisions with kinetic energy in the range of 40-50 MJ. It may be necessary to go for strength design or shared energy design for braces/legs, where the ship should dissipate considerable energy. Braces/legs should not suffer major local denting in order to maintain sufficient bending capacity. Unfortunately, there are no commonly agreed requirements from rules and design standards for a brace/leg to maintain compactness during deformation.

The work goal presented in this chapter is to gain deep insights of the deformation behavior of tubular members and ship-platform interactions, and to establish practical suggestions for safe design of platforms against collisions. This will be done through literature review, simplified

analytical analysis and numerical simulation of tubular braces and legs impacted by a ship bow and two ship stern structures using the NLFEA code LS-DYNA. The main work in this chapter is presented in **Paper 4** (Yu and Amdahl, 2017a), and also some part in Yu and Amdahl (2017c) and Yu and Amdahl (2017b).

5.2 Ship collision with rigid braces and legs

5.2.1 FE modelling of supply vessel bow and sterns

The studied objects are one bulbous bow and two stern sections, belonging to two 7500 tons displacement supply vessels with modern design. The finite element models are presented in Figures 5-3, 5-4 and 5-5. The two sterns are quite different, and stern No. 2 has a large vertical section.

The relative strength of the striking and struck objects are very sensitive to material strength and rupture. The power law model was used to model the plastic strain hardening of steel. It includes a yield plateau that delays the onset of hardening. The RTCL damage criterion (Tørnqvist, 2003) with proper mesh scaling was used to model fracture. The details of the FE models, material properties, boundary conditions, etc, are presented in the appended **Paper 4** (Yu and Amdahl, 2017a).

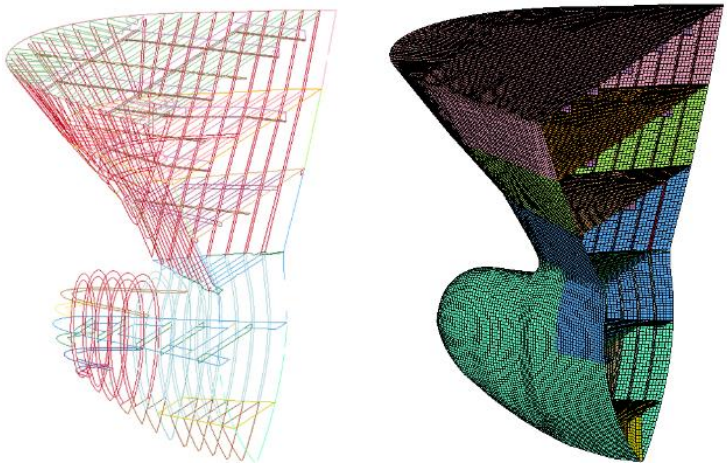

Figure 5-3. The FE model of the bulbous bow

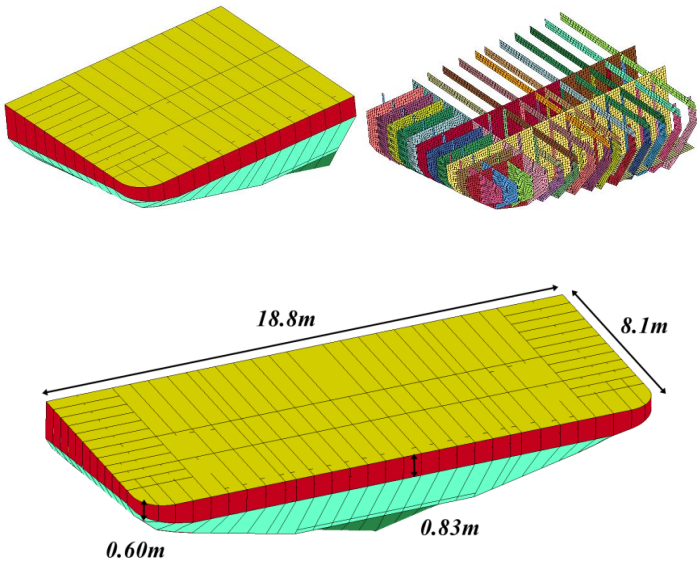

Figure 5-4. The finite element model of stern No. 1

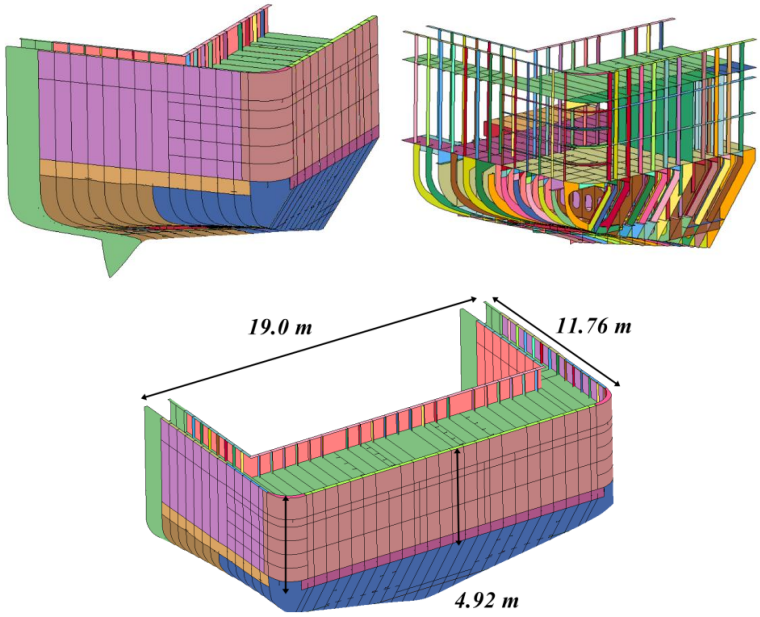

Figure 5-5. The finite element model stern No. 2

5.2.2 Resistance to penetration of rigid braces and legs

Rigid braces and legs are used first to crush the ship models. The resistance curves can be compared with the force levels in NORSOK/DNV RP C204. The standard vessel in the present

DNV-RP-C204 (2010) is a 5000-ton displacement supply, and the design resistance curves are given in Figure 5-6.

Take stern corner collisions with rigid tubes both in ship center line and at quarter width as an example. The tube diameters are 1.5 m and 10 m in correspondence with DNV rules. Collision with a rigid jacket leg with a batter of 1:8 and a diameter of 1.5m was also simulated. The force-displacement curves are plotted in Figure 5-7 for stern 1 and Figure 5-8 for stern 2 respectively, along with current design curves.

The collision forces of stern 1 follow the design curves well up to 1 m deformation, but becomes substantially larger beyond 2 m penetration. The sudden drop at a displacement of about 1m is caused by shell plate fracture. The force level for stern 2 exceeds the design curves substantially. Consequently, it is suggested that the standard design curve should follow the curves for the stronger vessel, i.e. stern 2.

For the 1.5 m rigid brace collisions, significant drops in the force level are observed for center collision, but not for quarter width collisions. The drops for center collision are due to shell plating fracture and buckling of the main girder. Design curves for stern end impacts are suggested to follow the curves of stern 2 in Figure 5-8.

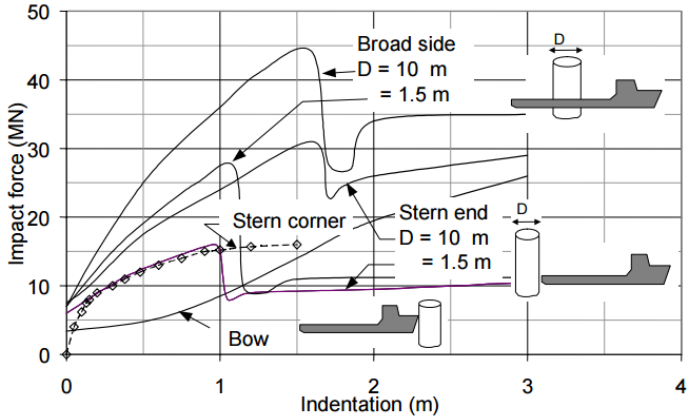

Figure 5-6. Recommended force-displacement curve for beam, bow and stern impacts (DNV, 2004)

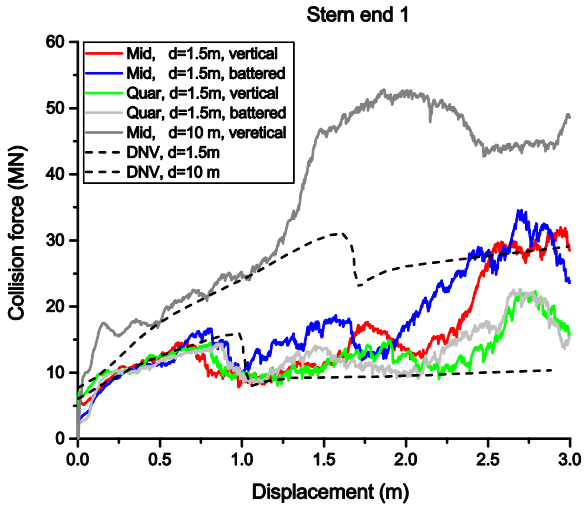

Figure 5-7. Force-deformation curves for the end of stern 1 collision against rigid braces

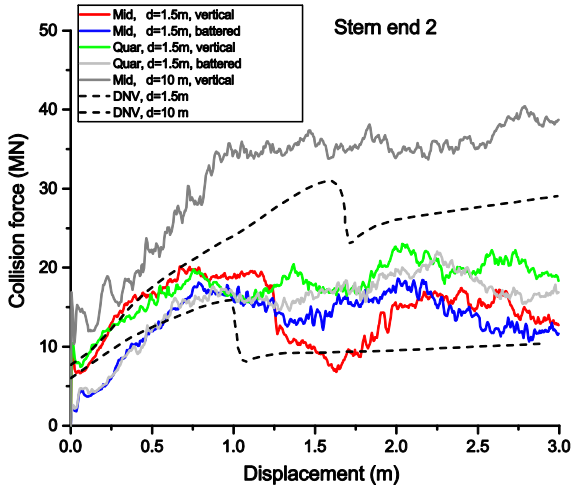

Figure 5-8. Force-deformation curves for the end of stern 2 collision against rigid braces

Resistance curves of bow collisions and stern corner collisions from numerical simulation and the present standard are compared in the appended **Paper 4**. Results show that the force levels in the present standard are low for the considerations of the modern ships, and should be increased accordingly.

5.3 Denting resistance of braces and legs subjected to lateral impacts

5.3.1 Extension of a local denting model

The formulas for the resistance of circular pipes to local denting have been reviewed in section 2.4.1, among which the Wierzbicki and Suh (1988) model gives a closed form analytical solution with the appealing form of simplicity.

$$R = 16\sqrt{\frac{2\pi}{3}\frac{D}{t}\frac{w_d}{D}}\cdot\frac{1}{4}\sigma_y t^2\sqrt{\left(1-\frac{1}{4}\left[1-\frac{N}{N_p}\right]^3\right)} \tag{5.1}$$

Where R is the indentation resistance, D is the tube diameter, t is the thickness, w_d is the denting depth. N and N_p are the instantaneous axial force, and the yield force in tension.

A factor that may limit its application is the assumption of point load. In real ship collisions, the loads are often distributed over a contact width denoted by B. This has been taken into account in the NORSOK denting resistance model given by:

$$R/R_c = \left(22+1.2\frac{B}{D}\right)\left(\frac{w_d}{D}\right)^{\frac{1.925}{3.5+\frac{B}{D}}}\cdot\sqrt{\frac{4}{3}\left(1-\frac{1}{4}\left[1-\frac{N}{N_p}\right]^3\right)} \tag{5.2}$$

The last term was borrowed from Wierzbicki and Suh (1988) to account for the effect of axial force on the leg. R_c is a characteristic resistance of the tube defined as:

$$R_c = \sigma_y\frac{t^2}{4}\sqrt{\frac{D}{t}} \tag{5.3}$$

The Wierzbicki and Suh (1988)'s derivation of energy dissipation is extended to account for distributed loads with a contact width of B using the following equation:

$$R = 16\left\{\sqrt{\frac{2\pi}{3}\frac{D}{t}\frac{w_d}{D}}\cdot\sqrt{1-\frac{1}{4}\left(1-\frac{N}{N_p}\right)^3}+\frac{B}{D}\right\}\cdot\frac{1}{4}\sigma_y t^2 \tag{5.4}$$

In the non-dimensional format, it reads:

$$\frac{R}{R_c} = 16\left\{\sqrt{\frac{2\pi}{3}\frac{w_d}{D}}\cdot\sqrt{1-\frac{1}{4}\left(1-\frac{N}{N_p}\right)^3}+\frac{B}{D}\sqrt{\frac{t}{D}}\right\} \tag{5.5}$$

In this way the resistance to denting is non-zero for zero indentation when the initial contact width $B > 0$.

5.3.2 Discussion of the models for local denting resistance

The local denting resistance models in *section 2.4.1* and *section 5.3.1* are studied by comparison with numerical simulation of braces impacted by rigid indenters with different widths. Two flat rigid indenters were modeled with a contact width of 0.6 m and 4.92 m, corresponding to the initial vertical height of the two sterns (see Figure 5-9). The tube had a length of 20 m, a diameter of 1.5 m and thickness varying from 30 mm to 50 mm. The tube ends were fixed against all motions.

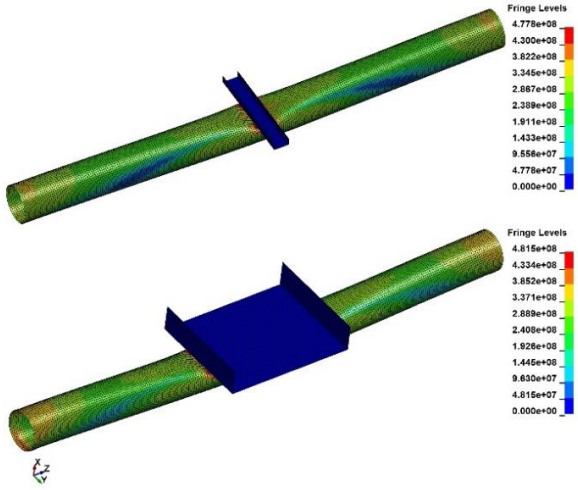

Figure 5-9. Impact responses of tubes with rigid indenters of different sizes

Comparison of the denting resistance obtained with different analytical models and numerical simulation is presented in Figure 5-10 for a tube thickness of 40 mm. Local indentation is defined as the original tube diameter less the residual 'diameter' of the dented cross section. It shows that the denting models predict the resistance for small contact widths reasonably well. For larger indentations, the force enters the bending and membrane stage. The membrane effect might be exaggerated by the boundary conditions assumed.

A detailed investigation of the NORSOK model and the modified Wierzbicki and Suh model is presented in Figure 5-11. The tube wall thickness varies from 30 mm to 50 mm. The NORSOK model works quite well for small contact width, but underestimates the resistance when the contact width is large. The underestimation increases with increasing tube wall thickness. The modified Wierzbicki and Suh model is more accurate for both small and large contact widths. The contact width effect is well captured by the second term in Eq. (5.4), which enables the denting force to start form a nonzero value.

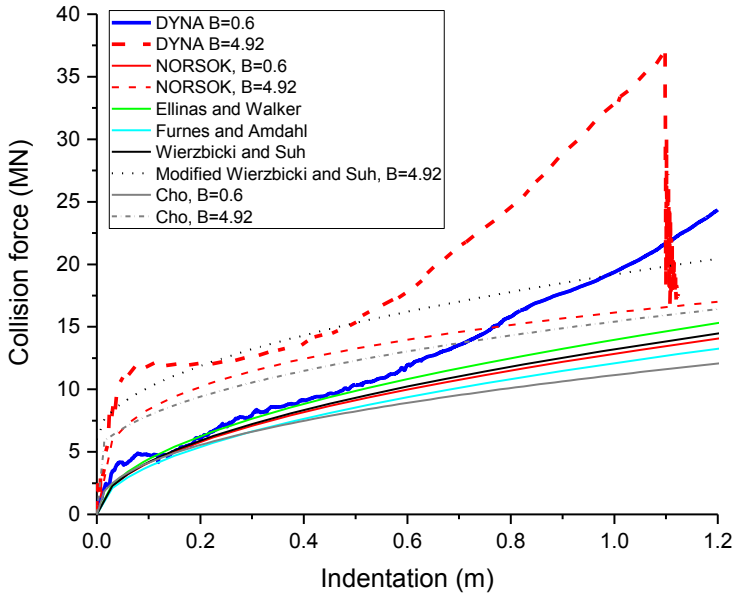

Figure 5-10. Comparison of denting resistances by DYNA simulations and analytical models

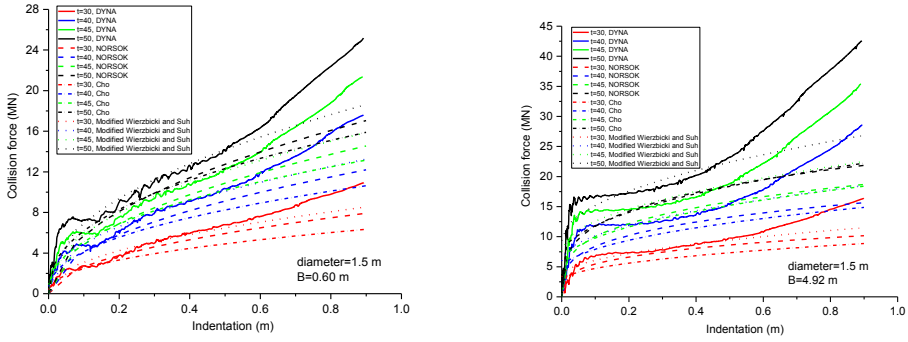

Figure 5-11. Comparison of denting resistances from impacts of a rigid indenter with contact widths B= 0.6 m and 4.92m

The NORSOK curve, the Cho model, the modified Wierzbicki and Suh model were further investigated where both the ship and braces were deformable. Stern corner impacts with a vertical brace were analysed. The brace length was 20 m, the diameter was 1.5 m and the wall thicknesses varied from 30 mm to 50 mm. The material yield stress was 285 MPa. The resistance curves are plotted in Figures 5-12 and 5-13. The dashed and dotted lines represent scenarios where the contact height is equal to the initial and maximum height of the stern corner for the two denting models, respectively.

The simulation shows that the denting resistance provided by both models is satisfactory, but the modified Wierzbicki and Suh model performs better for large contact heights and thick-walled tubes

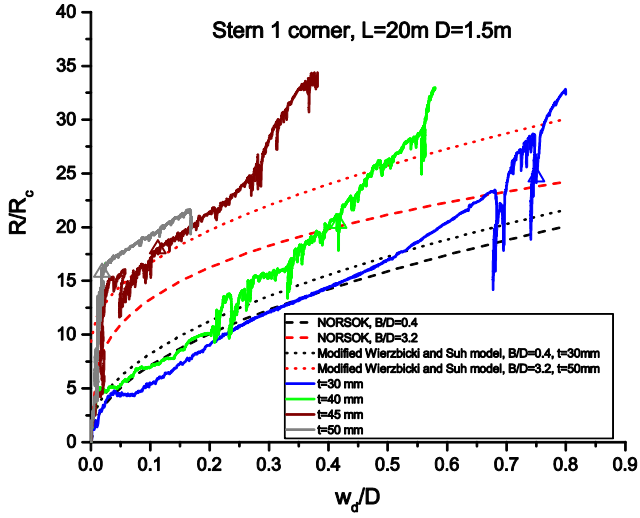

Figure 5-12. Comparison of denting resistance from impacts of the stern 1 corner

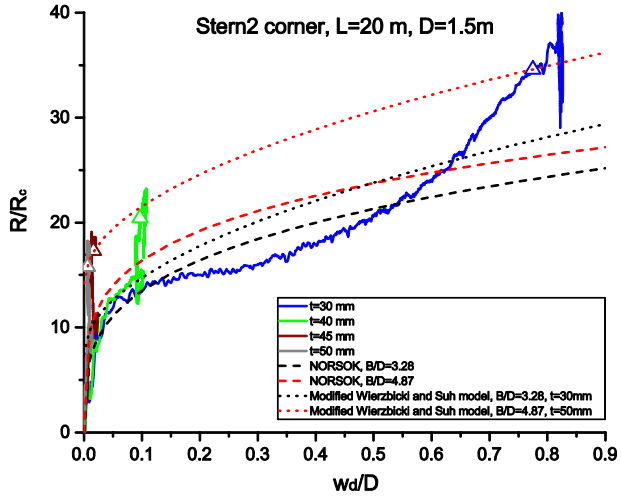

Figure 5-13. Comparison of denting resistance from impacts of the stern 2 corner

5.4 Transition from local denting to global bending

A brace/leg deforms first by local denting. The local indention decreases continuously the

plastic bending moment of the tube. There exists a certain transition indentation ratio, $w_{d,tran}/D$, beyond which the brace/leg starts to deform like a plastic mechanism. By further deformation, the resistance may remain constant, reduce or increase depending on the boundary conditions and the diameter over thickness ratio, see Figure 5-14.

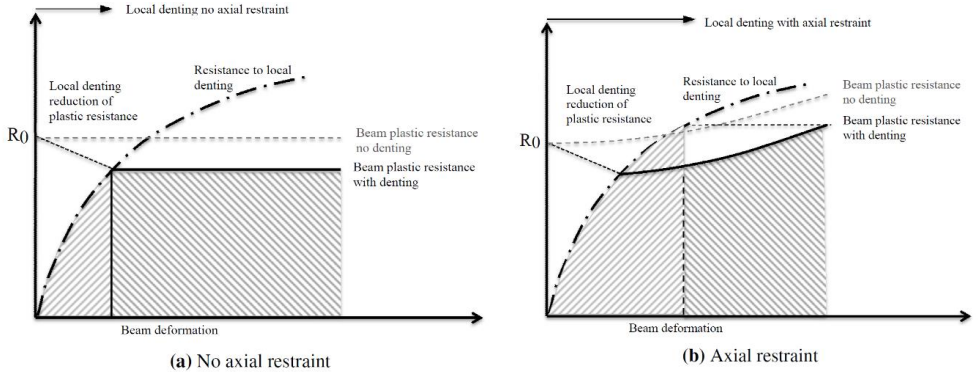

Figure 5-14. Plastic resistance vs beam deformation for varying axial restraint (From Storheim and Amdahl (2014)).

A few researchers have studied the transition from denting to global bending in the derivation of the resistance to denting, bending and membrane stretching, but little discussion on the transition indentation ratio exists. de Oliveira et al. (1982) proposed the following expression for the transition indentation ratio:

$$\frac{w_{d,tran}}{D} = 2(\lambda - \sqrt{\lambda^2 - 1}) \tag{5.6}$$

where

$$\lambda = 1 + \frac{\pi}{4} \cdot \left(\frac{L}{D}\right)^2 / \left(\frac{D}{t}\right) \tag{5.7}$$

According to Ellinas and Walker (1983), the transition indentation ratio can be found by solving the following equations:

$$\frac{w_{d,tran}}{D} = \left[16/K \cdot \frac{D}{L} \cdot \frac{D}{t}(1 + \cos\beta - \beta)\right]^2 \tag{5.8}$$

where

$$\beta = \left[1 - \frac{D}{t}\left\{\sqrt{16/9 \cdot \left(\frac{w_{d,tran}}{D}\right)^2 + \left(\frac{t}{D}\right)^2} - 4/3 \cdot \frac{w_{d,tran}}{D}\right\}\right] \cdot \sqrt{\frac{w_{d,tran}}{D}} \tag{5.9}$$

Neither model accounts for the contact width. If we combine the relatively conservative NORSOK denting model and the NORSOK residual bending-capacity model, a new expression is obtained for the characteristic transition indentation ratio $w_{d,tran}/D$ by solving:

$$\frac{R_0}{2R_c}\left(1+\sqrt{1-\frac{w_{d,tran}}{D}}-\sqrt{\frac{w_{d,tran}}{D}-\left(\frac{w_{d,tran}}{D}\right)^2}\right)=\left(22+1.2\frac{B}{D}\right)\left(\frac{w_{d,tran}}{D}\right)^{\frac{1.925}{3.5+\frac{B}{D}}} \tag{5.10}$$

For a brace with clamped ends, R_0 / R_c can be expressed as:

$$R_0 / R_c = 32\sqrt{\frac{D}{t}}\cdot\frac{D}{L-B} \tag{5.11}$$

$L-B$ is the effective brace length that is used to determine R_0. It is found that $w_{d,\text{tran}} / D$ depends only on two parameters, i.e. R_0 / R_c and B / D. This dependence is consistent with de Oliveira et al. (1982)'s model when B=0.

The transition indentation ratios predicted by the three models are compared with numerical simulations; refer **Paper 4**. It is found that all three models provide reasonably accurate predictions of $w_{d,tran}$/D for varying tube length, diameter and thickness. de Oliveira et al. (1982) model agrees best with numerical results. The proposed model has the advantage of accounting for the contact length. Numerical simulation results also show that there is a threshold $w_{d,tran}$/D value of 0.15, below which a brace/leg experiences negligible local denting before initiation of global bending. Figure 5-15 shows the variation of the transition indentation ratio for a large range of L/D and D/t values using de Oliveira et al. (1982) model. It is found that the large transition indentation ratios are concentrated in the region with small L/D and large D/t values.

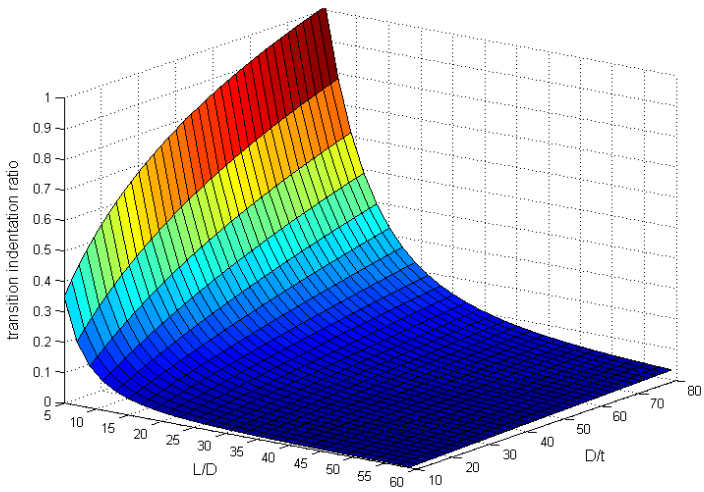

Figure 5-15. Variations of transition indentation ratios with L/D and D/t

The variations of $w_{d,tran}$/D with wall thickness, diameter and length are reflected in Eq. (5.11),

where R_0 / R_c varies with the powers of 3/2, -1/2 and -1 for the diameter, thickness and length of a brace/leg, respectively. Another important factor is the contact width B. On one hand, the contact width reduces the effective length in calculating R_0 and therefore gives a larger R_0 / R_c and subsequently a larger $w_{d,tran}/D$; on the other hand, the capability to resist local denting is enhanced with increasing contact width and this will reduce the $w_{d,tran}/D$. The tendency of decreasing $w_{d,tran}/D$ with increasing contact widths seems to be dominant.

5.5 Compactness requirements

5.5.1 A review of requirements to resist local denting

The existing requirements for a brace/leg to remain compact under lateral impact are generally based on experimental observations and numerical results, but theoretical supports are lacking.

Soares and Søreide (1983) proposed an analytical solution for the beam deformation of tubular members considering the interaction between bending moment and axial forces. Local denting was assumed to be negligible. Good agreement with numerical simulations was obtained for minor denting. They suggested that members with D/t of 35 or less and L/D up to 22, can be considered to maintain full bending capacity during sustained deformation in accordance with Sherman (1976)'s experimental observations.

The API rules (RP2A-WSD, 2000) prescribe $D/t < 9000/f_y; \left(f_y \, in \, MPa\right)$ to maintain full capacity trough plastic deformation. For $9000/f_y < D/t < 15000/f_y$, only limited capacity can be assumed.

The present NORSOK N004 (DNV, 2004) and DNV-RP-C204 (2010) require the following compactness criterion to avoid excessive local denting of the tube before the formation of a three-hinge collapse mechanism:

$$R_0 / R_c < 6 \tag{5.12}$$

Through observations of numerical simulations, Storheim and Amdahl (2014) showed that the criterion is overly conservative. They proposed to use R_c as a characteristic strength factor, and R_c should be larger than 1.7 for bow collisions and 1.3 for vessel side collisions to fulfill the compactness requirements.

Cerik et al. (2016) carried out extensive numerical simulations with ABAQUS and proposed to use the indicator R_0/R_c, to classify the impact responses of tubular members. Four response modes were suggested:

Mode 1: $R_0 / R_c < 6.5$; dominated by global bending

Mode 2: $6.5 \le R_0 / R_c \le 10$; dominated by both local denting and beam deformation, and local denting ceases immediately after plastic collapse.

Mode 3: $10 \le R_0 / R_c \le 23$; dominated by both local denting and beam deformation, and local denting continues after plastic collapse.

Model 4: $R_0 / R_c > 23$; dominated by local shell denting.

Mode 1 seems to agree with the present DNV-GL RP C204 standard (DNV-RP-C204, 2010).

5.5.2 Discussion

The existing compactness criteria and the transition indentation are connected. The R_0/R_c value in Eq. (5.11), depends on $D/(L-B)$ and D/t. If we assume conservatively that the contact width $B=0$, it is interesting to find that the R_0/R_c compactness criterion according to the NORSOK standard (DNV, 2004) and Cerik et al. (2016), and the D/t, L/D criterion by Sherman (1976) are similar, and by nature limits $w_{d,tran} / D$ to be within a certain range as indicated in Table 5-1. The API rules set limits only to the D/t values, and may not be sufficient to ensure compactness.

Table 5-1. The compactness criteria

	Sherman	Cerik et al.	NORSOK
Compactness criteria	D/t⩽35; L/D⩾22	R_0/R_c⩽6.5	R_0/R_c⩽6
Corresponding R_0/R_c	R_0/R_c⩽8.6	R_0/R_c⩽6.5	R_0/R_c⩽6
Corresponding w_{tran}/D	w_{tran}/D⩽0.12	w_{tran}/D⩽0.08	w_{tran}/D⩽0.07

The question arises: is it sufficient to limit the transition indentation ratio $w_{d,tran}/D$ to keep the cross sections compact during the beam bending phase? No, it is not; for stern corner 1 collision with the 20x1.0x20 tube, where the simulated $w_{d,tran}/D$ is only 0.008, local denting increases continuously during global bending as demonstrated by the plots in Figure 5-16(a). The front and rear sides of the brace is illustrated in Figure 5-17. Continuous increase of local denting is also observed for stern corner 1 collision with 20x1.6x20 tube where the transition indentation is large ($w_{d,tran}/D = 0.39$), see Figure 5-16(b). The membrane forces created by axially fixed ends may exaggerate local indentations at the late stage, but the simulations do prove the insufficiency of using the transition indentation ratio as a compactness criterion. In addition, the rear side deflection of the brace in Figure 5-16(b) is slightly negative in the denting phase, and this confirms the ovalization effect.

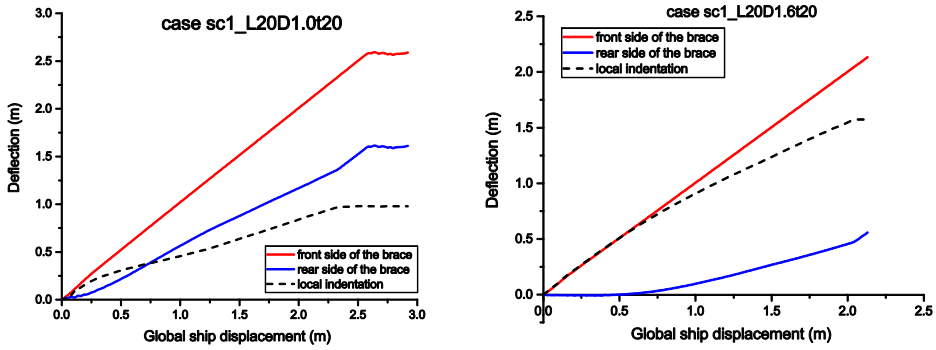

Figure 5-16. Deflection curves of nodes on the front and back sides of the brace (left): 20x1.0x20; (right) 20x1.6x20

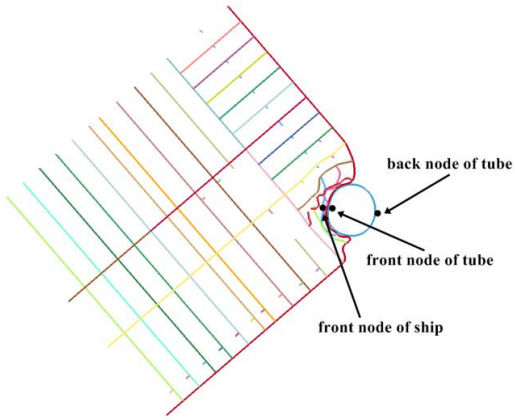

Figure 5-17. Sectional view of the ship stern corner-brace collision

To ensure compactness, the tube should be able to resist locally a certain force level for an indentation of, say for example 0.1D. This means that R_c should be larger than a certain value as proposed by Storheim and Amdahl (2014). They showed that the $R_0 / R_c < 6$ compactness requirement in NORSOK for bow-brace collisions was too conservative. However, it is found that the criterion itself is not necessarily conservative. Another requirement that is often assumed for strength design is that the plastic bending capacity of the brace R_0 should be no less than the maximum collision force $F_{\max}$ when the ship crushes into a rigid brace/leg, i.e. $R_0 \geq F_{\max}$. By satisfying both requirements, we obtain

$$R_c \geq \frac{F_{\max}}{6} \tag{5.13}$$

It is actually the combined requirement in Eq. (5.13) that is overly conservative.

5.6 Design of offshore tubular members against ship impacts

5.6.1 The effect of ship structure interactions

The ship platform interactions are illustrated with the stern end impact conditions as an example. The cases for ship bow and stern corner collisions can be found in the appended **Paper 4**.

Force deformation curves from simulation of stern end 1 and stern end 2 impacts on a vertical brace with 1.5 m diameter and varying thickness are plotted in Figures. 5-18 and 5-19. The brace length is 20 m. The collision force is plotted versus local denting and beam deformation of the brace as well as penetration of the stern end. The plastic collapse resistance for an undented brace, R_0, is indicated on the diagrams. The effective beam length is reduced for stern end 2 to account for the large contact height (4.92 m). For stern end 1 a concentrated contact force is assumed. During collision, the softer structure will deform and the impact force will be distributed over a larger contact area. This increases the resistance of the strong structure, and therefore there is an upward shift of the resistance curve for the stronger structure as shown in Figures. 5-18 and 5-19. In designing offshore platforms, load-deformation curves of ships and platforms are often established independently by disregarding the relative strength and assuming the other object as infinitely rigid. Shared energy design based on such independently obtained force curves may not give the correct energy distributions.

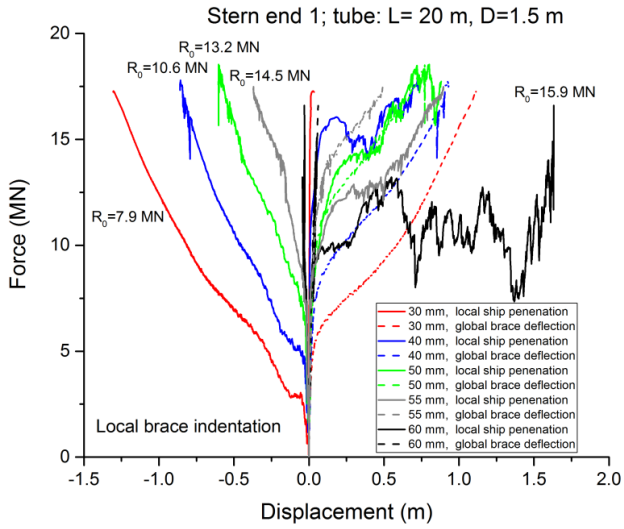

Figure 5-18. Force versus local indentation and beam deformation of brace and force-versus penetration of stern end 1-vertical brace with 1.5m diameter and varying thicknesses

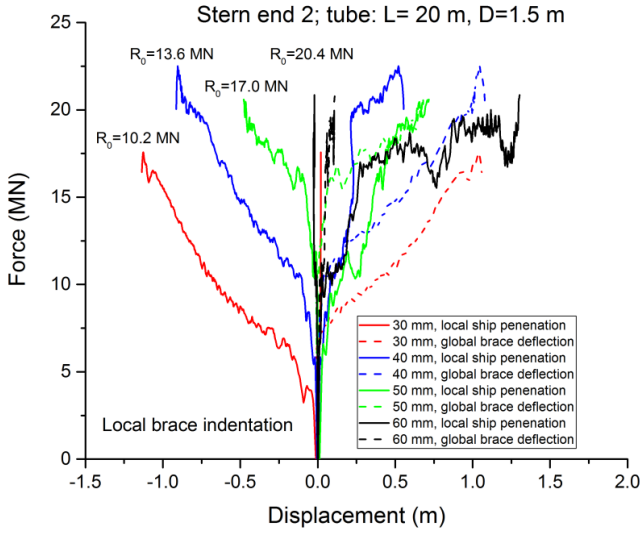

Figure 5-19. Force versus local indentation and beam deformation of brace and force-versus penetration of stern end 2 -vertical brace with 1.5m diameter and varying thicknesses

When the thickness is 30 mm, the brace undergoes severe denting and large beam deformation for stern end 1 impacts as shown in Figure 5-18. At maximum force, the cross-section is virtually flat and the brace acts predominantly by membrane tension, because the ultimate collapse resistance in bending (R_0 *=7.9 MN)* is small. The stern is not penetrated, even if the force level of 17 MN exceeds substantially the maximum resistance to penetration of a rigid brace, i.e. 12.5 MN. This illustrates the importance of interaction; the stern resistance to penetration by a dented brace is larger than that of a rigid brace.

The same behavior is experienced for a thickness of 40 mm, but ultimately, for a force level 16 MN, the brace starts to penetrate the ship. However, the brace has been pushed significantly into the tensile membrane action, and brace fracture due to excessive straining may take place. The stern's resistance to penetration continues to drop for 50 mm brace thickness, but significant brace denting and beam deformation take place. Evidently, the brace collapse resistance (R_0 = *13.2* MN) is not sufficient to avoid extensive brace damage. Only when the thickness is increased to 60 mm, with a collapse resistance of R_0 *=15.9* MN, neither local denting nor beam deformation take place. Thus, the transition to strength design takes place around 55-60 mm brace wall thickness for this brace configuration.

The brace response for stern end 2 impacts is similar, see Figure 5-19. The contact width is much larger for this vessel, so the stern's resistance to penetration increases, but this is also the case for the brace collapse resistance. For wall thicknesses up to 50 mm, the brace undergoes extensive denting, but with 60 mm thickness, the brace is capable of penetrating the stern

without local denting and beam bending. The corresponding $R_0 = 20.4$ MN is close to the stern's resistance to penetration. Again, for this brace configuration the transition to strength design takes place for brace wall thickness of 55-60 mm with the corresponding $R_c \sim 1.12\text{-}1.28$ MN; In addition, the bending resistance, R_0, accounting for the contact height, should exceed the stern's resistance to penetration.

5.6.2 Design against ship collisions

The design of platform braces/legs against ship impact may be carried out in the ductile, shared-energy or strength design domain. The governing factor is the resistance to plastic collapse in bending, R_0. If the resistance is larger than the force that the ship will produce when penetrated by a rigid tube, the ship will predominantly dissipate the collision energy, i.e. the brace/leg response is in the strength domain. Normally, the collapse in bending is calculated for a "perfect" circular pipe, which is representative for pipe with no or small dents. In order for this to be valid, the brace/leg must comply with compactness requirements, R_c, with respect to local denting. In addition to reducing R_0, any denting will also increase the ship force, because the resistance to penetration of the ship is larger for a dented pipe than a rigid pipe.

If R_0 is less than the ship's resistance to penetration, the brace/leg will be in the shared-energy or ductile domain with small or no contribution to the energy dissipation from the ship. Depending on the dimensions and material strength, the brace/leg may dissipate considerable energy by beam bending and later by membrane forces at large deformations provided that the ends have some restraint against inward motion. Any local denting will contribute to the energy dissipation as well. However, it may be advisable to avoid significant local denting for two reasons:

1. With little local denting, simple plastic beam theory applies
2. Local denting reduces the energy dissipation, and the resistance of sections dented beyond brace/leg radius is uncertain

On the other hand, denting plays a less role in membrane stage, because the axial capacity is in principle not impaired.

By analyzing numerical simulation results, a new compactness criterion, R_c, that depends on the maximum collision resistance of the ship bow penetrated by rigid braces/legs, F_{max}, is suggested for bow-brace collisions:

$$R_c \geq 1.9 \frac{F_{\max}}{24} \tag{5.14}$$

For stern corner collisions and stern end collisions, a constant R_c of 1.2 MN and 1.5 MN is suggested. Further details are given in the appended **Paper 4**.

Chapter 6

Resistance to large inelastic deformations of stiffened panels subjected to lateral loading

6.1 Introduction

Stiffened panels are widely used in ships, offshore platforms and other engineering structures. A typical stiffened panel in a ship side or bottom is shown in Figure 6-1. They are often exposed to the actions from explosions, ship collisions, violent water slamming, ice crushing and dropped objects. Potential consequences may vary from minor local deformations to major structural damage and plate rupture, causing compartment flooding or oil leakage. Consequently, it is crucial to estimate the resistance of stiffened panels with reasonable accuracy.

Experimental methods and NLFEA methods have often been applied to evaluate the deformation and resistance of stiffened panels, refer e.g. Alsos et al. (2009), Liu et al. (2015a) AbuBakar and Dow (2013), Xu and Soares (2012), Xu et al. (2013), Ghavami and Khedmati (2006), etc. Simplified methods are advantageous for early design purposes, but little work has been presented regarding simplified assessment of large deformation resistance of stiffened panels. The simplified model presented by Cho and Lee (2009) addressed only the energy dissipation after collision. Considering the confinement effect in the longitudinal and transverse directions, a few expressions for the resistance of stiffened panels under blast loads can be found in refs. Manolakos and Mamalis, 1988, Jiang and Olson, 1995, Schubak et al., 1991, Louca et al., 1998. The main focus was on the dynamic effects, and the plastic interaction (yield) functions for stress resultants were simplified. Schubak et al. (1993a,b) presented a rigid plastic model with clamped ends and partial end fixity subjected to uniformly distributed blast loads. The plastic neutral axis was assumed to coincide with the centroid axis, the plastic interaction curve was asymmetric and was later simplified as piecewise linear curves. Amdahl (2005) proposed a model for the resistance of stiffened panels with fixed end conditions subjected to explosions with more refined yield functions. Daley et al. (2016) developed a model for the resistance of flat bar stiffened plates subjected to ice loading: the effect of bending and shear was discussed while any axial force was not considered.

Jones (1973) proposed an analytical formulation that accounted for the effect of inward flexibility at beam ends. A drawback of this method was that the flexibility was proportional to the square of the deflection, which made it difficult to associate it with physical properties of a

structure. Hodge Jr (1974) and De Oliveria (1981) presented simple expressions where elastic translational and rotational flexibilities at the boundaries were accounted for. They showed that the translational stiffness at beam ends was crucial for the development of membrane forces during large deformation.

In this chapter, a simplified formulation is presented for the large deformation resistance of stiffened panels subjected to lateral loading, where axial flexibilities at the boundaries are accounted for. This is also presented in **Paper 5** (Yu et al., 2017).

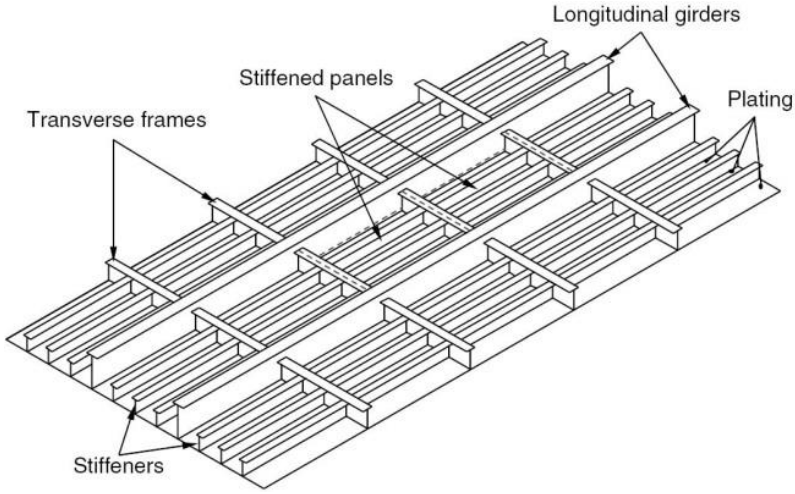

Figure 6-1. Stiffened panels

6.2 Yield functions based on generalized forces

The subject of this study is a stiffened panel with a vertically asymmetric I-profiles, as shown in Figures 6-1 and 6-2 (a). The areas of the plate flange, the top flange and the stiffener web are denoted A_p, A_t and A_w, respectively. h_w denotes the height of the web. It is presupposed that the area of the plate flange is larger than or equal to the area of the stiffener (top) flange and the web such that $A_p \geq A_w + A_t$. This assumption is valid for most stiffened panels used in ships and offshore installations.

The material is assumed to be rigid perfectly plastic with a yield strength of σ_y. The following approximations are introduced in the calculation of the plastic bending moment:

- The contribution from the large plate flange is small because the plastic neutral axis is located in the plate flange.
- The distance from the web toe to the true neutral axis, z_1, in the plate flange is neglected.
- The thickness of the stiffener top flange is assumed to be small compared to the web height, h_w, and is neglected.

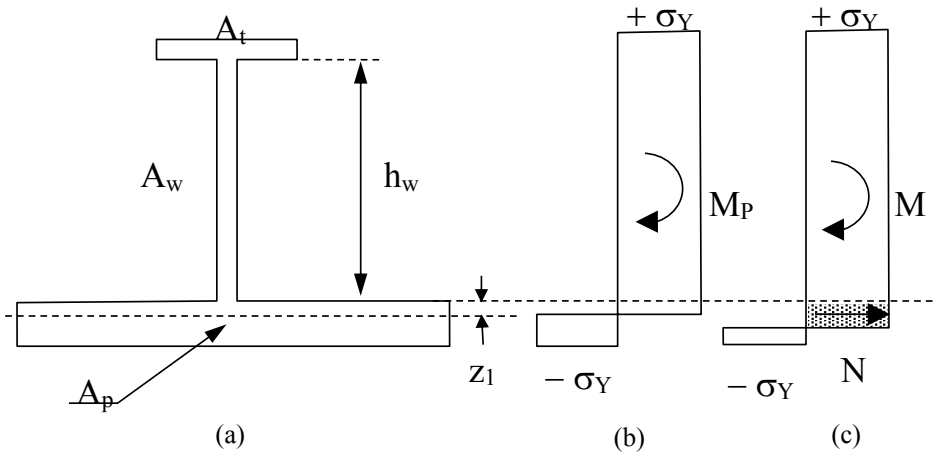

Figure 6-2. Stiffened panel cross section subjected to bending and tension

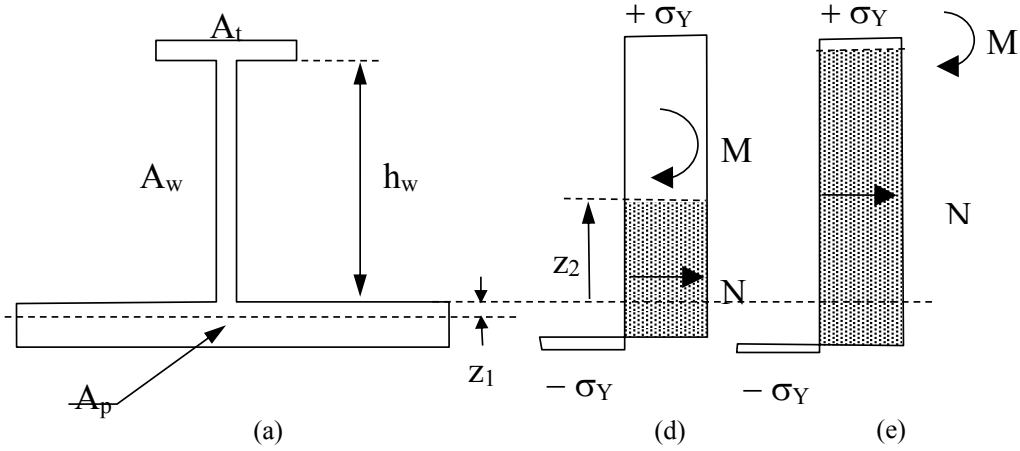

Figure 6-3. Plastic stress distribution in stage 2

In deriving the interaction functions, the effect of shear deformation is assumed to be negligible. If the cross section, that is fully plasticized in bending, is subjected to an increasing membrane tension force, as shown in Figure 6-2(c), a part of the compression field below the plastic neutral axis, z_1, has to change to yielding in tension. An equal area of the tension field above the plastic neutral axis will be "occupied" by the axial force, N. The total area "occupied" by the tension force is indicated by the shaded area in Figure 6-2(c). Depending on the magnitude of the axial force, the response of the stiffened panel may be split into four different stages.

- Stage 1: Tension force in the plate flange only; Figure 6-2(c)
- Stage 2: Tension force in the plate flange and web; Figure 6-3(d)
- Stage 3: Tension force in the plate flange, web and top flange; Figure 6-3(e)
- Stage 4: Pure tension force

Figure 6-4 shows the non-dimensional interaction functions of bending moments and axial forces for given A_p / A_s and A_w / A_t ratios. The A_p / A_s ratio plays a dominant role in determining the shape of the interaction curves, while the effect of the A_w / A_t ratio is smaller. The interaction curve approaches asymptotically that of a rectangular cross section when $A_p / A_s = 1$ and $A_w / A_t \to \infty$. The interaction becomes more linear for symmetric I-profiles.

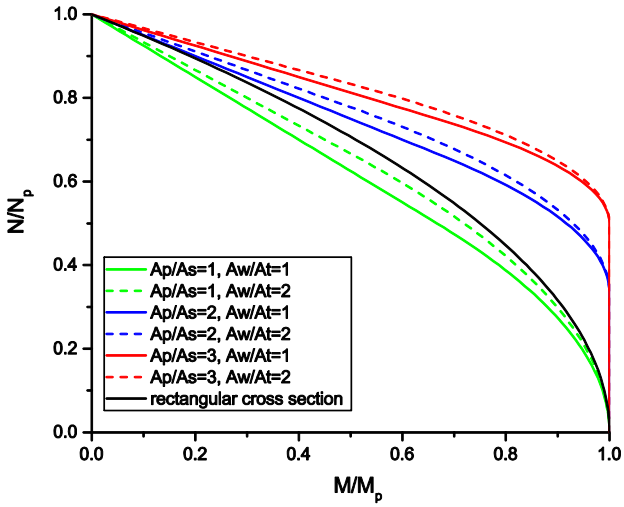

Figure 6-4. Non-dimensional interaction functions of bending moment and axial forces

6.3 Resistance of stiffened panels at finite deformations

A stiffener with associated plate flange under the action of a lateral load is shown in Figure 6-5. The detailed derivation for the resistance is presented in **Paper 5** (Yu et al., 2017), and is omitted here. Only the final expressions are summarized.

The non-dimensional resistance for the general loading case in Figure 6-5 reads:

$$\frac{P}{P_0} = \frac{M}{M_p} + \frac{Nw}{\beta M_p}; \quad \beta = \begin{cases} 1 & \text{free rotation} \\ 2 & \text{fixed rotation} \end{cases} \tag{6-1}$$

where:

$$P_0 = \beta M_p \left(\frac{1}{\alpha L_{eff}} + \frac{1}{1-\alpha\ L_{eff}} \right)$$
$$M_p = \sigma_y \left(\frac{1}{2} A_w h_w + A_t h_w \right) \tag{6-2}$$
$$N_p = \sigma_y A_e$$

The development of the membrane force is determined by:

$$\frac{N}{N_p} = \left(\frac{16}{\beta^2 c} \left(\frac{A_w}{A_e} \right)^2 - \left(2\frac{A_p}{A_e} - 1 \right) \right) \left[\exp\left(-\frac{\beta c}{4} \frac{A_e}{A_w} \frac{w}{h_w} \right) - 1 \right]$$
$$+ \frac{4}{\beta} \frac{A_w}{A_e} \frac{w}{h_w}; \quad \left(stage\,1,2,3 : \frac{N}{N_p} < 1 \right) \tag{6-3}$$
$$\frac{N}{N_p} = 1; \quad stage\,4$$

c is the non-dimensional stiffness factor $c = \dfrac{k_{eq} h_w^{\,2}}{\alpha\ 1-\alpha\ L_{eff} N_p}$.

The development of the bending moment is calculated from:

$$\frac{M}{M_p} = 1; \quad \left(stage\,1 : \frac{N}{N_p} \le \frac{2A_p}{A_e} - 1 \right)$$
$$\frac{M}{M_p} = 1 - \frac{1}{4} \frac{1}{1+2\dfrac{A_t}{A_w}} \left(\frac{A_e}{A_w} \right)^2 \left(\frac{N}{N_p} - \left(\frac{2A_p}{A_e} - 1 \right) \right)^2; \quad \left(stage\,2 : \frac{2A_p}{A_e} - 1 < \frac{N}{N_p} < 1 - \frac{2A_t}{A_e} \right) \tag{6-4}$$
$$\frac{M}{M_p} = \frac{\dfrac{A_e}{A_w}}{1+2\dfrac{A_t}{A_w}} \left(1 - \frac{N}{N_p} \right); \quad \left(stage\,3 : 1 - \frac{2A_t}{A_e} \le \frac{N}{N_p} < 1 \right)$$
$$M = 0; \quad stage\,4$$

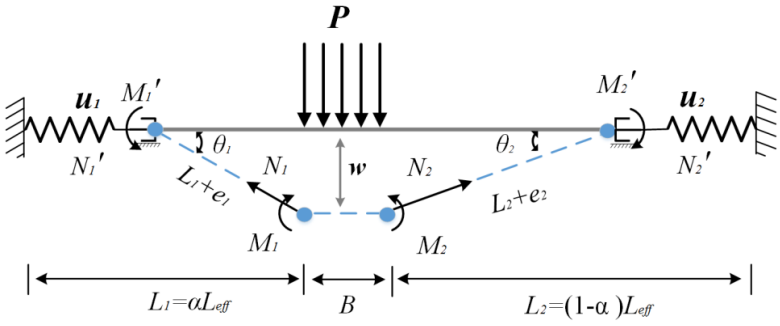

Figure 6-5. Beam collapse mechanism in a general loading condition

The resistance versus deformation is plotted in Figure 6-6 for stiffened panels with cross section T6 (see *section 6.4.1*) and various degrees of axial stiffness. When c approaches infinity, the solution converges correctly to the solution for fixed ends in the entire deformation range. For all values of c, when the deformation becomes sufficiently large, the resistance converges to the pure tension solution for fixed ends.

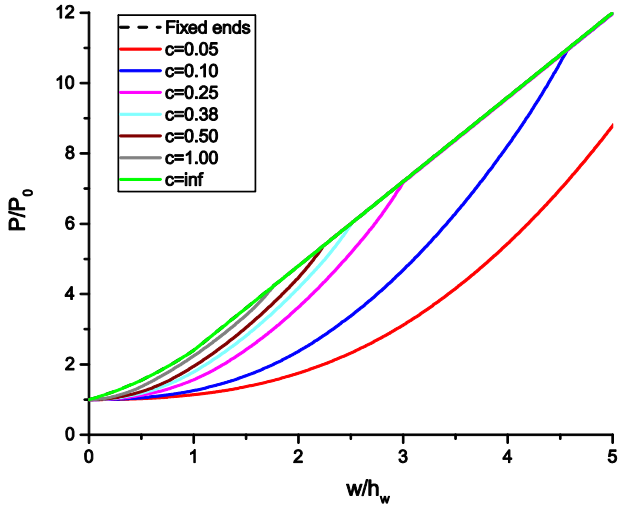

Figure 6-6. Resistance-displacement curves for fixed-end T6 stiffened panel given different translational stiffness

6.4 Comparison with nonlinear finite element analysis

6.4.1 Finite element models

To verify the simplified method, numerical simulations of 5 m stiffened panels struck by a flat indenter with a constant velocity of 0.2 m/s at mid-span were conducted with the nonlinear finite element code LS-DYNA 971. The studied stiffened panels are long enough to ensure that response is dominated by bending and axial force with negligible shear effect. The shear effect will be studied later with shorter stiffened panels. The panels had different A_p / A_s and A_w / A_t ratios and stiffener area $A_s = A_w + A_t$; refer to Table 6-1. The typical FE mesh is shown in Figure 6-7.

Table 6-1. Dimensions of different stiffened panel cross sections (Unit: mm)

Cross section type	A_p/A_s	A_w/A_t	A_p	A_w	A_t
T1	1	1	600 x 8	240 x 10	200 x 12
T2	1	2	600 x 8	200 x 16	160 x 10
T3	1	3	600 x 8	300 x 12	100 x 12
T4	2	1	600 x 8	150 x 8	120 x 10
T5	2	2	600 x 8	160 x 10	100 x 8
T6	2	3	600 x 8	180 x 10	100 x 6
T7	3	1	600 x 8	160 x 5	100 x 8
T8	3	3	600 x 8	120 x 10	50 x 8

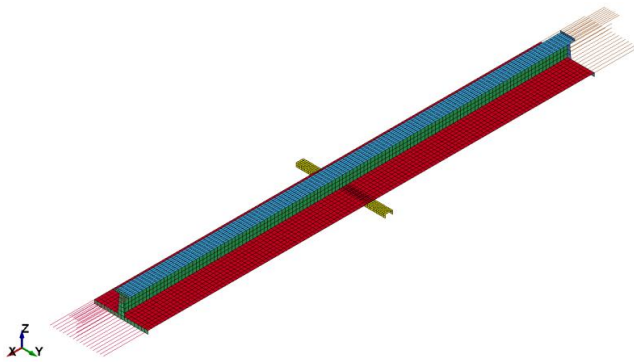

Figure 6-7. An example of a stiffened panel model

Two different materials were used, with stress-strain curves plotted in Figure 6-8. Because the simplified method is based on a rigid perfectly plastic material, material 1 had small, linear hardening. Moderate hardening is needed to avoid excessive concentrations of plastic strains in narrow regions, which would yield imprecise response predictions. Material 2 had a more realistic hardening, which was represented with the power law model. The material properties are given in Table 6-2. Fracture was not considered for material 1, whereas the RTCL fracture criterion (Tørnqvist, 2003) was used for material 2.

Table 6-2. Material properties for stiffened panels

Material	*Hardening type*	σ_y *(MPa)*	*E (GPa)*	*K (MPa)*	*n*	E_t *(MPa)*
Material 1	Linear	355	207	-	-	400
Material 2	Power law	355	207	780	0.22	-

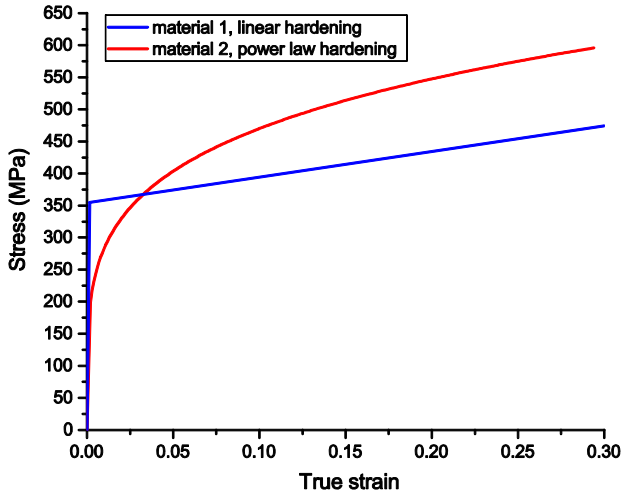

Figure 6-8. Stress-strain curves for the two materials

6.4.2 Resistance with infinite or finite stiffness against inward motion

The resistance-displacement curves predicted with the simplified method are compared with results from LS-DYNA for the cases in Table 6-1 in Figures 6-9 and 6-10. Good accuracy is found, especially for material 1 with soft hardening. For material 2 the simplified method tends to underestimate the resistance as the lateral deflection increases. The difference is especially apparent in the pure tension stage. This is because the forces are nondimensionalized with P_0 using the initial yield stress σ_y, while the resistance predictions, P, are based on the flow stress σ_{flow}. Thus, there is a slope difference of σ_{flow}/σ_y between the prediction and the simulated resistance curves. $\sigma_{flow}=\left(\sigma_y+\sigma_u\right)/2$ may be used instead of σ_y in the pure tension stage for materials with significant hardening. σ_u is the ultimate strength of the material. Local buckling of stiffeners may occur during deformation accompanied by a force drop, but this has limited influence on the prediction accuracy of the proposed simplified model because it mainly reduces the bending moment and has little influence on the membrane force. Buckling occurs usually after a displacement of several times the stiffener web height. The stiffened panel develops quickly into the full tension stage, with little bending moment remaining after a displacement of stiffener height, and the resistance is thus only slightly influenced by stiffener buckling. The effect of buckling may become important for shorter beams.

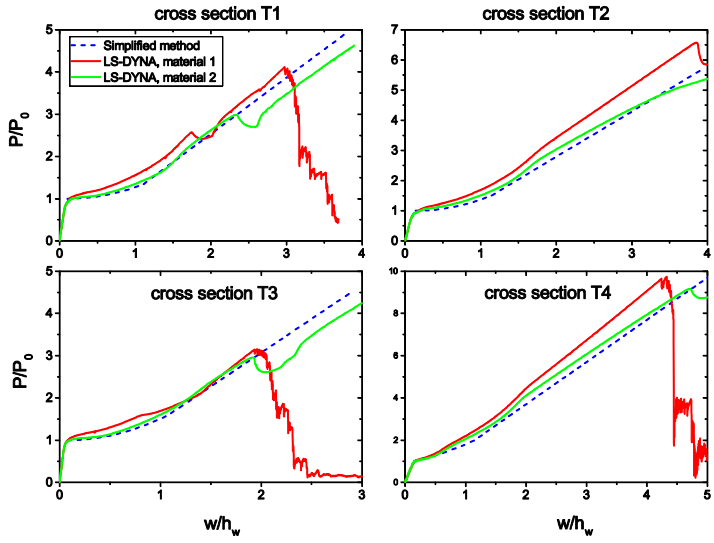

Figure 6-9. Nondimensional resistance curves for fixed-end stiffened panels with cross section T1-T4

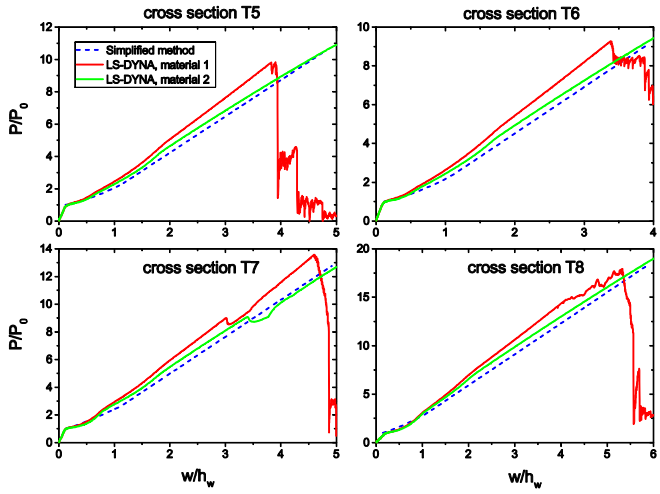

Figure 6-10. Nondimensional resistance curves for fixed-end stiffened panels with cross section T5-T8

Resistance curves for stiffened panels with finite translational stiffness, and material 2, are compared in Figure 6-11. The results agree well, notably when the axial stiffness is moderate. In the pure tension stage, the simplified model has a smaller slope due to missing hardening. The small force drops in the numerical simulations are due to local buckling which has limited influence. Resistance of stiffened plates with non-central loads and patch loads compared also quite well with numerical simulation. Details can be found in **Paper 5** (Yu et al., 2017).

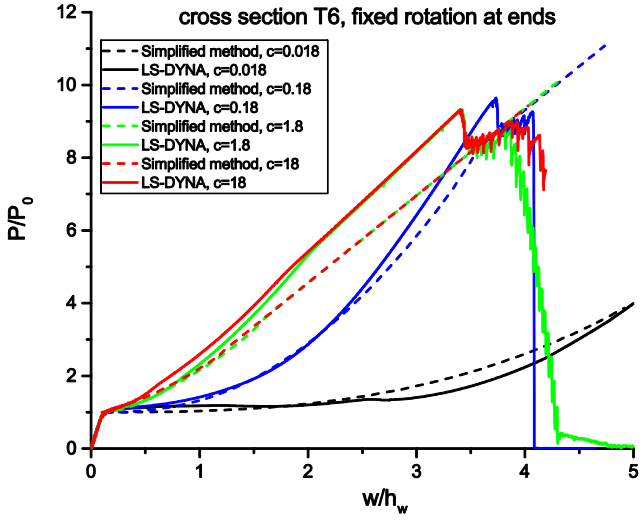

Figure 6-11. Nondimensional resistance for the T6 stiffened panels with fixed rotation conditions at the ends

6.4.3 Resistance to uniformly distributed loads

Figure 6-12 shows the force displacement curves for the four different cross sections subjected to uniformly distributed loads. The simplified method captures the general response quite well, but the capacity is somewhat underestimated. This may be because the assumption of using $0.5pL$ to approximate uniform distributed loads is only valid up to the plastic bending collapse, but not satisfied exactly in the membrane stage. The neglect of the material hardening may also contribute to the difference.

Fracture occurs much earlier in cases with uniformly distributed loads compared to those with point loads. This is because uniform loading gives much reduced central deflections if the same total force is applied, but the shear forces at the supports are equal for both scenarios being equal to $0.5\,pL$ at each end. For the same lateral deflection, the shear force at the support with uniform loading is twice the force with point loading, and fracture thus occurs early at the support under the combined action of bending, tension and shear.

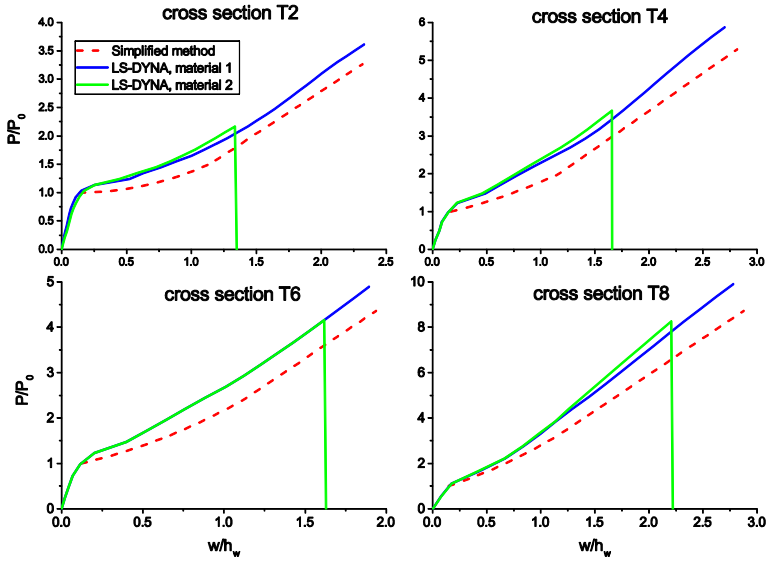

Figure 6-12. Resistance curves for stiffened panels subjected to uniformly distributed pressure loads

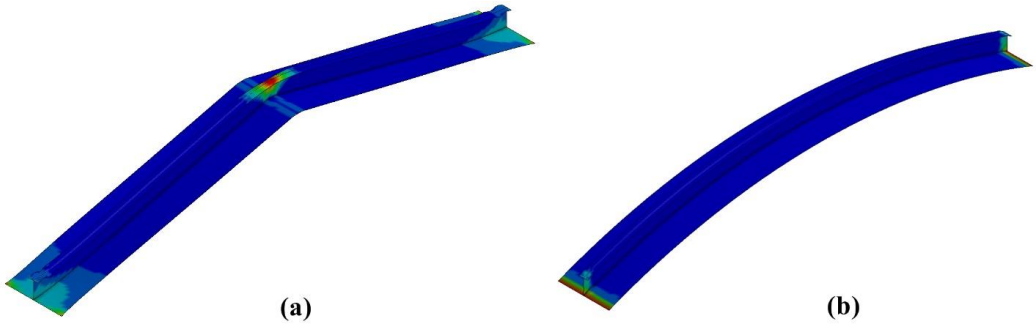

Figure 6-13. Strain distribution of deformed stiffened panels under (a) point loads and (b) uniform pressure loads

6.4.4 Panels stiffened with L-profiles

L-profile stiffeners are asymmetric and more susceptible to warping or tripping. Three different L-profiles defined in Table 6-3 were investigated. The effect of a bracket at stiffener mid-span to prevent tripping was also studied; refer to Figure 6-14. Resistance-deformation curves are plotted in Figure 6-15. The results showed that the bending moment capacity was reduced due to tripping and shear deformation. A tripping bracket at mid-span was found to ameliorate the situation. Again, the simplified resistance model gave acceptable results.

Table 6-3. Stiffened panel cross sections with L-profile stiffeners (Unit: mm)

Stiffener type	A_p/A_s	A_w/A_t	A_p	A_w	A_t
Type L1	1	1	600×8	240×10	80×30
Type L2	1	2	600×8	200×16	80×20
Type L6	2	3	600×8	180×10	60×10

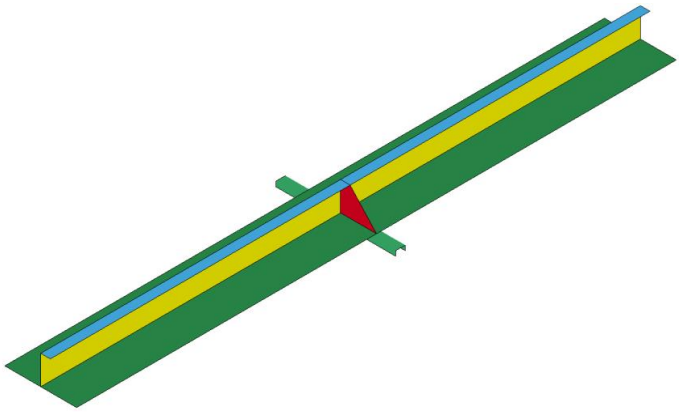

Figure 6-14. Impact scenario of a stiffened panel with L-profile stiffeners and a middle bracket

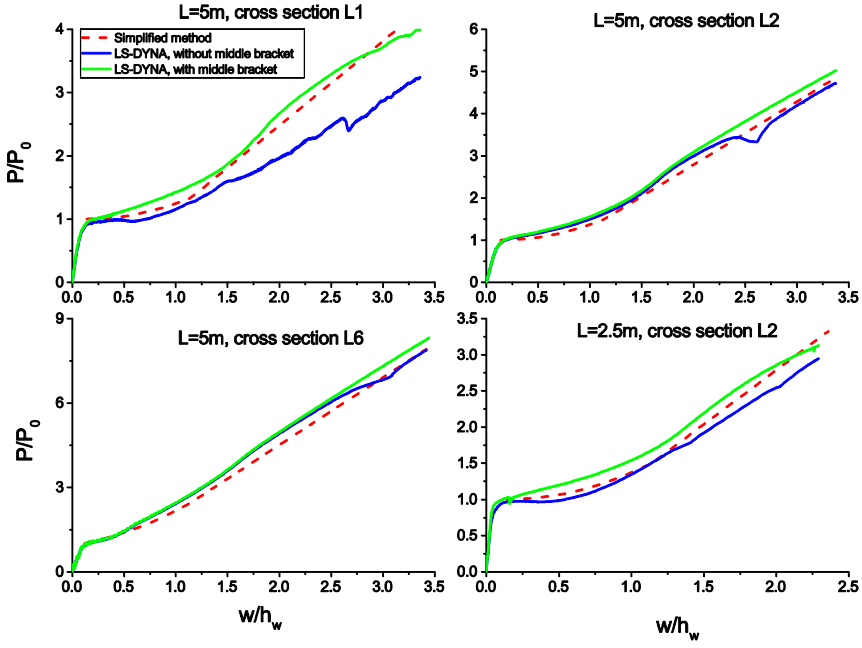

Figure 6-15. Nondimensional resistance curves for stiffened plates with L-profile stiffeners

6.4.5 The influence of transverse shear and inertial forces on the resistance

The simplified method is based on the assumption that the shear force is small and negligible. This may be the case for long, slender stiffened panels, but the effect of shear may become important and reduce the bending moment significantly. The effect of shear force is studied by letting the beam length vary such that L/h_w=12, 10, 8 and 5 for the T2 cross section. The resistance curves are plotted in Figure 6-16. They show that the shear effect becomes large for short beams. Thus the range of validity of the simplified models is $L/h_w \geq 10$.

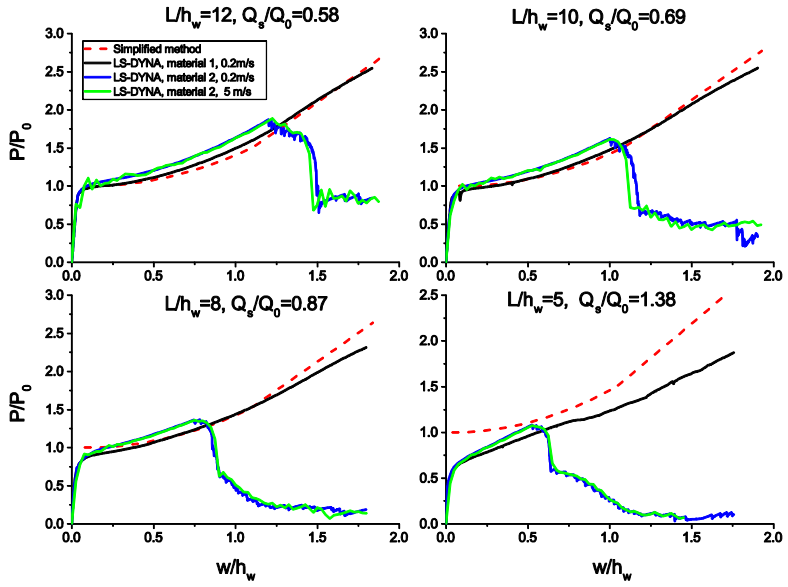

Figure 6-16. Nondimensional resistance-deformation curves for L/h_w=12, 10, 8 and 5

The influence of inertia forces is studied for the T6 stiffened panel under point load by varying the indenter speed. Material 1 is used, and any strain rate effects are not considered. The ends are fixed against inward motion. Figure 6-17 shows that the resistance oscillates in the initial stages, noticeably for the highest impact speed. The effect increases with increasing impact speed. The force tends to become stable as the indentation increases. The simplified method appears to be quite accurate as far as the average resistance is concerned, and the total dissipated energy is close to the static solution despite force oscillations.

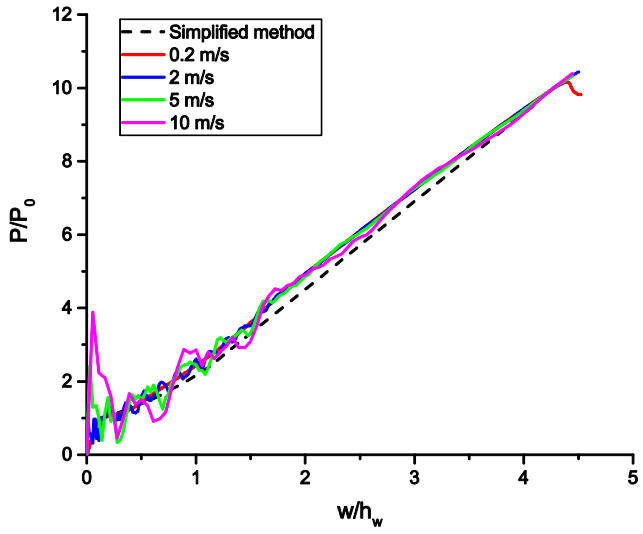

Figure 6-17. Resistance curves of the T6 stiffened panel for different impact velocities

Chapter 7

Conclusions and recommendations for future work

Ship collisions are rare events, but may cause severe consequences. It is crucial to assess accurately the structural response to collision actions, and to design crashworthy structures. The objective of the thesis is to improve the accuracy of ship collision simulations by developing advanced integrated methods, to shed light on the influence of coupling external and internal mechanics on the damage prediction of ship collisions, and to investigate the collision mechanics of tubular members and stiffened panels by means of numerical simulations and simplified analysis.

This final chapter concludes the thesis work and presents recommendations where future work may be usefully directed.

7.1 Conclusions

- **6DOF integrated simulation of ship collision**

A prevailing way to deal with ship collisions is to decouple the process into external dynamics and internal mechanics. The accuracy of the decoupled method is less compared to coupled methods. It is, however, very challenging to perform fully coupled NLFEA and few attempts have been reported in the literature. The present thesis described a method to couple the external and internal mechanics in LS-DYNA by the use of user subroutines.

Two models were developed and implemented by means of user subroutines into LS-DYNA for 6DOF integrated simulation of ship collision and grounding accidents, i) Hydrodynamic loads based on a maneuvering model and ii) Hydrodynamic loads based on linear potential flow theory. By comparison with the computer code SIMO, the methods were shown to be capable of predicting simultaneously the 6DOF ship motions and structural deformation with good efficiency and high accuracy. The major effects of fluid-structure interactions in ship collisions and groundings are well captured. The forward speed effect was found to have little influence on structural responses of ship collisions, and can be neglected. The proposed coupled methods can be used to improve simulation where the ship moves considerably and may be subjected to significant deflection.

- **Validity of the decoupled method**

The accuracy and the assumptions behind external mechanics models for decoupled analysis were discussed using the results from the coupled simulations. The 6DOF decoupled method is found to be capable of predicting the energy dissipation up to the end of the first impact period with reasonable accuracy. However, up to this point, structural damage cannot be predicted with the same accuracy. The predicted damage may deviate significantly in the transverse direction, especially for cases with small collision angles and long collision durations.

The equivalent added masses were found to vary with the shape of the collision curves, the collision duration, and the definitions of added masses. The frequency content of collision resistances is very dispersive, and it is difficult to find a representative frequency to determine the constant added mass for the external dynamic models. However, the varying added mass coefficients in sway and yaw were found to have little influence on the total energy absorption for large collision angle cases. In these cases, values that are typically used in present design guidance may be appropriate. The influence tends to become more important with decreasing collision angles.

The collision angle is assumed to be constant during collisions in external dynamic models. For short duration collisions, this is reasonable; but for cases with long durations or secondary impacts, the collision angle may change significantly, leading to large discrepancies with respect to energy dissipation and ship trajectories.

It is straight forward to determine the collision angle for the 2D external dynamic model, but not for the 3D model. The normal vector of the contact plane for a 3D external dynamic model should either be based on the surface of the striking or the struck object. For cases where both structures are deformable or where the geometry changes rapidly, the normal vector of the contact plane is difficult to identify. In some cases, the ship can be locked in the deformation of the struck object, and the 3D effect becomes limited.

It is not necessarily conservative to assume a restitution factor of 0 if the traditional kinematic restitution factor is used. The restitution ratio to maximize the total energy dissipation varies with cases. The maximum value can be unrealistic with a large restitution factor. Considering both aspects, it is recommended to use a restitution factor of 0.1 for engineering practice based on observation of numerical simulations

The periodic motions of the roll, pitch and heave may induce secondary impacts in ship collisions and groundings, which may increase the total energy dissipation significantly. The energy increase in secondary impacts comes mainly from friction contribution in the present study.

- **Collision with tubular members in offshore structures**

The standard design collision energy in the revised NORSOK N-003 standard is 50 MJ for bow impacts and 31 MJ for stern impacts. It is virtually impossible for braces/legs to absorb the

entire energy (i.e. ductile design). In such cases, it will be necessary to aim for strength design or shared energy design; i.e. the brace/leg should be capable of penetrating substantially into the ship structure. In order to obtain sufficient strength of braces/legs, local indentations should be kept small by satisfying the denting compactness criterion.

The deformation of tubular members includes stages of local denting, global bending and membrane stretching. The resistance models to local denting were reviewed. The NORSOK model was found to underestimate the denting resistance when the contact width is large. The underestimation increases with increasing tube wall thickness. The Wierzbicki and Suh model was extended to consider the contact width effect. The modified expression for the resistance versus local denting agrees well with the results of numerical simulations.

The concept of 'transition indentation ratio', $w_{d,tran/D}$, for braces and legs was discussed, where the deformation switches from local denting to plastic bending. The concept serves two main functions; one is to help judge the governing deformation modes of a tube with given tube dimensions and material properties. The other is that the transition ratio was found to have connection with the compactness criteria. The compactness criteria formulated in terms of the normalized resistance (R_0/R_c), and the length diameter ratio (L/D) together with the diameter/thickness ratio (D/t) are virtually the same, and by the very nature limit the transition ratio to a small value. It was found, however, that even for small transition ratios, local denting may still continue in the global bending stage. Hence, it is suggested to use the characteristic denting resistance parameter, R_c as the compactness requirement, following the recommendations by Storheim and Amdahl (2014). Based on numerical simulation results, R_c is suggested to be 1.2 MN for stern corner impacts, and 1.5 MN for stern end impacts. For bow collisions with horizontal and diagonal braces, $R_c = 1.9\ F_{max}/24$, where F_{max} is the maximum collision force.

The effect of ship-platform interaction on the distribution structural damage was identified and found to be significant. During collisions, the softer structure will deform and the impact force will be distributed over a larger contact area. This increases the resistance of the strong structure, and therefore there will be an upward shift of the resistance curve for the stronger structure. In collision checks of offshore platforms, load deformation curves of ships and platforms are often established independently by disregarding the relative strength and assuming the other object as infinitely rigid. Shared energy design based on such force curves may not give the correct energy distributions. It is suggested that a simple correction effect for the interaction should be implemented in the simplified formulations.

- **Resistance of stiffened panels subjected to lateral impacts**

A simplified formulation was proposed for the large deformation resistance of stiffened panels subjected to concentrated load, uniformly distributed load and patch loading. The panels may be simply supported or clamped against rotations at the ends with various degrees of restraints against inward motion. By comparison with NLFEA, the simplified formulation was shown to be capable of predicting the large deformation resistance curve with high accuracy, provided that the profile is compact and not subjected to tripping or very high utilization of the web in

shear. Care should be exercised to use the formulations for very asymmetric profiles, which are susceptible to tripping. A tripping bracket at mid span was found to ameliorate the situation in these cases. The method is a useful tool for quick assessment of the resistance of stiffened panels. The formulation will be implemented in the revised DNV-GL RP C204.

7.2 Recommendations for future work

It is recommended that the following topics be addressed in future work :

- The effects of waves, current and hydrodynamic interactions between the colliding bodies during collisions were not accounted for in the present coupled models, but the effect may be important.
- Fracture modeling is crucial for the accurate assessment of structural responses in ship collisions. The present simulations with the coupled models used a critical equivalent strain model for simplicity. This can be improved by combining the developed code with advanced fracture models, such as the RTCL and the BWH criteria.
- The effect of local indentation on the reduction of cross section bending capacity is still not fully understood. Different researchers presented quite different answers; refer Figure 2-16. It is advised to conduct experiments to gain deeper insights.
- The structural flexibilities of jacket and jack-up platforms may become important during collisions. Motions and vibrations of the structures may absorb considerable energy. It is still not clear how much energy can be absorbed by structural vibrations, and how the energy varies with different platforms. This should be investigated further. Preferably, simplified external dynamic models should be derived considering the effect of structural flexibilities.
- The simplified formulation for the deformation of stiffened panels is developed for static conditions, and can be used for low velocity impacts. The model can be extended to consider dynamic conditions with large velocity impacts and impact impulses. The accuracy for various T-, L- and bulb profiles with different spans should be further investigated by means of extensive parametric studies
- The usefulness of the coupled model should be further demonstrated by simulating collision scenarios against offshore structures, floating bridges etc. where more than 1 degree of freedom is activated during the collision and/or where the collision duration is significant.
- The coupled model should also be useful for grounding simulations. In this cases for shallow-water effects should be accounted for in determination of the hydrodynamic coefficients.
- Further studies should be carried out to establish recommendations for estimation of the collision angle to be used in with the decoupled 6DOF method when both structures are deformable or where the geometry changes rapidly.
- The proposed coupled models are still not stable enough for general purpose use. The reasons may be that the acceleration term was not directly provided by the subroutine, but

was estimated from velocity history. In addition, the constant timestep is required, which was enforced by using the mass scaling technique. The coupled models should be further improved with respect to the stableness and robustness.

References

ABUBAKAR, A. & DOW, R. 2013. Simulation of ship grounding damage using the finite element method. *International Journal of Solids and Structures,* 50**,** 623-636.

ADOUM, M. & LAPOUJADE, V. Examples' manual for* USER_LOADING option. Proc. 4th European LS-DYNA Users Conference, Ulm, Germany, 2003.

ALEXANDER, J. M. 1960. AN APPROXIMATE ANALYSIS OF THE COLLAPSE OF THIN CYLINDRICAL SHELLS UNDER AXIAL LOADING. *The Quarterly Journal of Mechanics and Applied Mathematics,* 13**,** 10-15.

ALSOS, H. S. & AMDAHL, J. 2007. On the resistance of tanker bottom structures during stranding. *Marine Structures,* 20**,** 218-237.

ALSOS, H. S. & AMDAHL, J. 2009. On the resistance to penetration of stiffened plates, Part I– Experiments. *International Journal of Impact Engineering,* 36**,** 799-807.

ALSOS, H. S., AMDAHL, J. & HOPPERSTAD, O. S. 2009. On the resistance to penetration of stiffened plates, Part II: Numerical analysis. *International Journal of Impact Engineering,* 36**,** 875-887.

ALSOS, H. S., HOPPERSTAD, O. S., TÖRNQVIST, R. & AMDAHL, J. 2008. Analytical and numerical analysis of sheet metal instability using a stress based criterion. *International Journal of Solids and Structures,* 45**,** 2042-2055.

AMDAHL, J. 1980. Impact Capacity of Steel Platforms and Tests on Large Deformations of Tubes and Transverse Loading. *Det norske Veritas, Progress Report***,** 80-0036.

AMDAHL, J. 1983. Energy absorption in ship-platform impacts. Doctoral Thesis, Norwegian Institute of technology.

AMDAHL, J. 2005. Static resistance of stiffened plates subjected to explosions. *FABIG Newsletter Issue 2005;41(R531):4–7*.

AMDAHL, J. & JOHANSEN, A. High-energy ship collision with jacket legs. The Eleventh International Offshore and Polar Engineering Conference, 2001. International Society of Offshore and Polar Engineers.

AMDAHL, J. & KAVLIE, D. Experimental and numerical simulation of double hull stranding. DNV-MIT workshop on mechanics of ship collision and grounding, 1992.

AMDAHL, J., WATAN, R., HU, Z. & HOLMÅS, T. Broad side ship collision with jacket legs: Examination of NORSOK N-004 Analysis Procedure. ASME 2012 31st International Conference on Ocean, Offshore and Arctic Engineering, 2012. American Society of Mechanical Engineers, 745-751.

BALA, S. & DAY, J. 2012. General guidelines for crash analysis in LS-DYNA. *Livermore Software Technology Corporation*.

BROWN, A. J. 2002. Collision scenarios and probabilistic collision damage. *Marine Structures,* 15**,** 335-364.

BULDGEN, L., LE SOURNE, H. & PIRE, T. 2014. Extension of the super-elements method to the analysis of a jacket impacted by a ship. *Marine Structures,* 38**,** 44-71.

CALLE, M. & ALVES, M. 2015. A review-analysis on material failure modeling in ship collision. *Ocean Engineering,* 106**,** 20-38.

CALLE, M. A., VERLEYSEN, P. & ALVES, M. 2017a. Benchmark study of failure criteria for ship

collision modeling using purpose-designed tensile specimen geometries. *Marine Structures,* 53**,** 68-85.

CALLE, M. A. G., OSHIRO, R. E. & ALVES, M. 2017b. Ship collision and grounding: Scaled experiments and numerical analysis. *International Journal of Impact Engineering,* 103**,** 195-210.

CARLEBUR, A. 1995. Full-scale collision tests. *Safety science,* 19**,** 171-178.

CERIK, B. C., SHIN, H. K. & CHO, S.-R. 2016. A comparative study on damage assessment of tubular members subjected to mass impact. *Marine Structures,* 46**,** 1-29.

CHO, S.-R., KWON, J.-S. & KWAK, D.-I. 2010. Structural Characteristics of Damaged Offshore Tubular Members. *Journal of Ocean Engineering and Technology,* 24**,** 1-7.

CHO, S.-R. & LEE, H.-S. 2009. Experimental and analytical investigations on the response of stiffened plates subjected to lateral collisions. *Marine Structures,* 22**,** 84-95.

CHO, S. R. 1990. Development of a simplified dynamic analysis procedure for offshore collisions. *Bulletin of the Society of Naval Architects of Korea,* 27**,** 72-82.

DALEY, C. G., DALEY, K. H., DOLNY, J. & QUINTON, B. W. T. 2016. Overload response of flatbar frames to ice loads. *Ships and Offshore Structures***,** 1-14.

DALEY, J. 2013. Mumbai high north platform disaster. *Proto-Type,* 1.

DE OLIVEIRA, J., WIERZBICKI, T., ABRAMOWICZ, W. & VERITAS, N. 1982. *Plastic Behaviour of Tubular Members Under Lateral Concentrated Loading*, Det norske Veritas, Research Division.

DE OLIVERIA, J. The behavior of steel offshore structures under accidental collisions. Offshore Technology Conference, 1981. Offshore Technology Conference.

DNV-RP-C204 2010. Recommended practice DNV-RP-C204. *DET NORSKE VERITAS*.

DNV-RP-C208 2013. Determination of Structural Capacity by Non-linear FE analysis Methods. *Det Norske Veritas*.

DNV 1981. Impact loads from boats. *Technical Note for Fixed Offshore Installations TN A,* 202.

DNV 2004. NORSOK Standard N004. Design of steel structures, Appendix A, design against accidental actions. Det Norske Veritas 2004.

EHLERS, S., BROEKHUIJSEN, J., ALSOS, H. S., BIEHL, F. & TABRI, K. 2008. Simulating the collision response of ship side structures: a failure criteria benchmark study. *International Shipbuilding Progress,* 55**,** 127-144.

EHLERS, S., TABRI, K., ROMANOFF, J. & VARSTA, P. 2012. Numerical and experimental investigation on the collision resistance of the X-core structure. *Ships and offshore structures,* 7**,** 21-29.

ELLINAS, C. & VALSGARD, S. 1985. Collisions and damage of offshore structures: a state-of-the-art. *Journal of energy resources technology,* 107**,** 297-314.

ELLINAS, C. P. & WALKER, A. C. Damage on offshore tubular bracing members. IABSE Colloquium on Ship Collisions With Bridges and Offshore Structures, Copenhagen, May, 1983. 253-261.

ENDO, H., YAMADA, Y., KITAMURA, O. & SUZUKI, K. 2002. Model test on the collapse strength of the buffer bow structures. *Marine Structures,* 15**,** 365-381.

FOSS, G. & EDVARDSEN, G. Energy Absorbtion During Ship Impact on Offshore Steel Structures. Offshore Technology Conference, 1982. Offshore Technology Conference.

FURNES, O. & AMDAHL, J. 1980. Ship collisions with offshore platforms. *Intermaritec'80*.

GAGNON, R. E. & WANG, J. 2012. Numerical simulations of a tanker collision with a bergy bit incorporating hydrodynamics, a validated ice model and damage to the vessel. *Cold Regions Science and Technology,* 81**,** 26-35.

GHAVAMI, K. & KHEDMATI, M. R. 2006. Numerical and experimental investigations on the compression behaviour of stiffened plates. *Journal of Constructional Steel Research,* 62**,** 1087-1100.

HALLQUIST, J. O. 2006. LS-DYNA theory manual. *Livermore software Technology corporation,* 3**,** 25-31.

HODGE JR, P. G. 1974. Post-yield behavior of a beam with partial end fixity. *International Journal of Mechanical Sciences,* 16**,** 385-388.

HOGSTRÖM, P. & RINGSBERG, J. W. 2012. An extensive study of a ship's survivability after collision–A parameter study of material characteristics, non-linear FEA and damage stability analyses. *Marine structures,* 27**,** 1-28.

HONG, L. 2009. Simplified analysis and design of ships subjected to collision and grounding. *PhD Thesis, Norwegian University of Science and Technology, Norway*.

HONG, L. & AMDAHL, J. 2008. Plastic mechanism analysis of the resistance of ship longitudinal girders in grounding and collision. *Ships and Offshore Structures,* 3**,** 159-171.

HONG, L. & AMDAHL, J. 2013. Rapid assessment of ship grounding over large contact surfaces: Taylor & Francis, Jeom Kee Paik and the Editorial Board of Ships and Offshore Structures are delighted to announce that the following paper has been awarded the 2012 Best Paper Award. *Ships and Offshore Structures,* 8**,** 1-2.

HU, Z., JØRGEN, A. & LIN, H. 2011. Verification of a simplified analytical method for predictions of ship groundings over large contact surfaces by numerical simulations. *Marine Structures,* 24**,** 436-458.

IMO 2015. International Maritime Organization, GISIS: Marine Casualties and Incidents, Cited 05. URL https://gisis.imo.org/Public/MCI/ Default.aspx.

JIA, H. & MOAN, T. Global Responses of Struck Ships in Collision With Emphasis on Hydrodynamic Effects. ASME 2010 29th International Conference on Ocean, Offshore and Arctic Engineering, 2010. American Society of Mechanical Engineers, 225-236.

JIANG, J. & OLSON, M. D. 1995. Rigid-plastic analysis of underwater blast loaded stiffened plates. *International Journal of Mechanical Sciences,* 37**,** 843-859.

JONES, N. 1973. Influence of in-plane displacements at the boundaries of rigid-plastic beams and plates. *International Journal of Mechanical Sciences,* 15**,** 547-561.

JONES, N. 2011. Structural impact. Cambridge university press.

JONES, N., BIRCH, S., BIRCH, R., ZHU, L. & BROWN, M. 1992. An experimental study on the lateral impact of fully clamped mild steel pipes. *Proceedings of the Institution of Mechanical Engineers, Part E: Journal of Process Mechanical Engineering,* 206**,** 111-127.

JONES, N. & SHEN, W. 1992. A theoretical study of the lateral impact of fully clamped pipelines. *Proceedings of the Institution of Mechanical Engineers, Part E: Journal of Process Mechanical Engineering,* 206**,** 129-146.

KARLSSON, U. B., RINGSBERG, J. W., JOHNSON, E., HOSEINI, M. & ULFVARSON, A. 2009. Experimental and numerical investigation of bulb impact with a ship side-shell structure. *Marine Technology,* 46**,** 16-26.

KITAMURA, O. 2002. FEM approach to the simulation of collision and grounding damage. *Marine*

Structures, 15**,** 403-428.

KVITRUD, A. Collisions between platforms and ships in Norway in the period 2001-2010. ASME 2011 30th International Conference on Ocean, Offshore and Arctic Engineering, 2011. American Society of Mechanical Engineers, 637-641.

LE SOURNE, H. A ship collision analysis program based on super-element method coupled with large rotational ship movement analysis tool. International Conference on Collision and Grounding of Ships, 2007. 131-138.

LE SOURNE, H., BESNARD, N., CHEYLAN, C. & BUANNIC, N. 2012. A Ship Collision Analysis Program Based on Upper Bound Solutions and Coupled with a Large Rotational Ship Movement Analysis Tool. *Journal of Applied Mathematics,* 2012**,** 27.

LEE, S., ZHAO, T. & NAM, J. Structural safety assessment of ship collision and grounding using FSI analysis technique. International conference" Collision and Grounding of Ships and Offshore Structures", ICCGS, 2013. 197-204.

LEE, S. G., BAEK, Y. H., LEE, I. H., YANG, K. K. & KIM, Y. Numerical simulation of 2D sloshing by using ALE2D technique of LS-DYNA and CCUP methods. 20th International Offshore and Polar Engineering Conference, ISOPE-2010, 2010 Beijing. 192-199.

LEE, S. G., KIM, J. K., NGUYEN, H. A. & NAM, J. H. Structural safety assessment of LNGC MARK III membrane type CCS under sloshing impact loading. 22nd International Offshore and Polar Engineering Conference, ISOPE-2012, 2012a Rhodes. 487-494.

LEE, S. G., NAM, J. H., KIM, J. K., ZHAO, T. & NGUYEN, H. A. Structural safety assessment of ship collision using FSI analysis technique. 22nd International Offshore and Polar Engineering Conference, ISOPE-2012, 2012b Rhodes. 753-762.

LEE, S. G. & ZHAO, T. Structural safety assessment of lngc ccs under iceberg collision using fsi analysis technique. 23rd International Offshore and Polar Engineering Conference, ISOPE 2013, 2013 Anchorage, AK. 1145-1155.

LEHMANN, E. & PESCHMANN, J. 2002. Energy absorption by the steel structure of ships in the event of collisions. *Marine Structures,* 15**,** 429-441.

LIU, J. & HU, Z. 2017. 3D analytical method for the external dynamics of ship collisions and investigation of the coefficient of restitution (In Chinese). *Chinese journal of ship research,* 12**,** 84-91.

LIU, B., VILLAVICENCIO, R. & GUEDES SOARES, C. 2015a. Simplified analytical method to evaluate tanker side panels during minor collision incidents. *International Journal of Impact Engineering,* 78**,** 20-33.

LIU, B., VILLAVICENCIO, R. & GUEDES SOARES, C. 2015b. Simplified method for quasi-static collision assessment of a damaged tanker side panel. *Marine Structures,* 40**,** 267-288.

LIU, Z. & AMDAHL, J. 2010. A new formulation of the impact mechanics of ship collisions and its application to a ship–iceberg collision. *Marine Structures,* 23**,** 360-384.

LOUCA, L. A., PAN, Y. G. & HARDING, J. E. 1998. Response of stiffened and unstiffened plates subjected to blast loading. *Engineering Structures,* 20**,** 1079-1086.

MAKER, B. N. & ZHU, X. 2000. Input parameters for metal forming simulation using LS-DYNA. *Livermore Software Technology Corporation,* 4**,** 43-46.

MANOLAKOS, D. E. & MAMALIS, A. G. 1988. Limit analysis for laterally loaded stiffened plates. *International Journal of Mechanical Sciences,* 30**,** 441-447.

MARINATOS, J. & SAMUELIDES, M. 2015. Towards a unified methodology for the simulation of

rupture in collision and grounding of ships. *Marine Structures,* 42**,** 1-32.

MINORSKY, V. 1958. An analysis of ship collisions with reference to protection of nuclear power plants. Sharp (George G.) Inc., New York.

MOAN, T., AMDAHL, J. & GERHARD, E. 2016. assessment of ship impact risk to offshore structures-new NORSOK N-003 guidelines. *Preceedings of the 3rd Offshore Structural Reliablity Conference (OSRC 2016)*.

MOTORA, S., FUJINO, M., SUGIURA, M. & SUGITA, M. 1971. Equivalent Added Mass of Ships in Collisions. *Selected papers from the journal of the Society of Naval Architects of Japan,* 7**,** 138-148.

NEWTON, I. 1686. Principia: Mathematical Principles of Natural Philosophy (and His System of the World)(1686). Reprinted by Univ. of CA Press.

NORRBIN, N. H. 1971. Theory and observations on the use of a mathematical model for ship manoeuvring in deep and confined waters. DTIC Document.

NORSOK-N003 2007. Action and action effects.

NORSOK-N004 2004. Design of steel structures. Rev.

OHTSUBO, H., KAWAMOTO, Y. & KUROIWA, T. 1994a. Experimental and numerical research on ship collision and grounding of oil tankers. *Nuclear engineering and design,* 150**,** 385-396.

OHTSUBO, H., KAWAMOTO, Y. & KUROIWA, T. 1994b. Experimental and numerical research on ship collision and grounding of oil tankers. *Nuclear engineering and design,* 150**,** 385-396.

PAIK, J.-K. & SHIN, B.-C. 1989. Damage effects on the ultimate strength of offshore tubular members. *Journal of Ocean Engineering and Technology,* 3**,** 77-86.

PAIK, J. 2007. Practical techniques for finite element modelling to simulate structural crashworthiness in ship collisions and grounding (Part II: Verification). *Ships and Offshore Structures,* 2**,** 81-85.

PEDERSEN, P. T. 2010. Review and application of ship collision and grounding analysis procedures. *Marine Structures,* 23**,** 241-262.

PEDERSEN, P. T. & LI, Y. 2009. On the global ship hull bending energy in ship collisions. *Marine Structures,* 22**,** 2-11.

PEDERSEN, P. T. & ZHANG, S. 1998. On impact mechanics in ship collisions. *Marine Structures,* 11**,** 429-449.

PEDERSEN, P. T. & ZHANG, S. 2000. Absorbed energy in ship collisions and grounding-revising Minorsky's empirical method. *Journal of Ship Research,* 44**,** 140-154.

PETERSEN, M. J. 1982. Dynamics of ship collisions. *Ocean Engineering,* 9**,** 295-329.

PETERSEN, M. J. & PEDERSEN, P. T. Collisions between ships and offshore platforms. Offshore Technology Conference, 1981. Offshore Technology Conference.

PIKE, K., BUTT, N., JOHNSON, D., PRYCE-ROBERTS, N. & VIGAR, N. 2013. 15 Years of shipping accidents: A review for WWF.

PILL, I. & TABRI, K. 2011. Finite element simulations of ship collisions: A coupled approach to external dynamics and inner mechanics. *Ships and Offshore Structures,* 6**,** 59-66.

POPOV, Y. N., FADDEEV, O., KHEISIN, D. & YAKOVLEV, A. 1969. Strength of ships sailing in ice. DTIC Document.

RP2A-WSD, A. Recommended practice for planning, designing and constructing fixed offshore platforms–working stress design–. Twenty-, 2000.

RUDAN, S., TABRI, K. & KLARIĆ, I. Analysis of sloshing interaction in ship collisions by means of

ALE finite element method. Proceedings of 5th International Conference on Collision and grounding of Ships, 2010. 229-234.

SAJDAK, J. & BROWN, A. 2005. Modeling longitudinal damage in ship collisions. *SSC-437, Ship Structure Committee*.

SALVESEN, N., TUCK, E. & FALTINSEN, O. 1970. Ship motions and sea loads. *Trans. SNAME,* 78**,** 250-287.

SAMUELIDES, E. & FRIEZE, P. 1989. Fluid-structure interaction in ship collisions. *marine Structures,* 2**,** 65-88.

SCHUBAK, R. B., OLSON, M. D. & ANDERSON, D. L. 1991. *Nonlinear Rigid-Plastic Analysis of Stiffened Plates under Blast Loads.*

SCHUBAK, R. B., OLSON, M. D. & ANDERSON, D. L. 1993a. Rigid-plastic modelling of blast-loaded stiffened plates—Part I: One-way stiffened plates. *International Journal of Mechanical Sciences,* 35**,** 289-306.

SCHUBAK, R. B., OLSON, M. D. & ANDERSON, D. L. 1993b. Rigid-plastic modelling of blast-loaded stiffened plates—Part II: Partial end fixity, rate effects and two-way stiffened plates. *International Journal of Mechanical Sciences,* 35**,** 307-324.

SERVIS, D. & SAMUELIDES, M. 2006. Implementation of the T-failure criterion in finite element methodologies. *Computers & Structures,* 84**,** 196-214.

SHERMAN, D. R. 1976. Test of circular steel tubes in bending. *Journal of the Structural Division,* 102**,** 2181-2195.

SIMONSEN, B. C. 1997. Ship grounding on rock—I. Theory. *marine Structures,* 10**,** 519-562.

SKALLERUD, B. & AMDAHL, J. 2002. *Nonlinear analysis of offshore structures*, Research Studies Press Baldock, Hertfordshire,, England.

SOARES, C. G. & SØREIDE, T. H. 1983. Plastic analysis of laterally loaded circular tubes. *Journal of Structural Engineering,* 109**,** 451-467.

SONG, M., KIM, E., AMDAHL, J., MA, J. & HUANG, Y. 2016. A comparative analysis of the fluid-structure interaction method and the constant added mass method for ice-structure collisions. *Marine Structures,* 49**,** 58-75.

SOREIDE, T., AMDAHL, J., EBERG, E., HELLAN, O. & HALMÅS, T. 1999. USFOS–a computer program for progressive collapse analysis of steel offshore structures. *Theory Manual. SINTEF Report STF71 F,* 88038.

SØREIDE, T. H. 1985. *Ultimate load analysis of marine structures,* [Y.y.], Tapir.

STORHEIM, M. 2016. Structural response in ship-platform and ship-ice collisions. *Doctoral thesis, Norwegian University of Science and Technology*.

STORHEIM, M., ALSOS, H. S., HOPPERSTAD, O. S. & AMDAHL, J. 2015a. A damage-based failure model for coarsely meshed shell structures. *International Journal of Impact Engineering,* 83**,** 59-75.

STORHEIM, M. & AMDAHL, J. 2014. Design of offshore structures against accidental ship collisions. *Marine Structures,* 37**,** 135-172.

STORHEIM, M. & AMDAHL, J. 2017. On the sensitivity to work hardening and strain-rate effects in nonlinear FEM analysis of ship collisions. *Ships and Offshore Structures,* 12**,** 100-115.

STORHEIM, M., AMDAHL, J. & MARTENS, I. 2015b. On the accuracy of fracture estimation in collision analysis of ship and offshore structures. *Marine Structures,* 44**,** 254-287.

SUN, B., HU, Z. & WANG, G. 2015. An analytical method for predicting the ship side structure

response in raked bow collisions. *Marine Structures,* 41**,** 288-311.

TABRI, K. 2010. Dynamics of ship collisions.

TABRI, K. 2012. Influence of coupling in the prediction of ship collision damage. *Ships and Offshore Structures,* 7**,** 47-54.

TABRI, K. & BROEKHUIJSEN, J. Influence of ship motions in the numerical prediction of ship collision damage. Advances in Marine Structures - Proceedings of the 3rd International Conference on Marine Structures, MARSTRUCT 2011, 2011. 391-397.

TABRI, K., BROEKHUIJSEN, J., MATUSIAK, J. & VARSTA, P. 2009a. Analytical modelling of ship collision based on full-scale experiments. *Marine Structures,* 22**,** 42-61.

TABRI, K., MÄÄTTÄNEN, J. & RANTA, J. 2008. Model-scale experiments of symmetric ship collisions. *Journal of Marine Science and Technology,* 13**,** 71-84.

TABRI, K., MATUSIAK, J. & VARSTA, P. 2009b. Sloshing interaction in ship collisions—An experimental and numerical study. *Ocean Engineering,* 36**,** 1366-1376.

TABRI, K., VARSTA, P. & MATUSIAK, J. 2010. Numerical and experimental motion simulations of nonsymmetric ship collisions. *Journal of Marine Science and Technology,* 15**,** 87-101.

TABY, J., MOAN, T. & RASHED, S. 1981. Theoretical and experimental study of the behaviour of damaged tubular members in offshore structures. *Norwegian Maritime Research,* 9**,** 26-33.

TABY, J. & MOAN, T. 1988. Ultimate strength and post-ultimate strength behavior of damaged tubular members in offshore structures.

THYS, M. 2013. Theoretical and experimental investigation of a free running fishing vessel at small frequency of encounter.

TØRNQVIST, R. 2003. *Design of crashworthy ship structures.* Technical University of Denmark Kgns Lyngby,, Denmark.

TRAVANCA, J. & HAO, H. 2014. Numerical analysis of steel tubular member response to ship bow impacts. *International Journal of Impact Engineering,* 64**,** 101-121.

UEDA, Y. & RASHED, S. 1985. Behavior of damaged tubular structural members. *Journal of energy resources technology,* 107**,** 342-349.

UEDA, Y. & RASHED, S. M. H. 1984. The idealized structural unit method and its application to deep girder structures. *Computers & Structures,* 18**,** 277-293.

VALSGARD, S. & JORGENSEN, L. Evaluation of Ship/Ship Collision Damage Using a Simplified Nonlinear Finite Element Procedure. Proceedings of the International Symposium on Practical Design in Shipbuilding, 1983. 16-22.

VAN BERLEKOM, W. B. & GODDARD, T. A. 1972. Maneuvering of large tankers. *Presented at the Annual Meeting of SNAME, Society of Naval Architects and Marine Engineers,* Paper #8.

VILLAVICENCIO, R., LIU, B. & SOARES, C. G. 2014. Experimental and numerical analysis of a tanker side panel laterally punched by a knife edge indenter. *Marine Structures,* 37**,** 173-202.

VREDEVELDT, A. & WEVERS, L. 1993. Full scale ship collision tests.

WALTERS, C. L. & VOORMEEREN, L. O. Consequences of using the plane stress assumption for damage calculations in crash analyses. ASME 2014 33rd International Conference on Ocean, Offshore and Arctic Engineering, 2014. American Society of Mechanical Engineers, V04BT02A011-V04BT02A011.

WANG, G., ARITA, K. & LIU, D. 2000. Behavior of a double hull in a variety of stranding or collision scenarios. *Marine Structures,* 13**,** 147-187.

WANG, G., SPENCER, J. & CHEN, Y. 2002. Assessment of a ship's performance in accidents. *Marine*

Structures, 15**,** 313-333.

WANG, S. & GUEDES SOARES, C. 2012. Analysis of the water impact of symmetric wedges with a multi-material Eulerian formulation. *International Journal of Maritime Engineering (IJME),* 154**,** 191-206.

WATAN, R. 2011. Analysis and Design of Columns in Offshore Structures subjected to Supply Vessel Collisions. *Master thesis Norwegian University of Science and Technology*.

WEVERS, L. J., VREDEVELDT, A. W., BUILDING, T., RESEARCH, C. & RESEARCH, N. I. F. M. 1999. *Full Scale Ship Collision Experiments 1998: Test of New Type Ship Side Structure, Royal Schelde, the Netherlands*, TNO.

WIERZBICKI, T. & ABRAMOWICZ, W. 1983. On the crushing mechanics of thin-walled structures. *Journal of Applied mechanics,* 50**,** 727-734.

WIERZBICKI, T. & SUH, M. 1988. Indentation of tubes under combined loading. *International Journal of Mechanical Sciences,* 30**,** 229-248.

WIKIPEDIA 2016. ship collision, https://en.wikipedia.org/wiki/Ship_collision.

WOISIN, G. Design against collision Int. Symp. Adv. Mar. Technol., Trondheim Norway, 1979. 1-28.

WOISIN, G., 1988. INSTANTANEOUS LOSS OF ENERGY IN UNSYMMETRIC SHIP COLLISION.

XU, M. & SOARES, C. G. 2012. Assessment of the ultimate strength of narrow stiffened panel test specimens. *Thin-Walled Structures,* 55**,** 11-21.

XU, M. C., YANAGIHARA, D., FUJIKUBO, M. & GUEDES SOARES, C. 2013. Influence of boundary conditions on the collapse behaviour of stiffened panels under combined loads. *Marine Structures,* 34**,** 205-225.

YAMADA, Y. & ENDO, H. 2008. Experimental and numerical study on the collapse strength of the bulbous bow structure in oblique collision. *Marine technology,* 45**,** 42-53.

YU, Z. & AMDAHL, J. 2016a. Buckling and fracture analysis of a side-shell structure subjected to collision loads. *internal report*.

YU, Z. & AMDAHL, J. 2016b. Full six degrees of freedom coupled dynamic simulation of ship collision and grounding accidents. *Marine Structures,* 47**,** 1-22.

YU, Z. & AMDAHL, J. 2016c. Influence of 6DOF ship motions in the damage prediction of ship collision and grounding accidents. *Proceedings of the 7th International Conference on Collision and Grounding of Ships and Offshore Structures, June 15-18, Ulsan, South Korea*.

YU, Z. & AMDAHL, J. 2017a. Analysis and design of offshore tubular members against ship impacts. *submitted to jounal*.

YU, Z. & AMDAHL, J. 2017b. Design of offshore tubular members against excessive local indentation under lateral impacts. *Proceedings of 6th International Conference on Marine Structures, MARSTRUCT 2017, Lisbon, Portugal.*

YU, Z. & AMDAHL, J. 2017c. A review of structural responses of offshore tubular structures subjected to ship impacts. *Submitted to jounal*.

YU, Z., AMDAHL, J. & SHA, Y. 2017. Large inelastic deformation resistance of stiffened panels subjected to lateral loading *submitted to jounal*.

YU, Z., AMDAHL, J. & STORHEIM, M. 2016a. A new approach for coupling external dynamics and internal mechanics in ship collisions. *Marine Structures,* 45**,** 110-132.

YU, Z., HU, Z., AMDAHL, J. & LIU, Y. 2013. Investigation on structural performance predictions of double-bottom tankers during shoal grounding accidents. *Marine Structures,* 33**,** 188-213.

YU, Z., HU, Z. & WANG, G. 2015. Plastic mechanism analysis of structural performances for stiffeners on bottom longitudinal web girders during a shoal grounding accident. *Marine Structures,* 40**,** 134-158.

YU, Z., SHEN, Y., AMDAHL, J. & GRECO, M. 2016b. Implementation of Linear Potential-Flow Theory in the 6DOF Coupled Simulation of Ship Collision and Grounding Accidents. *Journal of Ship Research*.

ZEINODDINI, M., PARKE, G. & HARDING, J. 2002. Axially pre-loaded steel tubes subjected to lateral impacts: an experimental study. *International Journal of Impact Engineering,* 27**,** 669-690.

ZHANG, A. & SUZUKI, K. 2007. A comparative study of numerical simulations for fluid–structure interaction of liquid-filled tank during ship collision. *Ocean Engineering,* 34**,** 645-652.

ZHANG, S., VILLAVICENCIO, R., ZHU, L. & PEDERSEN, P. T. 2017. Impact mechanics of ship collisions and validations with experimental results. *Marine Structures,* 52**,** 69-81.

Appendix A: appended papers

PAPER 1

Yu Z., Amdahl J., Storheim M.

A new approach for coupling external dynamics and internal mechanics in ship collisions

Published in

Marine Structures
Vol. 45, Pages 110-132, 2016

Marine Structures 45 (2016) 110–132

Contents lists available at ScienceDirect

Marine Structures

journal homepage: www.elsevier.com/locate/marstruc

A new approach for coupling external dynamics and internal mechanics in ship collisions

Zhaolong Yu [a, b, *], Jørgen Amdahl [a, b], Martin Storheim [a, b, c]

[a] Department of Marine Technology, Norwegian University of Science and Technology (NTNU), Norway
[b] Centre for Autonomous Marine Operations and Systems (AMOS), NTNU, Norway
[c] Center for Sustainable Arctic Marine and Coastal Technology (SAMCoT), NTNU, Norway

ARTICLE INFO

Article history:
Received 2 October 2015
Received in revised form 6 November 2015
Accepted 11 November 2015
Available online 30 November 2015

Keywords:
Ship collision
Coupled simulation
Maneuvering model
3DOF ship motions
Forward speed

ABSTRACT

This paper proposes a new model, which efficiently couples the external dynamics and internal mechanics in ship collision accidents. This method is especially useful for design purposes since the detailed ship hull profile is not needed.

Ship motions in the horizontal plane are considered. The collision forces are calculated using the explicit nonlinear finite element code LS-DYNA. The hydrodynamic forces in surge, sway and yaw are calculated using a traditional ship maneuvering model with a series of nondimensional coefficients determined from experiments. These forces are applied to the center of gravity (COG) of the ship with the user defined load subroutine in LS-DYNA and are solved together with structural response analysis during simulation.

The proposed 3DOF coupled method was applied to calculations of an offshore supply vessel colliding with a rigid plate and a submersible platform. The results were compared with those predicted by a decoupled method. Ship motions with the proposed method compared reasonably with SIMO simulations. The advantages and limitations of the method were further discussed in the view of the equivalent added masses.

* Corresponding author. Department of Marine Technology, Norwegian University of Science and Technology (NTNU), Norway.
E-mail address: zhaolong.yu@ntnu.no (Z. Yu).

http://dx.doi.org/10.1016/j.marstruc.2015.11.001
0951-8339/

1. Introduction

The aim of this paper is to present a coupled procedure in ship collisions to predict the detailed structural damage together with reasonable global motions. This method is especially useful for design purposes since the detailed ship hull profile is not needed.

Ship collisions and groundings are highly nonlinear, coupled dynamic processes involving large structural deformations and fluid structure interactions. It is challenging to include all the effects in one simulation. Various methods have thus been proposed since Minorsky [1] presented a simplified decoupled solution. In this method, the collision process is decoupled into two independent parts: external dynamics and internal mechanics. The external dynamics part deals with motions of the striking and struck ships. A basic assumption in the external dynamics is that the effects of fluid are represented by constant added masses. The velocities after collision can then be determined by the conservation of momentum principle. Pedersen and Zhang [2] proposed a closed form theoretical model for the planar external dynamics problem. Stronge [3] developed an advanced solution for 3D impacts. Liu and Amdahl [4] extended Stronge's work for 3D impact cases in a local coordinate system, allowing the geometric shape of vertical contact and objects with 3D eccentricities such as icebergs to be considered.

For the simplified analytical models of external dynamics, knowing the velocities of the striking and struck ships before and after collisions, the energy lost during a collision can be obtained. This lost kinetic energy is dissipated by structural deformations. In the internal mechanics analysis, the struck ship is normally fixed in space, and the striking ship moves along a prescribed path. The final penetration is obtained when the area under the force-penetration curve equals the energy loss resulting from the external dynamic calculations. Nonlinear finite elementcodes such as LS-DYNA or ABAQUS are often used to determine the force-penetration curve; An alternative is to use simplified methods, which allow for fast estimation of the force-penetration curve with reasonable accuracy. Examples of simplified analytical methods can be found in Hong and Amdahl [5], Simonsen [6], Yu et al. [7], etc.

The decoupled method is well suited for a right angle collision when the struck ship is initially motionless. However, often a ship collision does not take place at a right angle, in which case the exact ship path cannot be specified beforehand. Tabri [8] compared the penetration predicted by the decoupled approach with model test results. He found that for unsymmetrical ship collisions, the decoupled approach failed to predict the penetration paths, and the error could be very large. He also found that the dissipated energy given by the decoupled method was typically within a reasonable range, but for cases when the struck ship had a forward speed, the error of the energy dissipation could be considerable. In addition, Motora et al. [9] found that the assumption of constant added masses was often not a good approximation. He showed both experimentally and analytically that the equivalent added masses depended on the collision duration and the variation of collision forces with time. Collisions with longer durations would yield larger equivalent added masses. These effects are not captured in the decoupled approach.

For a more accurate prediction of ship motions and structural responses, a few researchers have turned to the coupled solution. Samuelides [10] developed a code to solve the coupled right-angle collisions. Petersen [11] suggested a coupled simulation procedure, taking into account the transient effects of hydrodynamic loads. The strip theory was used and sectional added masses and damping were calculated using an approximate method. Ship motions were restricted to be in the horizontal plane. Tabri et al. [12] extended the simulation technique to full 6DOF for models of both the striking and struck ships. Brown [13] developed a Simplified Collision (SIMCOL) Model, which was capable of coupling the internal and external mechanics in planar motions. SIMCOL was especially useful in the preliminary design stage. Mitsubishi developed a program entitled MCOL to deal with rigid body dynamics. LeSourne [14] coupled the MCOL code and the super-element method [15] to tackle the internal and external mechanics simultaneously.

These methods emphasized more on external dynamics while the collision forces were simplified. For example, Petersen [11] simplified the collision forces with four nonlinear springs. Tabri et al. [12] assumed homogeneity of ship stiffness and represented the collision forces by integrating the

normal and tangential tractions over the contact surface between the colliding bodies. The super-element method used collision resistances based on simplified analytical solutions [14,15].

Recently, the Arbitrary Lagrangian Eulerian (ALE) finite element method has become available in some nonlinear finite element applications. This facilitates a fully coupled simulation of ship collisions. Traditional Lagrangian meshes are used to model the structures. In the fluid domain, Eulerian meshes are adopted to avoid possible large mesh distortions. Within each time step, the fluid and structure domains are simultaneously calculated, and the forces and boundary conditions are transferred between the two domains. The solver for the fluid domain is based on laminar flow theory, which should be sufficiently accurate for ship collision analysis. Examples of ALE ship collision analyses are found in Lee et al. [16], Rudan et al. [17], etc. However, this fully coupled ALE method requires considerable modeling efforts and large computation resources. Full-ship collision simulations with the ALE method are rarely carried out. This limits its applicability for engineering problems.

Viewing from literature, the collision and grounding area has long been troubled by evaluating internal mechanics and external dynamics simultaneously in one simulation. The major obstacle is that in most numerical codes used for structural analysis, the effect of surrounding water cannot be included efficiently. Most previous coupled models in literature emphasized ship motions in external dynamics, but the detailed structural damage in internal mechanics cannot be obtained. The ALE method is capable of coupling external and internal mechanics, but the simulation is too time-extensive and presents a number of additional challenges. Therefore, a simple and computationally fast method that includes all significant effects is needed for ship collision and grounding analysis.

This paper presents a useful tool, the user-defined load subroutine (LOADUD) and the user common subroutine (USERCOMM) in LS-DYNA, with which a traditional maneuvering model is implemented to represent major effects of the fluid. The maneuvering model uses a mathematical model with a series of non-dimensional coefficients based on experiments. It gives a steady-state representation of hydrodynamic loads in the horizontal plane. The internal mechanics is directly calculated with LS-DYNA; thus, the two parts are efficiently coupled. Ship motions with the proposed coupled method compared reasonably with SIMO. SIMO [18] is a computer program for the simulation of motions and behaviors of floating vessels, which gives a transient solution. Added masses and damping coefficients calculated with potential flow theory can be directly imported into SIMO. Ship collision forces can be applied as an external force vector.

With the proposed 3DOF coupled model, several ship collision simulations with rigid plates and with a semi-submersible platform are carried out. The results are compared with those predicted by the decoupled method. The validity and accuracy of the decoupled method is discussed. For a better understanding of the advantages and limitations, the proposed method is further discussed in the view of equivalent added masses proposed by Motora et al. [9].

The advantages of the proposed hybrid coupled approach can be summarized as follows:

1. The method is capable of efficiently coupling global ship motions and structural responses with reasonable accuracy and little additional computational cost.
2. Previous coupled models generally emphasize global motions and the collision forces and structural damage are usually simplified. In the proposed method, the internal mechanics are directly calculated with LS-DYNA; thus, the collision forces and the damage extent of the structures can be predicted with quite high accuracy while the global motions are predicted reasonably.
3. No external routines are needed to fulfill coupling; thus, it can be widely used.

2. The new coupled method

2.1. The maneuvering hydrodynamic model

The equations of motion constitute the mathematical model of the problems. It is convenient to introduce two coordinate systems, see Fig. 1. One is the earth-fixed coordinate system $X_0O_0Y_0$, and the other, XOY, is fixed to the body, with its origin located at the COG of the ship.

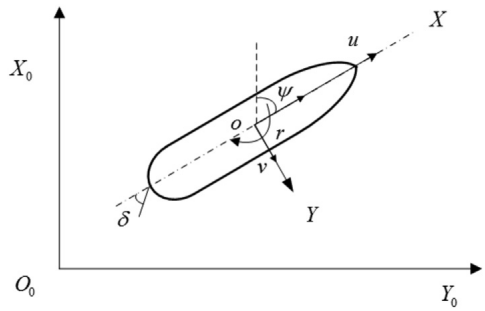

Fig. 1. Coordinate systems.

The governing equations of motion according to Newton's law are given in Eqs. (1)–(3) with reference to the body frame.

$$m\left(\dot{u} - ru - x_G r^2\right) = X_{hydro} + X_{dist} \tag{1}$$

$$m\left(\dot{v} + ru + x_G \dot{r}^2\right) = Y_{hydro} + Y_{dist} \tag{2}$$

$$I_{zz}\dot{r} + mx_G(\dot{v} + ru) = N_{hydro} + N_{dist} \tag{3}$$

The left hand sides of the equation system represent the inertial contributions referring to a ship-fixed coordinate system, and the right sides represent forces or moments acting on the ship. The superscript dot signifies time derivative. u, v, r are the velocities in surge, sway and yaw, respectively. x_G is the position coordinate of the ship COG in the longitudinal x direction. The subscript 'hydro' stands for hydrodynamic forces and moments in calm water, and 'dist' stands for disturbance forces and moments due to wind, waves, current, and, in this case, the collision forces.

The maneuvering model proposed by Norrbin [19] is used for the hydrodynamic forces. The coefficients are nondimensionalized by means of Froude scaling. The nondimensionalized force expressions are:

$$\begin{aligned} X_h = {} & X_{u/u/}u/u/ + X_{uuu/u/}u^3\Big/u/ + X_{vr}vr + (X_G + X_{rr})r^2 + X_{u/v/vv}u/v\Big/v^2 \\ & + X_{cc\delta\delta}c^2\delta^2 + X_{vv}v^2 + X_{uvv}uv^2 + X_{c/c/\delta\delta}c/c\Big/\delta^2 + X_{c/c/v}c/c/v + X_{c/c/\beta\delta}c/c/\beta\delta \end{aligned} \tag{4}$$

$$\begin{aligned} Y_h = {} & Y_{ur}ur + Y_{uur}u^2r + Y_{/u/v}\Big/u/v + Y_{u/u/v}u/u/v + Y_{/v/v}\Big/v/v + Y_{/r/r}r/r/ \\ & + Y_{/v/r}r/v/ + Y_{v/r/}v/r/ + Y_{cc\delta}c^2\delta + Y_{c/c/\delta}c/c/\delta + Y_{c/c/\beta/\beta/\delta}c/c/\beta/\beta/\delta \end{aligned} \tag{5}$$

$$\begin{aligned} N_h = {} & N_{/u/r}\Big/u/r + N_{u/u/r}u/u/r + N_{uv}uv + N_{uuv}u^2v + N_{/v/v}\Big/v/v \\ & + N_{/r/r}r/r/ + N_{/v/r}r/v/ + N_{v/r/}v/r/ + N_{cc\delta}c^2\delta + N_{c/c/\beta/\beta/\delta}c/c/\beta/\beta/\delta \end{aligned} \tag{6}$$

Where ψ is the yaw angle, δ is the rudder angle, ρ is the water density, n is the nominal propeller revolution rate, c is the flow velocity at the rudder and μ is the engine output ratio. u, v and r are the velocity in surge, sway and yaw, respectively.

The nondimensional parameters are:

$$X_{hydro} = \frac{X_{hydro}}{mg}, u = \frac{u}{\sqrt{gL_{pp}}}, v = \frac{v}{\sqrt{gL_{pp}}}, r = \frac{r}{\sqrt{g/L_{pp}}}, \beta = \frac{v}{u}, n = \frac{n}{\sqrt{g/L_{pp}}}, t = \frac{t}{\sqrt{L_{pp}/g}} \tag{7}$$

where β is the drift angle, and L_{pp} is the length between the perpendiculars of the ship.

The origin of the body-fixed coordinate system is set at the ship's center of gravity to eliminate nonzero x_G terms in Eqs. (1)–(3). The nondimensional motion equations are given by:

$$(1 - X_{\dot{u}})\dot{u} = X_h + X_{dist} \tag{8}$$

$$(1 - Y_{\dot{v}})\dot{v} - Y_{\dot{r}}\dot{r} = Y_h + Y_{dist} \tag{9}$$

$$-N_{\dot{v}}\dot{v} + \left(\frac{I_{zz}}{mL_{pp}{}^2} - N_{\dot{r}}\right)\dot{r} = N_h + N_{dist} \tag{10}$$

The nondimensional coefficients used in this paper are based on experiments from Berlekom et al. SNAME 1972 [20]. A series of tests investigating the maneuverability of large tankers was conducted in the Swedish State Shipbuilding Experimental Tank (SSPA) in the 1970s. Berlekom et al. [20] recalculated the experimental results according to an essentially quadratic fit using the 'SSPA steering and maneuvering simulator' and presented a series of nondimensionalized coefficients based on Norrbin's [19] mathematical model. The influence of several parameters on ship maneuverability was investigated, which allowed users to modify the coefficients depending on ship deadweight, L/B ratios and rudder sizes.

2.2. User-defined load and user common subroutine in LS-DYNA

The user-defined load subroutine (LOADUD) has been used in limited applications. An example is a paper by Adoum and Lapoujade [21], which contains a few basic examples demonstrating the application of LOADUD.

The user-defined load subroutine in LS-DYNA allows users to define nodal loads or pressure loads as a function of displacements, velocities, accelerations and user-defined inputs. This is sufficient to facilitate implementation of the traditional maneuvering model to represent the hydrodynamic loads.

However, a problem arises when applying the added mass forces. Nodal accelerations in the user load subroutine are only available for deformable bodies. If a deformable body is to be used to represent a hull girder, the body will generate large structural vibrations and nodal accelerations will oscillate intensively, leading to wrong results.

To solve this acceleration problem, the user common (USERCOMM) subroutine is used to track the velocity history of rigid bodies. The nodal accelerations are then approximated as:

$$a_n = \frac{V_n - V_{n-2}}{t_n - t_{n-2}} \tag{11}$$

where V_n and V_{n-2} are used instead of V_n and V_{n-1} because the code will otherwise yield numerical instabilities.

The time step is typically in the magnitude of 10^{-6} s in ship collision simulation. The nodal accelerations are updated every 10^{-3} s for maintaining good efficiency without losing accuracy. Results from turning circle simulations in LS-DYNA agree reasonably with results from Berlekom et al. [20], which confirms the correct implementation. The maneuvering motions are not the major concern in the ship collision and grounding analysis, and are thus not presented.

2.3. Comparison of ship motions with SIMO simulations

SIMO is used to verify the proposed coupled method. The supply vessel specified in Section 3.1 is accelerated to a forward velocity of 2.25 m/s before it is subjected to collision loads. Hydrodynamic coefficients are calculated with the software HydroD [22] based on the boundary element method. The ship panel model is shown in Fig. 2. An oblique impact case with the collision angle of 56° is used. The collision forces, which are shown in Section 4.2.1, are applied to the SIMO model as a time-dependent force vector. The resulting ship motions in surge, sway and yaw are shown in Fig. 3.

Compared to SIMO calculations, the proposed hybrid coupled method can predict ship motions reasonably well. The surge motion obtains a good match, while the sway and yaw motions are slightly underestimated. This is mainly because the equivalent added mass coefficients in sway and yaw that are used in the coupled method are overestimated. Nevertheless, the deviation is quite small. This shows that the proposed method can predict the global ship motions during collision accidents with reasonable accuracy.

3. Model description and case studies

Several ship collision cases with a rigid plate and a semi-submersible platform are investigated using the proposed coupled model. The models of the striking vessel and the platform are described below.

3.1. The striking ship

This is a supply vessel with a bulbous bow. The principal dimensions of the vessel are given in Table 1. The finite element model of the ship bow is shown in Fig. 4. The element size is generally 120 mm. The plate thickness varies from 7 mm for the decks to 12.5 mm in the bulb. The stiffener spacing is approximately 600 mm, with ring stiffeners and breast hooks of approximately 250 × 15 mm in the bulb. The bulbous part is almost cylindrical and is relatively strong. The forecastle protrudes 1.2 m ahead of the bulb.

The ship's hull girder is represented by two rigid beams from the bow back toward the center of gravity. The beam properties are calibrated to represent correctly the total inertia of the ship with respect to the center of gravity. Because only planar motions are considered, large values are given to the moments of inertia in roll, pitch and the added mass in heave. The maneuvering forces as user-defined loads are applied at the COG of the ship located at the center of the blue beam in Fig. 5.

3.2. The submersible platform

The platform is a four-legged semisubmersible with ring-pontoons. The global motion is small and has little interaction with local deformations. Only the front part of the column including the sponson at the impact point is modeled; see Fig. 6.

An elastic-plastic material model with power-law hardening is used. The yield stress is 275 MPa. As shown in Kõrgesaar and Romanoff [23], the fracture strain is mesh size dependent. A constant failure

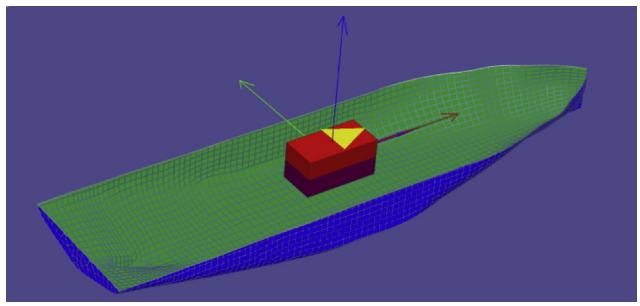

Fig. 2. The ship panel model.

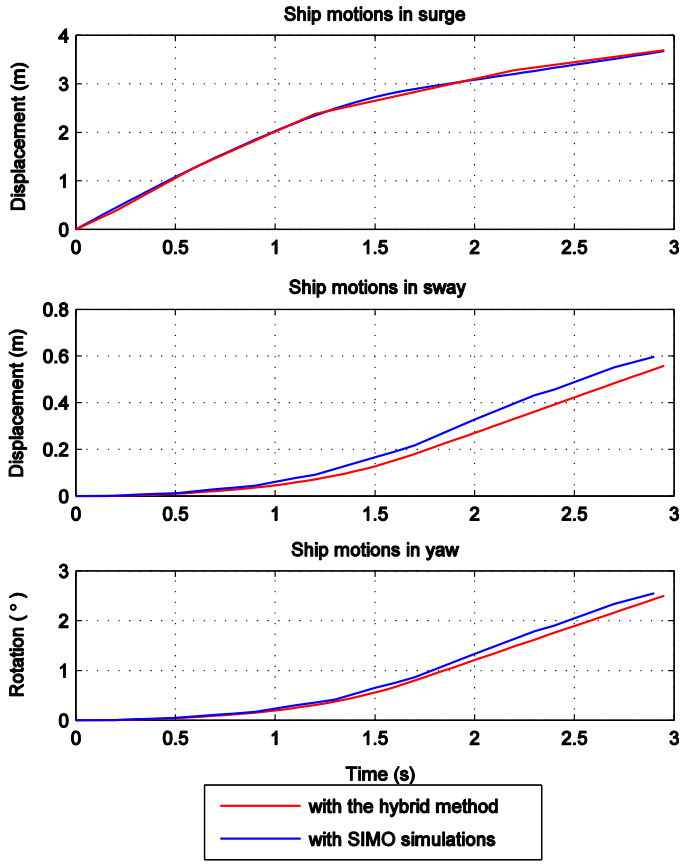

Fig. 3. A comparison of ship motion in surge, sway and yaw.

strain of 0.3 is used for simplicity. The model has mesh size in the range of 90 mm in the region where large deformations are expected, and this gives, on average, three elements over a stiffener web and a minimum of five elements in the plate between each stiffener. Gross plate thickness including corrosion allowance is used, with thicknesses in the range of 18–25 mm.

The mass of the platform is considerably larger than that of the striking ship. Hence, the platform motions are very small and therefore neglected for simplicity. The nodes on the platform boundary edges, marked in black in Fig. 6, are constrained against all translations and rotations. Two schemes of contact are used, self-contact and master-slave contact. The self-contact enables contact of the structures if they deform onto themselves. The master-slave contact is applied between the striking vessel and the platform. The friction coefficient is set as 0.3 at all the contacts. In this study, the Belytschko-Lin-Tsay shell elements, with five integration points through the thickness, are used for both the ship and the platform. This element type is selected as the default shell element in LS-DYNA because of its computational efficiency due to the co-rotational and velocity-strain formulation. Hourglass deformation modes are controlled using the stiffness-based hourglass control option, with a stiffness factor of 0.03. The calculation shows that the hourglass energy is less than 2% of the internally dissipated strain energy.

3.3. Simulation cases

Several cases are simulated with the proposed coupled method. The cases are summarized in Table 2. An initial speed of 2.25 m/s of the striking ship is assumed, and this gives an initial kinetic energy of 19 MJ.

Table 1
Principal dimensions of the striking vessel.

Displacement	7500 ton
Length	90 m
Breadth	18.8 m
Depth	7.6 m
Draft	6.2 m

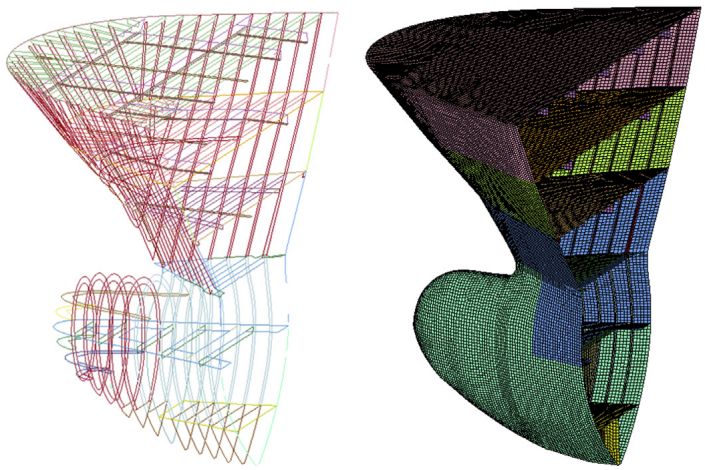

Fig. 4. The FE model of the bulbous bow.

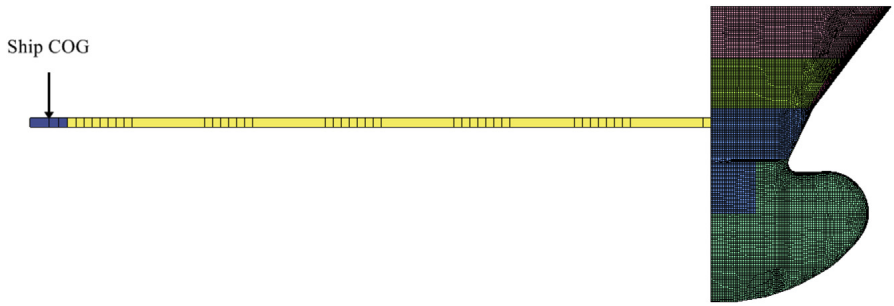

Fig. 5. The FE model of the striking ship.

4. A comparative study using the decoupled approach

4.1. Basic assumptions of the decoupled approach

A local coordinate $\xi\eta$ system is established in Fig. 7 with the ξ direction normal to the contact point, following the approach by Pedersen and Zhang [2]. The ships are allowed to rebound from each other in the ξ direction by introducing a coefficient of restitution e defined as:

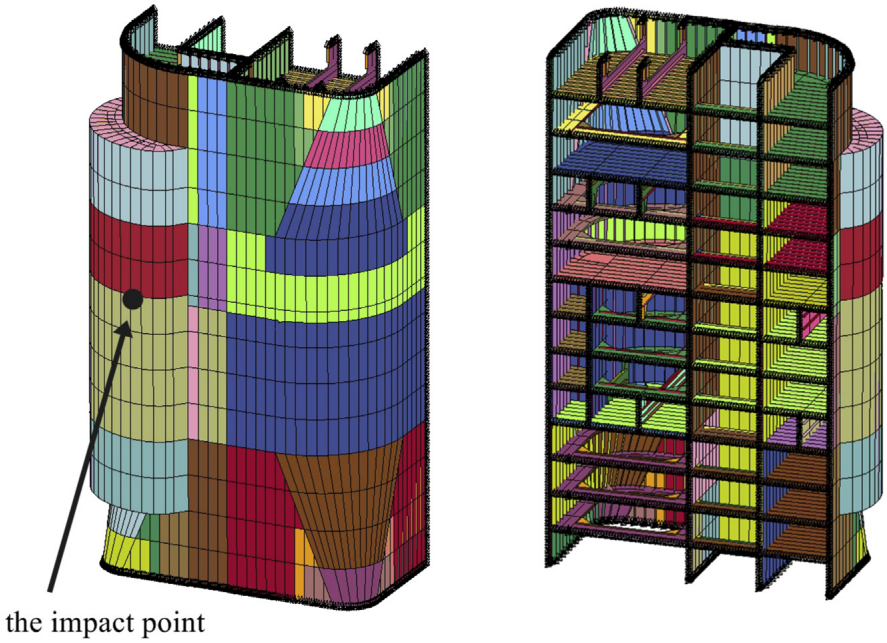

Fig. 6. FE models of the semi-sub platform column.

$$e = \left| \frac{\dot{\xi}(t=T)}{\dot{\xi}(t=0)} \right| \tag{12}$$

Where $\dot{\xi}(t=0)$ and $\dot{\xi}(t=T)$ represent the relative velocities of the striking and struck ships in the ξ direction normal to the contact plane before collision at $t=0$ and after collision at $t=T$, respectively. The relative velocity in the ξ direction at the end of the impact can be directly obtained as $-e\cdot\dot{\xi}(t=0)$. The parameter e is 0 for an entirely plastic collision and is 1 for a perfect elastic collision. The ratio of impact impulses in the η and ξ direction $\mu = I_{\eta 0}/I_{\xi 0}$ is introduced to judge whether the striking and struck ships will stick or slide against each other.

If $|\mu| \leq |\mu_0|$ (μ_0 is the static friction coefficient), the two ships will stick together, and the relative velocity after collision is zero in the η direction. The collision forces are assumed to satisfy the relation $F_\eta = \mu \cdot F_\xi$, where μ is the ratio of impact impulses.

If $|\mu| > |\mu_0|$, the two ships will glance off each other. Then, $F_\eta = \mu_0 \cdot F_\xi$ according to Coulomb's friction law.

With these assumptions, the relative velocities in the ξ and η directions and the subsequent dissipated energy after the collision are readily obtained. It is implicitly assumed that the angles α and β do not change during the collision process.

4.2. Ship collision with a rigid plate

The simple ship collision cases with a rigid plate is first studied, which means $\alpha = \beta$ in Fig. 7. Liu and Amdahl [4]'s 3D model is used for calculations with the decoupled method.

4.2.1. Sliding scenario

The ship will slide along the rigid plate for the collision scenarios with angles of 35°, 44° and 56°. A top view of the collision scenarios before and after collision is presented in Fig. 8 for case C1-35 and case C1-56. Case C1-44 is similar and is not presented. Here the phrase 'after collision' means the

Table 2
Case definitions.

Case no.	Struck object	Collision angle (°)	Initial velocity (m/s)
C1-35	Rigid plate	35	2.25
C1-44	Rigid plate	44	2.25
C1-56	Rigid plate	56	2.25
C1-80	Rigid plate	80	2.25
C2-56	Platform	56	2.25

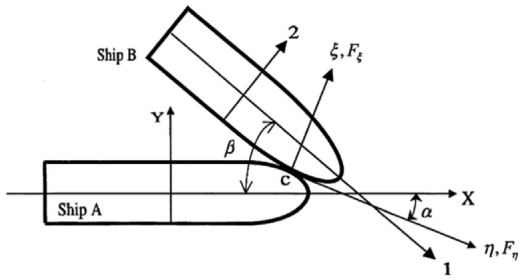

Fig. 7. The coordinate system used for ship collision analysis, according to Pedersen and Zhang [2].

moment when the contact forces decrease to zero. The time histories of the planar motions for the three cases are shown in Fig. 9. It is observed that smaller collision angles give larger sway and yaw motions after collision, and the surge velocity drops more slowly. This is because the transverse force component and the yaw moment increase as the collision angle decreases from 56° to 35° while the longitudinal force component decreases.

Three coordinate systems are used, namely the global earth fixed coordinate, the ship fixed coordinate and the local coordinate at the impact point; see Fig. 10. The collision force curves are represented in the earth-fixed $X_0O_0Y_0$ coordinate and are shown in Fig. 11. The collision forces change drastically at about 1.3 s for case C1-56 because the bulbous bow starts to be crushed at this time. During sliding, Coulomb's friction law $F_\eta = \mu_0 \cdot F_\xi$ is assumed in the decoupled approach. When transformed into the global coordinate system, the ratio of the vertical and horizontal forces are expressed as:

$$\lambda = \frac{F_{Y_0}}{F_{X_0}} = \frac{F_\xi \cdot \cos\alpha - F_\eta \cdot \sin\alpha}{F_\xi \cdot \sin\alpha + F_\eta \cdot \cos\alpha} \tag{13}$$

This force ratio versus collision angle in the global coordinate system is given in Fig. 12. Note that this ratio is only valid for sliding cases, and $\mu_0 = 0.3$ is used in the simulations. The force ratios for cases C1-35 and C1-56 using the coupled approach are shown in Fig. 13. The vertical and horizontal forces decrease to zero after collision, and the force ratio then becomes 0/0. It is set to be zero for simplicity. It is observed that, despite the occurrence of small oscillations, the force ratio remains a constant value in general. According to Fig. 12, the decoupled method predicts force ratios of 0.31 and 0.79 for cases C1-56 and C1-35, respectively. These values agree well with the simulation results shown in Fig. 13. The same also goes for case C1-44, which confirms the assumption of a constant force ratio in the decoupled approach for sliding rigid plate impacts.

A comparison of the dissipated internal and friction energy for the three cases predicted by the hybrid coupled method and the decoupled method is shown in Fig. 14. The restitution factor is set to zero as it is typically used. It is observed that the dissipated strain energy predicted by the decoupled method is generally reasonable, but the error of friction energy can be considerable.

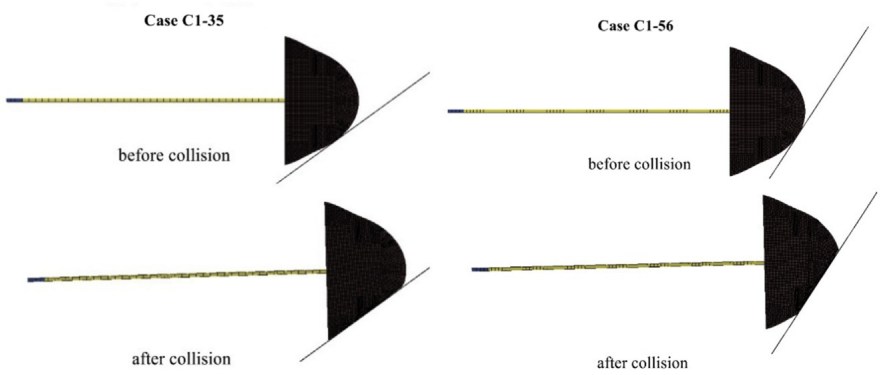

Fig. 8. A top view of the ship-rigid plate collision before and after collision.

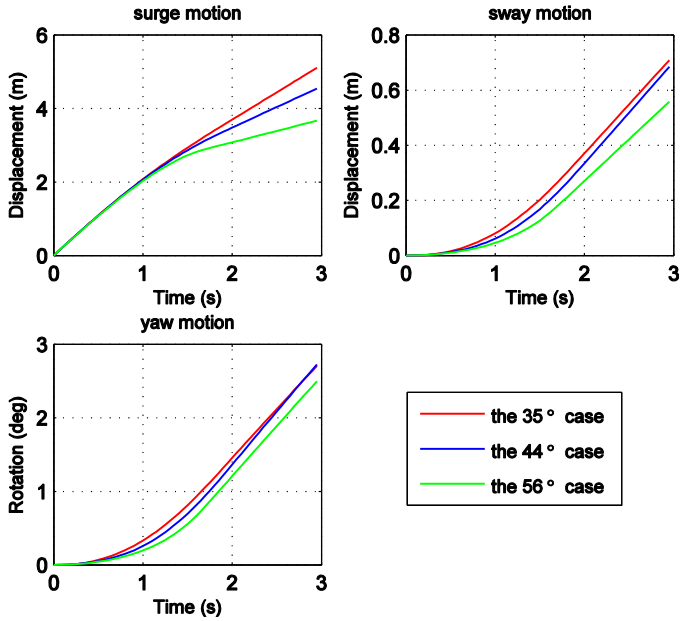

Fig. 9. The time histories of ship motions.

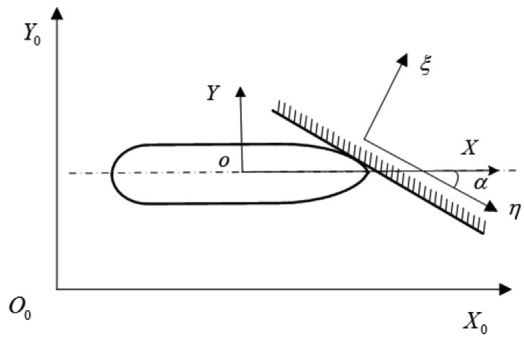

Fig. 10. The three coordinate systems.

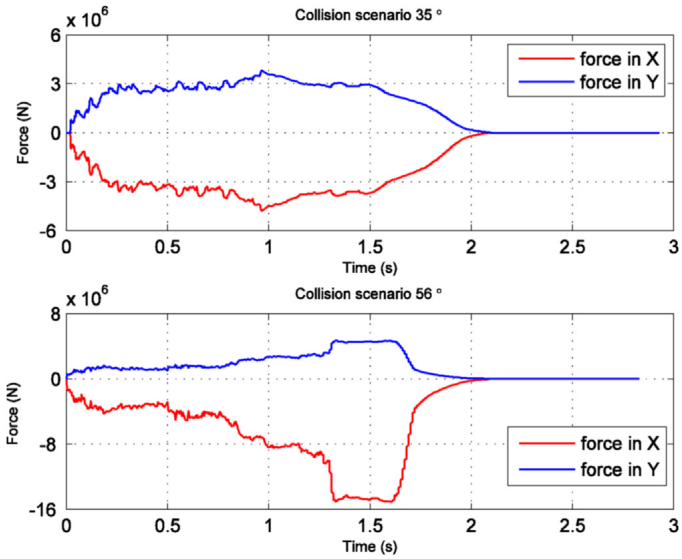

Fig. 11. The time sequence of collision force in the global coordinate system.

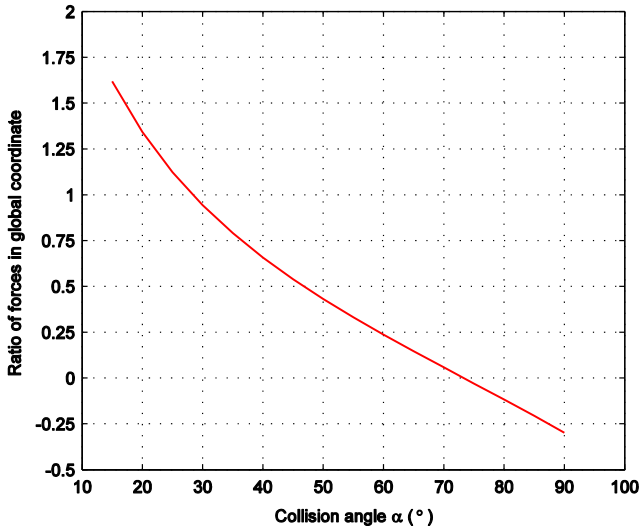

Fig. 12. The ratio of forces versus collision angles in the global coordinate system.

Take case C1-35 as an example. The variation of dissipated energy with the restitution factor using the decoupled method is shown in Fig. 15. It is observed that the internal energy reaches its maximum when e equals to 0 and decreases with increasing restitution factor. However, the friction energy continuously increases with e because friction energy is also dissipated in the unloading phase. The gradient is virtually linear. The total energy is maximized when a restitution factor of about 0.5 is used. It is clear that the commonly used restitution value of zero is not conservative.

A challenge of the decoupled approach is how to decide the value of the restitution factor. It is recommended to adjust the restitution factor to the value, with which the friction energy is properly

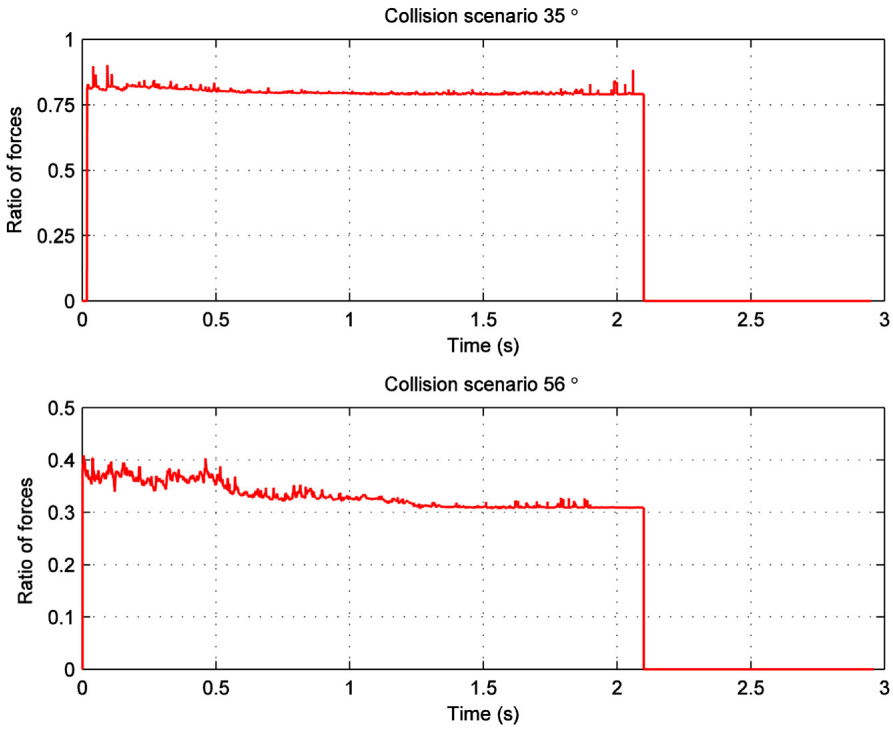

Fig. 13. The ratio of vertical and horizontal forces in the global coordinate system.

predicted. This is because the internal energy is very sensitive to the collision angle changes while the friction energy is not. As an example, the decoupled method predicts an internal energy dissipation of 11.51 MJ and 10.47 MJ for a collision angle of 56° and 54° respectively, with corresponding energy dissipation due to friction as 4.78 MJ and 4.84 MJ. The friction energy dissipation does not change much with yaw motions, while the change of the predicting internal energy is large.

With the above method for the restitution factor, the dissipated strain/internal energy is compared in Table 3. The strain energy is found to decrease more slowly than the friction energy increases, and the total energy obtained a better agreement.

It is interesting to find from Fig. 14 that at the moment when the internal energy stops increasing, the friction energy with the coupled method agrees very well with the decoupled method. This is because the velocity normal to the contact plane decreases to zero, and the restitution factor is exactly zero at this time. After that, the unloading stage initiates. The ship starts to be rebounded in the normal direction and the stored elastic energy starts to be released. The elastic energy is quite small, but the friction energy dissipation is still considerable in this stage, in particular for the smallest collision angle 35°.

4.2.2. Sticking scenario

Case C1-80 is analyzed. The impact geometries before and after the collision are shown in Fig. 16. The rebound velocity after collision in the coupled simulation is 0.175 m/s in the longitudinal direction and is negligible transversely. The restitution factor is $V_{after}/V_{initial} = 0.175/2.25 = 0.078$ if the decoupled method is to be used.

The force ratio is approximately $\mu = I_{\eta 0}/I_{\xi 0} = 0.18$ in the local $\xi\eta$ coordinate system and is about 0 when transformed to the global coordinate system with Eq. (13). The collision forces in the longitudinal and transverse directions and the force ratios with the coupled method are given in Fig. 17. It is observed that the force ratio varies significantly but remains within ±0.1.

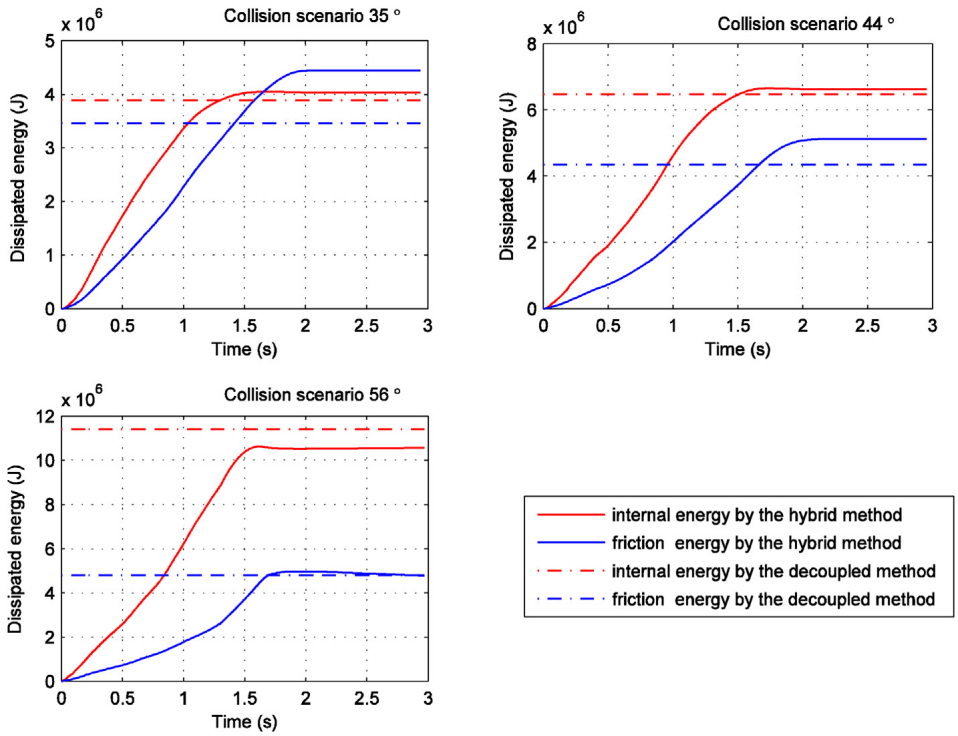

Fig. 14. A comparison of the dissipated energy.

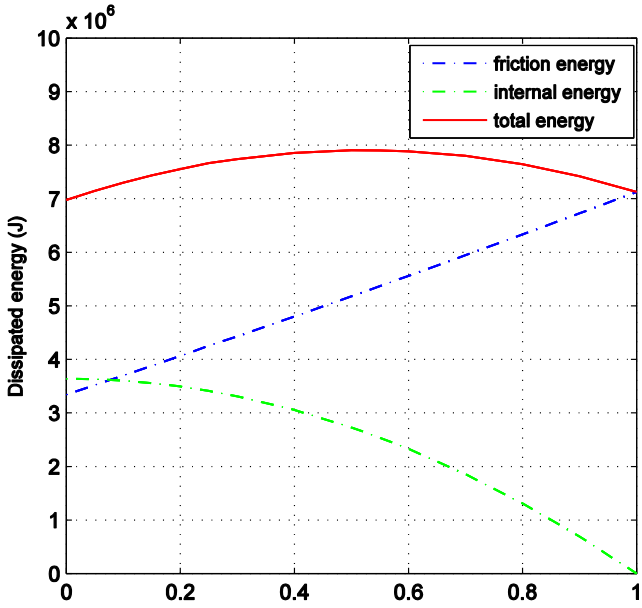

Fig. 15. Variation of dissipated energy with the restitution factor for the 35° collision case.

Table 3
A comparison of the dissipated strain/friction energy.

The collision angle (°)	The coupled method (MJ)	The decoupled method (MJ) when $e = 0$	The decoupled method (MJ) with selected e
35	4.03/4.44	3.89/3.45	3.30/4.44 (e = 0.304)
44	6.62/5.12	6.48/4.34	6.15/5.12 (e = 0.17)
56	10.56/4.78	11.40/4.79	11.40/4.79 (e = 0)

The curves of dissipated energy are shown in Fig. 18. The total energy is well predicted because almost all of the kinetic energy is dissipated. The internal energy is overestimated to some extent and the friction energy is underestimated. This is mainly caused by the assumption of constant force ratios. However, as the total energy is often the major concern, the decoupled approach is considered reasonable.

4.3. Ship collision with a platform

The decoupled approach uses the initial contact point to determine the collision angle and does not consider that it may change during the collision. However, during a sliding collision, the contact point will move and the collision angle will change, especially for objects with a curved contour. This will challenge the accuracy of the decoupled method.

A sliding collision case C2-56 between a supply vessel and a semisubmersible platform is studied. The initial impact point is on the sponson on the cylindrical column, as shown in Fig. 6. The collision geometry at the initial contact and at the end of the contact period is shown in Fig. 19. The yaw angle after collision is approximately 2.8°, which is much larger than that of the rigid plate collision.

The collision resistances and force ratios are compared in Fig. 20. The duration of the collision process is much longer than that in a rigid collision because both the striking and the stuck objects deform and dissipate energy. In addition, the bulbous part of the bow is not involved in the collision, which leads to milder changes of the contact forces.

Unlike the rigid plane collision, the force ratio oscillates more. In the first 2 s, it oscillates about a mean value of 0.28. This value is close to the 0.31 predicted by the decoupled method. However, the force ratio decreases after 2 s and oscillates about zero until the end of the collision.

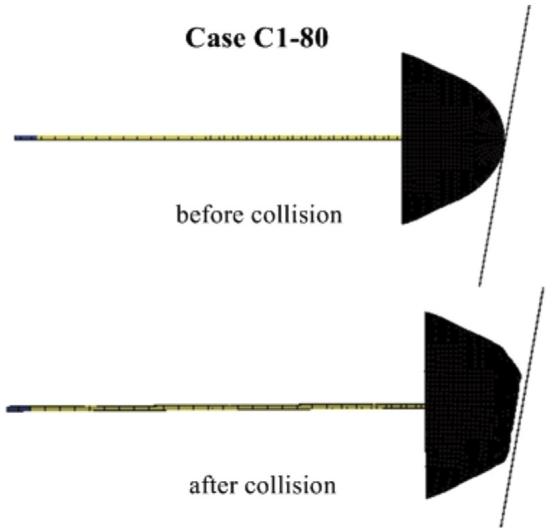

Fig. 16. The scenario before and after the collision.

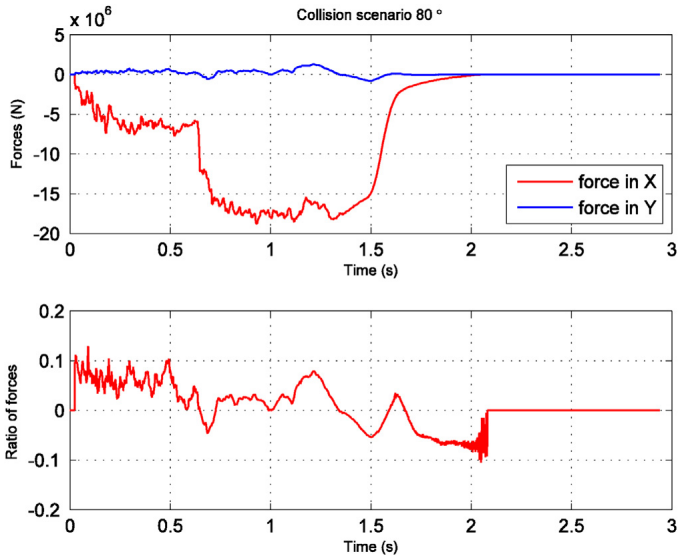

Fig. 17. The collision forces and force ratio.

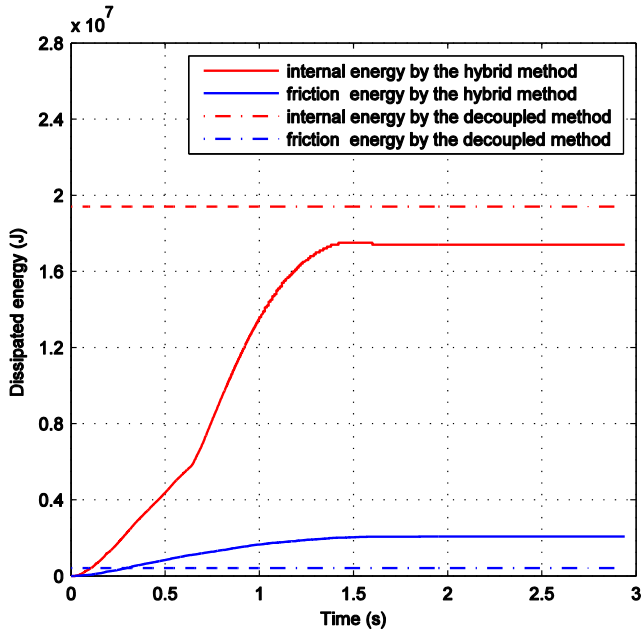

Fig. 18. The time sequence of dissipated energy during a ship collision.

For a better understanding of the underlying mechanism of the force ratio variations, snapshots at several points of time during the collision are given in Fig. 21. For the first 2 s, the contact area is approximately symmetric to the initial contact point, as shown in Fig. 21 (a). The collision angle and force ratio remain unchanged. However, the sliding motion becomes intense after 2 s and the yaw angle increases. The deformed part of the ship bow tends to leave the platform column such that the contact region becomes unsymmetrical. This increases the effective collision angle as shown in Fig. 21 (b)–(d).

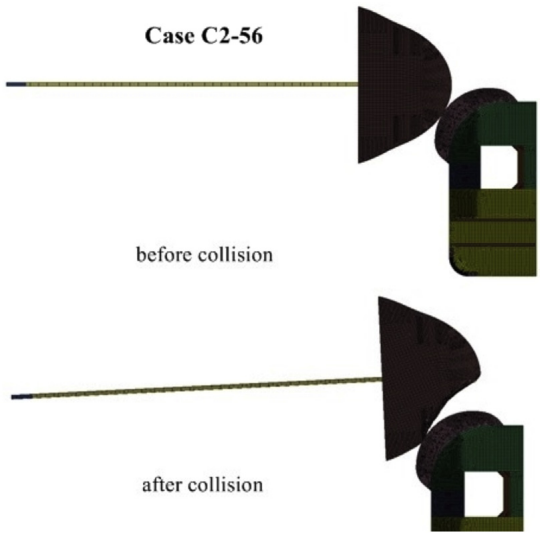

Fig. 19. The collision scenario with the semisubmersible platform.

According to Fig. 12, an increase of the collision angle yields a decrease of the force ratio in the global coordinate system. The force ratio with a mean value of approximately zero from 3 s to the end corresponds to a collision angle of 73°. A measure of the separation point at the collision end gives a collision angle of 67°, which is very close to the predicted value. The change of the collision angle is

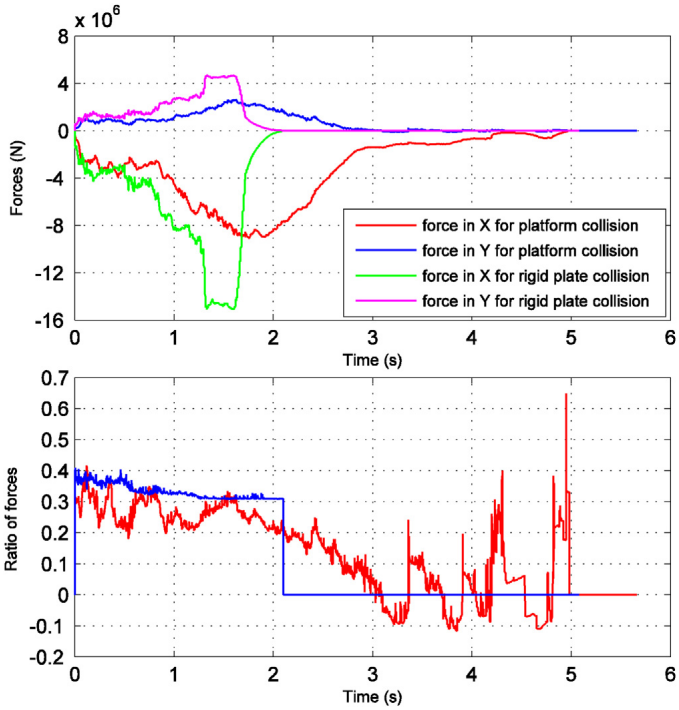

Fig. 20. Comparison of the ratio of forces.

quite considerable and is due to the curved geometry of the struck object as well as the deformation of the bow.

The energy dissipation curves are compared in Fig. 22. It is observed that the decoupled approach predicts lower strain and friction energy. This is unconservative. It is found that most strain energy is dissipated in the first 2 s before unloading and the internal and friction energy at this time agree quite well with the predictions by the decoupled approach. This is consistent with previous conclusions. However, in the unloading phase, the collision angle changes a lot and the rate of energy increase also changes. This change is clearly observed for the platform collision case, but is not obvious for the rigid plate collision because the change of the collision angle induced by the yaw motion is relatively small.

The structural damage of the ship bow at the end of the collision is given in Fig. 23 using the coupled and decoupled method. The collision end for the coupled model represents the moment when the collision forces decrease to zero. For the decoupled method, the collision end means that the ship bow crushes to the points where the dissipated energy in the internal mechanics equals to the energy predicted with the external dynamic models.

It is observed that the two methods predict different structural damage. With the decoupled method where the ship moves in a prescribed manner, the deformation of the ship bow structure conforms to the contour of the platform column and is arc shaped. With the proposed coupled method where the supply vessel is free to move sideways, the penetration normal to the contact plane is smaller and the transverse damage extension is larger. The deformation is no longer circular but elliptical. The coupled method gives more realistic and accurate predictions of energy dissipation and structural damage compared to the decoupled method.

5. Discussions of the coupled method

5.1. Time dependence of added masses

The coefficients for the maneuvering model are mainly based on model tests. However, these tests essentially give ship responses in the steady state, not in the transient phase. To test how well this

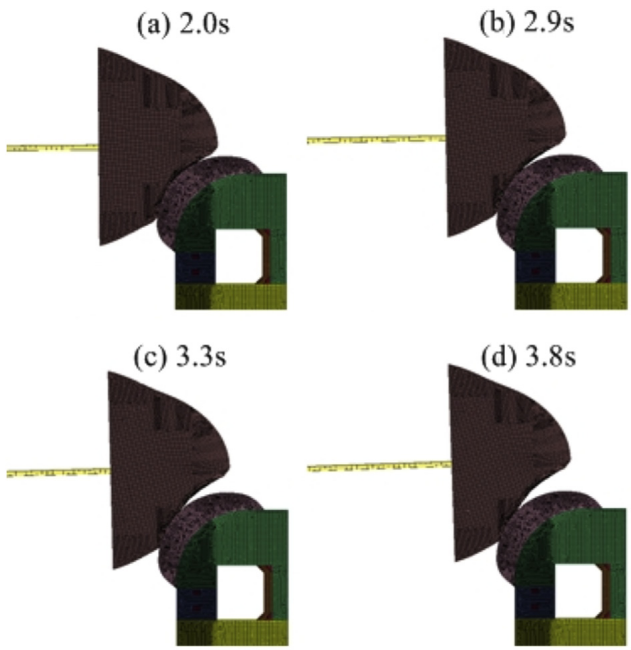

Fig. 21. Snapshots during ship collision with the semisubmersible platform.

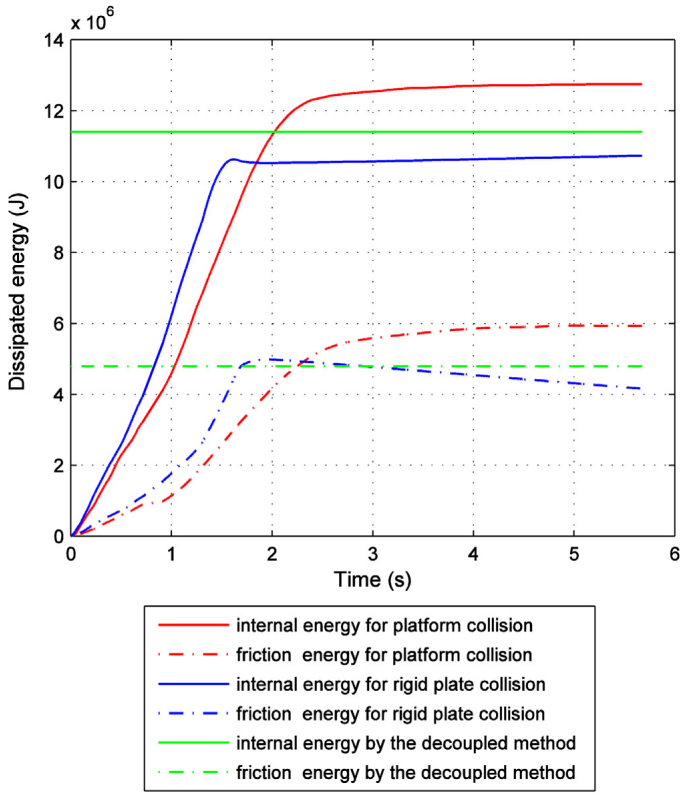

Fig. 22. A comparison of the dissipated energy during ship collision.

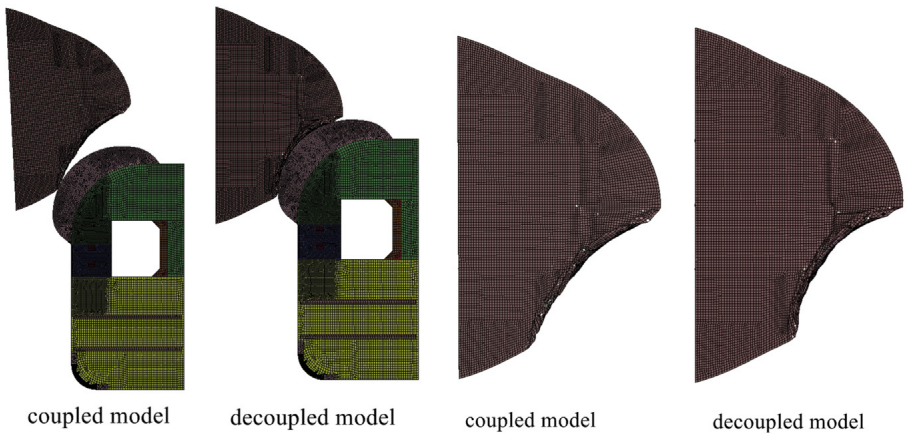

Fig. 23. Structural damage at the end of the collision by the coupled and decoupled methods.

model can simulate the problem, the maneuvering model is studied using definitions of equivalent added masses proposed by Motora et al. [9]. Motora et al. [9] found that there were no time-independent constant value of added mass coefficients. They introduced three definitions of equivalent added mass, which gave exact values for accelerations, momentum and absorbed energy,

respectively. The added masses based on momentum similitude M'_m and energy similitude M'_e were given by:

$$M + M'_m = \frac{\int_0^t f(\tau)d\tau}{v(t)} \tag{14}$$

$$M + M'_e = \frac{\int_0^t f(\tau)v(\tau)d\tau}{\frac{1}{2}v^2(t)} \tag{15}$$

where $f(\tau)$ and $v(\tau)$ are the collision force and velocity at time τ, respectively.

Samuelides [24] considered a central and right-angled collision, and thus only the sway motion was excited for the struck ship after collision. The striking ship moved with an initial forward speed V_0 and the struck ship was motionless initially. After collision, the velocities of the striking and struck ships at a disengagement were V_{1a} and V_{2a} respectively. The equivalent added masses in this case were expressed as:

$$M'_m = M'_2 + \frac{\int_0^{t_d}\left(\int_0^t h(\tau)\dot{s}_2(t-\tau)d\tau\right)dt}{V_{2a}} \tag{16}$$

$$M'_e = M'_2 + \frac{2\int_0^{s_{2m}}\left(\int_0^t h(\tau)\dot{s}_2(t-\tau)d\tau\right)ds}{V_{2a}^2} \tag{17}$$

Where M'_2 is added mass of the struck ship at infinite frequency, $h(\tau)$ is the impulse response function, t_d is the collision duration and s_{2m} is the maximum rigid body displacement of the struck ship.

It is clear to see the time dependency of the equivalent added masses from Eqs. (16) and (17). According to potential theory, the convolution integral term increases with time and approaches a constant value when the transient effects die out. The is consistent with the time dependent equivalent added mass curve obtained by Motora et al. [9] in Fig. 24. Motora et al. [9] investigated the equivalent added masses both analytically and experimentally. The principal dimensions of the ship model in their experiments are shown in Table 4. The ship model was accelerated to sway by a constant external force, and the equivalent added masses were calculated.

The maneuvering model is studied in the view of equivalent added masses. The maneuvering coefficients used in this study are adjusted according to the ship model scale and the L/B ratio in Table 4. The initial forward speed is set to zero. The same external force is applied to the COG in the sway direction. Resulting curves with respect to the equivalent added mass based on energy similitude are shown in Fig. 24. The time representation is in model scale, and 1 s in the model test corresponds to 7.6 s in full-scale trials.

It is worthwhile to clarify the meaning of the analytical curve by Motora et al. [9]. As an example, a collision accident with a duration of 0.5 s in model scale is assumed. If a constant added mass should be used to obtain exactly the same energy at 0.5 s, the added mass coefficient should be 1.1 according to the curve. At the intersection points of the two curves in Fig. 24, the energy is predicted exactly the same with both methods.

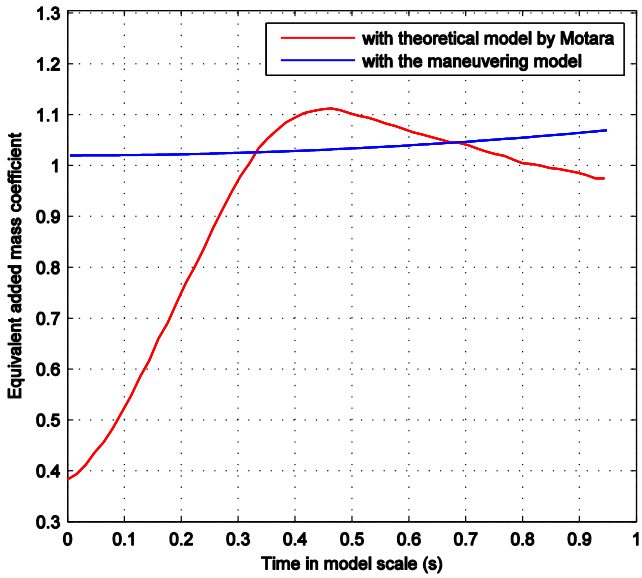

Fig. 24. The equivalent added mass during collision.

It is observed that the maneuvering model is consistent with Motora's experiments when motions become steady. According to Fig. 24, the maneuvering model is suitable for collision durations longer than 0.3 s in model scale, which is approximately 2.3 s in full scale. For a collision incident with a duration shorter than 2.3 s, transient effects predominate and the added mass is overestimated. In such short duration collision cases, an empirical approximation of added masses as a function of collision durations proposed by Petersen and Pedersen [25] can be useful, which is given as:

$$dm = a(\infty) + k(a(0) - a(\infty)) \tag{18}$$

where $a(0)$ and $a(\infty)$ are the limit values of the frequency-dependent added masses when the frequency approaches zero and infinity, respectively. The factor k, is given as a function of the duration of a collision in a normalized form.

5.2. Effects of forward speed on added masses

In Motora's experiment, the ship was only allowed to move in the sway direction. However, ships typically have forward speeds in real cases. In this study, a constant forward speed of 1.0 m/s is assumed in the model scale, which corresponds to 7.6 m/s in the full scale. The same external stepwise force is applied on the ship's COG in sway. The equivalent added masses are compared in Fig. 25. It is

Table 4
Principal dimensions of the ship model by Motora et al. [10].

L_{pp}	2000 mm
B	327.6 mm
D	227.6 mm
d	119.0 mm
Δ	53.0 kg
C_b	0.664
C_p	0.672
C_w	0.826

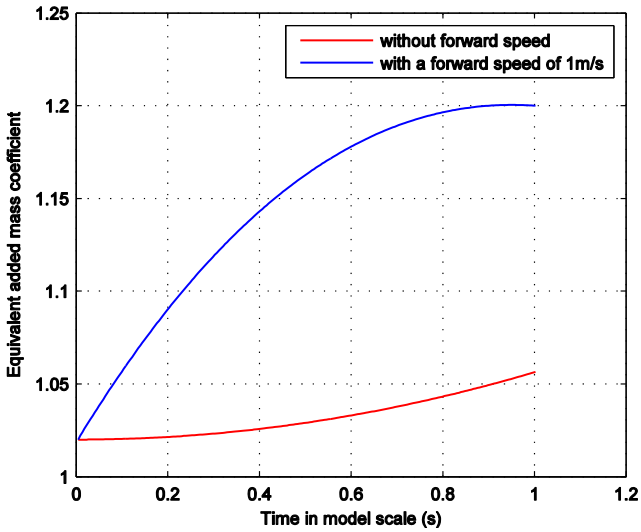

Fig. 25. The influence of forward speed on the added mass in sway.

observed that the coefficient in sway increases much faster when there is a forward speed. This is because a small negative yaw angle is induced due to coupling terms among velocities. If the ship is assumed to be a slender body and can be simplified as a foil, the yaw angle then acts as the attack angle. The induced lift force is proportional to U^2 according to the lifting surface theory and acts opposite to the external force. The equivalent added mass in sway thus increases.

Some coupled ship collision models are based on the transient equations, but they often do not include the forward speed effect. The maneuvering model used in this paper is capable of accounting for the forward speed effect and the coupling between sway and yaw motions, but the transient effects cannot be captured. In view of the large collision forces and the small Froude number, both methods are reasonably accurate.

6. Concluding remarks

A coupled procedure is proposed in this paper to predict the detailed structural damage together with reasonable global motions in ship collision accidents. Several impact cases are simulated, and the results are compared with predictions by a decoupled method. The conclusions are as follows:

1. The proposed coupled method is capable of simultaneously calculating external and internal mechanics in ship collisions with reasonable accuracy and at manageable computational costs. Unlike most previous coupled models, the internal mechanics in the coupled method are calculated with LS-DYNA; thus, collision forces and structural damage can be predicted with high precision.
2. The maneuvering model gives a crude approximation of hydrodynamic loads capturing the major effects of the fluid. However, the global motions are verified to be of reasonable accuracy for the purpose of structural design. The forward speed is shown to have an influence on the equivalent added masses. The present model considers only ship motions in the horizontal plane, and it will be extended to consider the full 6DOF ship motions in future work.
3. The collision angle will change during a sliding collision due to the yaw motion and the curved geometrical contour of the striking and struck objects. This may challenge the accuracy of the decoupled method, especially when the collision angle changes are large. The coupled method is capable of considering the effect of a changing collision angle and predicting the global motions and the structural deformations with good accuracy.

4. For sticking collisions, the decoupled approach predicts the energy contributions from the internal energy and the friction energy with less precision because of the assumption of constant force ratios. The prediction is reasonable in view of total energy dissipation.

Acknowledgments

This work has been funded by the Research Council of Norway (NFR) through the Centers of Excellence funding scheme, project AMOS (project no. 50053806) at the Norwegian University of Science and Technology (NTNU). This support is gratefully acknowledged by the authors.

References

[1] Minorsky V. An analysis of ship collisions with reference to protection of nuclear power plants. New York: Sharp (George G.) Inc.; 1958.
[2] Pedersen PT, Zhang S. On impact mechanics in ship collisions. Mar Struct 1998;11(10):429–49.
[3] Stronge WJ. Impact mechanics. Cambridge University Press; 2004.
[4] Liu Z, Amdahl J. A new formulation of the impact mechanics of ship collisions and its application to a ship–iceberg collision. Mar Struct 2010;23(3):360–84.
[5] Hong L, Amdahl J. Rapid assessment of ship grounding over large contact surfaces: Taylor & Francis, Jeom Kee Paik and the Editorial Board of Ships and Offshore Structures are delighted to announce that the following paper has been awarded the 2012 Best Paper Award. Ships Offshore Struct 2013;8(1):1–2.
[6] Simonsen BC. Ship grounding on rock—I. Theory. Mar Struct 1997;10(7):519–62.
[7] Yu Z, Hu Z, Wang G. Plastic mechanism analysis of structural performances for stiffeners on bottom longitudinal web girders during a shoal grounding accident. Mar Struct 2015;40(0):134–58.
[8] Tabri K. Influence of coupling in the prediction of ship collision damage. Ships Offshore Struct 2012;7(1):47–54.
[9] Motora Seizo, Fujino Masataka, Sugiura Masanori, Sugita Matsuji. Equivalent added mass of ships in collisions. J Soc Naval Archit Jpn 1971;7:138–48.
[10] Samuelides E, Frieze P. Fluid-structure interaction in ship collisions. Mar Struct 1989;2(1):65–88.
[11] Petersen MJ. Dynamics of ship collisions. Ocean Eng 1982;9(4):295–329.
[12] Tabri K, Varsta P, Matusiak J. Numerical and experimental motion simulations of nonsymmetric ship collisions. J Mar Sci Technol 2010;15(1):87–101.
[13] Brown AJ. Collision scenarios and probabilistic collision damage. Mar Struct 2002;15(4–5):335–64.
[14] Le Sourne H. A ship collision analysis program based on super-element method coupled with large rotational ship movement analysis tool. In: International Conference on Collision and Grounding of Ships; 2007.
[15] Lützen M, Simonsen BC, Pedersen PT. Rapid prediction of damage to struck and striking vessels in a collision event. In: Proceedings of ship structures for the new millennium: Supporting Quality in Shipbuilding, Arlington; 2000.
[16] Sang-Gab Lee, Jae-Hyung Nam, Jin-Kyung Kim, Tuo Zhao, Hong-Anh Nguyen. Structural safety assessment of ship collision using FSI analysis technique. In: 22nd International Offshore and Polar Engineering Conference, ISOPE-2012; 2012 [Rhodes].
[17] Rudan S, Tabri K, Klarić I. Analysis of sloshing interaction in ship collisions by means of ALE finite element method. In: International Conference on Collision and grounding of Ships, Espoo, Finland, 2010; 2010.
[18] Marintek Report SIMO – User's manual Version 4.0 rev0. 2012.
[19] Norrbin NH. Theory and observations on the use of a mathematical model for ship manoeuvring in deep and confined waters. 1971. DTIC Document.
[20] Van Berlekom WB, Goddard TA. Maneuvering of large tankers. In: Presented at the Annual Meeting of SNAME, Society of Naval Architects and Marine Engineers; 1972. Paper #8.
[21] Adoum M, Lapoujade V. Examples' manual for* USER_LOADING option. In: Proc. 4th European LS-DYNA Users Conference, Ulm, Germany; 2003.
[22] DNV. HydroD user manual. 2014.
[23] Körgesaar M, Romanoff J. Influence of mesh size, stress triaxiality and damage induced softening on ductile fracture of large-scale shell structures. Mar Struct 2014;38:1–17.
[24] Samuelides E. Structural dynamic and rigid body response coupling in ship collisions. Doctoral thesis. University of Glasgow; 1984.
[25] Petersen MJ, Pedersen PT. Collisions between ships and offshore platforms. In: Offshore Technology Conference; 1981.

Appendix A: appended papers

PAPER 2

Yu Z., Amdahl J.

Full six degrees of freedom coupled dynamic simulation of ship collision and grounding accidents

Published in

Marine Structures
Vol. 47, Pages 1-22, 2016

Marine Structures 47 (2016) 1–22

Contents lists available at ScienceDirect

Marine Structures

journal homepage: www.elsevier.com/locate/marstruc

Full six degrees of freedom coupled dynamic simulation of ship collision and grounding accidents

Zhaolong Yu [a, b, *], Jørgen Amdahl [a, b]

[a] Centre for Autonomous Marine Operations and Systems (AMOS), Norwegian University of Science and Technology (NTNU), Trondheim, Norway
[b] Department of Marine Technology, Norwegian University of Science and Technology (NTNU), Trondheim, Norway

ARTICLE INFO

Article history:
Received 3 December 2015
Received in revised form 23 February 2016
Accepted 21 March 2016
Available online 31 March 2016

Keywords:
Ship collision and grounding
The hybrid method
Ship motions
6DOF
Coupled simulation

ABSTRACT

By taking advantage of the user-defined load subroutine (*loadud*) and the user common subroutine (*usercomm*) in LS-DYNA, the authors proposed a new coupled approach for simultaneously calculating structural damage and the planar 3DOF ship motions in ship collisions. The coupled procedure aimed at predicting the detailed structural damage together with reasonable global ship motions. This paper extends the method to consider the full 6DOF ship motions; thus, ship collision as well as grounding accidents can be properly handled. This method is particularly useful for design purposes because the detailed ship hull profile is not needed.

A traditional ship maneuvering model is used for the in-plane surge, sway and yaw degrees of freedom with a series of nondimensional coefficients determined from experiments. It is assumed that the out-of-plane degrees of freedom are not coupled with the in-plane ship motions, and there is no coupling among roll, pitch and heave motions. The implementation is verified through free decay tests, and the obtained natural periods show good agreement with theoretical results.

Several collision and grounding cases are simulated in which a supply vessel crashes into rigid plates with different orientations. The effects of the roll motion, the heave and pitch motions and the full 6DOF motions are studied. The results are compared with those from a 6DOF decoupled method. Ship motions through the proposed method compare reasonably well with SIMO results. It is found that several consecutive impacts may occur in the simulation of one collision case due to the periodic motions. This is not taken into account in the decoupled method, which makes this method unconservative.

1. Introduction

Ship collisions and groundings are highly nonlinear, coupled dynamic processes involving large structural deformations and fluid structure interactions. To simulate the collision process accurately, it is necessary to couple the fluid and structure domains efficiently. However, this coupling is still challenging to implement. The major obstacle is that in most numerical

* Corresponding author.Centre for Autonomous Marine Operations and Systems (AMOS), Norwegian University of Science and Technology (NTNU), Trondheim, Norway.
E-mail address: zhaolong.yu@ntnu.no (Z. Yu).

http://dx.doi.org/10.1016/j.marstruc.2016.03.001
0951-8339/

codes used for structural analysis, the effect of surrounding water cannot be included efficiently. Various methods are proposed to simplify the problem.

In the past decades, the most widely used method for ship collision analysis is that pioneered by Minorsky [1] in which the collision problem is decoupled into external dynamics and internal mechanics. Examples of theoretical models for external dynamics can be found in Pedersen and Zhang [2] for planar 3DOF ship motions and in Liu and Amdahl [3] for 6DOF ship motions. Liu and Amdahl's model allowed the geometric shape of vertical contact and objects with 3D eccentricities such as icebergs to be considered. The energy determined in the external dynamics analysis is dissipated as strain energy in the assessment of the internal mechanics, where the ship is typically supposed to move in a displacement-controlled manner. The decoupled method is simple to apply and provides reasonable accuracy of the energy prediction in most cases. However, ship paths are not well predicted, and the error of the final penetration into the struck ship can be as large as 80% according to Tabri [4]. In addition, the effects of the fluid are considered to be constant added masses that may lead to further inaccuracies.

For a more accurate prediction of ship motions and structural responses, a few researchers have turned to the coupled solution. Petersen [5] suggested a coupled simulation procedure, taking into account the transient effects of hydrodynamic loads. The strip theory was used, and sectional added masses and damping were calculated through the use of an approximate method. Ship motions were restricted to the horizontal plane. Tabri et al. [6] extended the simulation technique to full 6DOF for models of both the striking and struck ships. Brown [7] developed a Simplified Collision (SIMCOL) model that was capable of coupling the internal and external mechanics of the planar motions. SIMCOL was especially useful in the preliminary design stage. Mitsubishi developed a program entitled MCOL (Mitsubishi Collision) to address rigid body dynamics. Le Sourne [8] coupled the MCOL code with the super element method [9] to tackle the internal and external mechanics simultaneously. The MCOL code has also been used by Tørnqvist [10] for symmetric collisions and by Biehl et al. [11] for collisions between a push barge and a rigid wall. The above methods are usually based on certain simplifications of the collision forces. For example, Petersen [5] simplified the collision forces with four nonlinear springs. Tabri et al. [6] assumed the homogeneity of ship stiffness and represented the collision forces by integrating the normal and tangential tractions over the contact surface between the colliding bodies. The super element method uses the collision resistances of the simplified analytical solutions [8,9].

An alternative approach to coupling local deformations and global ship motions is the Arbitrary Lagrangian Eulerian (ALE) finite element method in which the model is divided into two domains: a fluid domain and a structure domain. Traditional Lagrangian meshes are used in the structure domain. In the fluid domain, Eulerian meshes are adopted to avoid possible large mesh distortions. Within each time step, the fluid and structure domains are simultaneously calculated, and forces and boundary conditions are transferred. The huge number of structural and fluid elements for a full ship simulation and the complex solvers in both domains require considerable computation capacity. Therefore, full-ship collision simulations through the ALE method are rarely reported in the literature. More often, the ALE method is carried out for studying the sloshing interaction between the fluid and structures, such as in Rudan et al. [12] and Zhang and Suzuki [13].

Yu et al. [14] presented useful tools, the user-defined load subroutine and the user common subroutine in LS-DYNA, with which the planar 3DOF ship motions and structural deformations are efficiently coupled. The effects of the fluid were calculated through the use of a traditional ship maneuvering model on the basis of experiments. The hydrodynamic forces were applied as a force vector to the rigid beam model. This paper further extends the method to consider the full 6DOF ship motions during ship collisions and groundings. Decay tests for roll, pitch and heave are carried out to verify the implementation of the user load and to ensure that the correct natural periods are obtained. Several collision and grounding cases, in which a supply vessel crashes into rigid plates with different orientations, are simulated through the 6DOF coupled method. The effects of the roll motion, the heave and pitch motions and the full 6DOF motions are studied. The results are compared with those from a 6DOF decoupled approach and are discussed in some detail. It is interesting to observe that several consecutive contacts do occur in the simulation of one collision case, and the secondary impacts will make the 6DOF decoupled method very unconservative in some cases. Ship motions through the proposed 6DOF coupled method compared reasonably well with the results using SIMO. SIMO [15] is a computer program for the simulation of the motion and behavior of floating vessels. The added masses and damping forces, which are calculated with potential hydrodynamic theory, can be directly imported. Ship collision forces can be applied as an external force vector.

The proposed coupled method is shown to be capable of efficiently coupling structural deformation and the 6DOF ship motions. Unlike most previous coupled models, the internal mechanics are calculated through the use of LS-DYNA; thus, the collision forces and damage extents of structures can be predicted with high accuracy, while the global motions are predicted reasonably well. In addition, the method can be widely used because no external routines are needed. Therefore, this method constitutes a promising tool for coupled ship collision and grounding analysis.

2. The coupling algorithm using LS-DYNA

2.1. LS-DYNA for structural analysis

LS-DYNA is a general purpose finite element code for analyzing the large deformation static and dynamic response of structures. It is widely used in the automotive and offshore industries for crash and impact analysis. LS-DYNA uses the explicit central difference scheme to integrate the equation of motions. For maintaining solution stability, the timestep size should

not exceed the required critical timestep [16]. The penalty based contact algorithm allow to treat difficult contact problems. A variety of element formulations and material constitutive models are available in LS-DYNA.

For ship collision and grounding problems, the nonlinear FEA have exhibited great capabilities to simulate the complicated problems by comparing with experimental tests. Yamada and Endo [17] investigates the collapse strength and the mechanism of the bulbous bow structure in case of an oblique collision by experiments and LS-DYNA, and fairly good agreement was achieved. Paik [18] presented practical finite element (FE) modelling techniques to simulate structural crashworthiness in ship collisions and grounding, and the application examples agreed well with experimental results. More experimental validation of numerical simulation using the NLFEA can also be found in Amdahl and Kavlie [19] and Ohtsubo et al. [20].

A wide range of numerical parameters have to be determined when conducting the NLFEA. This requires good expertise and engineering judgement. Recommendations of numerical setups for ship collision simulations can be found in Storheim [21], Sajdak and Brown [22] and Paik [23].

2.2. Theory of hydrodynamic loads

2.2.1. The planar 3 degrees of freedom

The maneuvering model in Yu et al. [14] is still used to consider the in-plane 3DOF ship motions. The theory is briefly introduced.

The governing equations of motion according to Newton's law are given in Eqs. (1)–(3) with reference to the body frame. The origin of the body fixed XOY coordinate is located at the center of gravity (COG) of the ship as shown in Fig. 1.

$$m\left(\dot{u} - ru - x_G r^2\right) = X_{hydro} + X_{dist} \tag{1}$$

$$m\left(\dot{v} + ru + x_G \dot{r}^2\right) = Y_{hydro} + Y_{dist} \tag{2}$$

$$I_{zz}\dot{r} + mx_G(\dot{v} + ru) = N_{hydro} + N_{dist} \tag{3}$$

The left hand sides of the equation system represent the inertial contributions referring to the coordinate XOY, and the right sides represent forces or moments acting on the ship. The superscript dot signifies time derivative. u,v,r are the velocities in surge, sway and yaw, respectively. x_G is the position coordinate of the ship COG in the longitudinal x direction. The subscript 'hydro' stands for hydrodynamic forces and moments in calm water, and 'dist' stands for disturbance forces and moments due to wind, waves, current, and, in this case, the collision forces.

The maneuvering model proposed by Norrbin [24] is used for the hydrodynamic forces. The coefficients are non-dimensionalized by means of Froude scaling. The nondimensionalized force expressions are:

$$X_h = X_{u/u/}u/u/ + X_{uuu/u/}u^3\Big/u/ + X_{vr}vr + (X_G + X_{rr})r^2 + X_{u/v/vv}u/v\Big/v^2 + X_{cc\delta\delta}c^2\delta^2 + X_{vv}v^2 + X_{uvv}uv^2 + X_{c/c/\delta\delta}c/c\Big/\delta^2 + X_{c/c/v}c/c/v + X_{c/c/\beta\delta}c/c/\beta\delta \tag{4}$$

$$Y_h = Y_{ur}ur + Y_{uur}u^2r + Y_{/u/v}\Big/u/v + Y_{u/u/v}u/u/v + Y_{/v/v}\Big/v/v + Y_{/r/r}r/r/ + Y_{/v/r}r/v/ + Y_{v/r/}v/r/ + Y_{cc\delta}c^2\delta + Y_{c/c/\delta}c/c/\delta + Y_{c/c/\beta/\beta/\delta}c/c/\beta/\beta/\delta \tag{5}$$

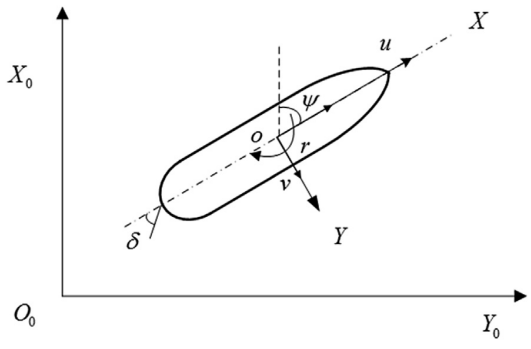

Fig. 1. Coordinate systems.

$$N_h = N_{/u/r}\Big/u/r + N_{u/u/r}u/u/r + N_{uv}uv + N_{uuv}u^2v + N_{/v/v}\Big/v/v + N_{/r/r}r/r/ + N_{/v/r}r/v/ + N_{v/r/}v/r/ + N_{cc\delta}c^2\delta + N_{c/c/\beta/\beta/\delta}c/c/\beta/\beta/\delta \quad (6)$$

where ψ is the yaw angle, δ is the rudder angle, ρ is the water density, n is the nominal propeller revolution rate, c is the flow velocity at the rudder andμ is the engine output ratio. u, v and r are the velocity in surge, sway and yaw, respectively.

The nondimensional coefficients in Eqs (4)–(6) are given in Berlekom et al. SNAME 1972 [25] based on experiments. The coefficients can be adjusted according to ship deadweights, Length/Beam (L/B) ratios and rudder sizes, such that this can applied to a wide range of vessels.

The maneuvering model is a steady-state representation of ship hydrodynamic forces. Yu et al. [14] proved that it was suitable for collision accidents with durations longer than approximately 2 s. For collisions with durations shorter than 2 s, the equivalent added masses can be adjusted according to an empirical expression proposed by Petersen and Pedersen [26]. More details can be found in Yu et al. [14] and Berlekom et al. SNAME 1972 [25].

2.2.2. The out-of-plane 3 degrees of freedom

It is assumed that the out-of-plane ship motions are not coupled with the in-plane ship motions and there is no coupling among roll, pitch and heave motions. Then, the roll, pitch and heave can be simplified as three separate single degree of freedom spring-damper vibration subsystems.

The governing equations are then:

$$(M_{33} + A_{33})\ddot{z} + B_{33}\dot{z} + C_{33}z = 0 \quad (7)$$

$$(I_{44} + A_{44})\ddot{\alpha} + B_{44}\dot{\alpha} + C_{44}\alpha = 0 \quad (8)$$

$$(I_{55} + A_{55})\ddot{\beta} + B_{55}\dot{\beta} + C_{55}\beta = 0 \quad (9)$$

where A_{33},A_{44},A_{55} are added masses for heave, roll and pitch, respectively. α and β are the roll and pitch angles, and z is the heave displacement. The restoring forces are

$$C_{33} = \rho g A_w \quad (10)$$

$$C_{44} = \rho g \nabla \bullet GM_T \quad (11)$$

$$C_{55} = \rho g \nabla \bullet GM_L \quad (12)$$

whereA_w is the water plane area, ∇ is the ship displacement, and GM_T and GM_L are the transverse and longitudinal metacentric heights, respectively.

By moving terms of the motion equations to the left side, the hydrodynamic forces for heave, roll and pitch are expressed as:

$$F_{33} = -A_{33}\ddot{z} - B_{33}\dot{z} - C_{33}z \quad (13)$$

$$M_{44} = -A_{44}\ddot{\alpha} - B_{44}\dot{\alpha} - C_{44}\alpha \quad (14)$$

$$M_{55} = -A_{55}\ddot{\beta} - B_{55}\dot{\beta} - C_{55}\beta \quad (15)$$

The natural period of oscillation for a single degree of freedom vibration system is given by

$$T = 2\pi\sqrt{\frac{I + A}{C}} \quad (16)$$

According to the linear potential flow theory, the surge, heave and pitch motions are coupled, and the sway, roll and yaw motions are coupled. The natural frequency of each degree of freedom is determined by solving the coupled system. The coupling effect is assumed to be of secondary importance in ship collision problems, so the roll, pitch and heave are simplified as independent single degree of freedom systems with natural periods determined by Eq. (16). The idea is to ensure that the same natural periods are used with this simplified model and with the linear potential flow theory for roll, heave and pitch. In this paper, the added masses for heave, pitch and roll are determined by using empirical equations proposed by Popov et al. [27]. The equations are shown in the appendix. Given the calculated natural periods from the potential theory code HydroD, the values of restoring terms for the proposed method are readily obtained according to Eq. (16).

The damping effect is usually considered secondary in ship collision and grounding problems. In this paper, the damping terms for roll, pitch and heave are expressed empirically as n fraction of the value of the critical damping:

$$B = nB_{crit} = n\left\{2[(I+A)C]^{0.5}\right\} \tag{17}$$

2.3. Coupling hydrodynamic loads computation and structural analysis

The coupling between nonlinear FEM structural solver and the hydrodynamic model based on the maneuvering model is made possible by the use of the user defined load subroutine (LOADUD). The user-defined load subroutine has found limited application in literature. A paper by Adoum and Lapoujade [28], which contains several basic examples demonstrating the application of LOADUD is useful to start with. The user-defined load subroutine in LS-DYNA provides the nodal information of displacements, velocities, accelerations and user-defined inputs and allows users to define nodal loads or pressure loads as a function of the information. This should be sufficient to implement the current model. However, a problem arises when applying the added mass forces as nodal accelerations in the user load subroutine are only available for deformable bodies, but not for rigid bodies. If a deformable body is to be used to represent the hull girder, the body will generate large structural vibrations and nodal acceleration oscillations that will yield wrong results.

The hull girder is therefore represented with a rigid beam and the velocity histories of ship COG are used to approximate the accelerations as:

$$a_n = \frac{V_n - V_{n-2}}{t_n - t_{n-2}} \tag{18}$$

whereV_n and V_{n-2} are used instead of V_n and V_{n-1} because the code will otherwise yield numerical instabilities.

It should be noted that LOADUD gives nodal information only in the current timestep and the information will be cleared upon moving to the next step. Therefore, the user common subroutine (USERCOMM) variables are introduced to store the velocity histories of ship COG. Information in the user common variables will not be erased from one timestep to next. The coupling algorithm between structural and hydrodynamic solvers is shown in Fig. 2.

During simulation, LS-DYNA first passes nodal displacements, velocities of ship COG in the current timestep to the user subroutine. The velocity histories of COG are then stored with the user common subroutine. The time increment is typically in the order of 10^{-6} s in ship collision simulations. In order to maintain efficiency without losing accuracy, the velocity histories are stored every 400 steps, i.e. around every 10^{-3}s.

With the above information, the hydrodynamic loads can be calculated in the user load subroutine. The obtained hydrodynamic loads are applied in the ship COG, and the program goes back again to the structural solver. LS-DYNA solver then calculates structural deformation and global motions, and gives motion information for the next timestep.

More detailed procedures for calculating the 6DOF hydrodynamic loads are given in Fig. 3. The motion information provided from LS-DYNA is expressed in the global earth-fixed $X_0O_0Y_0$ coordinate, and it should first be transformed into the local body-fixed XOY coordinate. As the maneuvering model is expressed in a dimensionless form, the motion information thus needs to be nondimensionalized before calculating the hydrodynamic loads. After loads calculation, the forces are dimensionalized and transformed back into the global $X_0O_0Y_0$ coordinate system.

HydroD and SIMO softwares are used for verifying the proposed method as shown in Fig. 2. With the ship panel model, HydroD calculates the hydrodynamic coefficients and the natural periods of roll, pitch and heave of the vessel. The obtained natural periods are used as inputs of the proposed method to ensure that exactly the same natural periods are used for both methods. The obtained 6DOF forces and moments from LS-DYNA and the hydrodynamic coefficients are imported into SIMO. SIMO then calculates the global motion response of the vessel under the action of collision forces. The results can then be compared to those with the proposed method.

3. Model description of application examples with the proposed procedure

As an example for the application of the proposed procedure, a supply vessel is assumed to crash into rigid plates with different orientations. Thus, different components of ship motions are excited such that both collision and grounding scenarios can be well represented.

3.1. The striking ship

A modern supply vessel with a bulbous bow is selected as the striking ship for the study. The principal dimensions of the vessel design are given in Table 1. The bow Finite Element (FE) model is shown in Fig. 4. The element size is generally 120 mm. The shell plate thickness is 12.5 mm in the bulb and 10 mm in the forecastle. The thickness of the decks and stringers varies between 7 and 12.5 mm. The frame spacing is 600 mm. Ring stiffeners and breast hooks of approximately 250 × 15 mm are provided in the bulb. The bulbous part is almost cylindrical and is relatively strong. The forecastle protrudes 1.2 m ahead of

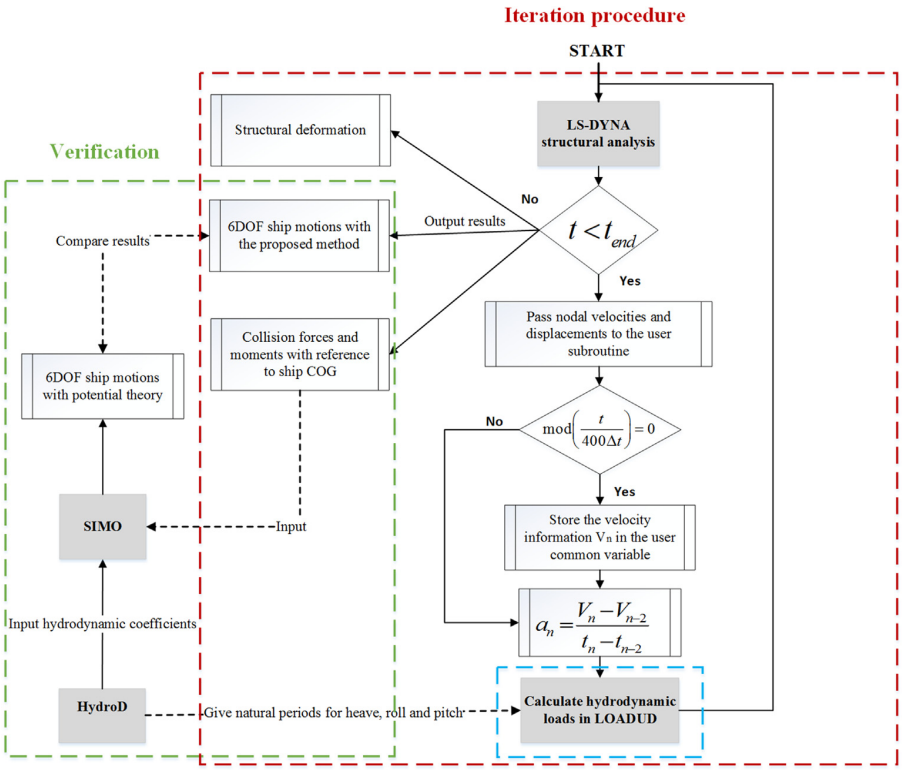

Fig. 2. Illustration of the coupling algorithm.

the bulb. The material model MAT_18 in LS-DYNA is used, which is an elastic–plastic material model with the power-law hardening. The yield stress is 275 MPa, and the power law parameters K and n are 746 MPa and 0.24, respectively. A constant failure strain of 0.3 is used for simplicity, disregarding the effect of the mesh size dependency. The strain rate effect is not considered.

The bow is crushed against a rigid wall. The crushing force vs. the deformation of the bulb and the stern of the bow is plotted in Fig. 5 and are compared with the design curve in NORSOK N-004. It is found that the force levels are comparable, which demonstrates that design curve is quite representative for this bow configuration. It should be noted that the NORSOK curve was developed in 1981 based on a raked bow, not a bulbous bow. The behavioral differences have been discussed by Storheim and Amdahl [29].

It is found that the bulb is stronger than the stem and the force level is much higher. Several force peaks are found in the bulb force–displacement curve. They coincide with the collapse of the shell between bulb ring frames.

The ship's hull girder is represented by a long beam from the bow back toward the center of gravity. Because the user-defined load subroutine does not allow the application of bending moments, the user has to transform the bending moments into force couples. Therefore, several small beams are created to facilitate the application of the bending moments in roll, pitch and yaw (see Fig. 6). Accounting for the contribution of the bow model, we calibrated the beam properties to represent correctly the total mass and inertia of the ship with respect to the center of gravity. The added masses of surge, sway and yaw are determined by the maneuvering model given by Van Berlekom and Goddard [25]. The added masses of the other 3DOF and the radius of gyration for ships are determined through empirical equations given by Popov et al. [27]. The 6DOF forces and moments as user-defined loads are applied at the Center of Gravity (COG) of the ship, as shown in Fig. 6.

3.2. Implementation of the 6DOF coupled method

The roll, pitch and heave natural periods of the striking ship are calculated as 10.05 s, 5.98 s and 6.79 s, respectively, through the boundary element method using HydroD [30]. The ship panel model is shown in Fig. 7. To obtain exactly the same natural periods in LS-DYNA, the transverse GM_T and longitudinal GM_L metacentric heights and the water plane area A_w were theoretically calculated to be 1.8 m, 103.2 m and 1212.6 m^2, respectively, through Eqs. (10)–(12) and (16). These values are

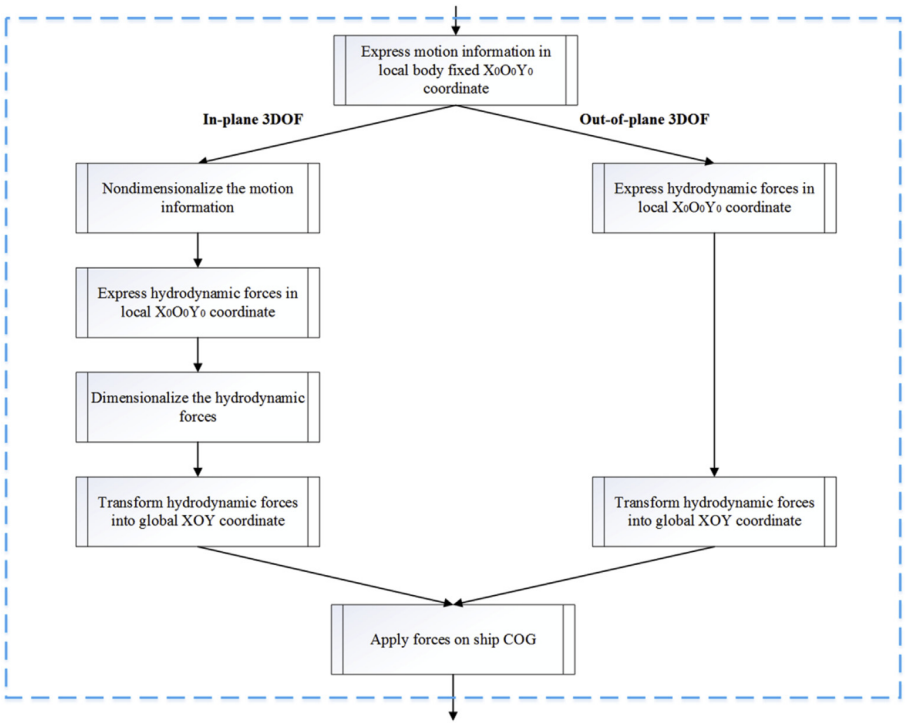

Fig. 3. Procedures for calculating hydrodynamic loads.

Table 1
Principal dimensions of the striking vessel.

Displacement	7500 ton
Length	90 m
Breadth	18.8 m
Depth	7.6 m
Draft	6.2 m

within a reasonable range and are used in the user-defined load subroutine. The damping terms were estimated to be 8%, 1% and 9% of the corresponding critical damping for roll, pitch and heave, respectively [31].

Decay tests were carried out to test the accuracy of acceleration estimation using Eq. (18) and to ensure the correct natural periods are applied. The forces were applied to a simple cross-shaped model consisting of several rigid beams that was given the same mass and inertia as the ship. The model is given in Fig. 8. The moments are transformed into force couples and applied on the beam ends. The free decay curves from the numerical simulations are shown in Fig. 9. It is observed that the periods are in good agreement with the theoretical values, which confirms the correct implementation of the user load and the good accuracy of the acceleration estimation provided by Eq. (18). Then, the proposed method can be readily applied following the procedure in Figs. 2 and 3.

3.3. Simulation cases

Three scenarios are defined according to the orientation of the rigid plates, as shown in Fig. 10. The scenarios are (1) colliding with oblique plates, (2) grounding on a sloping sea floor and (3) crashing into rigid plates with a normal vector of $\overline{n}_1$. For each scenario, several cases are simulated with different attack angles. The cases are defined in Table 2. An initial forward speed of 2.25 m/s is used for all the cases. This gives a kinetic energy of 19 MJ of the ship. The total energy can be larger when the fluid effect is included.

In scenario 1, the heave and pitch motions are small and negligible, while the planar 3DOF and the roll motion are significant. The sway, roll and yaw motions are negligible in scenario 2, but the coupled heave and pitch motions are

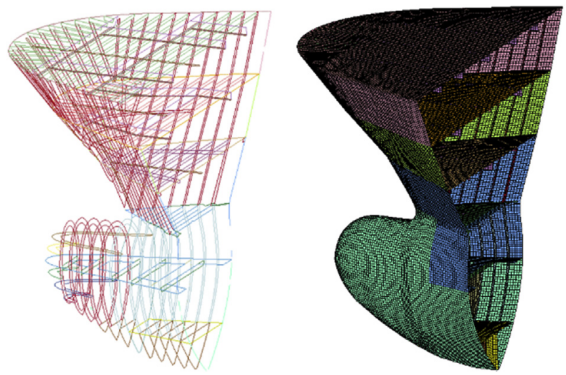

Fig. 4. The FE model of the bulbous bow.

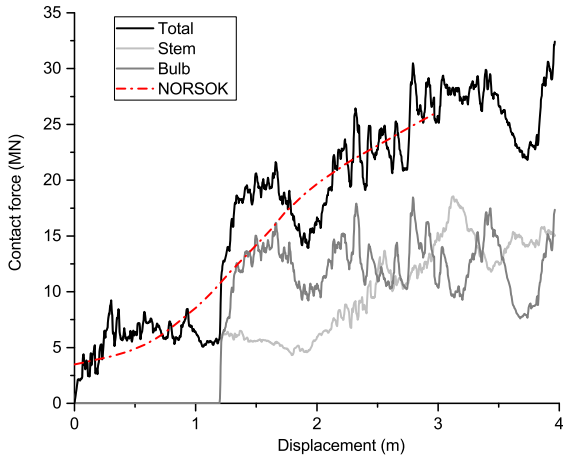

Fig. 5. The FE model of the striking ship.

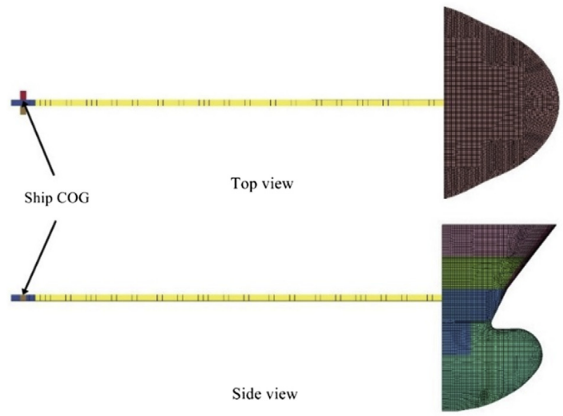

Fig. 6. The FE model of the striking ship.

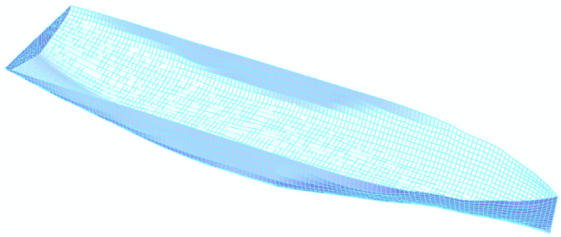

Fig. 7. The ship panel model.

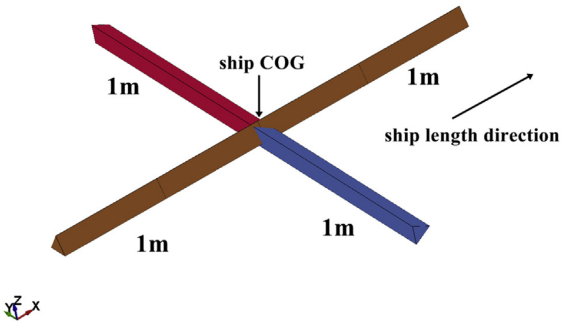

Fig. 8. The ship panel model.

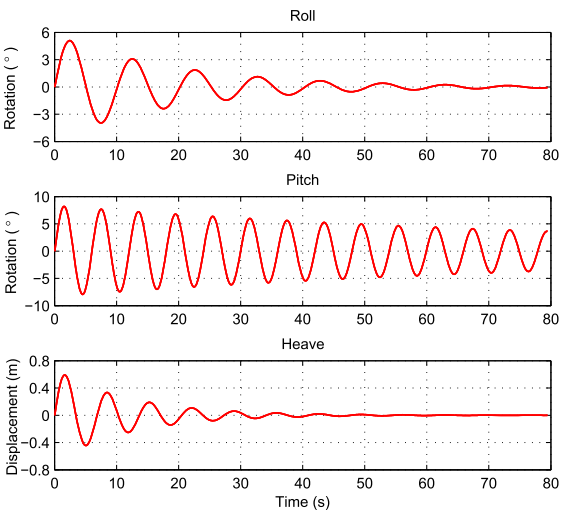

Fig. 9. The free decay test curves with LS-DYNA.

considerable. For case C3 in scenario 3, the normal vector of the rigid plate is $\vec{n}_1 = [-0.74, 0.24, 0.63]$, where all of the 6DOF ship motions are significant.

4. Verification of ship motions with SIMO simulations

The SIMO software [15] is a computer program for the simulation of the motion and behavior of floating vessels. It is used to verify ship motions predicted by the hybrid method in this study. Three typical cases are selected: the oblique collision case (C1-56), the grounding case (C2-45) and the collision-grounding case (C3).

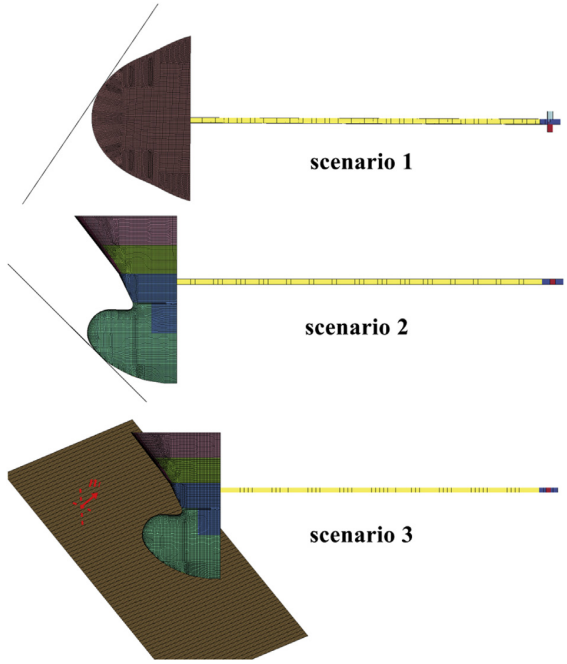

Fig. 10. The collision and grounding scenarios.

Table 2
Case definitions.

Case no.	Scenario no.	Attack angle
C1-35	1	35
C1-44	1	44
C1-56	1	56
C1-66	1	66
C1-80	1	80
C2-45	2	45
C2-60	2	60
C2-75	2	75
C3	3	–

In the SIMO simulation, the supply vessel is accelerated to a forward velocity of 2.25 m/s before it is subjected to collision loads. The hydrodynamic forces are calculated through the use of the HydroD software [30]. The ship panel model is shown in Fig. 7. The collision forces shown in *Sections 5, 6 and 7*, are applied to the SIMO model as a time-dependent force vector. The corresponding resulting ship motions are shown in Figs. 11–13.

The agreement between the 6DOF hybrid coupled method and SIMO is generally good for surge, sway, yaw and heave. For the roll and pitch motions, the peak values are captured, but the curves may deviate after the first peak. This may be due to the neglect of both the coupling effects among different motions and the memory effects of hydrodynamic forces. Nevertheless, the error is considered small in view of other uncertainties related to ship collision damage assessment, and acceptable for structural design purposes. It is therefore concluded that, the proposed method is capable of coupling the internal mechanics and the external mechanics, yielding the detailed structural damage and reasonably accurate 6DOF global motions. Work is underway to implement the complete linear potential flow theory such that both the coupling effects and the memory effects can be well included.

5. The influence of roll motion in ship collisions

In the first place, we studied the effect of the roll motion on a ship colliding with an oblique rigid plate. Ship orientations before and after collision are shown in Fig. 14 for cases C1-44 and C1-56. Here, the phrase “after collision” means the moment

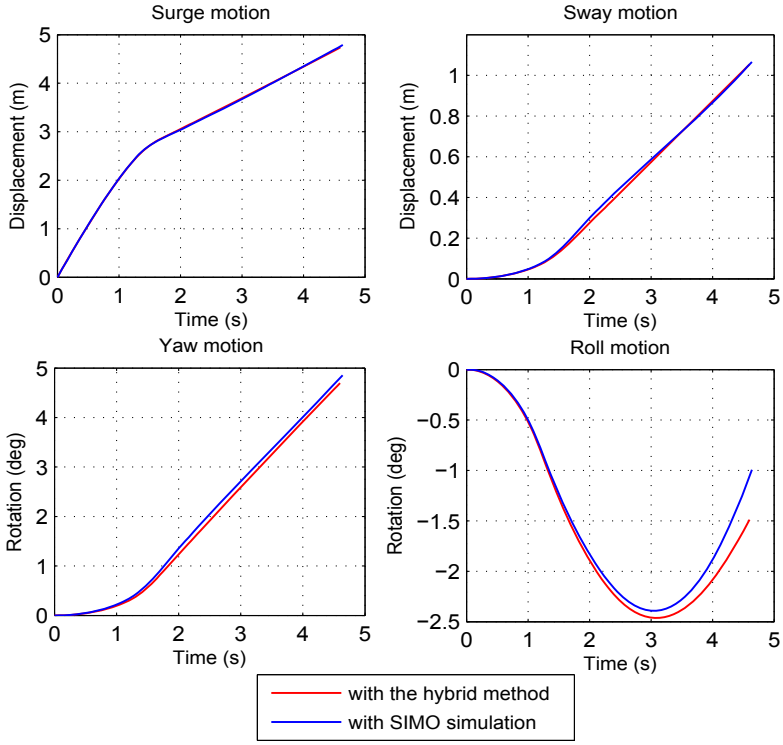

Fig. 11. A comparison of ship motions for the oblique collision case (C1-56).

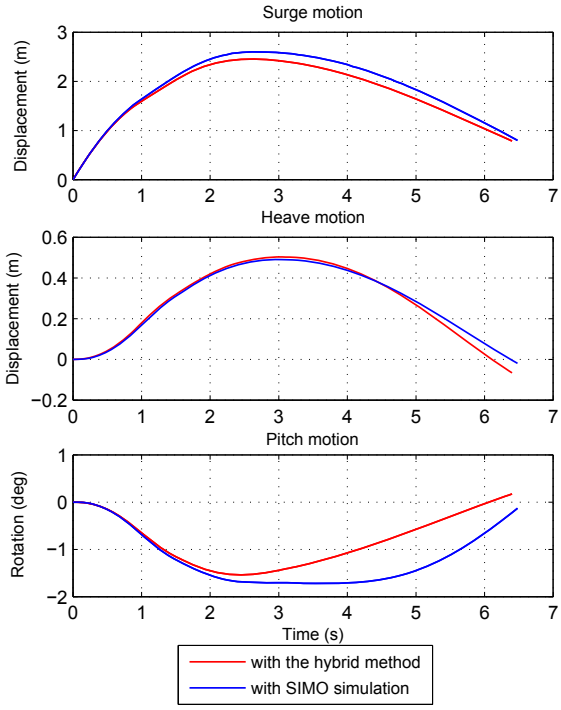

Fig. 12. A comparison of ship motions for the grounding case (C2-45).

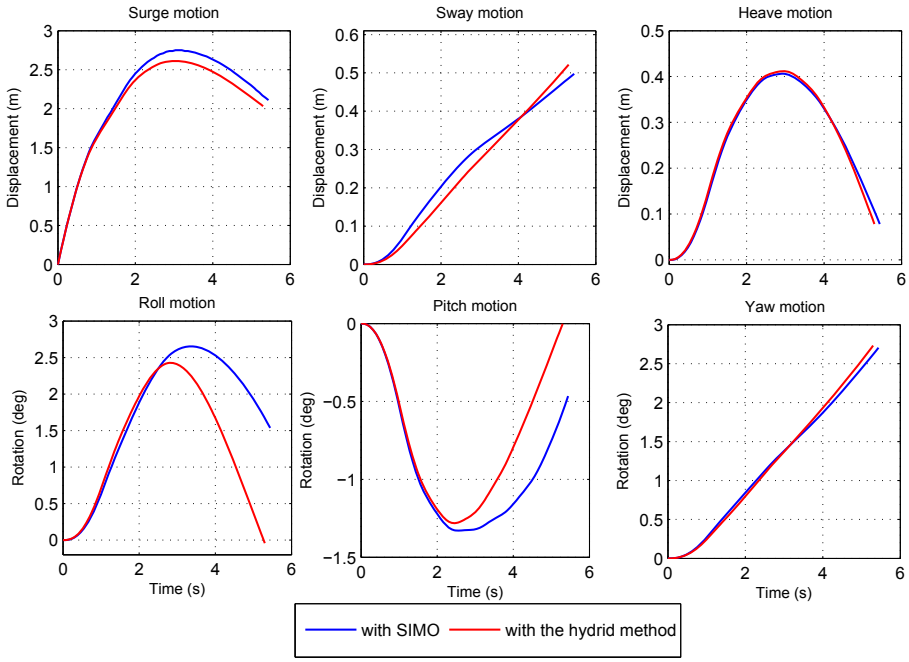

Fig. 13. A comparison of ship motions for case C3.

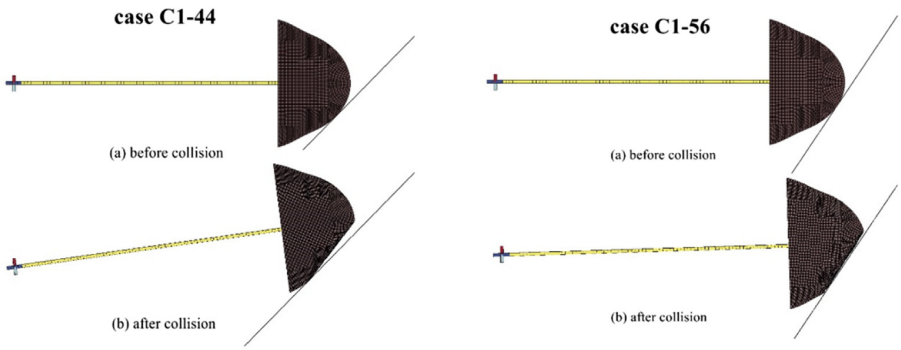

Fig. 14. The collision scenarios before and after collision.

when collision forces decrease to zero. A front view of the collision process at several time points for case C1-44 is shown in Fig. 15. The roll motion, both forward and reverse, can be clearly observed.

The time histories of the roll and yaw angles in cases C1-44 and C1-56 are shown in Fig. 16. In Figs. 14 and 16, it is observed that the yaw and roll angles behave quite differently in the two cases. The yaw angle is much larger in case C1-44, and the roll motion is more intense. This is mainly because in case C1-56, the bulbous bow gets involved in the collision process. As the bulb is located below the ship COG and is very strong, it gives a large bending moment in roll that tends to counteract that produced by deformations of the upper bow. The resultant bending moment in roll is therefore small.

In case C1-44, there is no contact between the bulb and the rigid plate during the collision, and the roll motion is intense. This is also observed in the collision force histories for cases C1-44 and C1-56 presented in Figs. 17 and 18, respectively. In Fig. 18, $f1$ and $f2$ represent the collision forces from the upper bow structures and the bulbous bow, respectively. The collision forces are given in the right-handed global XYZ coordinate, as shown in Fig. 19.

We compared the collision forces that were obtained through the use of two different methods–the 6DOF hybrid method and the 3DOF coupled method–for cases C1-44 and C1-56, as shown in Figs. 17 and 18, respectively. The heave and pitch motions are small and negligible in both cases when the 6DOF hybrid method is used. In Fig. 17, it is observed that the peak

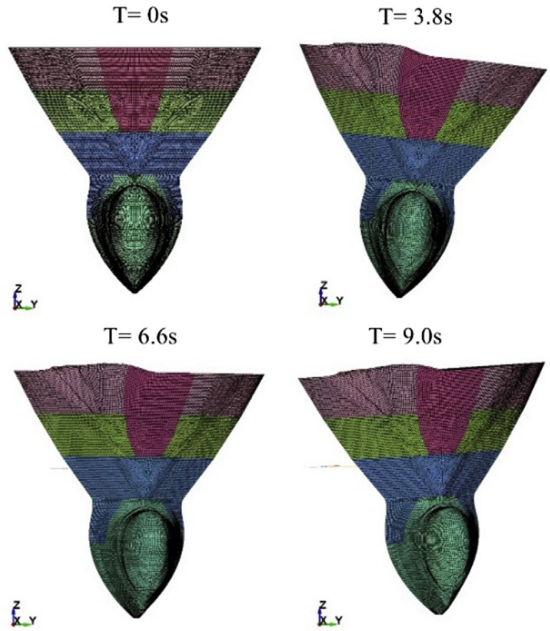

Fig. 15. Snapshots of the collision process for case C1-44.

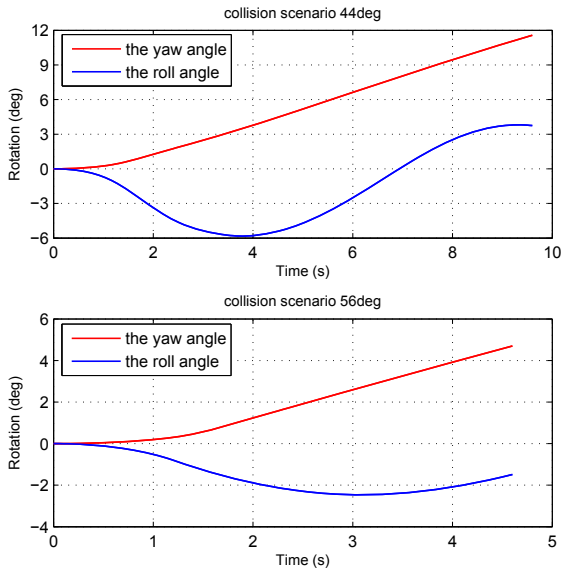

Fig. 16. The time history of roll and yaw angles during collision.

forces are quite similar, but the peak values last shorter when the roll motion is considered. This is reasonable because the roll gives a velocity at the collision point that tends to separate ships at the contact point. In case C1-56, because the bulbous bow is lower than the ship COG, the roll motion increases the contact duration of the bulbous bow but shortens the whole collision duration.

In the 6DOF decoupled method in Liu and Amdahl [3], it is assumed that the normal and tangential friction factors μ_n and μ_t are constant and are given as

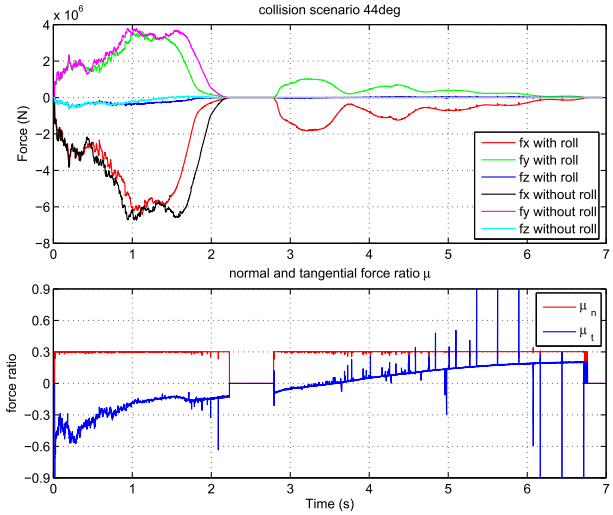

Fig. 17. The collision forces and force ratio for impact case C1-44.

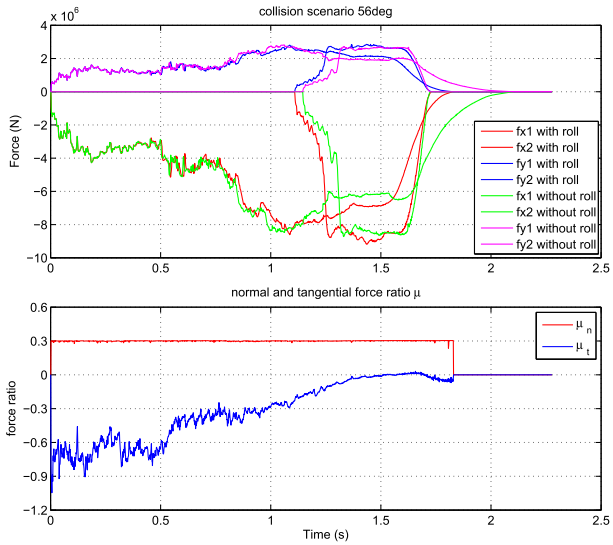

Fig. 18. The collision forces and force ratio for impact case C1-56.

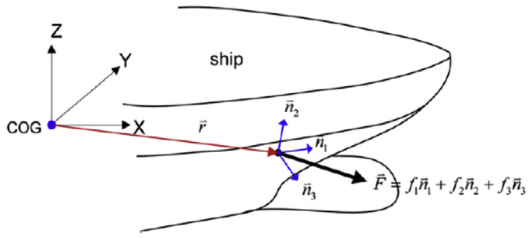

Fig. 19. Collision point geometry and the coordinate systems, after Liu and Amdahl [3].

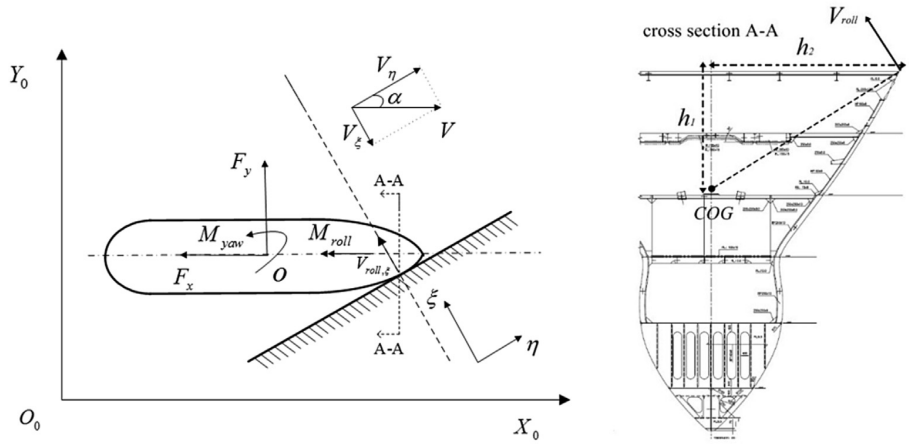

Fig. 20. Loads on the ship and velocities during collision.

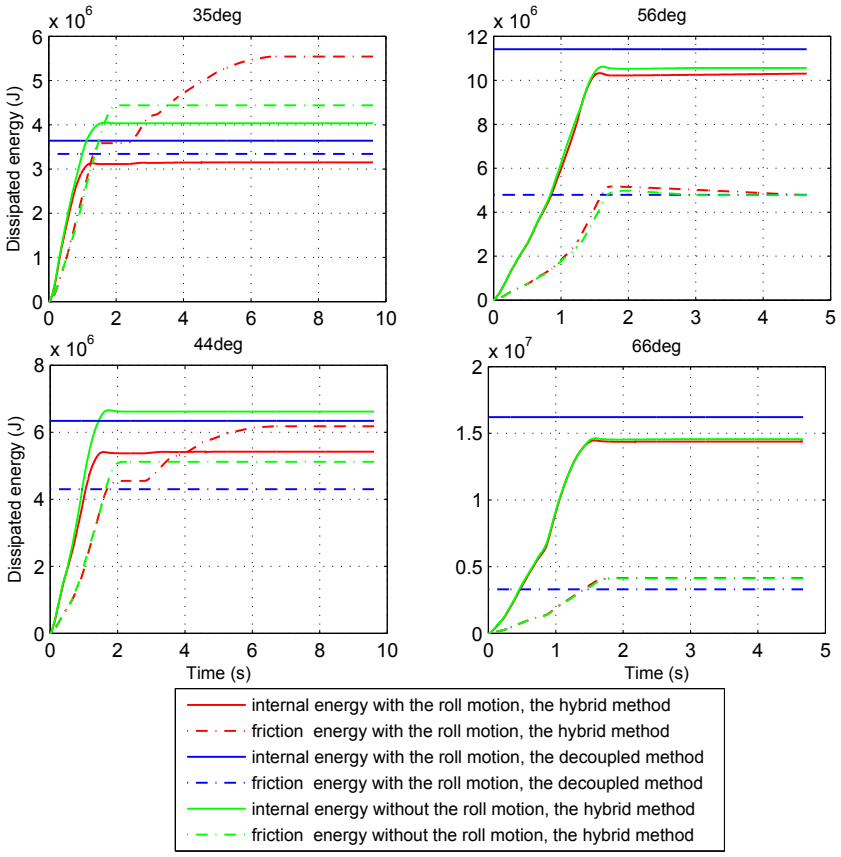

Fig. 21. A comparison of dissipated energy.

$$\mu_n = sign(dp_1)\frac{\sqrt{dp_1^2 + dp_2^2}}{dp_3} \tag{19}$$

$$\mu_t = \frac{dp_2}{dp_1} \tag{20}$$

where dp_1,dp_2 anddp_3 are the impulses in each direction in the local coordinate, as shown in Fig. 19 (Liu and Amdahl [3]). For sliding cases, μ_n is assumed to be equal to the sliding friction coefficient.

According to Figs. 18 and 19, the normal force ratio is almost constant despite small oscillations and is equal to the sliding friction coefficient 0.3. This is consistent with the conclusions in Yu, Amdahl [14]. However, the tangential force ratio is not quite constant. This may lead to inaccurate energy contributions in the n_1 and n_2 directions, but the sum of the energy from force contributions in the n_1 and n_2 directions is not necessarily inaccurate because the equilibrium value of the tangential force ratio is close to 0, as predicted by Eq. (20).

In case C1-44 in Fig. 17, it is interesting to find that when the roll motion is considered, the collision forces drop to zero at 2.1 s and remain at zero for approximately 0.7 s. After that, a second collision occurs and lasts much longer than the first collision. This is also observed in case C1-35 where the bulb is not involved and the roll motion is intense. This second collision is mainly due to the roll motion. The collision typically ends when the velocity of the collision point in the normal ξ direction decreases to zero and rebound starts. The roll motion gives a velocity in the normal ξ direction, $V_{roll,\xi}$, that is opposite to the ship normal velocityV_ξ(see Fig. 20).

The ship normal velocity at the contact point decreases with the occurrence of the sway, yaw and roll motions. When $V_\xi - V_{sway,\xi} - V_{yaw,\xi} - V_{roll,\xi} \leq 0$, the contact points separate, and the collision ends. However, unlike sway and yaw motions, the roll motion is periodic. After$V_{roll,\xi}$ reaches its maximum, it will decrease or even change direction. This causes a second collision to occur. A second collision is not observed in cases C1-56 and C1-66 because the involvement of the bulb makes the roll motion much milder, as shown in Fig. 16. It seems that the roll angular velocity rather than the roll angle governs whether secondary impacts occur. According to Fig. 20, $V_{roll,\xi}$ is given as

$$V_{roll,\xi} = V_{roll}\cdot\frac{h_1}{\sqrt{h_1^2 + h_2^2}}\cdot\cos\alpha = \dot{\theta}h_1\cos\alpha \tag{21}$$

In case C1-44, $h_1 = 6.2$ m and$h_2 = 3.8$ m; the roll angular velocity $\dot{\theta} = 0.05$ rad/s at 2.1 s. Then $V_{roll,\xi}$ is calculated as 0.22 m/s, which is not small.

We compared the dissipated internal and friction energy obtained through the use of three different methods–the planar 3DOF hybrid coupled method, the full 6DOF hybrid method and the 6DOF decoupled method–for the four impact cases, as shown in Fig. 21. A second collision takes place in cases C1-35 and C1-44 but not in cases C1-56 and C1-66. It is observed that in cases C1-56 and C1-66 where the roll angular velocity is small, the energy obtained through the 6DOF hybrid method is slightly lower than that obtained through the 3DOF hybrid method, but the difference is very small. However, in cases C1-35 and C1-44 where the roll angular velocity is considerable, the difference is large even at the end of the first collision. This is because the roll motion absorbs considerable kinetic energy.

It is observed that in the cases with a second collision, the 6DOF decoupled method captures the energy only at the end of the first collision period. This is unconservative. In cases C1-35 and C1-44, the internal energy is generally overestimated by the 6DOF decoupled method, while the friction energy is underestimated by this method. This is because the restitution factor is assumed to be zero. As shown in Yu et al. [14], it is not conservative to assume a zero restitution factor through the use of the decoupled method.

In addition, for the impact cases with secondary collisions, we calculated the internal and friction energy, using the 6DOF coupled method, as 3.15 MJ and 5.55 MJ, respectively, for case C1-35 and as 5.42 MJ and 6.18 MJ, respectively, for case C1-44 at the end of the whole collision. Using the 3DOF coupled method, we calculated 4.03 MJ and 4.44 MJ for case C1-35 and 6.62 MJ and 5.12 MJ for case C1-44. It is interesting to see that although the contributions from the internal and friction energy are different, the total energy after the second collision is similar for the 3DOF and 6DOF hybrid coupled methods. This is because of the periodic roll motion. If the plate is long enough, the energy absorbed by the roll motion at the end of the first collision will be dissipated in the second collision. The internal and friction contributions are different because the collision-induced yaw angle is large, as shown in Fig. 16. Therefore, it is recommended to use the planar 3DOF decoupled method rather than the 6DOF decoupled method because the latter method will significantly underestimate the total energy when a second collision occurs.

Fig. 22 presents the penetration paths of the collision cases in scenario 1 that were evaluated by the decoupled method, the 3DOF coupled method and the 6DOF coupled method. The markers on the curves represent the points where the collision ends. For the decoupled method, “the collision end” means the point where the demand for internal energy dissipation is complied with. For the coupled method, “the collision end” represents the moment when the collision forces decrease to zero.

It is observed that the decoupled approach predicts a shorter transverse extent but deeper penetrations normal to the contact plane, which is often more serious with respect to flooding or cargo spill. The deviation is especially clear for small

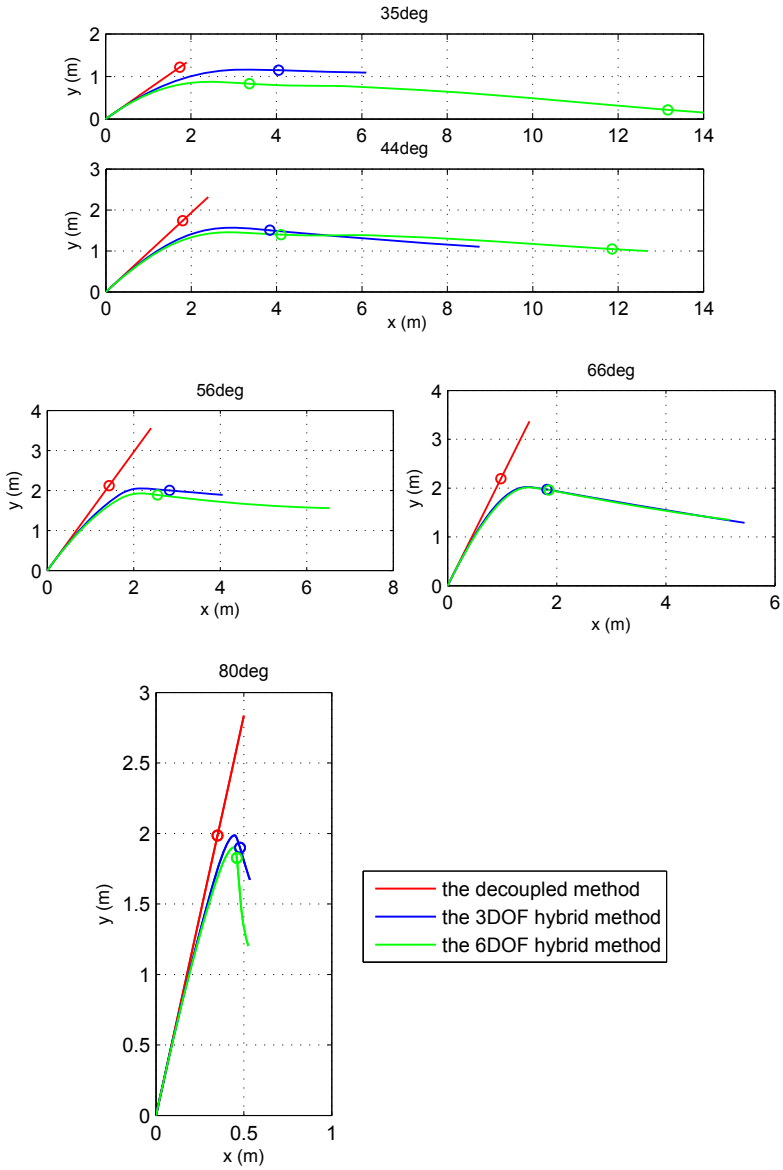

Fig. 22. Penetration paths of the striking ship.

collision angles. The extent of transverse damage is underestimated by approximately 50% for the 35°, 44°, 56° and 66° impact cases where the striking ship and the rigid plate slide over each other. The deviation is small for cases with large collision angles (e.g., see case C1-80). In cases with secondary impacts, the decoupled method is not able to capture a second collision. As ship structures are not homogeneous in general, the structural damage can be very different for different collision paths. Tabri and Broekhuijsen [32] compared the deformation energy at the instant when the inner hull is breached by using the decoupled method and a coupled method. They found that the difference in the deformation energy between the two methods could be up to 90% due to the path deviation.

The path deviation is caused mainly by the yaw motion. The roll motion also has some influence, as shown in the comparison between the blue and green curves in Fig. 22. The maximum penetration is smaller when the roll motion is considered. In general, when more degrees of freedom are released, more kinetic energy will remain after collision. This is because the structures have less motion constraints, and the colliding bodies separate more easily; thus, less strain energy is dissipated.

6. The influence of heave and pitch motions in ship grounding accidents

Using the 6DOF hybrid method, we studied the effects of heave and pitch motions when the ship grounds over an inclined, rigid plate. The planar degrees of freedom are small and negligible. The surge, heave and pitch motions are in a common vertical plane similar with the planar 3DOF problem. However, one large difference is that the heave and pitch motions are periodic due to restoring terms, while the sway and yaw motions are not.

The grounding scenarios before and during grounding for case C2-45 are shown in Fig. 23, where the pitch angle, although small, can be clearly observed. Typically, the pitch angle is approximately $0^{\circ}-2^{\circ}$ in ship collision and grounding accidents, but the bow can move up meters in view of the large ship length. Ship motion histories of surge, heave and pitch for three grounding cases (C2-45, C2-60 and C2-75) are shown in Fig. 24. It is observed that as the inclination angle increases, the heave and pitch motions will reduce. This is because the force component in the vertical z direction decreases. In addition, as shown in Fig. 24, unlike in the other two cases, the pitch motion in the grounding case C2-75 starts with a positive angle. This is because no sliding occurs in this case, and the ship then rotates clockwise about the collision point. However, the amplitude is very small.

The grounding resistances in the global XYZ coordinate are given in Fig. 25. In case C2-45, a second grounding also occurs, and in case C2-60, a third and a fourth grounding even occur. Note that here the plate is assumed to be infinitely long, which may not represent the true grounding situations. The results indicate that ships may contact the sea floor and lift off several times due to heave and pitch motions. The underlying principle is similar to the one for the roll motion.

The energy dissipation curves for the three grounding cases are shown in Fig. 26. Because of the long plate approximation, nearly all ship energy needs to be dissipated anyhow except for the small energy portion from the rebound velocity. However, it is still interesting to see how well the 6DOF decoupled method works until the end of the first contact period.

It is observed that the energy dissipated in the secondary impacts is considerable in case C2-45 but is negligible in case C2-60. This is because the 45° grounding angle gives larger vertical force components and the heave and pitch motions are more intense. This induces an early separation, and the remaining kinetic energy is still substantial and is dissipated in the subsequent impacts.

According to Fig. 26, the decoupled approach gives a reasonable estimation of the dissipated energy after the first grounding. However, this method is not necessarily conservative (e.g., see the grounding case C2-45).

7. The influence of 6DOF ship motions in “collision-grounding” events

The 6DOF motion coupling is studied in case C3, where the rigid plate is rotated to a skew angle. The normal vector of the rotated rigid plate is $\vec{n}_1 = [-0.74, 0.24, 0.63]$ (see Fig. 10).

The 6DOF ship motion curves can be seen in the SIMO verification in Fig. 13. The collision force histories and the normal and tangential force ratios are shown in Fig. 27. It is observed that the normal force ratio is always valid for the decoupled method, as was previously shown. The tangential force ratio is generally valid up to the end of the first collision. It is found that the instantaneous tangential force ratio changes its sign after some time. This is because the friction force in the n_2 direction changes its sign when the ship slides down from the peak (See Fig. 28 for the trajectory of ship motions along the rigid plate during collision.). According to Fig. 28, the ship moves up along the plate to the peak point and then slides back to the water plane. During the process, the coupled effects of 6DOF ship motions can be clearly observed.

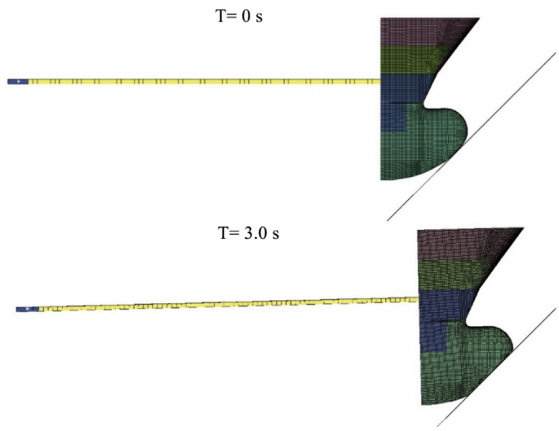

Fig. 23. The grounding scenarios before and during grounding for case C2-45.

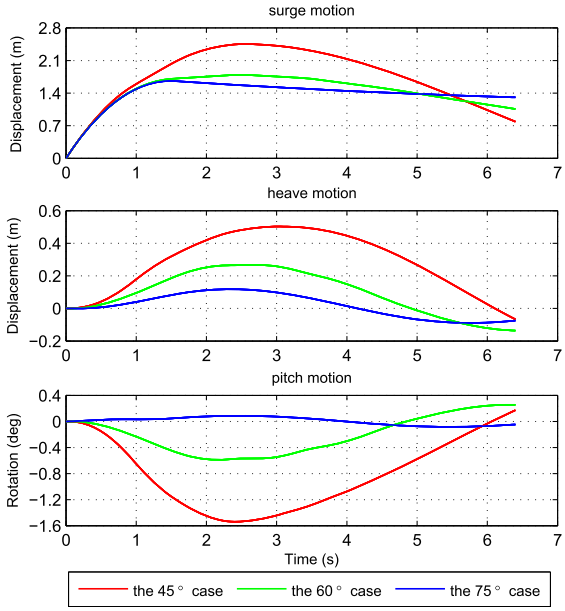

Fig. 24. Ship motions for the three grounding cases.

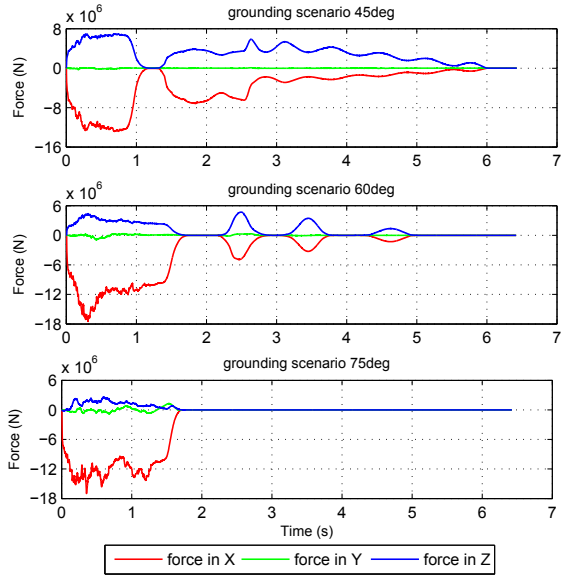

Fig. 25. Grounding force histories for the three cases.

In Fig. 27, a second collision is also observed, and it is interesting to find that during the second collision, the forces are oscillating with a period of approximately 0.7 s. This may be because the coupling of motions is oscillatory and tends to separate the collision contacts but is not intense enough to fully detach them.

As shown in Fig. 29, we compared the dissipated energy obtained through two different methods–the proposed hybrid method and the decoupled method. The waterline angle α and the normal frame angle $\beta^{'}$ in Liu and Amdahl [3]'s model are calculated as $\alpha = 72.1^{\circ}, \beta^{'} = 38.7^{\circ}$. It is found that the 6DOF decoupled method gives reasonable predictions of the dissipated energy at the end of the first collision. However, it is not necessarily conservative.

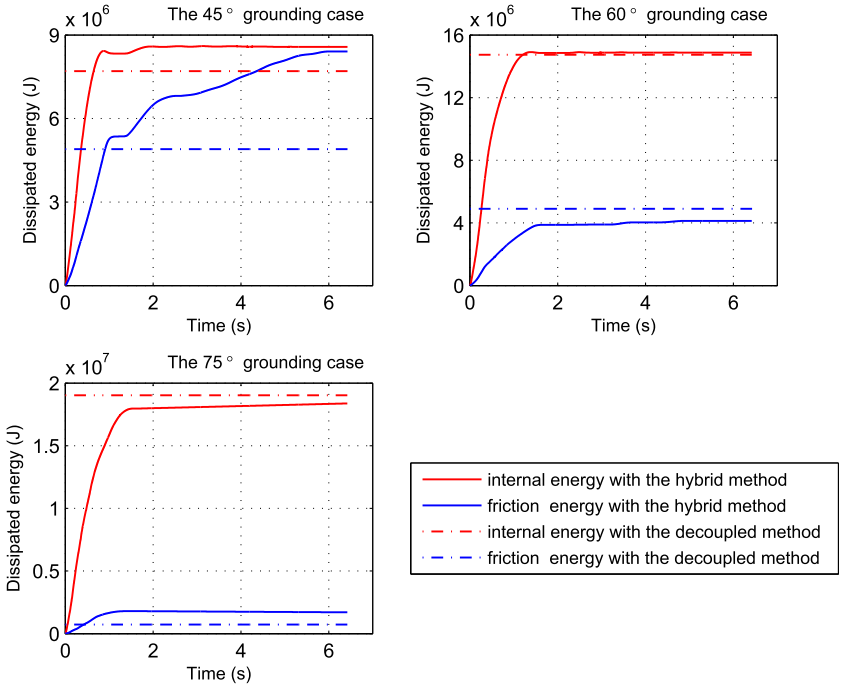

Fig. 26. The dissipated energy during grounding for the three cases.

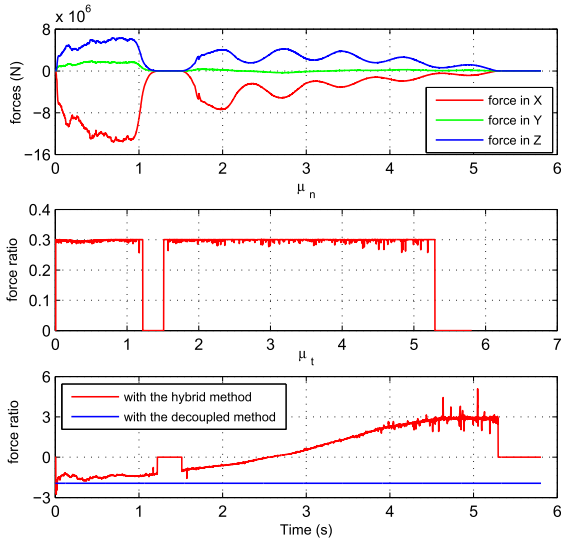

Fig. 27. The collision forces and the normal and tangential force ratios.

8. Concluding remarks

The 3DOF hybrid coupled method has been successfully extended to consider the full 6DOF ship motions in the simulation of collision and grounding accidents using LS-DYNA. Several application scenarios have been analyzed, where a supply vessel bow collides with a rigid body with different orientations. The results are compared with those obtained using a 6DOF decoupled method. The conclusions are as follows:

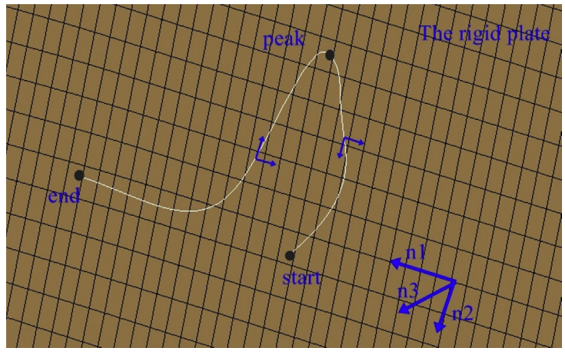

Fig. 28. Trajectory of ship motions along the rigid plate during collision.

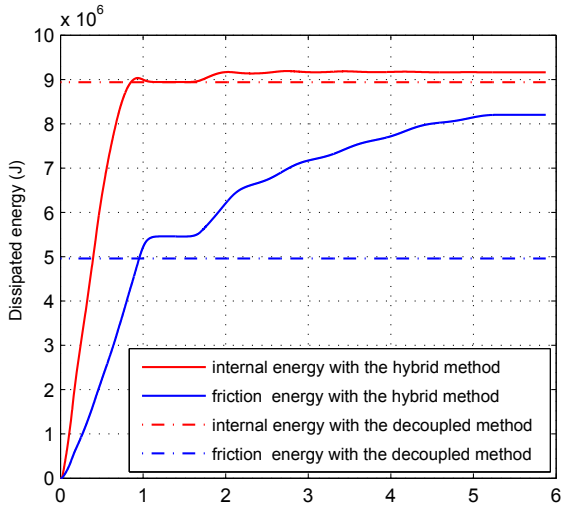

Fig. 29. A comparison of the dissipated energy.

1 The 6DOF coupled method is capable of efficiently coupling the external dynamics and the internal mechanics in ship collision and grounding events, yielding both detailed structural damage and 6DOF global motions. This model uses an approximation of the hydrodynamic loads that captures the major effects of the fluid. The global motions obtained through this model have been compared with those calculated by SIMO. The accuracy is reasonable notably in view of other uncertainties related to collision damage assessment. Work is underway to include the complete linear potential flow theory to further improve the accuracy of structural damage assessment.
2 The involvement of all of the 6DOF ship motions will generally reduce the strain energy dissipation at the end of the first impact period and increase the remaining kinetic energy of the ship. However, secondary impacts may occur because of the periodic motions of roll, pitch and heave, which will increase the total strain energy dissipation.
3 The 6DOF decoupled method can predict the dissipated energy with reasonable accuracy as far as the end of the first impact period is concerned. It may not be conservative with respect to the demand for energy dissipation. If secondary collisions occur, the total energy dissipation and structural damage will increase. This energy increase can be large in some cases, but cannot be captured by the decoupled method. The potential limitation of the decoupled approach should therefore be great.

Acknowledgments

This work has been funded by the Research Council of Norway (NFR) through the Centers of Excellence funding scheme, project AMOS (Grant No. 223254) at the Norwegian University of Science and Technology (NTNU). This support is gratefully acknowledged by the authors.

Appendix

For the purpose of investigating the ice loads exerted on ship structures, Popov et al. [27] derived a series of empirical equations to assess the added mass factor and radius of gyration for ships. Eqs. (A.1), (A.2) and (A.6) for added mass coefficients in the surge, sway and yaw degrees of freedom are not used in this paper but are presented anyway.

$$\widehat{m}_x = 0 \tag{A.1}$$

$$\widehat{m}_y = 2T/B \tag{A.2}$$

$$\widehat{m}_z = 2/3\left(BC_{wp}^2\right)\Big/\left(TC_b(1+C_{wp})\right) \tag{A.3}$$

$$\widehat{j}_{xx} = 0.25 \tag{A.4}$$

$$\widehat{j}_{yy} = B/\left(T(3-2C_{wp})(3-C_{wp})\right) \tag{A.5}$$

$$\widehat{j}_{zz} = 0.3 + 0.05L/B \tag{A.6}$$

$$\widehat{R}_{xx}^2 = C_{wp}B^2\Big/(11.4C_m) + H^2\Big/12 \tag{A.7}$$

$$\widehat{R}_{yy}^2 = 0.07C_{wp}L^2 \tag{A.8}$$

$$\widehat{R}_{zz}^2 = L^2\Big/16 \tag{A.9}$$

References

[1] Minorsky V. An analysis of ship collisions with reference to protection of nuclear power plants. New York: Sharp (George G.) Inc; 1958.
[2] Pedersen PT, Zhang S. On impact mechanics in ship collisions. Mar Struct 1998;11(10):429–49.
[3] Liu Z, Amdahl J. A new formulation of the impact mechanics of ship collisions and its application to a ship–iceberg collision. Mar Struct 2010;23(3):360–84.
[4] Tabri K. Influence of coupling in the prediction of ship collision damage. Ships Offshore Struct 2012;7(1):47–54.
[5] Petersen MJ. Dynamics of ship collisions. Ocean Eng 1982;9(4):295–329.
[6] Tabri K, Varsta P, Matusiak J. Numerical and experimental motion simulations of nonsymmetric ship collisions. J Mar Sci Technol 2010;15(1):87–101.
[7] Brown AJ. Collision scenarios and probabilistic collision damage. Mar Struct 2002;15(4–5):335–64.
[8] Le Sourne H. A ship collision analysis program based on super-element method coupled with large rotational ship movement analysis tool. In: International conference on collision and grounding of ships; 2007.
[9] Lützen M, Simonsen BC, Pedersen PT. Rapid prediction of damage to struck and striking vessels in a collision event. In: Proceedings of ship structures for the new millennium: supporting quality in shipbuilding; 2000. Arlington.
[10] Tørnqvist R. Design of crashworthy ship structures. Denmark: Technical University of Denmark Kgns Lyngby; 2003.
[11] Biehl F, Kunz K, Lehmann E. Collisions of inland waterway vessels with fixed structures: load–deformation relations and full scale simulations. In: Proceedings of 4th international conference on collision and grounding of ships; 2007.
[12] Rudan S, Tabri K, Klarić I. Analysis of sloshing interaction in ship collisions by means of ALE finite element method. In: International conference on collision and grounding of ships, Espoo, Finland, 2010.; 2010.
[13] Zhang A, Suzuki K. A comparative study of numerical simulations for fluid–structure interaction of liquid-filled tank during ship collision. Ocean Eng 2007;34(5–6):645–52.
[14] Yu Z, Amdahl J, Storheim M. A new approach for coupling external dynamics and internal mechanics in ship collisions. Mar Struct 2015, 45, 110-132.
[15] Marintek. SIMO - User's manual Version 4.0 rev0. Marintek Report. 2012.
[16] Hallquist JO. LS-DYNA theory manual, 3. Livermore software Technology corporation; 2006. p. 25–31.
[17] Yamada Y, Endo H. Experimental and numerical study on the collapse strength of the bulbous bow structure in oblique collision. Mar Technol 2008; 45(1):42–53.
[18] Paik J. Practical techniques for finite element modelling to simulate structural crashworthiness in ship collisions and grounding (Part II: verification). Ships Offshore Struct 2007;2(1):81–5.
[19] Amdahl J, Kavlie D. Experimental and numerical simulation of double hull stranding. In: DNV-MIT workshop on mechanics of ship collision and grounding; 1992.
[20] Ohtsubo H, Kawamoto Y, Kuroiwa T. Experimental and numerical research on ship collision and grounding of oil tankers. Nucl Eng Des 1994;150(2):385–96.
[21] Storheim M. Structural response in ship-platform and ship-ice collisions. Doctoral thesis. Norwegian University of Science and Technology; 2016.
[22] Sajdak J, Brown A. Modeling longitudinal damage in ship collisions. SSC-437, Ship Structure Committee. 2005.
[23] Paik J. Practical techniques for finite element modeling to simulate structural crashworthiness in ship collisions and grounding (Part I: theory). Ships Offshore Struct 2007;2(1):69–80.
[24] Norrbin NH. Theory and observations on the use of a mathematical model for ship manoeuvring in deep and confined waters. 1971 [DTIC Document].
[25] Van Berlekom WB, Goddard TA. Maneuvering of large tankers. In: Presented at the annual meeting of SNAME, society of naval architects and marine engineers; 1972. Paper #8.
[26] Petersen MJ, Pedersen PT. Collisions between ships and offshore platforms. In: Offshore Technology conference; 1981 [Offshore Technology Conference].
[27] Popov YN, et al. Strength of ships sailing in ice. 1969 [DTIC Document].
[28] Adoum M, Lapoujade V. Examples' manual for* USER_LOADING option. In: Proc. 4th European LS-DYNA users conference, Ulm, Germany; 2003.
[29] Storheim M, Amdahl J. Design of offshore structures against accidental ship collisions. Mar Struct 2014;37:135–72.
[30] DNV. HydroD user manual. 2014.
[31] Ferreira MD, de Oliveira MC, Carvalho RC, Sphaier SH. Asymmetric FPSO roll response due to the influence of lines arrangement. In: ASME 2012 31st international conference on ocean, offshore and arctic engineering. American Society of Mechanical Engineers; 2012. p. 267–77.
[32] Tabri K, Broekhuijsen J. Influence of ship motions in the numerical prediction of ship collision damage. In: Advances in Marine Structures - Proceedings of the 3rd International Conference on Marine Structures. MARSTRUCT; 2011. 2011.

Appendix A: appended papers

PAPER 3

Yu Z., Shen Y., Amdahl J., Greco M.

Implementation of linear potential-flow theory in the 6DOF coupled simulation of ship collision and grounding accidents

Published in

Journal of Ship Research
Vol. 60 (3), Pages 119-144, 2016

Is not included due to copyright

Appendix A: appended papers

PAPER 4

Yu Z., Amdahl J.

Analysis and design of offshore tubular members against ship impacts

Submitted to journal

Is not included due to copyright

Appendix A: appended papers

PAPER 5

Yu Z., Amdahl J., Sha Y.

Large inelastic deformation resistance of stiffened panels subjected to lateral loading

Submitted to journal

Is not included due to copyright

Previous PhD theses published at the Departement of Marine Technology
(earlier: Faculty of Marine Technology)
NORWEGIAN UNIVERSITY OF SCIENCE AND TECHNOLOGY

Report No.	Author	Title
	Kavlie, Dag	Optimization of Plane Elastic Grillages, 1967
	Hansen, Hans R.	Man-Machine Communication and Data-Storage Methods in Ship Structural Design, 1971
	Gisvold, Kaare M.	A Method for non-linear mixed -integer programming and its Application to Design Problems, 1971
	Lund, Sverre	Tanker Frame Optimalization by means of SUMT-Transformation and Behaviour Models, 1971
	Vinje, Tor	On Vibration of Spherical Shells Interacting with Fluid, 1972
	Lorentz, Jan D.	Tank Arrangement for Crude Oil Carriers in Accordance with the new Anti-Pollution Regulations, 1975
	Carlsen, Carl A.	Computer-Aided Design of Tanker Structures, 1975
	Larsen, Carl M.	Static and Dynamic Analysis of Offshore Pipelines during Installation, 1976
UR-79-01	Brigt Hatlestad, MK	The finite element method used in a fatigue evaluation of fixed offshore platforms. (Dr.Ing. Thesis)
UR-79-02	Erik Pettersen, MK	Analysis and design of cellular structures. (Dr.Ing. Thesis)
UR-79-03	Sverre Valsgård, MK	Finite difference and finite element methods applied to nonlinear analysis of plated structures. (Dr.Ing. Thesis)
UR-79-04	Nils T. Nordsve, MK	Finite element collapse analysis of structural members considering imperfections and stresses due to fabrication. (Dr.Ing. Thesis)
UR-79-05	Ivar J. Fylling, MK	Analysis of towline forces in ocean towing systems. (Dr.Ing. Thesis)
UR-80-06	Nils Sandsmark, MM	Analysis of Stationary and Transient Heat Conduction by the Use of the Finite Element Method. (Dr.Ing. Thesis)
UR-80-09	Sverre Haver, MK	Analysis of uncertainties related to the stochastic modeling of ocean waves. (Dr.Ing. Thesis)
UR-81-15	Odland, Jonas	On the Strength of welded Ring stiffened cylindrical Shells primarily subjected to axial Compression
UR-82-17	Engesvik, Knut	Analysis of Uncertainties in the fatigue Capacity of

		Welded Joints
UR-82-18	Rye, Henrik	Ocean wave groups
UR-83-30	Eide, Oddvar Inge	On Cumulative Fatigue Damage in Steel Welded Joints
UR-83-33	Mo, Olav	Stochastic Time Domain Analysis of Slender Offshore Structures
UR-83-34	Amdahl, Jørgen	Energy absorption in Ship-platform impacts
UR-84-37	Mørch, Morten	Motions and mooring forces of semi submersibles as determined by full-scale measurements and theoretical analysis
UR-84-38	Soares, C. Guedes	Probabilistic models for load effects in ship structures
UR-84-39	Aarsnes, Jan V.	Current forces on ships
UR-84-40	Czujko, Jerzy	Collapse Analysis of Plates subjected to Biaxial Compression and Lateral Load
UR-85-46	Alf G. Engseth, MK	Finite element collapse analysis of tubular steel offshore structures. (Dr.Ing. Thesis)
UR-86-47	Dengody Sheshappa, MP	A Computer Design Model for Optimizing Fishing Vessel Designs Based on Techno-Economic Analysis. (Dr.Ing. Thesis)
UR-86-48	Vidar Aanesland, MH	A Theoretical and Numerical Study of Ship Wave Resistance. (Dr.Ing. Thesis)
UR-86-49	Heinz-Joachim Wessel, MK	Fracture Mechanics Analysis of Crack Growth in Plate Girders. (Dr.Ing. Thesis)
UR-86-50	Jon Taby, MK	Ultimate and Post-ultimate Strength of Dented Tubular Members. (Dr.Ing. Thesis)
UR-86-51	Walter Lian, MH	A Numerical Study of Two-Dimensional Separated Flow Past Bluff Bodies at Moderate KC-Numbers. (Dr.Ing. Thesis)
UR-86-52	Bjørn Sortland, MH	Force Measurements in Oscillating Flow on Ship Sections and Circular Cylinders in a U-Tube Water Tank. (Dr.Ing. Thesis)
UR-86-53	Kurt Strand, MM	A System Dynamic Approach to One-dimensional Fluid Flow. (Dr.Ing. Thesis)
UR-86-54	Arne Edvin Løken, MH	Three Dimensional Second Order Hydrodynamic Effects on Ocean Structures in Waves. (Dr.Ing. Thesis)
UR-86-55	Sigurd Falch, MH	A Numerical Study of Slamming of Two-Dimensional Bodies. (Dr.Ing. Thesis)
UR-87-56	Arne Braathen, MH	Application of a Vortex Tracking Method to the Prediction of Roll Damping of a Two-Dimension Floating Body. (Dr.Ing. Thesis)

UR-87-57	Bernt Leira, MK	Gaussian Vector Processes for Reliability Analysis involving Wave-Induced Load Effects. (Dr.Ing. Thesis)
UR-87-58	Magnus Småvik, MM	Thermal Load and Process Characteristics in a Two-Stroke Diesel Engine with Thermal Barriers (in Norwegian). (Dr.Ing. Thesis)
MTA-88-59	Bernt Arild Bremdal, MP	An Investigation of Marine Installation Processes – A Knowledge - Based Planning Approach. (Dr.Ing. Thesis)
MTA-88-60	Xu Jun, MK	Non-linear Dynamic Analysis of Space-framed Offshore Structures. (Dr.Ing. Thesis)
MTA-89-61	Gang Miao, MH	Hydrodynamic Forces and Dynamic Responses of Circular Cylinders in Wave Zones. (Dr.Ing. Thesis)
MTA-89-62	Martin Greenhow, MH	Linear and Non-Linear Studies of Waves and Floating Bodies. Part I and Part II. (Dr.Techn. Thesis)
MTA-89-63	Chang Li, MH	Force Coefficients of Spheres and Cubes in Oscillatory Flow with and without Current. (Dr.Ing. Thesis
MTA-89-64	Hu Ying, MP	A Study of Marketing and Design in Development of Marine Transport Systems. (Dr.Ing. Thesis)
MTA-89-65	Arild Jæger, MH	Seakeeping, Dynamic Stability and Performance of a Wedge Shaped Planing Hull. (Dr.Ing. Thesis)
MTA-89-66	Chan Siu Hung, MM	The dynamic characteristics of tilting-pad bearings
MTA-89-67	Kim Wikstrøm, MP	Analysis av projekteringen for ett offshore projekt. (Licenciat-avhandling)
MTA-89-68	Jiao Guoyang, MK	Reliability Analysis of Crack Growth under Random Loading, considering Model Updating. (Dr.Ing. Thesis)
MTA-89-69	Arnt Olufsen, MK	Uncertainty and Reliability Analysis of Fixed Offshore Structures. (Dr.Ing. Thesis)
MTA-89-70	Wu Yu-Lin, MR	System Reliability Analyses of Offshore Structures using improved Truss and Beam Models. (Dr.Ing. Thesis)
MTA-90-71	Jan Roger Hoff, MH	Three-dimensional Green function of a vessel with forward speed in waves. (Dr.Ing. Thesis)
MTA-90-72	Rong Zhao, MH	Slow-Drift Motions of a Moored Two-Dimensional Body in Irregular Waves. (Dr.Ing. Thesis)
MTA-90-73	Atle Minsaas, MP	Economical Risk Analysis. (Dr.Ing. Thesis)
MTA-90-74	Knut-Aril Farnes, MK	Long-term Statistics of Response in Non-linear Marine Structures. (Dr.Ing. Thesis)
MTA-90-75	Torbjørn Sotberg, MK	Application of Reliability Methods for Safety Assessment of Submarine Pipelines. (Dr.Ing.

		Thesis)
MTA-90-76	Zeuthen, Steffen, MP	SEAMAID. A computational model of the design process in a constraint-based logic programming environment. An example from the offshore domain. (Dr.Ing. Thesis)
MTA-91-77	Haagensen, Sven, MM	Fuel Dependant Cyclic Variability in a Spark Ignition Engine - An Optical Approach. (Dr.Ing. Thesis)
MTA-91-78	Løland, Geir, MH	Current forces on and flow through fish farms. (Dr.Ing. Thesis)
MTA-91-79	Hoen, Christopher, MK	System Identification of Structures Excited by Stochastic Load Processes. (Dr.Ing. Thesis)
MTA-91-80	Haugen, Stein, MK	Probabilistic Evaluation of Frequency of Collision between Ships and Offshore Platforms. (Dr.Ing. Thesis)
MTA-91-81	Sødahl, Nils, MK	Methods for Design and Analysis of Flexible Risers. (Dr.Ing. Thesis)
MTA-91-82	Ormberg, Harald, MK	Non-linear Response Analysis of Floating Fish Farm Systems. (Dr.Ing. Thesis)
MTA-91-83	Marley, Mark J., MK	Time Variant Reliability under Fatigue Degradation. (Dr.Ing. Thesis)
MTA-91-84	Krokstad, Jørgen R., MH	Second-order Loads in Multidirectional Seas. (Dr.Ing. Thesis)
MTA-91-85	Molteberg, Gunnar A., MM	The Application of System Identification Techniques to Performance Monitoring of Four Stroke Turbocharged Diesel Engines. (Dr.Ing. Thesis)
MTA-92-86	Mørch, Hans Jørgen Bjelke, MH	Aspects of Hydrofoil Design: with Emphasis on Hydrofoil Interaction in Calm Water. (Dr.Ing. Thesis)
MTA-92-87	Chan Siu Hung, MM	Nonlinear Analysis of Rotordynamic Instabilities in Highspeed Turbomachinery. (Dr.Ing. Thesis)
MTA-92-88	Bessason, Bjarni, MK	Assessment of Earthquake Loading and Response of Seismically Isolated Bridges. (Dr.Ing. Thesis)
MTA-92-89	Langli, Geir, MP	Improving Operational Safety through exploitation of Design Knowledge - an investigation of offshore platform safety. (Dr.Ing. Thesis)
MTA-92-90	Sævik, Svein, MK	On Stresses and Fatigue in Flexible Pipes. (Dr.Ing. Thesis)
MTA-92-91	Ask, Tor Ø., MM	Ignition and Flame Growth in Lean Gas-Air Mixtures. An Experimental Study with a Schlieren System. (Dr.Ing. Thesis)
MTA-86-92	Hessen, Gunnar, MK	Fracture Mechanics Analysis of Stiffened Tubular Members. (Dr.Ing. Thesis)

MTA-93-93	Steinebach, Christian, MM	Knowledge Based Systems for Diagnosis of Rotating Machinery. (Dr.Ing. Thesis)
MTA-93-94	Dalane, Jan Inge, MK	System Reliability in Design and Maintenance of Fixed Offshore Structures. (Dr.Ing. Thesis)
MTA-93-95	Steen, Sverre, MH	Cobblestone Effect on SES. (Dr.Ing. Thesis)
MTA-93-96	Karunakaran, Daniel, MK	Nonlinear Dynamic Response and Reliability Analysis of Drag-dominated Offshore Platforms. (Dr.Ing. Thesis)
MTA-93-97	Hagen, Arnulf, MP	The Framework of a Design Process Language. (Dr.Ing. Thesis)
MTA-93-98	Nordrik, Rune, MM	Investigation of Spark Ignition and Autoignition in Methane and Air Using Computational Fluid Dynamics and Chemical Reaction Kinetics. A Numerical Study of Ignition Processes in Internal Combustion Engines. (Dr.Ing. Thesis)
MTA-94-99	Passano, Elizabeth, MK	Efficient Analysis of Nonlinear Slender Marine Structures. (Dr.Ing. Thesis)
MTA-94-100	Kvålsvold, Jan, MH	Hydroelastic Modelling of Wetdeck Slamming on Multihull Vessels. (Dr.Ing. Thesis)
MTA-94-102	Bech, Sidsel M., MK	Experimental and Numerical Determination of Stiffness and Strength of GRP/PVC Sandwich Structures. (Dr.Ing. Thesis)
MTA-95-103	Paulsen, Hallvard, MM	A Study of Transient Jet and Spray using a Schlieren Method and Digital Image Processing. (Dr.Ing. Thesis)
MTA-95-104	Hovde, Geir Olav, MK	Fatigue and Overload Reliability of Offshore Structural Systems, Considering the Effect of Inspection and Repair. (Dr.Ing. Thesis)
MTA-95-105	Wang, Xiaozhi, MK	Reliability Analysis of Production Ships with Emphasis on Load Combination and Ultimate Strength. (Dr.Ing. Thesis)
MTA-95-106	Ulstein, Tore, MH	Nonlinear Effects of a Flexible Stern Seal Bag on Cobblestone Oscillations of an SES. (Dr.Ing. Thesis)
MTA-95-107	Solaas, Frøydis, MH	Analytical and Numerical Studies of Sloshing in Tanks. (Dr.Ing. Thesis)
MTA-95-108	Hellan, Øyvind, MK	Nonlinear Pushover and Cyclic Analyses in Ultimate Limit State Design and Reassessment of Tubular Steel Offshore Structures. (Dr.Ing. Thesis)
MTA-95-109	Hermundstad, Ole A., MK	Theoretical and Experimental Hydroelastic Analysis of High Speed Vessels. (Dr.Ing. Thesis)
MTA-96-110	Bratland, Anne K., MH	Wave-Current Interaction Effects on Large-Volume Bodies in Water of Finite Depth. (Dr.Ing. Thesis)
MTA-96-111	Herfjord, Kjell, MH	A Study of Two-dimensional Separated Flow by a Combination of the Finite Element Method and

		Navier-Stokes Equations. (Dr.Ing. Thesis)
MTA-96-112	Æsøy, Vilmar, MM	Hot Surface Assisted Compression Ignition in a Direct Injection Natural Gas Engine. (Dr.Ing. Thesis)
MTA-96-113	Eknes, Monika L., MK	Escalation Scenarios Initiated by Gas Explosions on Offshore Installations. (Dr.Ing. Thesis)
MTA-96-114	Erikstad, Stein O., MP	A Decision Support Model for Preliminary Ship Design. (Dr.Ing. Thesis)
MTA-96-115	Pedersen, Egil, MH	A Nautical Study of Towed Marine Seismic Streamer Cable Configurations. (Dr.Ing. Thesis)
MTA-97-116	Moksnes, Paul O., MM	Modelling Two-Phase Thermo-Fluid Systems Using Bond Graphs. (Dr.Ing. Thesis)
MTA-97-117	Halse, Karl H., MK	On Vortex Shedding and Prediction of Vortex-Induced Vibrations of Circular Cylinders. (Dr.Ing. Thesis)
MTA-97-118	Igland, Ragnar T., MK	Reliability Analysis of Pipelines during Laying, considering Ultimate Strength under Combined Loads. (Dr.Ing. Thesis)
MTA-97-119	Pedersen, Hans-P., MP	Levendefiskteknologi for fiskefartøy. (Dr.Ing. Thesis)
MTA-98-120	Vikestad, Kyrre, MK	Multi-Frequency Response of a Cylinder Subjected to Vortex Shedding and Support Motions. (Dr.Ing. Thesis)
MTA-98-121	Azadi, Mohammad R. E., MK	Analysis of Static and Dynamic Pile-Soil-Jacket Behaviour. (Dr.Ing. Thesis)
MTA-98-122	Ulltang, Terje, MP	A Communication Model for Product Information. (Dr.Ing. Thesis)
MTA-98-123	Torbergsen, Erik, MM	Impeller/Diffuser Interaction Forces in Centrifugal Pumps. (Dr.Ing. Thesis)
MTA-98-124	Hansen, Edmond, MH	A Discrete Element Model to Study Marginal Ice Zone Dynamics and the Behaviour of Vessels Moored in Broken Ice. (Dr.Ing. Thesis)
MTA-98-125	Videiro, Paulo M., MK	Reliability Based Design of Marine Structures. (Dr.Ing. Thesis)
MTA-99-126	Mainçon, Philippe, MK	Fatigue Reliability of Long Welds Application to Titanium Risers. (Dr.Ing. Thesis)
MTA-99-127	Haugen, Elin M., MH	Hydroelastic Analysis of Slamming on Stiffened Plates with Application to Catamaran Wetdecks. (Dr.Ing. Thesis)
MTA-99-128	Langhelle, Nina K., MK	Experimental Validation and Calibration of Nonlinear Finite Element Models for Use in Design of Aluminium Structures Exposed to Fire. (Dr.Ing. Thesis)
MTA-99-	Berstad, Are J., MK	Calculation of Fatigue Damage in Ship Structures.

129		(Dr.Ing. Thesis)
MTA-99-130	Andersen, Trond M., MM	Short Term Maintenance Planning. (Dr.Ing. Thesis)
MTA-99-131	Tveiten, Bård Wathne, MK	Fatigue Assessment of Welded Aluminium Ship Details. (Dr.Ing. Thesis)
MTA-99-132	Søreide, Fredrik, MP	Applications of underwater technology in deep water archaeology. Principles and practice. (Dr.Ing. Thesis)
MTA-99-133	Tønnessen, Rune, MH	A Finite Element Method Applied to Unsteady Viscous Flow Around 2D Blunt Bodies With Sharp Corners. (Dr.Ing. Thesis)
MTA-99-134	Elvekrok, Dag R., MP	Engineering Integration in Field Development Projects in the Norwegian Oil and Gas Industry. The Supplier Management of Norne. (Dr.Ing. Thesis)
MTA-99-135	Fagerholt, Kjetil, MP	Optimeringsbaserte Metoder for Ruteplanlegging innen skipsfart. (Dr.Ing. Thesis)
MTA-99-136	Bysveen, Marie, MM	Visualization in Two Directions on a Dynamic Combustion Rig for Studies of Fuel Quality. (Dr.Ing. Thesis)
MTA-2000-137	Storteig, Eskild, MM	Dynamic characteristics and leakage performance of liquid annular seals in centrifugal pumps. (Dr.Ing. Thesis)
MTA-2000-138	Sagli, Gro, MK	Model uncertainty and simplified estimates of long term extremes of hull girder loads in ships. (Dr.Ing. Thesis)
MTA-2000-139	Tronstad, Harald, MK	Nonlinear analysis and design of cable net structures like fishing gear based on the finite element method. (Dr.Ing. Thesis)
MTA-2000-140	Kroneberg, André, MP	Innovation in shipping by using scenarios. (Dr.Ing. Thesis)
MTA-2000-141	Haslum, Herbjørn Alf, MH	Simplified methods applied to nonlinear motion of spar platforms. (Dr.Ing. Thesis)
MTA-2001-142	Samdal, Ole Johan, MM	Modelling of Degradation Mechanisms and Stressor Interaction on Static Mechanical Equipment Residual Lifetime. (Dr.Ing. Thesis)
MTA-2001-143	Baarholm, Rolf Jarle, MH	Theoretical and experimental studies of wave impact underneath decks of offshore platforms. (Dr.Ing. Thesis)
MTA-2001-144	Wang, Lihua, MK	Probabilistic Analysis of Nonlinear Wave-induced Loads on Ships. (Dr.Ing. Thesis)
MTA-2001-145	Kristensen, Odd H. Holt, MK	Ultimate Capacity of Aluminium Plates under Multiple Loads, Considering HAZ Properties. (Dr.Ing. Thesis)
MTA-2001-146	Greco, Marilena, MH	A Two-Dimensional Study of Green-Water

		Loading. (Dr.Ing. Thesis)
MTA-2001-147	Heggelund, Svein E., MK	Calculation of Global Design Loads and Load Effects in Large High Speed Catamarans. (Dr.Ing. Thesis)
MTA-2001-148	Babalola, Olusegun T., MK	Fatigue Strength of Titanium Risers – Defect Sensitivity. (Dr.Ing. Thesis)
MTA-2001-149	Mohammed, Abuu K., MK	Nonlinear Shell Finite Elements for Ultimate Strength and Collapse Analysis of Ship Structures. (Dr.Ing. Thesis)
MTA-2002-150	Holmedal, Lars E., MH	Wave-current interactions in the vicinity of the sea bed. (Dr.Ing. Thesis)
MTA-2002-151	Rognebakke, Olav F., MH	Sloshing in rectangular tanks and interaction with ship motions. (Dr.Ing. Thesis)
MTA-2002-152	Lader, Pål Furset, MH	Geometry and Kinematics of Breaking Waves. (Dr.Ing. Thesis)
MTA-2002-153	Yang, Qinzheng, MH	Wash and wave resistance of ships in finite water depth. (Dr.Ing. Thesis)
MTA-2002-154	Melhus, Øyvin, MM	Utilization of VOC in Diesel Engines. Ignition and combustion of VOC released by crude oil tankers. (Dr.Ing. Thesis)
MTA-2002-155	Ronæss, Marit, MH	Wave Induced Motions of Two Ships Advancing on Parallel Course. (Dr.Ing. Thesis)
MTA-2002-156	Økland, Ole D., MK	Numerical and experimental investigation of whipping in twin hull vessels exposed to severe wet deck slamming. (Dr.Ing. Thesis)
MTA-2002-157	Ge, Chunhua, MK	Global Hydroelastic Response of Catamarans due to Wet Deck Slamming. (Dr.Ing. Thesis)
MTA-2002-158	Byklum, Eirik, MK	Nonlinear Shell Finite Elements for Ultimate Strength and Collapse Analysis of Ship Structures. (Dr.Ing. Thesis)
IMT-2003-1	Chen, Haibo, MK	Probabilistic Evaluation of FPSO-Tanker Collision in Tandem Offloading Operation. (Dr.Ing. Thesis)
IMT-2003-2	Skaugset, Kjetil Bjørn, MK	On the Suppression of Vortex Induced Vibrations of Circular Cylinders by Radial Water Jets. (Dr.Ing. Thesis)
IMT-2003-3	Chezhian, Muthu	Three-Dimensional Analysis of Slamming. (Dr.Ing. Thesis)
IMT-2003-4	Buhaug, Øyvind	Deposit Formation on Cylinder Liner Surfaces in Medium Speed Engines. (Dr.Ing. Thesis)
IMT-2003-5	Tregde, Vidar	Aspects of Ship Design: Optimization of Aft Hull with Inverse Geometry Design. (Dr.Ing. Thesis)
IMT-	Wist, Hanne Therese	Statistical Properties of Successive Ocean Wave

2003-6		Parameters. (Dr.Ing. Thesis)
IMT-2004-7	Ransau, Samuel	Numerical Methods for Flows with Evolving Interfaces. (Dr.Ing. Thesis)
IMT-2004-8	Soma, Torkel	Blue-Chip or Sub-Standard. A data interrogation approach of identity safety characteristics of shipping organization. (Dr.Ing. Thesis)
IMT-2004-9	Ersdal, Svein	An experimental study of hydrodynamic forces on cylinders and cables in near axial flow. (Dr.Ing. Thesis)
IMT-2005-10	Brodtkorb, Per Andreas	The Probability of Occurrence of Dangerous Wave Situations at Sea. (Dr.Ing. Thesis)
IMT-2005-11	Yttervik, Rune	Ocean current variability in relation to offshore engineering. (Dr.Ing. Thesis)
IMT-2005-12	Fredheim, Arne	Current Forces on Net-Structures. (Dr.Ing. Thesis)
IMT-2005-13	Heggernes, Kjetil	Flow around marine structures. (Dr.Ing. Thesis
IMT-2005-14	Fouques, Sebastien	Lagrangian Modelling of Ocean Surface Waves and Synthetic Aperture Radar Wave Measurements. (Dr.Ing. Thesis)
IMT-2006-15	Holm, Håvard	Numerical calculation of viscous free surface flow around marine structures. (Dr.Ing. Thesis)
IMT-2006-16	Bjørheim, Lars G.	Failure Assessment of Long Through Thickness Fatigue Cracks in Ship Hulls. (Dr.Ing. Thesis)
IMT-2006-17	Hansson, Lisbeth	Safety Management for Prevention of Occupational Accidents. (Dr.Ing. Thesis)
IMT-2006-18	Zhu, Xinying	Application of the CIP Method to Strongly Nonlinear Wave-Body Interaction Problems. (Dr.Ing. Thesis)
IMT-2006-19	Reite, Karl Johan	Modelling and Control of Trawl Systems. (Dr.Ing. Thesis)
IMT-2006-20	Smogeli, Øyvind Notland	Control of Marine Propellers. From Normal to Extreme Conditions. (Dr.Ing. Thesis)
IMT-2007-21	Storhaug, Gaute	Experimental Investigation of Wave Induced Vibrations and Their Effect on the Fatigue Loading of Ships. (Dr.Ing. Thesis)
IMT-2007-22	Sun, Hui	A Boundary Element Method Applied to Strongly Nonlinear Wave-Body Interaction Problems. (PhD Thesis, CeSOS)
IMT-2007-23	Rustad, Anne Marthine	Modelling and Control of Top Tensioned Risers. (PhD Thesis, CeSOS)
IMT-2007-24	Johansen, Vegar	Modelling flexible slender system for real-time simulations and control applications
IMT-2007-25	Wroldsen, Anders Sunde	Modelling and control of tensegrity structures.

		(PhD Thesis, CeSOS)
IMT-2007-26	Aronsen, Kristoffer Høye	An experimental investigation of in-line and combined inline and cross flow vortex induced vibrations. (Dr. avhandling, IMT)
IMT-2007-27	Gao, Zhen	Stochastic Response Analysis of Mooring Systems with Emphasis on Frequency-domain Analysis of Fatigue due to Wide-band Response Processes (PhD Thesis, CeSOS)
IMT-2007-28	Thorstensen, Tom Anders	Lifetime Profit Modelling of Ageing Systems Utilizing Information about Technical Condition. (Dr.ing. thesis, IMT)
IMT-2008-29	Refsnes, Jon Erling Gorset	Nonlinear Model-Based Control of Slender Body AUVs (PhD Thesis, IMT)
IMT-2008-30	Berntsen, Per Ivar B.	Structural Reliability Based Position Mooring. (PhD-Thesis, IMT)
IMT-2008-31	Ye, Naiquan	Fatigue Assessment of Aluminium Welded Box-stiffener Joints in Ships (Dr.ing. thesis, IMT)
IMT-2008-32	Radan, Damir	Integrated Control of Marine Electrical Power Systems. (PhD-Thesis, IMT)
IMT-2008-33	Thomassen, Paul	Methods for Dynamic Response Analysis and Fatigue Life Estimation of Floating Fish Cages. (Dr.ing. thesis, IMT)
IMT-2008-34	Pákozdi, Csaba	A Smoothed Particle Hydrodynamics Study of Two-dimensional Nonlinear Sloshing in Rectangular Tanks. (Dr.ing.thesis, IMT/ CeSOS)
IMT-2007-35	Grytøyr, Guttorm	A Higher-Order Boundary Element Method and Applications to Marine Hydrodynamics. (Dr.ing.thesis, IMT)
IMT-2008-36	Drummen, Ingo	Experimental and Numerical Investigation of Nonlinear Wave-Induced Load Effects in Containerships considering Hydroelasticity. (PhD thesis, CeSOS)
IMT-2008-37	Skejic, Renato	Maneuvering and Seakeeping of a Singel Ship and of Two Ships in Interaction. (PhD-Thesis, CeSOS)
IMT-2008-38	Harlem, Alf	An Age-Based Replacement Model for Repairable Systems with Attention to High-Speed Marine Diesel Engines. (PhD-Thesis, IMT)
IMT-2008-39	Alsos, Hagbart S.	Ship Grounding. Analysis of Ductile Fracture, Bottom Damage and Hull Girder Response. (PhD-thesis, IMT)
IMT-2008-40	Graczyk, Mateusz	Experimental Investigation of Sloshing Loading and Load Effects in Membrane LNG Tanks Subjected to Random Excitation. (PhD-thesis, CeSOS)
IMT-2008-41	Taghipour, Reza	Efficient Prediction of Dynamic Response for Flexible amd Multi-body Marine Structures. (PhD-

		thesis, CeSOS)
IMT-2008-42	Ruth, Eivind	Propulsion control and thrust allocation on marine vessels. (PhD thesis, CeSOS)
IMT-2008-43	Nystad, Bent Helge	Technical Condition Indexes and Remaining Useful Life of Aggregated Systems. PhD thesis, IMT
IMT-2008-44	Soni, Prashant Kumar	Hydrodynamic Coefficients for Vortex Induced Vibrations of Flexible Beams, PhD thesis, CeSOS
IMT-2009-45	Amlashi, Hadi K.K.	Ultimate Strength and Reliability-based Design of Ship Hulls with Emphasis on Combined Global and Local Loads. PhD Thesis, IMT
IMT-2009-46	Pedersen, Tom Arne	Bond Graph Modelling of Marine Power Systems. PhD Thesis, IMT
IMT-2009-47	Kristiansen, Trygve	Two-Dimensional Numerical and Experimental Studies of Piston-Mode Resonance. PhD-Thesis, CeSOS
IMT-2009-48	Ong, Muk Chen	Applications of a Standard High Reynolds Number Model and a Stochastic Scour Prediction Model for Marine Structures. PhD-thesis, IMT
IMT-2009-49	Hong, Lin	Simplified Analysis and Design of Ships subjected to Collision and Grounding. PhD-thesis, IMT
IMT-2009-50	Koushan, Kamran	Vortex Induced Vibrations of Free Span Pipelines, PhD thesis, IMT
IMT-2009-51	Korsvik, Jarl Eirik	Heuristic Methods for Ship Routing and Scheduling. PhD-thesis, IMT
IMT-2009-52	Lee, Jihoon	Experimental Investigation and Numerical in Analyzing the Ocean Current Displacement of Longlines. Ph.d.-Thesis, IMT.
IMT-2009-53	Vestbøstad, Tone Gran	A Numerical Study of Wave-in-Deck Impact usin a Two-Dimensional Constrained Interpolation Profile Method, Ph.d.thesis, CeSOS.
IMT-2009-54	Bruun, Kristine	Bond Graph Modelling of Fuel Cells for Marine Power Plants. Ph.d.-thesis, IMT
IMT 2009-55	Holstad, Anders	Numerical Investigation of Turbulence in a Sekwed Three-Dimensional Channel Flow, Ph.d.-thesis, IMT.
IMT 2009-56	Ayala-Uraga, Efren	Reliability-Based Assessment of Deteriorating Ship-shaped Offshore Structures, Ph.d.-thesis, IMT
IMT 2009-57	Kong, Xiangjun	A Numerical Study of a Damaged Ship in Beam Sea Waves. Ph.d.-thesis, IMT/CeSOS.
IMT 2010-58	Kristiansen, David	Wave Induced Effects on Floaters of Aquaculture Plants, Ph.d.-thesis, CeSOS.

IMT 2010-59	Ludvigsen, Martin	An ROV-Toolbox for Optical and Acoustic Scientific Seabed Investigation. Ph.d.-thesis IMT.
IMT 2010-60	Hals, Jørgen	Modelling and Phase Control of Wave-Energy Converters. Ph.d.thesis, CeSOS.
IMT 2010- 61	Shu, Zhi	Uncertainty Assessment of Wave Loads and Ultimate Strength of Tankers and Bulk Carriers in a Reliability Framework. Ph.d. Thesis, IMT/ CeSOS
IMT 2010-62	Shao, Yanlin	Numerical Potential-Flow Studies on Weakly-Nonlinear Wave-Body Interactions with/without Small Forward Speed, Ph.d.thesis,CeSOS.
IMT 2010-63	Califano, Andrea	Dynamic Loads on Marine Propellers due to Intermittent Ventilation. Ph.d.thesis, IMT.
IMT 2010-64	El Khoury, George	Numerical Simulations of Massively Separated Turbulent Flows, Ph.d.-thesis, IMT
IMT 2010-65	Seim, Knut Sponheim	Mixing Process in Dense Overflows with Emphasis on the Faroe Bank Channel Overflow. Ph.d.thesis, IMT
IMT 2010-66	Jia, Huirong	Structural Analysis of Intect and Damaged Ships in a Collission Risk Analysis Perspective. Ph.d.thesis CeSoS.
IMT 2010-67	Jiao, Linlin	Wave-Induced Effects on a Pontoon-type Very Large Floating Structures (VLFS). Ph.D.-thesis, CeSOS.
IMT 2010-68	Abrahamsen, Bjørn Christian	Sloshing Induced Tank Roof with Entrapped Air Pocket. Ph.d.thesis, CeSOS.
IMT 2011-69	Karimirad, Madjid	Stochastic Dynamic Response Analysis of Spar-Type Wind Turbines with Catenary or Taut Mooring Systems. Ph.d.-thesis, CeSOS.
IMT - 2011-70	Erlend Meland	Condition Monitoring of Safety Critical Valves. Ph.d.-thesis, IMT.
IMT – 2011-71	Yang, Limin	Stochastic Dynamic System Analysis of Wave Energy Converter with Hydraulic Power Take-Off, with Particular Reference to Wear Damage Analysis, Ph.d. Thesis, CeSOS.
IMT – 2011-72	Visscher, Jan	Application of Particla Image Velocimetry on Turbulent Marine Flows, Ph.d.Thesis, IMT.
IMT – 2011-73	Su, Biao	Numerical Predictions of Global and Local Ice Loads on Ships. Ph.d.Thesis, CeSOS.
IMT – 2011-74	Liu, Zhenhui	Analytical and Numerical Analysis of Iceberg Collision with Ship Structures. Ph.d.Thesis, IMT.
IMT – 2011-75	Aarsæther, Karl Gunnar	Modeling and Analysis of Ship Traffic by Observation and Numerical Simulation. Ph.d.Thesis, IMT.

Imt – 2011-76	Wu, Jie	Hydrodynamic Force Identification from Stochastic Vortex Induced Vibration Experiments with Slender Beams. Ph.d.Thesis, IMT.
Imt – 2011-77	Amini, Hamid	Azimuth Propulsors in Off-design Conditions. Ph.d.Thesis, IMT.
IMT – 2011-78	Nguyen, Tan-Hoi	Toward a System of Real-Time Prediction and Monitoring of Bottom Damage Conditions During Ship Grounding. Ph.d.thesis, IMT.
IMT- 2011-79	Tavakoli, Mohammad T.	Assessment of Oil Spill in Ship Collision and Grounding, Ph.d.thesis, IMT.
IMT- 2011-80	Guo, Bingjie	Numerical and Experimental Investigation of Added Resistance in Waves. Ph.d.Thesis, IMT.
IMT- 2011-81	Chen, Qiaofeng	Ultimate Strength of Aluminium Panels, considering HAZ Effects, IMT
IMT- 2012-82	Kota, Ravikiran S.	Wave Loads on Decks of Offshore Structures in Random Seas, CeSOS.
IMT- 2012-83	Sten, Ronny	Dynamic Simulation of Deep Water Drilling Risers with Heave Compensating System, IMT.
IMT- 2012-84	Berle, Øyvind	Risk and resilience in global maritime supply chains, IMT.
IMT- 2012-85	Fang, Shaoji	Fault Tolerant Position Mooring Control Based on Structural Reliability, CeSOS.
IMT- 2012-86	You, Jikun	Numerical studies on wave forces and moored ship motions in intermediate and shallow water, CeSOS.
IMT- 2012-87	Xiang ,Xu	Maneuvering of two interacting ships in waves, CeSOS
IMT- 2012-88	Dong, Wenbin	Time-domain fatigue response and reliability analysis of offshore wind turbines with emphasis on welded tubular joints and gear components, CeSOS
IMT- 2012-89	Zhu, Suji	Investigation of Wave-Induced Nonlinear Load Effects in Open Ships considering Hull Girder Vibrations in Bending and Torsion, CeSOS
IMT- 2012-90	Zhou, Li	Numerical and Experimental Investigation of Station-keeping in Level Ice, CeSOS
IMT- 2012-91	Ushakov, Sergey	Particulate matter emission characteristics from diesel enignes operating on conventional and alternative marine fuels, IMT
IMT- 2013-1	Yin, Decao	Experimental and Numerical Analysis of Combined In-line and Cross-flow Vortex Induced Vibrations, CeSOS

IMT-2013-2	Kurniawan, Adi	Modelling and geometry optimisation of wave energy converters, CeSOS
IMT-2013-3	Al Ryati, Nabil	Technical condition indexes doe auxiliary marine diesel engines, IMT
IMT-2013-4	Firoozkoohi, Reza	Experimental, numerical and analytical investigation of the effect of screens on sloshing, CeSOS
IMT-2013-5	Ommani, Babak	Potential-Flow Predictions of a Semi-Displacement Vessel Including Applications to Calm Water Broaching, CeSOS
IMT-2013-6	Xing, Yihan	Modelling and analysis of the gearbox in a floating spar-type wind turbine, CeSOS
IMT-7-2013	Balland, Océane	Optimization models for reducing air emissions from ships, IMT
IMT-8-2013	Yang, Dan	Transitional wake flow behind an inclined flat plate-----Computation and analysis, IMT
IMT-9-2013	Abdillah, Suyuthi	Prediction of Extreme Loads and Fatigue Damage for a Ship Hull due to Ice Action, IMT
IMT-10-2013	Ramìrez, Pedro Agustìn Pèrez	Ageing management and life extension of technical systems- Concepts and methods applied to oil and gas facilities, IMT
IMT-11-2013	Chuang, Zhenju	Experimental and Numerical Investigation of Speed Loss due to Seakeeping and Maneuvering. IMT
IMT-12-2013	Etemaddar, Mahmoud	Load and Response Analysis of Wind Turbines under Atmospheric Icing and Controller System Faults with Emphasis on Spar Type Floating Wind Turbines, IMT
IMT-13-2013	Lindstad, Haakon	Strategies and measures for reducing maritime CO2 emissons, IMT
IMT-14-2013	Haris, Sabril	Damage interaction analysis of ship collisions, IMT
IMT-15-2013	Shainee, Mohamed	Conceptual Design, Numerical and Experimental Investigation of a SPM Cage Concept for Offshore Mariculture, IMT
IMT-16-2013	Gansel, Lars	Flow past porous cylinders and effects of biofouling and fish behavior on the flow in and around Atlantic salmon net cages, IMT
IMT-17-2013	Gaspar, Henrique	Handling Aspects of Complexity in Conceptual Ship Design, IMT
IMT-18-2013	Thys, Maxime	Theoretical and Experimental Investigation of a Free Running Fishing Vessel at Small Frequency of Encounter, CeSOS
IMT-19-2013	Aglen, Ida	VIV in Free Spanning Pipelines, CeSOS

IMT-1-2014	Song, An	Theoretical and experimental studies of wave diffraction and radiation loads on a horizontally submerged perforated plate, CeSOS
IMT-2-2014	Rogne, Øyvind Ygre	Numerical and Experimental Investigation of a Hinged 5-body Wave Energy Converter, CeSOS
IMT-3-2014	Dai, Lijuan	Safe and efficient operation and maintenance of offshore wind farms ,IMT
IMT-4-2014	Bachynski, Erin Elizabeth	Design and Dynamic Analysis of Tension Leg Platform Wind Turbines, CeSOS
IMT-5-2014	Wang, Jingbo	Water Entry of Freefall Wedged – Wedge motions and Cavity Dynamics, CeSOS
IMT-6-2014	Kim, Ekaterina	Experimental and numerical studies related to the coupled behavior of ice mass and steel structures during accidental collisions, IMT
IMT-7-2014	Tan, Xiang	Numerical investigation of ship's continuous- mode icebreaking in leverl ice, CeSOS
IMT-8-2014	Muliawan, Made Jaya	Design and Analysis of Combined Floating Wave and Wind Power Facilities, with Emphasis on Extreme Load Effects of the Mooring System, CeSOS
IMT-9-2014	Jiang, Zhiyu	Long-term response analysis of wind turbines with an emphasis on fault and shutdown conditions, IMT
IMT-10-2014	Dukan, Fredrik	ROV Motion Control Systems, IMT
IMT-11-2014	Grimsmo, Nils I.	Dynamic simulations of hydraulic cylinder for heave compensation of deep water drilling risers, IMT
IMT-12-2014	Kvittem, Marit I.	Modelling and response analysis for fatigue design of a semisubmersible wind turbine, CeSOS
IMT-13-2014	Akhtar, Juned	The Effects of Human Fatigue on Risk at Sea, IMT
IMT-14-2014	Syahroni, Nur	Fatigue Assessment of Welded Joints Taking into Account Effects of Residual Stress, IMT
IMT-1-2015	Bøckmann, Eirik	Wave Propulsion of ships, IMT
IMT-2-2015	Wang, Kai	Modelling and dynamic analysis of a semi-submersible floating vertical axis wind turbine, CeSOS
IMT-3-2015	Fredriksen, Arnt Gunvald	A numerical and experimental study of a two-dimensional body with moonpool in waves and current, CeSOS
IMT-4-2015	Jose Patricio Gallardo Canabes	Numerical studies of viscous flow around bluff bodies, IMT

IMT-5-2015	Vegard Longva	Formulation and application of finite element techniques for slender marine structures subjected to contact interactions, IMT
IMT-6-2015	Jacobus De Vaal	Aerodynamic modelling of floating wind turbines, CeSOS
IMT-7-2015	Fachri Nasution	Fatigue Performance of Copper Power Conductors, IMT
IMT-8-2015	Oleh I Karpa	Development of bivariate extreme value distributions for applications in marine technology,CeSOS
IMT-9-2015	Daniel de Almeida Fernandes	An output feedback motion control system for ROVs, AMOS
IMT-10-2015	Bo Zhao	Particle Filter for Fault Diagnosis: Application to Dynamic Positioning Vessel and Underwater Robotics, CeSOS
IMT-11-2015	Wenting Zhu	Impact of emission allocation in maritime transportation, IMT
IMT-12-2015	Amir Rasekhi Nejad	Dynamic Analysis and Design of Gearboxes in Offshore Wind Turbines in a Structural Reliability Perspective, CeSOS
IMT-13-2015	Arturo Jesùs Ortega Malca	Dynamic Response of Flexibles Risers due to Unsteady Slug Flow, CeSOS
IMT-14-2015	Dagfinn Husjord	Guidance and decision-support system for safe navigation of ships operating in close proximity, IMT
IMT-15-2015	Anirban Bhattacharyya	Ducted Propellers: Behaviour in Waves and Scale Effects, IMT
IMT-16-2015	Qin Zhang	Image Processing for Ice Parameter Identification in Ice Management, IMT
IMT-1-2016	Vincentius Rumawas	Human Factors in Ship Design and Operation: An Experiential Learning, IMT
IMT-2-2016	Martin Storheim	Structural response in ship-platform and ship-ice collisions, IMT
IMT-3-2016	Mia Abrahamsen Prsic	Numerical Simulations of the Flow around single and Tandem Circular Cylinders Close to a Plane Wall, IMT
IMT-4-2016	Tufan Arslan	Large-eddy simulations of cross-flow around ship sections, IMT

IMT-5-2016	Pierre Yves-Henry	Parametrisation of aquatic vegetation in hydraulic and coastal research,IMT
IMT-6-2016	Lin Li	Dynamic Analysis of the Instalation of Monopiles for Offshore Wind Turbines, CeSOS
IMT-7-2016	Øivind Kåre Kjerstad	Dynamic Positioning of Marine Vessels in Ice, IMT
IMT-8-2016	Xiaopeng Wu	Numerical Analysis of Anchor Handling and Fish Trawling Operations in a Safety Perspective, CeSOS
IMT-9-2016	Zhengshun Cheng	Integrated Dynamic Analysis of Floating Vertical Axis Wind Turbines, CeSOS
IMT-10-2016	Ling Wan	Experimental and Numerical Study of a Combined Offshore Wind and Wave Energy Converter Concept
IMT-11-2016	Wei Chai	Stochastic dynamic analysis and reliability evaluation of the roll motion for ships in random seas, CeSOS
IMT-12-2016	Øyvind Selnes Patricksson	Decision support for conceptual ship design with focus on a changing life cycle and future uncertainty, IMT
IMT-13-2016	Mats Jørgen Thorsen	Time domain analysis of vortex-induced vibrations, IMT
IMT-14-2016	Edgar McGuinness	Safety in the Norwegian Fishing Fleet – Analysis and measures for improvement, IMT
IMT-15-2016	Sepideh Jafarzadeh	Energy effiency and emission abatement in the fishing fleet, IMT
IMT-16-2016	Wilson Ivan Guachamin Acero	Assessment of marine operations for offshore wind turbine installation with emphasis on response-based operational limits, IMT
IMT-17-2016	Mauro Candeloro	Tools and Methods for Autonomous Operations on Seabed and Water Coumn using Underwater Vehicles, IMT
IMT-18-2016	Valentin Chabaud	Real-Time Hybrid Model Testing of Floating Wind Tubines, IMT
IMT-1-2017	Mohammad Saud Afzal	Three-dimensional streaming in a sea bed boundary layer
IMT-2-2017	Peng Li	A Theoretical and Experimental Study of Wave-induced Hydroelastic Response of a Circular Floating Collar
IMT-3-2017	Martin Bergström	A simulation-based design method for arctic maritime transport systems

IMT-4-2017	Bhushan Taskar	The effect of waves on marine propellers and propulsion
IMT-5-2017	Mohsen Bardestani	A two-dimensional numerical and experimental study of a floater with net and sinker tube in waves and current
IMT-6-2017	Fatemeh Hoseini Dadmarzi	Direct Numerical Simualtion of turbulent wakes behind different plate configurations
IMT-7-2017	Michel R. Miyazaki	Modeling and control of hybrid marine power plants
IMT-8-2017	Giri Rajasekhar Gunnu	Safety and effiency enhancement of anchor handling operations with particular emphasis on the stability of anchor handling vessels
IMT-9-2017	Kevin Koosup Yum	Transient Performance and Emissions of a Turbocharged Diesel Engine for Marine Power Plants
IMT-10-2017	Zhaolong Yu	Hydrodynamic and structural aspects of ship collisions